Vibration Test

for

Graphite Shielding Structure

March, 1972

BUILDING RESEARCH INSTITUTE
CONSTRUCTION MINISTRY, JAPAN

Name of Members

Kyoji NAKAGAWA
Hiroshi YAMAHARA
Norihiko OSAKI
Makoto WATABE
Yoji MURATA
Yoshikazu KITAGAWA
Kenkichi SAWADA

Osamu KAWAGUCHI
Shigehiko MATSUMOTO
Hideki ITO
Kinji AKINO
Muneaki KATO
Seiya TAMURA
Sachihito ISHIZAKI
Naoji AOKI

CONTENTS

Chapter 1 Introduction

This report covers the study and tests performed to examine the seismic resistant stability of the graphite shielding and its supporting structures which are used for the fast breeder reactors. This experimental work was undertaken by the Construction Ministry's Building Research Institute working as the mainstay of the study group upon the request of the Power Reactor and Nuclear Fuel Development Corporation (PNC). The experiment planning and the evaluation of the experimental results were managed and undertaken by a committee especially formed with the participation of experts and specialists in the respective concerned fields.

For the vibration and seismic tests, the large capacity vibration-shaking table at the National Disaster Defense Center was used by the courtesy of said Center, and the test was conducted in cooperation with the Center's technical staff.

Taking this opportunity, our sincere appreciation is hereby expressed for all the courtesies and assistance rendered in the development of this experiment by the following named organizations:

National Disaster Defense Center
Ohbayashi Gumi, Co.
Kyowa Dengyo Co.
Showa Denko Co.
Shimizu Construction Co.
Japan Atomic Power Co.
Hitachi Seisakusho, Co.

and particularly, for the group of students of the Tokyo Denki University who actively participated in the actual tests and analysis.

Vibration Test Schedule

Date		Type and Scope of Tests
July	12	STATIC Tilting test
July	14	DYNAMIC Setting of test specimens and measuring instruments including electric wiring. Test Run Measuring Points: Accelerometers 21 points 25 gal const Pins 2 50 gal const Keys 2 100 gal const 150 gal const
July	15	Draw up resonance curves Test No. 15-1 Test No. 15-3 100 gal const 400 gal const Test No. 15-2 Test No. 15-4 200 gal const Free vibration
July	*16	Test No. 16-1 Test No. 16-4 100 gal 100 gal const Test No. 16-2 Test No. 16-5 400 gal 400 gal const Test No. 16-3 Test No. 16-6 Random wave Random wave (1) Tokachi The same as No. 16-3 (2) El centro (3) Hiroo (4) El centro*
July	17	Test No. 16-7 Test No. 16-8 100 gal const 400 gal const Test No. 16-9 Random wave

July	18	Test No. 18-1 200 gal const Test No. 18-2 100 gal const Test No. 18-3 200 gal const	Test No. 18-4 400 gal const resonance Test No. 18-5 Free vibration Compulsory displacement
July	19	X direction mode produced Test No. 19-1 100 gal const Test No. 19-2 400 gal const	Test No. 19-3 Random wave (1) Tokachi (2) Hiroo (3) El centro (4) El centro* (5) El centro
July	21	Test No. 21-1 100 gal const Test No. 21-2 400 gal const Test No. 21-3 Random wave (1) Tokachi (2) Hiroo (3) El centro (4) El centro* (5) El centro*	Test No. 21-4 100 gal const Test No. 21-5 400 gal const Test No. 21-6 Random wave
July	22	Breaking Test Test No. 22-1 800 gal const Test No. 22-2 Constant speed (9 cm/sec) Test No. 22-3 Random wave (1) Tokachi (2) Hiroo (3) El centro	Test No. 22-4 Random wave (1) Tokachi (2) Hiroo (3) El centro (4) El centro* (5) El centro Test No. 22-5 1600 gal Test No. 22-6 Constant speed (20 cm/sec) Test No. 22-7

July	23	
		Note: El centro* : Response wave at the installed Floor due to El centro.

Static Loading Test Schedule

Date		Type and Scope of Tests
Aug.	16	Key compression tests, No. 1, 2 and 3. Strength and collapse test
Aug.	17	Key bending tests, No. 1, 2 and 3. Strength and collapse test
Aug.	19	Plate spring rigidity test, No. 1, 2 and 3.
		1-layer 3-row blocks compression test, No. 1. Strength and collapse test
Aug.	20	1-layer 3-row blocks compression test, No. 2. Strength and collapse test
Aug.	23	1-layer 3-row blocks compression test, No. 3. Strength and collapse test
Aug.	24	3-layer 3-row blocks compression tests No. 2, and 3.
		(test No. 1 failed due to certain fault.) Strength and collapse test
Aug.	26	1-layer 3-row blocks tensile test No. 1 This test failed due to erroneous fitting of jigs.
Sept.	10	1-layer 3-row blocks tensile test No. 2. Strength and collapse test
Sept.	13	1-layer 3-row blocks tensile test No. 3. Strength and collapse test
Oct.	6	Supplemental key compression tests No. 4, 5 and 6.
Oct.	13	3-layer 3-row blocks traverse force test No. 1.
		Strength and collapse test
Oct.	15	3-layer 3-row blocks traverse force test No. 2.
		Strength and collapse test

Chapter 2 Summary

2. 1 Purpose of Test and Plan

Fig. II-I shows the schematic drawings of the Graphite Shielding Structure which is the subject of this research and experiment work. As stated in the Introduction the purpose of this experiment work is to make qualitative and quantitative studies on the behaviors of the graphite shielding structure at the time of a strong seismic disturbance.

At the time of an earthquake, as the upper section of the Graphite Shielding Structure indicates a larger acceleration response, the Dynamic behavior of the structure upper section poses an important problem. In this experiment, the graphite blocks from the top down to the 11th lays as per Fig. II-I are the subject of this vibration tests.

For the test model of this type of vibration experiment, the material with a size 1/2 of the actual size are employed and subjected to a series of vibration tests by use of a large capacity vibration table installed at the Science and Technology Agency's National Disaster Defense Center located at the foot of Mt. Tsukuba, Ibaragi Pref.

In order to get acquainted with the behaviors of the graphite blocks under a strong seismic disturbance, it is necessary to measure and determine various involved factors such as the degree of stress, displacement, and acceleration of the graphite blocks themselves during the vibration tests, as well as the status of shearing stress of the graphite keys which hold and link the respective blocks together, the stress distribution of the supporting pins holding the blocks to the safety vessel and around the vicinity of the supporting pins, stress distribution of the safety vessel, and the acceleration distribution. Also the static test by lateral force applied on the tilted vibration test model is though necessary as a base to measure the dynamic behaviors during the vibration movement. For this reason, the static tilting test by tilting the vibration model is planned to be performed on the vibration table prior to the vibration test.

Furthermore, in order to gather and obtain basic information and data on the mechanical characteristics of graphite material, and on transmission of the shearing force of blocks and keys as an assembly of blocks, a series of so called static loading tests are scheduled to be undertaken at the material strength testing laboratory of the Construction Ministry's Building Research Institute.

2. 2 Static Loading Test

In the first place, a series of static loading tests are to be conducted for the purpose of obtaining various data and values on graphite material such as its tensile and compression strength, shear strength, yield points, elongation, elastic constant, plasticity coefficient, Poisson's ratio, specific gravity, static friction coefficient, dynamic friction coefficient, etc. Then, the static test of the rigidity of plate springs which play the cushioning role on the horizontal contact face between the graphite blocks and the primary sodium piping tunnel is to be conducted to obtain the plate spring's rigidity.

As the test specimen to be used for this experiment, three blocks are to be selected as one layer and (1) one unit is placed horizontalwise which is one-layer and 3-rows, and (2) one unit each is laid in the direction of depth and sidewise forming 3-layer and 3-rows. Here, it is also planned to conduct a set of static loading tests to obtain the knowledge on the shear strength of the graphite blocks as an assembly held together with keys, and the stress of the keyes, as well as the transfer mechanism of the shearing force between the blocks.

In consideration of the non-uniformity or struggling of both the test specimens and the measurement methods, it is made a principle in the static loading test to prepare three specimens of the same type materials so that the test is to be conducted three times by the same test method.

2. 3 Static Tilting Test by Tilting Test Model

Measurement of any dynamic stress or displacement involves varied aspects of inaccuracy and uncertainty as it often lacks in stability and stationary as comparing with the measurement of those of the statics. In this sense, it is important that the static strain and displacement must have been measured by tilting the test model and applying to them a static force in the lateral direction of the model by component of force of gravity. Furthermore, by comparison of the dynamic test results with the results of this static tilting test, it may as well be able to get acquainted with the indications of what degree of vibration effect can be brought about by the dynamic test results. In addition, it is considered necessary especially to conduct a static tilting test because of the considerable number of statistical variance among the various measured values caused by the impact occurring among the graphite blocks in the

course of a vibration test.

The tilt of specimens in this test is in the orthogonal directions of both X and Y, in which directions, the vibration is applied. The maximum tilt-angle is 45^{o} while the test also is performed at 30^{o}.

A device for the tilting of the specimen is specially designed and made, and the crane-hoist on the shaking table is used to maintain the specimen in the tilted angle.

2. 4 Vibration Test by Vibration Test Model

The vibration is in the same direction as in the case of the static tilting test (orthogonal directions of both X and Y). The type and scope of the applied vibration are of 0. 5 Hz to 20 Hz sinusoidal waves of constant acceralation the actual recorded seismic waves of the Tokachi Off-shore earthquakes compensated in consideration of the size simulation of the model, and the responded wave for the base of the Graphite Shielding Structure to the input of the El Centro Earthquakes EW (May 18, 1940) for the structures.

At the final stage of the vibration test, an ultimate collape test of the model is planned to be undertaken using the maximum vibration-shaking capacity of the shaking-table in order to see the braking behavior of the model.

The main objectives of the measurement are placed on the folowing five points: Acceleration response values of the respective sections, shearing stress of graphite keys, relative displacement between graphite blocks, bending stress of the supporting pins, and bending stress of the cylinder (the safety vessel).

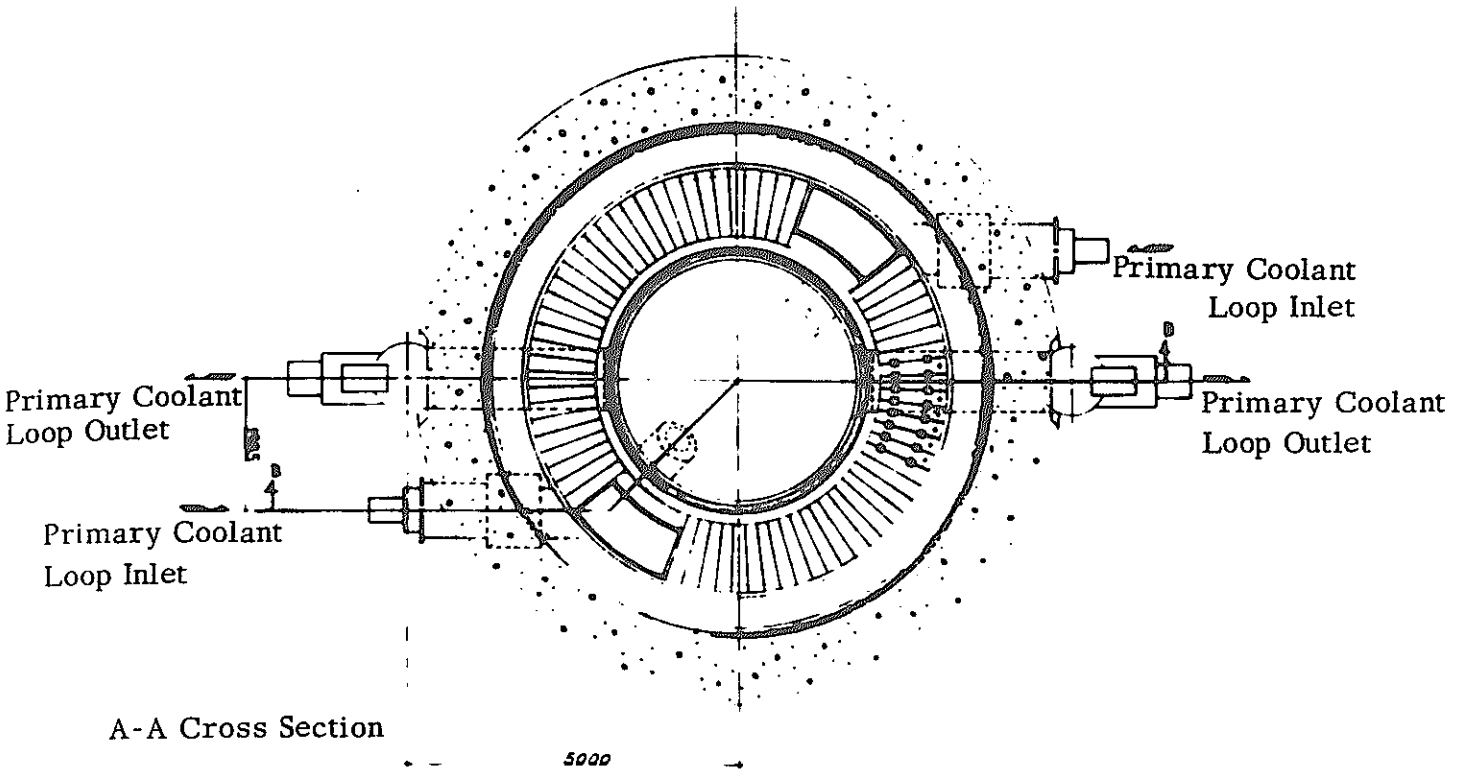

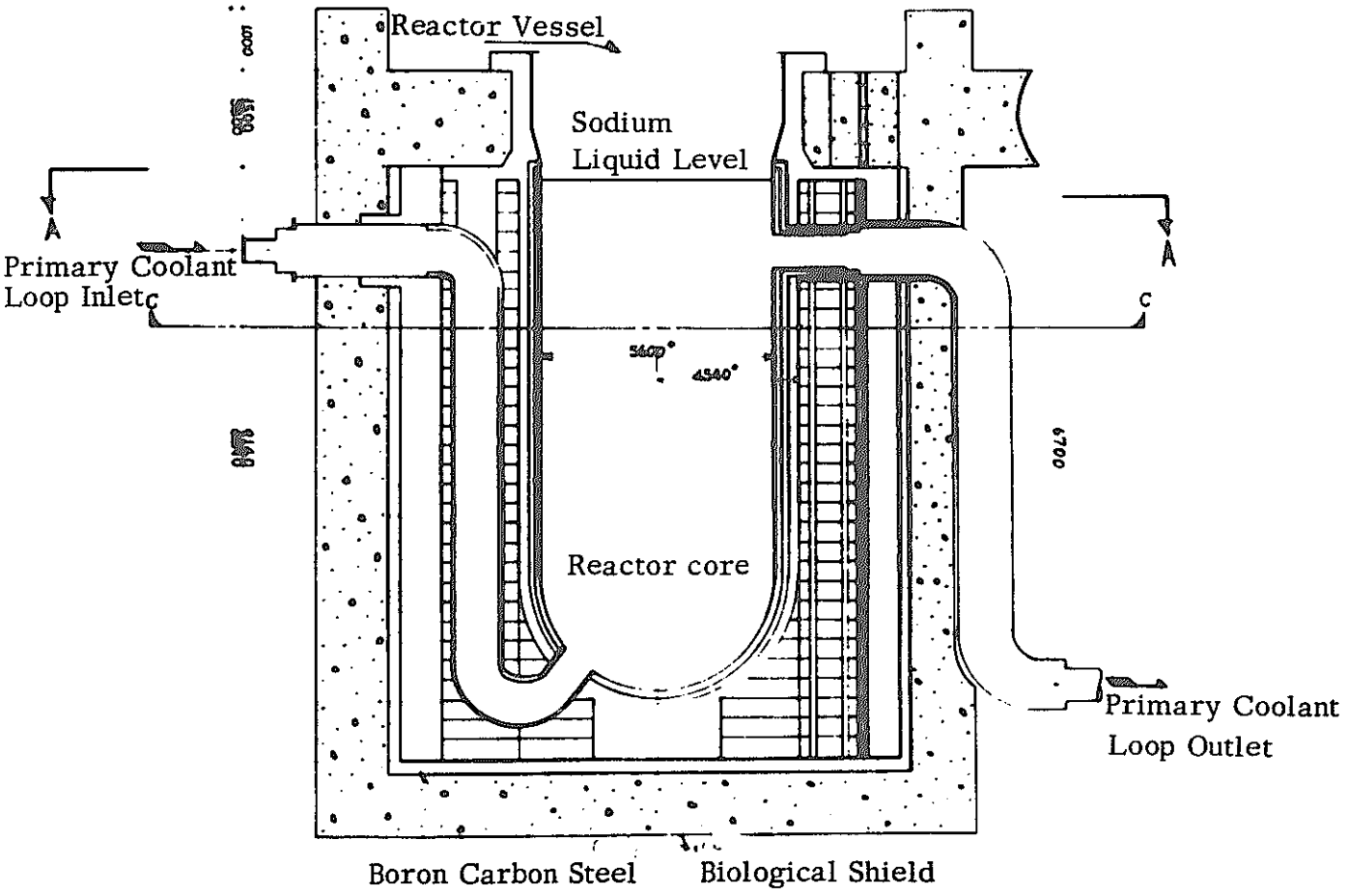

B-B Cross Section

A model of 1/2 of the actural size of C-C upper section is used for the experiments (The 11th layer from the uppermost section of the graphite blocks).

Fig. II-I

Chapter 3 Description of Test Model

3. 1 Static Loading Test Specimens

As described in the preceding Chapter, a static loding test is undertaken in order to examine the mechanical properties of graphite material, and similarly, the mechanical characteristics of graphite block held together by keys, as well as to determine the mechanical behavior of the plate springs which support the graphite. These test specimens which have been prepared for this experiment have a measured graphite density of 1. 78 g/cm^3 respectively.

3. 1. 1 Rigidity Test of Plate Springs

The horizontal direction vibration pattern of the graphite itself which is supported in the horizontal direction of the plate spring will be greatly influenced by the rigidity of the plate spring. Accordingly, the test is to be conducted under an actual use-condition with a slight change in the supporting condition for the purpose of facilitating the measurement of "displacement". The actual dimensions of the plate springs are shown in Fig. III-I-I.

3. 1. 2 Compressive Test of Keys

The compression test of keys is conducted aiming at obtaining the data of compression strength of graphite as a material, and its modulus of elasticity under compression, load deformation under compression as well as the Poisson's Ratio.

3. 1. 3 Bending Loading Test of Keys

By undertaking a bending loading test of keys, the tensile strength and the shearing strength of the keys as a material are examined. The actual dimensions of the keys are the same as when the compression test was performed. The dimensions are shown in Fig. II-I-II and III-I-III respectively.

3. 1. 4 Compressive and Tensile Loading Tests of 1-Layer 3-Row Blocks

This type of compression and tensile loading tests are performed to get acquainted with the shearing force transfer mechanism of the keys which hold together the three blocks in a row, and the behavior of the blocks themselves under force. As

shown in Fig. III-I-IV, the stress transfer in each of the four keys, the compression stress in each of the blocks as well as the tensile stress distribution among the blocks are examined in the process of the experiment, and finally to find out which section of these blocks may first surrender to a breakdown. The dimensions of each specimen are given in Fig. III-I-IV.

3. 1. 5 Compressive Loading Test of 3-Layer 3-Row Blocks

By assembling nine blocks, this type of experiment is aimed at determining how the shearing stress will transfer to each of the blocks. Also by this experiment, the bending stress and the shearing stress on the pins and keys which support the blocks are examined. The actual dimensions of the test specimens are as shown in Fig. III-I-V.

3. 1. 6 Traverse Direction Loading Test of 3-Layer 3-Row Blocks

The objectives of this type of experiment are almost the same as in the previous Paragraph. But in this case, as the loading is applied laterally sidewise, the behavior of pins is different from the case of compression loading. Also the transfer mechanism of the shearing stress through the key must be somewhat different. So, this experiment is particularly aimed at determining such differences. The actual dimensions of the test specimens are exactly the same as in the case of the compression test of the 3-layer 3-row shielding block specimens. The dimensions of the graphite shielding blocks are as given in Fig. III-I-VI.

3. 2 Vibration Test Model

The test model employed for this experiments is a 1/2 scale model of the actual size graphite shielding block assembly supported by pins and keys, and also the test model has similarty of the structural elements such as the opening and penetration for the primary coolant piping.

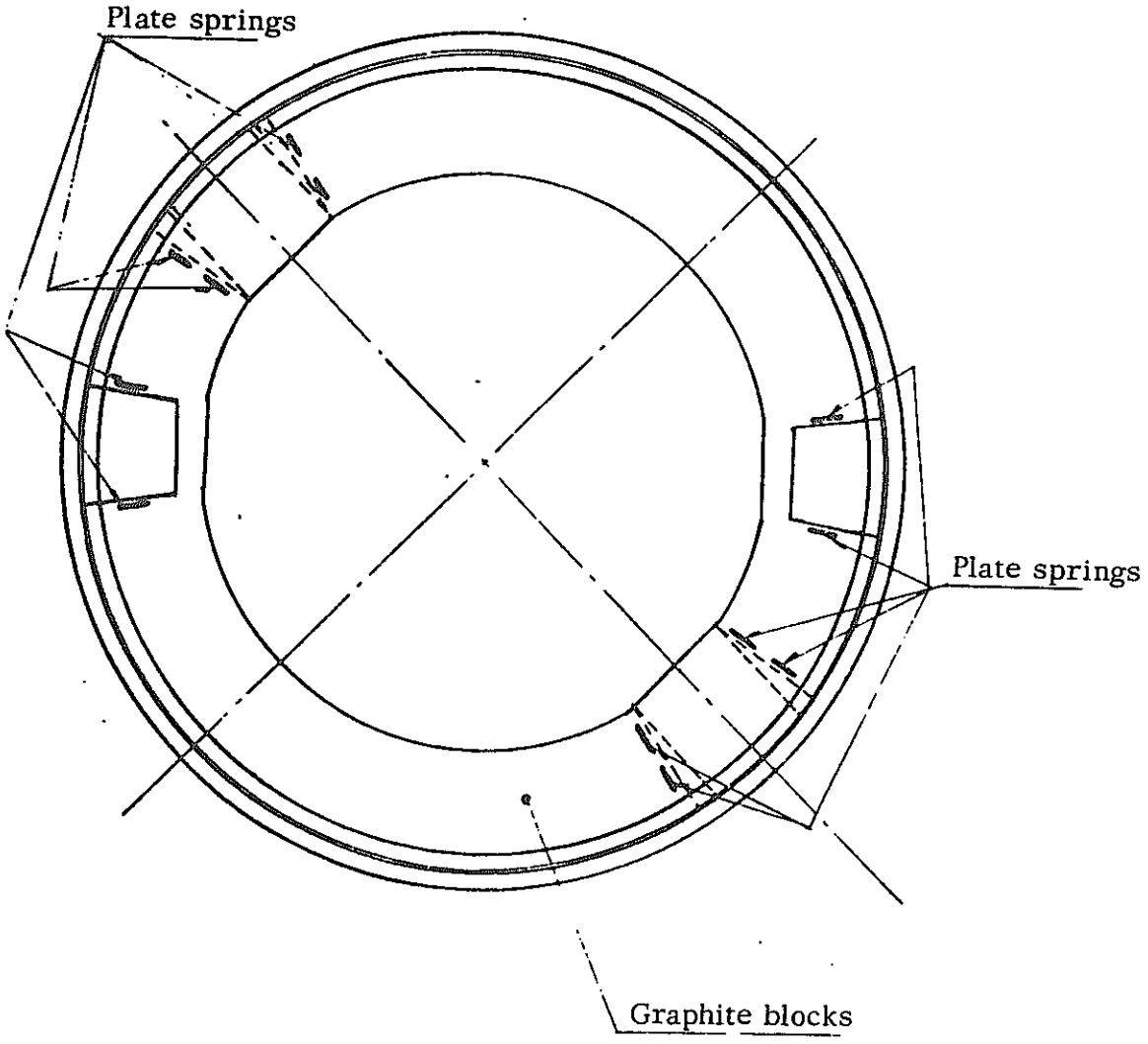

Fig. III-I-I_1 Location of Plate Springs

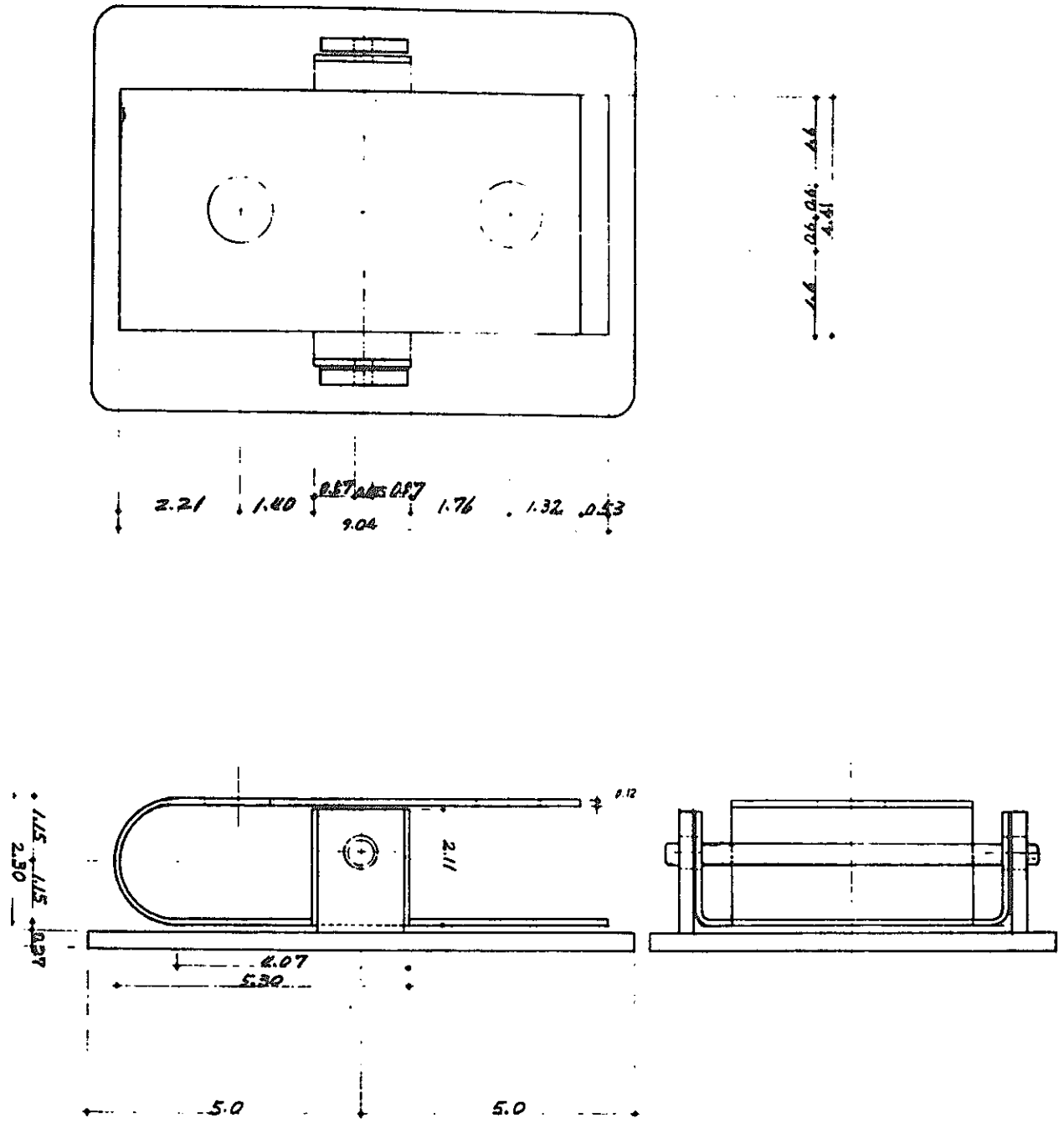

Fig. III-I-I_2 Dimensions of Specimens Used for Rigidity Test of Plate Spring (S: 1/1)

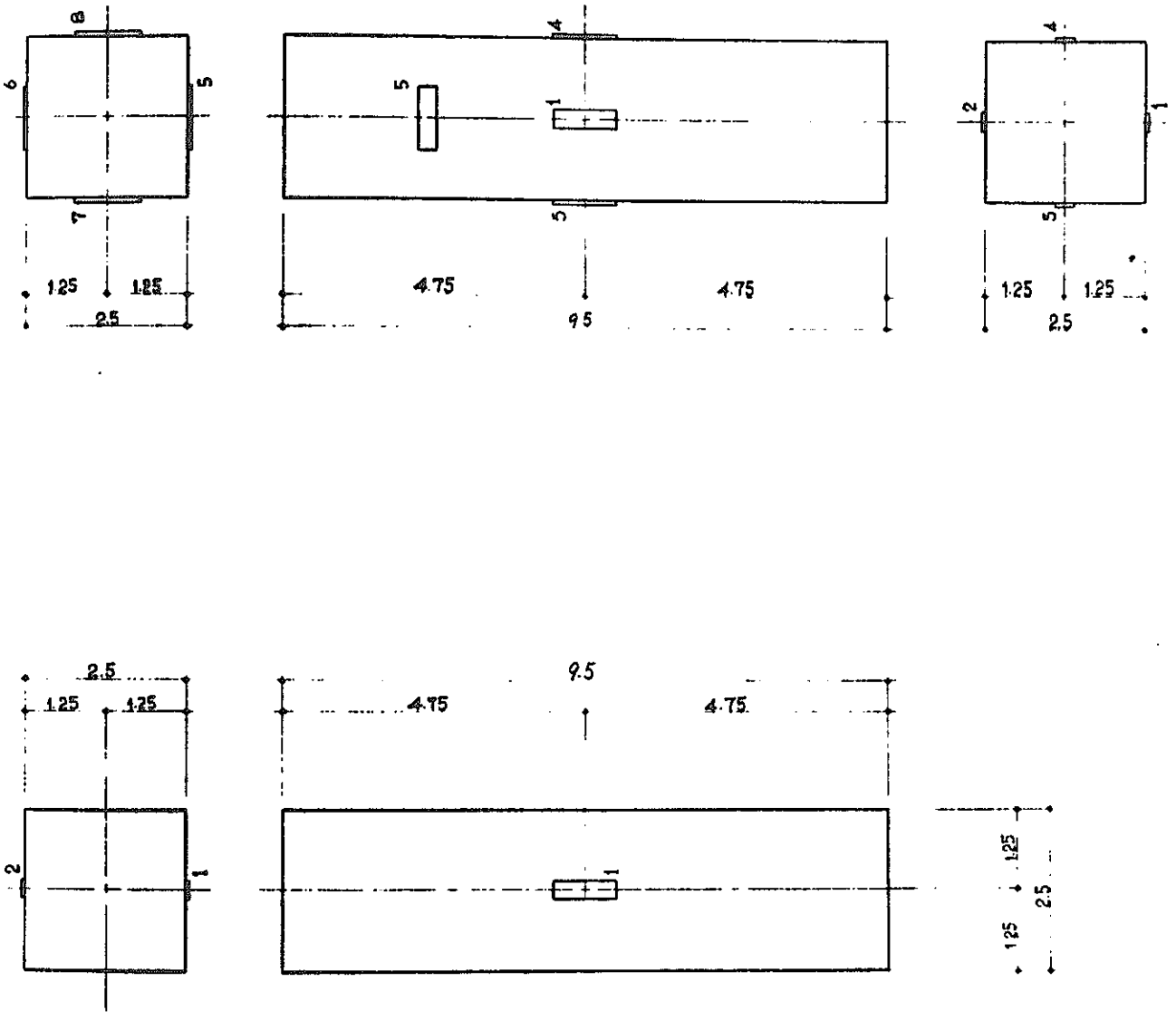

Fig. III-I-II Dimensions of Specimen Used for Key Compressive Test

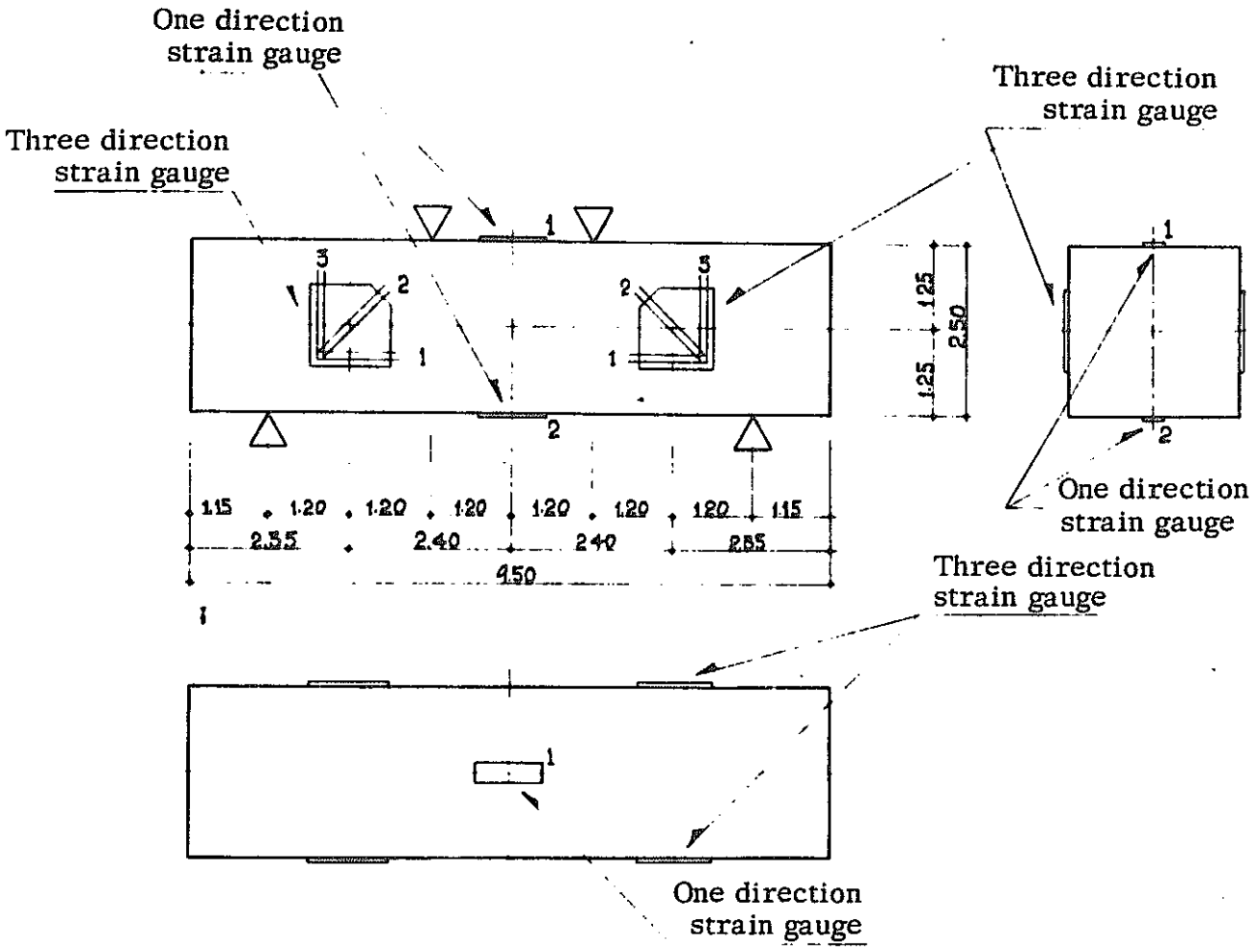

Fig. III-I-III Specimens Used for Bending and Shearing Test of Graphite Keys

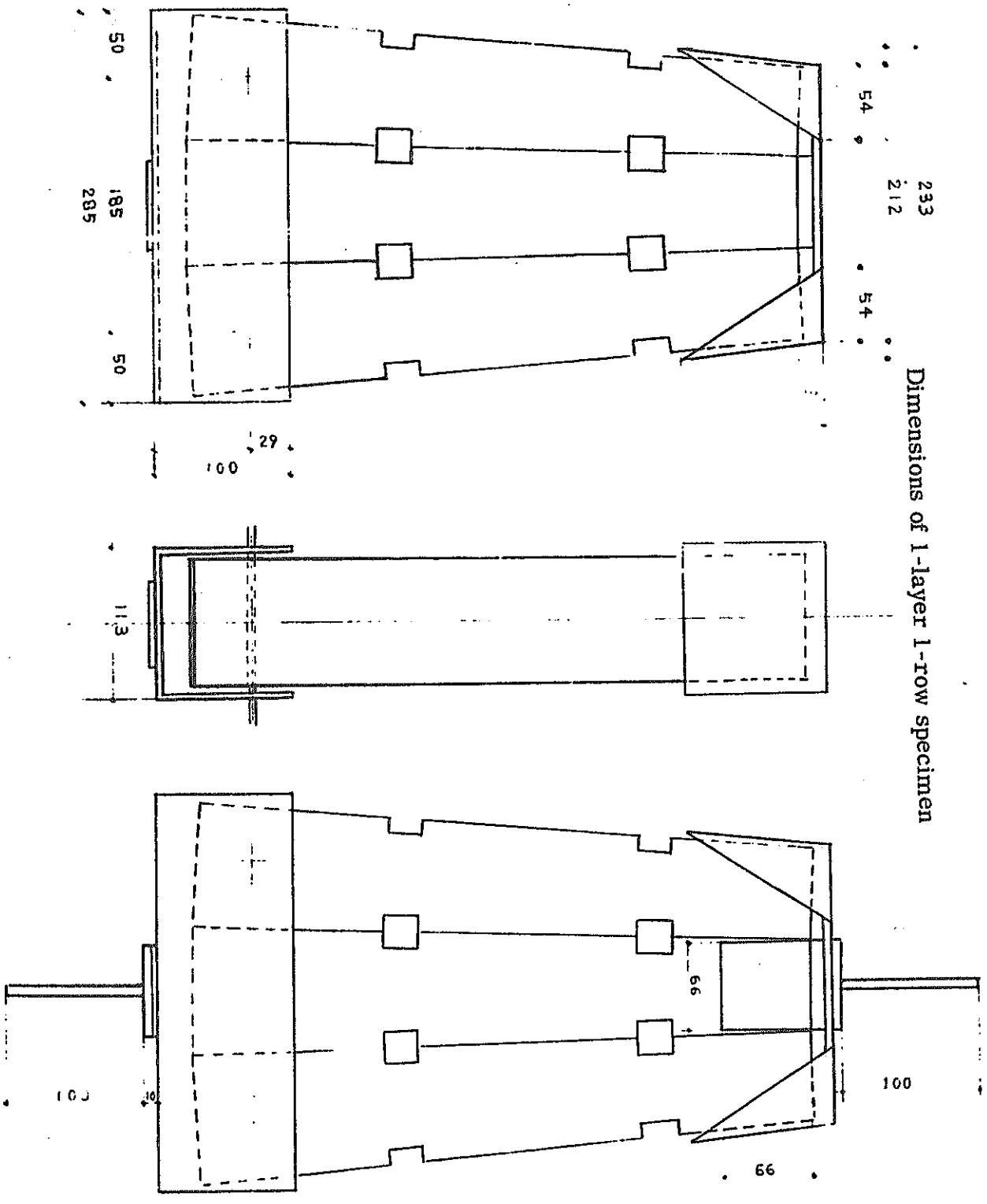

Dimensions of 1-layer 1-row specimen

Fig. III-I-IV Dimensions of 1-Layer 3-Row Shielding Blocks

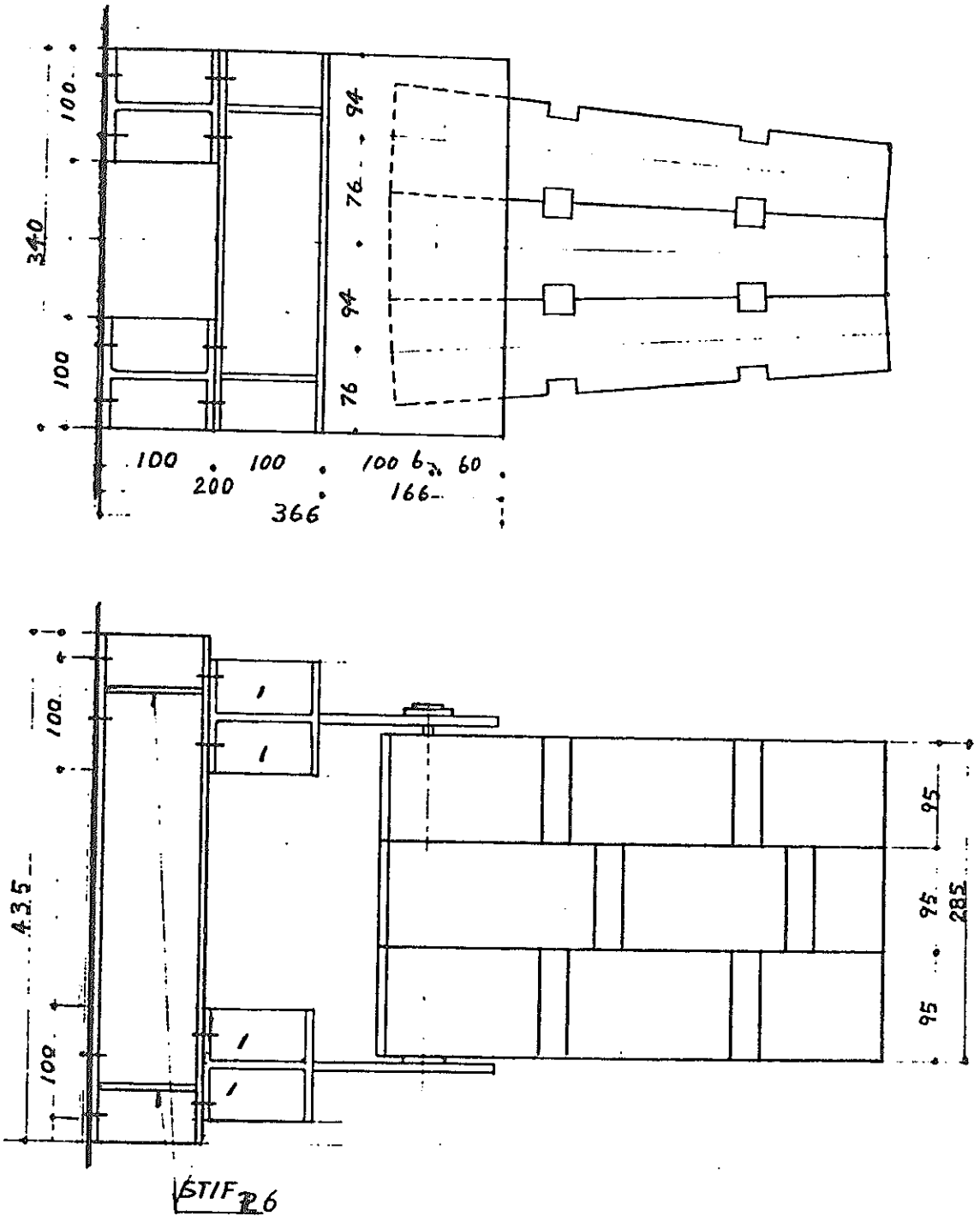

Dimensions of Specimens for Compression and Bending Tests (S: 1/5)

Fig. III-I-V

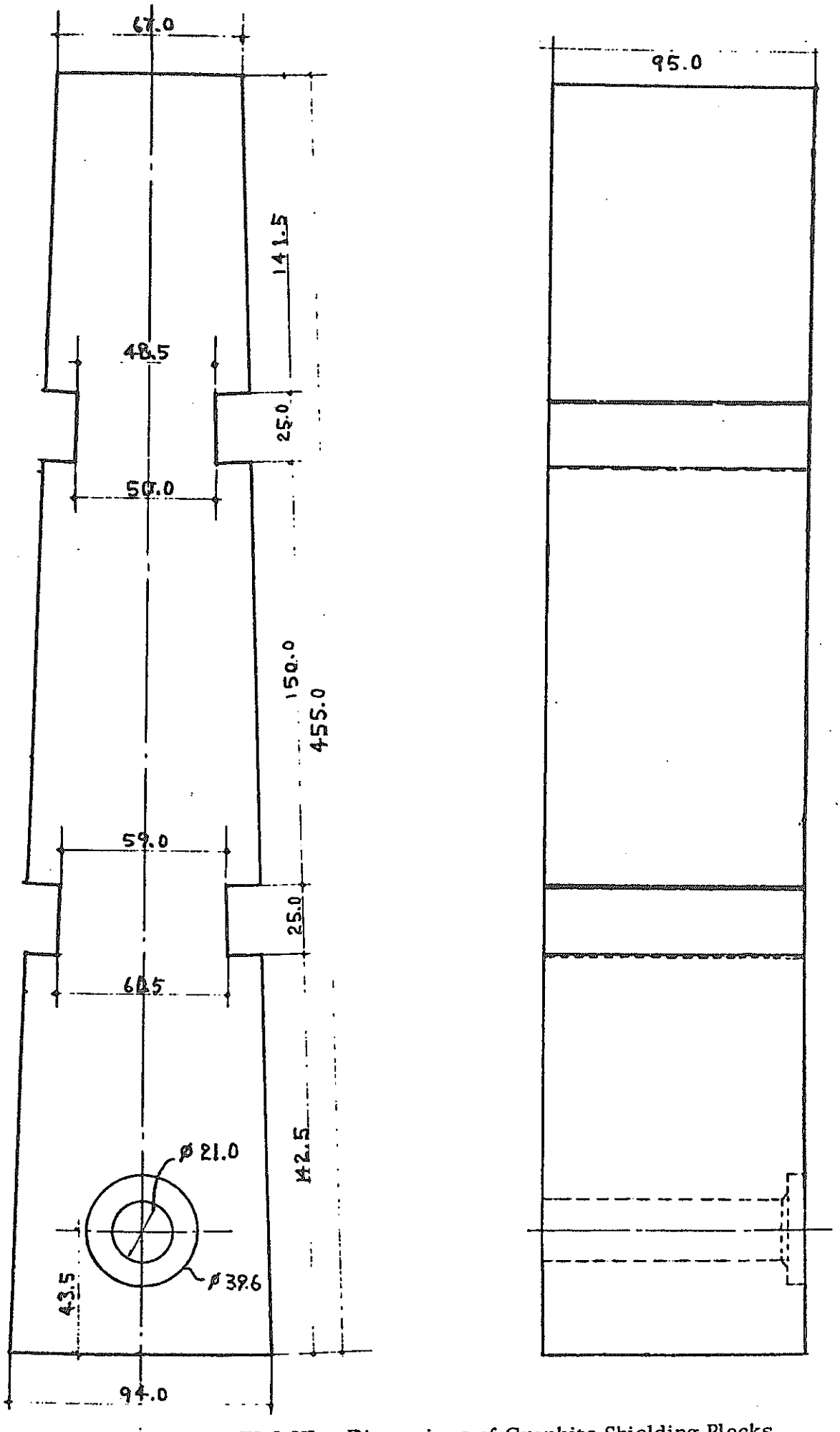

Fig. III-I-VI Dimensions of Graphite Shielding Blocks

Chapter 4 Static Loading Test

4. 1 Test Method and Results

A static loading test is performed for the same purpose as mentioned in the preceding Chapter. The test method adopted in each case of the tests is given as follows:

4. 1. 1 Compressive Loading Test of Plate Springs:

Measuring Method and Measuring Points

The locations of strain gauges and dial-gauges, and the applied points of load are as shown in Fig. IV-I-I. A vertical type Amsler compression testing machine of 1,000 Kg is used. For the measuring instruments, SM-60AT; Strain Meter, Switching & Balancing Box SS-24 R are employed. The load test by a pilot test is performed applying load on the plate spring with step by step of 2 Kg each until the upper face of the plate spring contacts the shaft. 20-steps of pressure application are as given below:

Load by step (Unit: Kg):

0, 2, 4, 6, 8, 10, ... 44, 46, 48, 50, 52 .....

No repeated load test measuring is conducted since it is within the range of its elasticity, until the upper face of the plate spring contacts the shaft.

Experiment Results:

The calculation formula to obtain the relation between the deformation volume and the force is introduced from the virtual work method and is computed by use of the following formulation.

$$\delta = \int \frac{M\bar{M}}{E\,I}\,dx \qquad \text{..... (4-1)}$$

M-Diagram

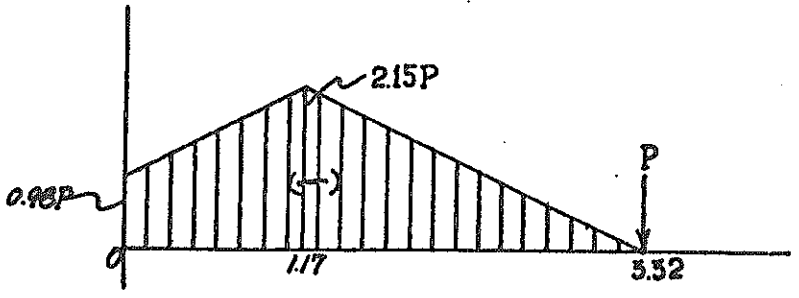

$\bar{M}$-Diagram

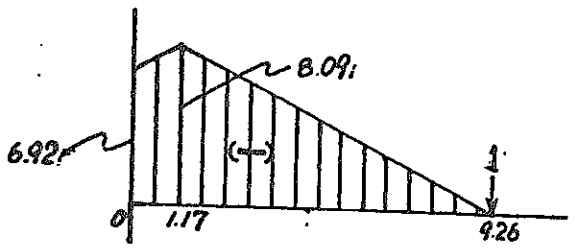

M-Diagram

$0.98P + Px$ $(0 \leqq x \leqq 1.17)$

$3.32P - Px$ $(1.17 \leqq x \leqq 3.32)$ (4.2)

0 $(3.32 \leqq x \leqq 9.26)$

$\bar{M}$-Diagram

$6.92 + x$ $(0 \leqq x \leqq 1.17)$

$9.26 - x$ $(1.17 \leqq x \leqq 9.26)$ (4.3)

$$E = 2.1 \times 10^6 \text{ kg/cm}^2 \quad (4.4)$$

$$I = \frac{b D^3}{12} = \frac{4.41 \times 0.12^3}{12} = 635.04 \times 10^{-6} \text{ (cm}^4\text{)} \quad (4.5)$$

Eq. (4-1) is substituted by Eqs. (4.2), (4.3), (4.4), and (4.5).

$$\delta = \int_0^{1.17} \frac{P(0.98 + x)(6.92 + x)}{2.1 \times 10^6 \times 635.04 \times 10^{-6}} dx + \int_{1.17}^{3.32} \frac{P(3.32 - x)(9.26 - x)}{2.1 \times 10^6 \times 635.04 \times 10^{-6}} dx$$

$$+ \int_{3.32}^{9.26} 0. \, dx = 23.18347P \times 10^{-2}$$

Consequently, the deformation volume is: $\delta = 23.18P \times 10^{-2}$ (4.6)

Where, as seen from the Graph IV-a, as the experimental values can be predicted by the calculation formula (4-1), it is assumed that the rigidity of the plate spring of the actual spring may be calculated by the formula of (4-1).

M-Diagram

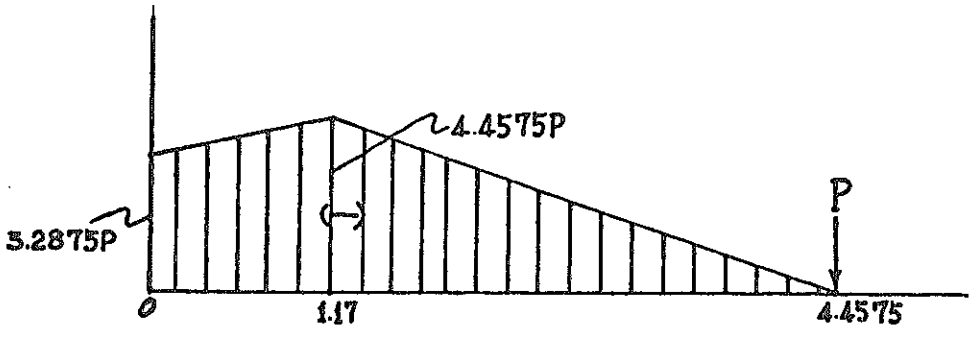

$\bar{M}$-Diagram

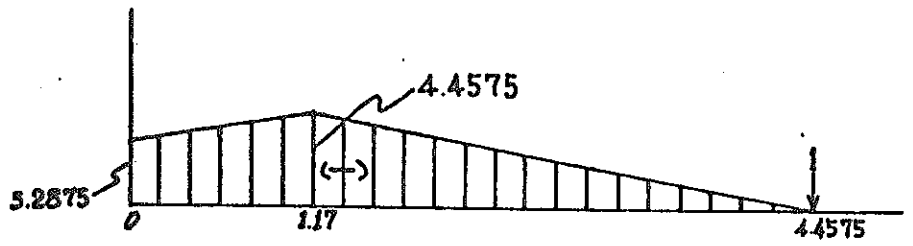

M-Diagram	$3.2875P + Px$	$(\ 0 \leqq x \leqq 1.17)$
	$4.4575P - Px$	$(1.17 \leqq x \leqq 4.4575)$
$\bar{M}$-Diagram	$3.2875 + x$	$(\ 0 \leqq x \leqq 1.17)$
	$4.4575 - x$	$(1.17 \leqq x \leqq 4.4675)$

$$\delta = \int_0^{1.17} \frac{P(3.2875 + x)^2}{2.1 \times 10^6 \times 635.04 \times 10^{-6}}\, dx + \int_{1.17}^{4.4575} \frac{P(4.4757 - x)^2}{2.1 \times 10^6 \times 635.04 \times 10^{-6}}\, dx$$

$$= 22.14116P \times 10^{-2} \text{ mm}$$

Consequently, the deformation volume is: $\delta = 22.14P \times 10^{-2}$ mm (4.7)

Where, Eq. (4.6) and (4.7) are expressed in Graph IV-I-1.

4.1.2 Compressive Loading Test of Keys

Measuring Method and Measuring Points:

The locations of strain gauges and the points of load are shown in Fig. IV-I-II. A 20-ton Amsler compression testing machine is used. The load test by steps is performed applying load by 100 kg each after confirmed by the pilot test. In this test the gauges are adhered on the surface of the specimens, and the load is applied evenly on the entire keys.

Experiment Results:

The maximum compression stress "σc" (t/cm^2) is computed by following formula as collapse load "P"(t), and the cross section of keys "A" (cm^2):

$$\sigma c = \frac{P}{A} \text{ (t/cm}^2\text{)} \qquad (4.8)$$

Specimens	Collapse Load (kg)	Cross Section (cm^2)	
I	$P_1 = 2,770$	$A = 6.25$	
II	$P_2 = 3,080$	$A = 6.25$	(4.9)
III	$P_3 = 3,290$	$A = 6.25$	

Substituting (4. 9) with (4. 8), the maximum compression stress of each specimen is sought as follows:

$$\sigma c_1 = \frac{2,770}{6.25} = 0.4432 \ (t/cm^2)$$

$$\sigma c_2 = \frac{3,080}{6.25} = 0.4928 \ (t/cm^2)$$

$$\sigma c_3 = \frac{3,290}{6.25} = 0.5264 \ (t/cm^2)$$

Obtaining the mean value of these σc_1, σc_2 and σc_3, and then make it the maximum compression stress "σc"

$$\bar{\sigma} c = \frac{1}{3} (\sigma c_1 + \sigma c_2 + \sigma c_3) = \frac{1}{3} (0.4432 + 0.4928 + 0.5264) = 0.4875 \ (t/cm^2)$$

The equation to obtain the standard deviation is:

$$S^2 = \frac{1}{N} (\Sigma \sigma c_1 \sim N^2) - (\bar{\sigma} c^2) \qquad (4.10)$$

$$N = 3$$

$$\Sigma \sigma c^2_{1\sim3} = \sigma^2 c_1 + \sigma^2 c_2 + \sigma^2 c_3 = 0.7164 \qquad (4.11)$$

$$\bar{\sigma} c^2 = 0.2377$$

When the standard deviation is sought by substituting (4. 10) with (4. 11), it is as follows:

$$S = \sqrt{\frac{1}{3} (0.7164) - 0.2377}$$

$$= 0.0332$$

Consequently, the maximum compression stress " c" of the graphite is:

$$\sigma c \geqq \bar{\sigma} c - 3S = 0.3879 \ (t/cm^2)$$

Relating to Poisson's Ratio:

The equation for Poisson's Ratio "ν ", as the strain in the stress direction as V, and the strain in the parpendicular direction to the stress as H, may be:

$$\nu = \frac{(-)H}{V} \qquad (4.12)$$

When Poisson's ratio is sought by computing the experiment results using Eq. (4. 12), it is:

$$\nu = 0.1468$$

Whereby, the graphite Poisson ratio is set at 0. 1468.

The above is represented in Graph IV-I-2 taking ν for longitudinal axis and σ

for the abscissa axis.

Young Modulus under Compression:

The equation for computation of Young modulus E(t/cm^2) under compression, as the longitudinal strain defined ϵ , and the stress defined σ (t/cm^2), may be:

$$E = \frac{\sigma}{\epsilon} \quad (t/cm^2) \qquad (4.14)$$

The experiment results are computed by Eq. (4. 14) and is expressed in Graph IV-I-3. As seen from the Graph, the Young modulus under compression is classified into three steps, and Young modulus at each step is obtained as follows:

Range of Strain	Young odulus under Compression
$0 \times 10^{-6} \leq \epsilon \leq 2220 \times 10^{-6}$	55. 470 (t/cm^2)
$2220 \times 10^{-6} \leq \epsilon \leq 5894 \times 10^{-6}$	40. 526 (t/cm^2)
$5894 \times 10^{-6} \leq \epsilon$	32. 694 (t/cm^2)

4. 1. 3 Bending Loading Test of Keys

Measuring Method and Measuring Points:

Fig. IV-I-III shows the locations of strain gauges pasted and the points of load. A 1, 000 kg vertical type compression testing equipment is used. The load test in steps is performed by applying 20kg load at each step in more than 10-steps minimum, after confirmed by the pilot test.

Experiment Results:

As for the maximum tensile stress, the equation to compute the maximum tensile stress σt (t/cm^2), as the bending momentum defined M (t. cm) and the cross section modulus as Z (cm^3), is as follows:

$$\sigma t = \frac{M}{Z} \quad (t/cm^2) \qquad (4.15)$$

M-Diagram

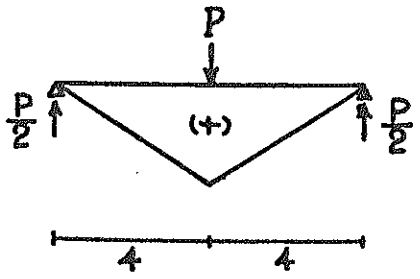

$$M = \frac{P}{2} \times 4 = 2P \ (t \cdot cm)$$

$$Z = \frac{b\,D^2}{6} = \frac{2.5^3}{6} = 2.604\ cm^3$$

Specimen	Breakdown Load
I	$P_1 = 0.23$
II	$P_2 = 0.24$
III	$P_3 = 0.251$
IV	$P_4 = 0.224$

(4. 16)

The values of above M and Z (4. 16) are substituted by (4. 15) and the maximum tensile stress σt of each specimen is sought as follows:

$$\sigma t_1 = \frac{2 \times 0.23}{2.604} = 0.17665\ (t/cm^2)$$

$$\sigma t_2 = \frac{2 \times 0.24}{2.604} = 0.18433\ (t/cm^2)$$

$$\sigma t_3 = \frac{2 \times 0.251}{2.604} = 0.19278\ (t/cm^2)$$

$$\sigma t_4 = \frac{2 \times 0.244}{2.604} = 0.17204\ (t/cm^2)$$

Where the obtained mean values of these σt_1, σt_2, σt_3, and σt_4 shall be the maximum tensile stress.

$$\bar{\sigma} t = \frac{1}{4}(\sigma t_1 + \sigma t_2 + \sigma t_3 + \sigma t_4)$$

$$= \frac{1}{4}(0.17665 + 0.18433 + 0.19278 + 0.17204)$$

$$= 0.18145$$

Where, the standard deviation is sought:

N = 4

$$\Sigma\, \sigma t_{1 \sim 4} = 0.13194 \qquad (4.17)$$

$$\bar{\sigma} t^2 = 0.03294$$

The standard deviation S is obtained by substituting (4. 17) by (4. 10) as per the following expression:

$$S = \sqrt{\frac{1}{4} \times 0.13194 - 0.03294}$$

$$= 0.0067$$

Consequently, the maximum tensile stress σt of the graphite is:

$$\sigma t \geq \bar{\sigma} t - 3S = 0.161\ (t/cm^2)$$

Relation between Shear Stress and Shear Deformation:

M-Diagram

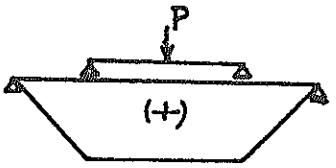

Q-Diagram

The above is shown in Graph IV-I-4 and IV-I-5 indicating the shear stress ($P/2A$ t/cm^2) in a longitudinal axis and the shear deformation in a traverse axis.

4. 1. 4 Compressive and Tensile Loading Tests of 1-Layer 3-Row Blocks

Measurement Method:

The location of strain gauges pasted and the points of load are indicated in Fig. IV-I-IV and 100-ton hydraulic pressure type compression testing equipment is used. The compression test is performed in more than 10-step load applying method with 500 kg load each on the basis of pre-calculation. For the tensile test, the measurement is conducted similarly in more than 10-step load application at 300 kg each step.

Test Results

For the computation of the principal plane, the principal stress and the shearing deformation of the graphite specimens at location where gauges are adhered, the measured values (strain) of the test are used. The 3-direction strain values indicated on the gauges are shown as follows:

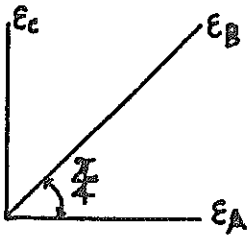

Strain Values on 3-Direction Gauges

Fig. IV-I-1

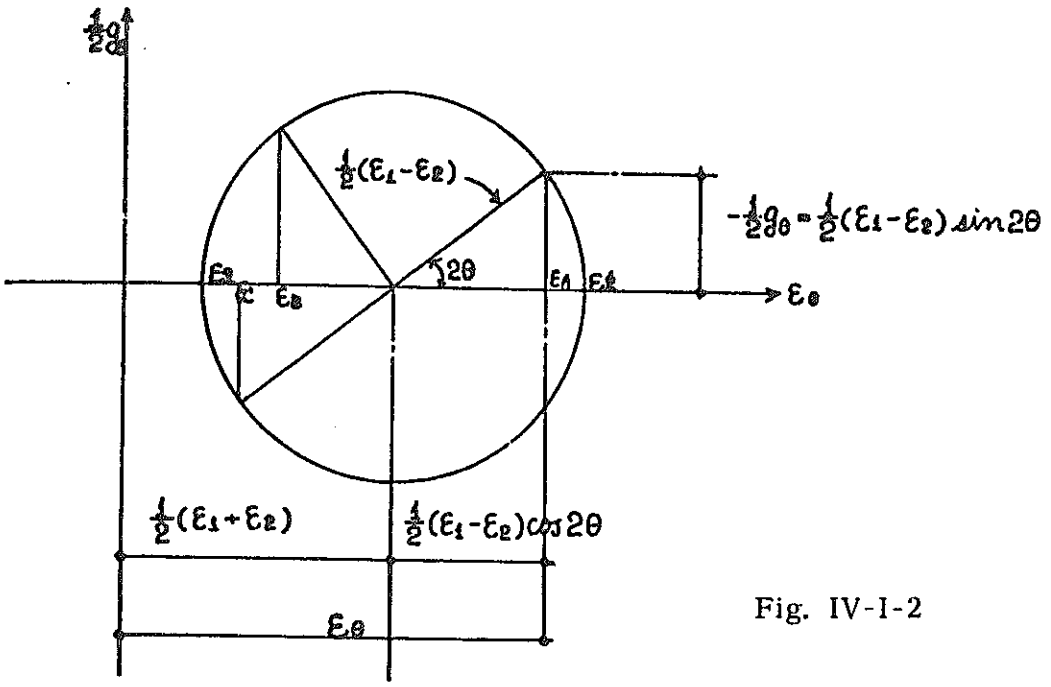

Fig. IV-I-2

The equations to compute the principal strain are given as follows:

$$\gamma^2 = \left(\frac{\epsilon_A - \epsilon_C}{2}\right)^2 + \left(\frac{\epsilon_A + \epsilon_C - 2\epsilon_B}{2}\right)^2 \tag{4.18}$$

$$\frac{1}{2}g = -\frac{1}{2}\left(\epsilon_A + \epsilon_C - 2\epsilon_B\right) \tag{4.19}$$

$$\epsilon_1 = \frac{1}{2}\cdot\left(\epsilon_A + \epsilon_C\right) + |\gamma| \tag{4.20}$$

$$\epsilon_2 = \frac{1}{2}\cdot\left(\epsilon_A + \epsilon_C\right) - |\gamma| \tag{4.21}$$

$$\tan 2\theta = \frac{\epsilon_A + \epsilon_C - 2\epsilon_B}{\epsilon_A - \epsilon_C} \tag{4.22}$$

From Eqs. (4.18), (4.19), (4.20), (4.21) and (4.22) ϵ_1 and ϵ_2 are obtained. When the principal stress σ_1 and σ_2 are sought, they are as follows:

$$\epsilon_1 = \frac{1}{E}\cdot\left(\sigma_1 - \nu\sigma_2\right) \tag{4.23}$$

$$\epsilon_2 = \frac{1}{E}\cdot\left(-\nu\sigma + \sigma_2\right) \tag{4.24}$$

The solution of the simultaneous equations of (4.23) and (4.24) is:

$$\sigma_1 = \frac{E(\epsilon_1 + \nu\epsilon_2)}{1 - \nu^2}\left(t/cm^2\right) \tag{4.25}$$

$$\sigma_2 = \frac{E(\nu\epsilon_1 + \epsilon_2)}{1 - \nu^2}\left(t/cm^2\right) \tag{4.26}$$

Then, the direction of the principal plane of stress is sought:

The direction of the principal plane of stress expressed from the Eq. (4. 22) is as follows:

$$\theta' = \tan^{-1}\left(\frac{\epsilon_A + \epsilon_C - 2\epsilon_B}{\epsilon_A - \epsilon_C}\right) \cdot \frac{180^O}{\pi} \cdot \frac{1}{2} \qquad (4.27)$$

Then, the shear-rigidity coefficient G is obtained by the following equation:

$$G = \frac{E}{2(1+\nu)} \qquad (4.28)$$

4. 1. 5 Compression Loading Test of 3-Layer 3-Row Blocks

Measuring Method and Measuring Points:

The locations of strain gauges adhered and the positions of load are as shown in Fig. IV-I-V. A 20-ton hydraulic long-column type compression testing equipment is used for the test. On the basis of pre-calculated results, it is programmed to apply a load of 300 kg for each step until it adds up to more than 10 steps. In this case of test, the load position is changed with repetition of test. For preparation of this 3-layer 3-row test specimen blocks, a jig has been especially made and provided as shown by Fig. IV-I-V_2.

Experiment Results:

The calculation of each block's shearing force is made by the following method:

As shown by the following diagram, each block is coded by Y_1 and Y_3:

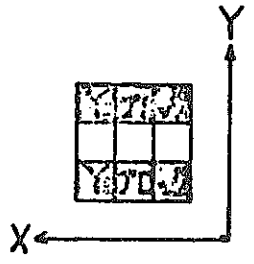

When the shearing stress of each key of No. 10, No. 11, No. 12, No. 13, No. 30, No. 31, No. 32, and No. 33 is expressed by $\tau 10$, $\tau 11$, $\tau 12$, $\tau 13$, $\tau 30$, $\tau 31$, $\tau 32$, and $\tau 33$, as there are only four keys which have the gauges adhered, such as Key No. 10, No. 11, No. 30 and No. 31, the load points of 1, 2, 3, 4, 5, 6 and 9 are represented as $\tau 12 = \tau 10$, $\tau 13 = \tau 11$, $\tau 32 = \tau 30$, and $\tau 33 = \tau 31$, and for the load points of 7 and 8, $\tau 12 = \tau 11$, $\tau 12 = \tau 11$, $\tau 13 = \tau 10$,

$\tau 33 = \tau 31$, and $\tau 33 = \tau 30$.

The shearing force of Y_1 blocks is:

$$\frac{(\tau 10 + \tau 11 + \tau 12 + \tau 13) \cdot A}{P} \times 100 \ (\%) \qquad (4.37)$$

and the shearing force of Y_3 blocks:

$$\frac{(\tau 30 + \tau 31 + \tau 32 + \tau 33) \cdot A}{P} \times 100 \ (\%) \qquad (4.38)$$

The results are shown in Graph IV-I-10, IV-I-11, IV-I-12, IV-I-13, IV-I-14, IV-I-15, IV-I-16, IV-I-17, and IV-I-18.

The computation of the moment M for each pin where gauge adhered, as the cross section modulus of pin where gauge adhered defined Z and the elastic coefficient of steel defined E, and the strain at the point as ϵ it is:

$$M = Z \cdot E \cdot \epsilon \qquad (t \cdot cm) \qquad (4.39)$$

$$Z = \frac{\pi \cdot d^3}{32} = \frac{3.14 \cdot 1.2^3}{32} \ (cm^3) \qquad (4.40)$$

$$E = 2.1 \times 10^3 \ (t/cm^2)$$

Eq. (4.40) is introduced into Eq. (4.39) to obtain the moment. Provided, however, as the support condition of pin-1 is not exactly the same as in the case of other 2 pins, the support status of the other two pins is considered as merely of a simple beam, and modified values are sought as follows:

M-Diagram

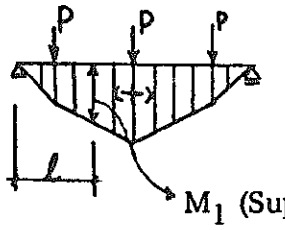

M_1 (Support condition of other two pins)

$$M_1 = \frac{3}{2} P\ell - P \cdot \frac{1}{2}\ell$$

$$= P \cdot \ell \ (t \cdot cm)$$

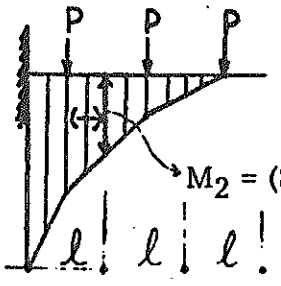

M_2 = (Support condition of P_1)

$$M_2 = P \cdot \frac{3}{2}\ell + P \cdot \frac{1}{2}\ell$$

$$= 2\,P\,\ell \quad (t \cdot cm)$$

There form, $M_1 = \frac{1}{2} \cdot M_2$

Consequently, the moment of P_1 is one half (1/2) of the experiment results as shown by Graph IV-I-19, IV-I-20, IV-I-21, IV-I-22 and IV-I-23.

4. 1. 6 Traverse Direction Compressive Loading Test of 3-Layer 3-Row Blocks

Measuring Method and Measuring Points:

The locations of the strain gauge adhesion and the load positions are as shown in Fig. IV-I-V_1 and IV-I-V_2. A jack is used as a device to apply force. The load weight is read by means of a load-cell. The load is applied step by step in more than 10 steps in accordance with the precalculated program. In this test, the load position is changed with repetition of test. For this test of 3-layer 3-row blocks, a specially designed jig as indicated by Fig. IV-I-V_2 is employed.

Experiment Results:

With respect to the compression between the experimental values of the shearing stress of keys and their theoretical ones, the computation is made by the following manner:

An equation is introduced to obtain the shearing stress of the keys by setting the shearing stress as τ, the statical moment of area as S, the geometrical moment of inertia as I, the shearing force as Q, the traverse thickness of the block as t, the length of the block as B, and the width of the key as K:

$$\tau = \frac{B}{2K} \cdot \frac{S \cdot Q}{I \cdot t} \quad (t/cm^2) \qquad (4.41)$$

From the dimensions of specimen as given in Fig. III-1-IV,

K = 2. 5 (cm)

B = 41. 15 (cm)

The shearing force Q is, Q = P (t).

In the case of the load position 1 (Refer to Fig. IV-I-V_2):

$$I_1 = \frac{28.5 \times 21.3^3}{12} = 22951.0428 \ (cm^4)$$

$$S_1 = 28.5\ (10.65 - 4)\ \frac{(10.65 - 4)}{2} + 4 \qquad (cm^3)$$

$$= 1388.2704 \ (cm^3)$$

Seeking the shearing stress by substituting them with Eq. (4.41), it is:

$$\tau_1 = \frac{41.15}{2 \times 2.5} \times \frac{1388.2704}{22951.0428 \times 28.5} \times P$$

$$= 0.017467P \ (t/cm^2)$$

This is shown in Graph IV-I-25.

4.2 Consideration on Static Loading Test

4.2.1 Mechanical Properties of Graphite Material under Room Temperature

From the results of the experiments and the reference to the results as reported by "Manufacturing Experiment of JEFR Shielding Graphite" (Showa Denko, Feb. 27, 1971), it is considered the contents in Table 4.2.1 suggests an overall situation. (Note: Refer to Table 18 and 19 "Immerged 8 Specimen" of the above mentioned report).

Table 4.2.1 Mechanical Properties of Graphite

	Elastic Modulus $\epsilon \leqq 100\mu$	$\epsilon \leqq 2200\mu$	Poisson's Ratio	Cmprs'n strength	Tnsl Strength	Bend strength	Shear Stregnth	Sharpi Imp-St
	t/cm^2 $\bar{X}, \sigma$	t/cm^2 $\bar{X}$	$\bar{X}$	kg/cm^2 $\bar{X}, \sigma$	kg/cm^2 $\bar{X}, \sigma$	kg/cm^2 $\bar{X}, \sigma$	kg/cm^2 $\bar{X}, \sigma$	$kg \cdot m$ $\bar{X}, \sigma$
⊥⊥ Direction	116.3, 5.4	55.5	0.1468	470, 28	148, 25	237, 48	186, 17	0.17, 0.03
+ Direction	75.8, 7.3			444, 40	110, 18	184, 43	169, 13	0.11, 0.03

Note: $\bar{X}$ represents the mean value.

σ is for standard deviation.

4. 2. 2 Properties and Characteristic of Spring

It has been ascertained that the relation between deformation and load, when calculated by a normal method, has hardly any appreciable difference from the values obtained by experiment (Refer to Graph VI-I-1). The relation between the strain and loading the spring's circular end section corresponds to the actual measured values when calculated with a modification of distance of point of force mechanism. For this reason, in the analysis of the dynamic force test, the modified values are employed.

4. 2. 3 Shearing Behavior of Keys under Static Loading

If the simple collapse load from the material test results is defined by P_{cr} and the collapse load from the actual experiment by Pb, it is:

$$\frac{Pb}{P_{cr}} = 0.524 \text{ (mean value)}$$

The cause is not due to the effect of imbalance of the shearing force distribution nor that the final collapse has occurred with the keys, but it is because of the following situation. Namely, with the increase of load, a partial collapse does take place on the corner points of the keys which causes wide openings between the blocks, while at the same time, the keys have sunk into the openings and act as wedges to apply an internal force in a parpendicular direction together with the load.

As this internal force will cause a bending stress to the blocks, the bending collapse of blocks determines the ultimate load. Since the above described phenomenon will inevitably occur in any blocks which are assembled in this type of form, for the virtual force of the key-blocks, it will be desirable to take the maximum shear-strength due to material test of $\frac{Pb}{Pcr}$ fold = 0. 5.

On the other hand, when the shearing force distribution upon the shear keys on both sides of four blocks is examined, the respective keys' share of force becomes even and uniform as the load weight increases as is considered from Fig. IV-I-6 ~ Fig. IV-I-8. The apportion rate of force is 100%/4 = 25% and the maximum concentration factor under load of 6 tons is (Fig. IV-I-8 Key No. 12 shows 38%) $\frac{38}{25}$ = 1. 52, and the mean value is $\frac{32}{25}$ = 1. 28, which may be considered as the stress concentration factor. The ratio between the maximum shearing stress within key's E max and the conventional mean shearing force τ mean as assumed from the experiment results is:

$$\frac{E \max}{\tau \text{ mean}} = \frac{0.074 \text{ t/cm}^2 \times 1.11}{0.063 \text{ t/cm}^2} = 1.298$$

This value is, so to speak, the stress concentration factor, and also that is supported from the analytical results using the finite element method analysis. The ratio between the maximum shearing force of the keys τ F max and τ mean is not so large ratio as seen from the following expression:

$$\frac{\tau \text{ F max}}{\tau \text{ mean}} = \frac{0.0453 \text{ t/cm}^2}{0.0378 \text{ t/cm}^2} = 1.2 \quad \text{(900 kg shearing stress per key)}$$

When this ratio is compared with the value obtained from the previously calculated shearing force of keys, the value indicates an approximate concordance rate of keys (1.28 : 1.33).

4.2.4 Stress Distribution of Graphite Blocks in the Vicinity of Keys

Viewing the principal stress at the indent-corner as represented in Fig. IV-I-6, the maximum compression force is 0.164 t/cm^2, of which ration to the expected mean compression stress of $\frac{1.5 \text{ t}}{1.25 \times 9.5} = 0.126 \text{ t/cm}^2$ is 1.3, and the stress concentration at this section is considered 1.3. Also this value corresponds with the stress concentration of keys described in Section 4.2.3.

4.2.5 Bending Strength of Pins

The maximum ultimate strength of blocks against the radial direction assumed from the 3-layer 3-row experiment results is 4.65 ton/2 = 2.32 ton. When the yielding stress of pins is assumed to be 2.4 ton/cm^2, the maximum ultimate strength calculated under the same condition is 11.4 kg. Namely, it has the final safety factor of $\frac{46.50}{11.4} = 203.5$. As the calculated values of 3 blocks as one unit is 7.6 kg, when a load of 7.06 x 203.5 = 1436 kg is applied on a single block in the radial direction, the block-unit will collapse. Since the weight of one single block is 6.5 kg, it is $\frac{1435}{6.5} = 221$, and it is assumed it can withstand an acceleration force of 211 g.

Meanwhile, the maximum ultinate strength of pins when a load is applied in a tangential direction is substantially low quite unlike in the radial direction. Considering three blocks as one unit (horizontal direction), the maximum resisting strength is 450 kg which is 150 kg per each single block. As their load is applied sidewise from the top, if this load is substituted by the center gravity force, it will be 340.7 kg. The gravity acceleration factor on the center-gravity is $\frac{189.3 \text{ kg}}{6.5 \text{ kg}} = 52.4$ g. That is, it is assumable that when the gravitational acceleration of 52.4 g is spplied in the

tangential direction, the great deformation of pins will occur and will cause a collapse of the blocks.

4. 2. 6 Allowable Acceleration Values (β) Assumed from Static Loading Tests.

$$\beta = \frac{\text{shearing cross section of keys} \cdot \text{shearing strength}}{\text{Stress concentration}} \cdot \frac{B}{\ell} \cdot \frac{1}{W} \times \rho$$

Where B is the block's width (4. 3 cm), ℓ is the distance from pin to the center gravity (17. 8 cm), and ρ is the load reduction rate by key's wedge action (0. 5).

With regard to pins, as previously produced, β = 52. 4.

The yielding load and the maximum load in the static loading test other than the material test are as shown in Table 4. 2. 2.

Table 4. 2. 2 Maximum Load and Yielding Load

Specimens	Max Load (kg)	Yield Load (kg)	Max/Yield
1. 1-Layer 3-Row Compression Test			
No. 1	8350 kg	5000 kg	1. 67
No. 2	7800 kg	5000 kg	1. 56
No. 3	8200 kg	5500 kg	1. 49
2. 1-Layer 3-Row Tensile Test	1800 kg (Bending)	Unknown (1500 kg)	1. 2
3. 3-Layer 3-Row Compression Test	4650 kg	3000 kg	1. 55
4. 3-Layer 3-Row Traverse Direction Force Test			
No. 1	671. 1 kg	500 kg	1. 34*
No. 2	691. 67 kg	450 kg	1. 53

* This value is used in 5-3 Tilt Test.

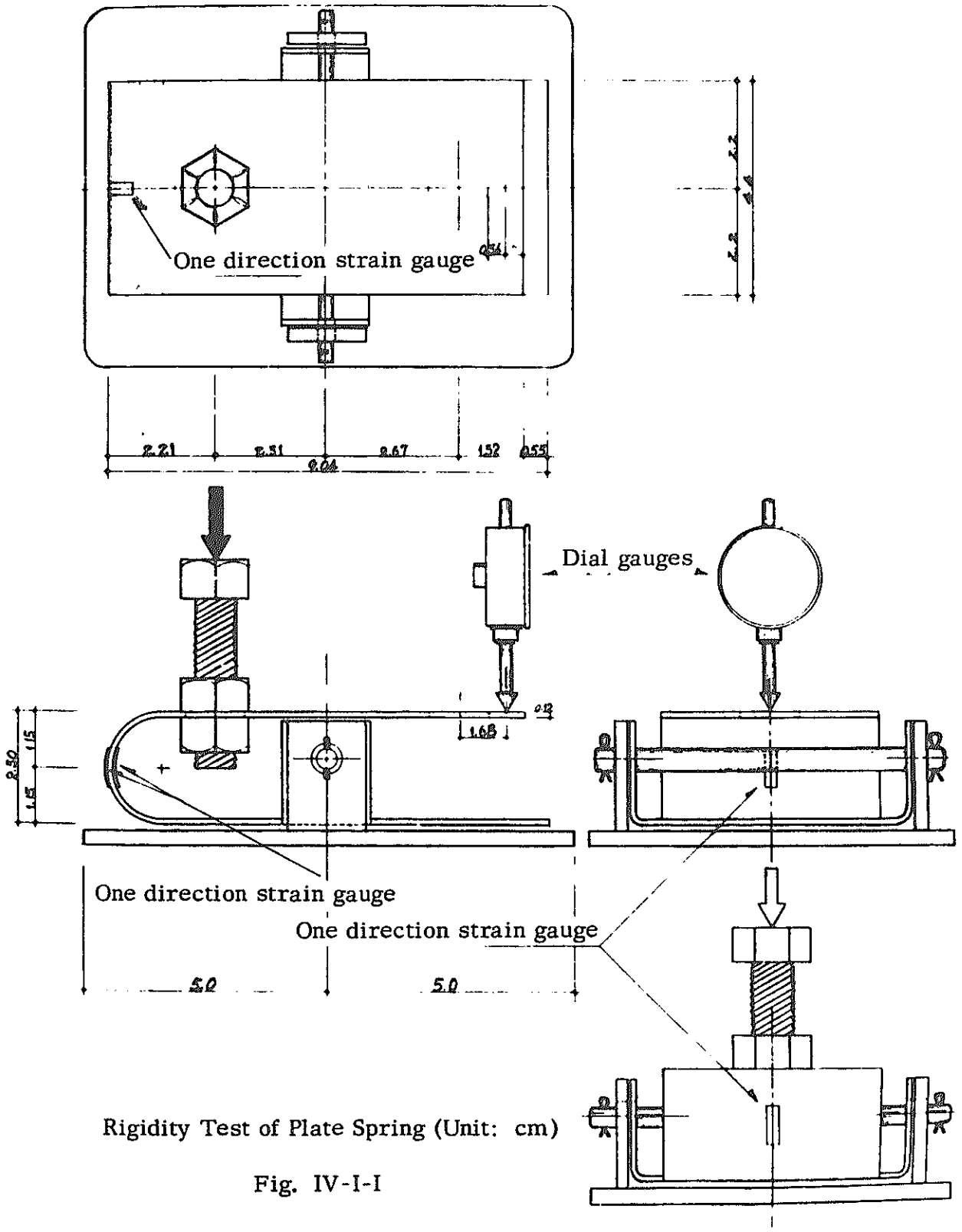

Rigidity Test of Plate Spring (Unit: cm)

Fig. IV-1-1

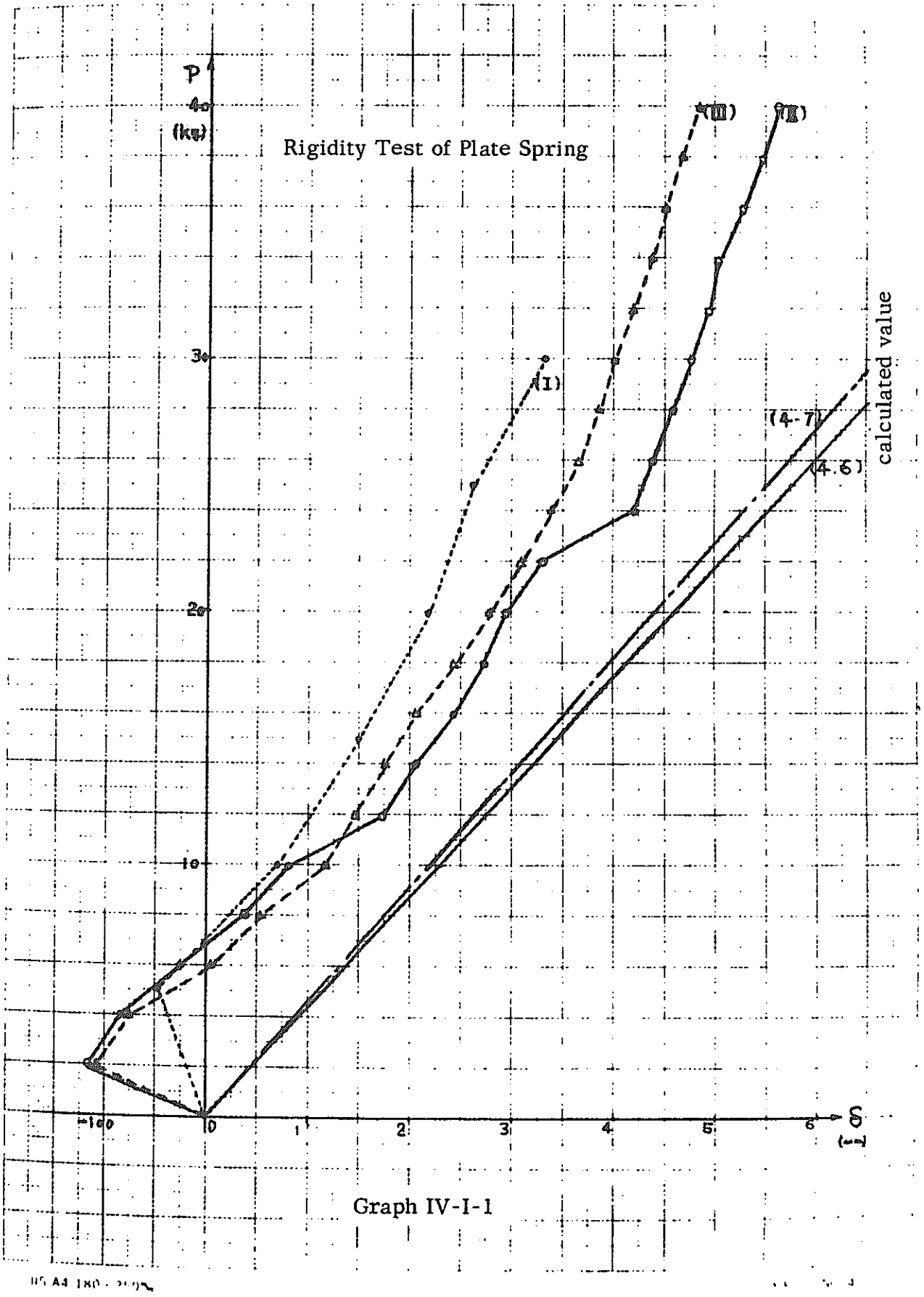
Rigidity Test of Plate Spring
P
(kg)
4
3
2
1
0
-100
1
2
3
4
5
6
δ
(mm)
(I)
(II)
(III)
(4-7)
(4-6)
calculated value

Graph IV-I-1

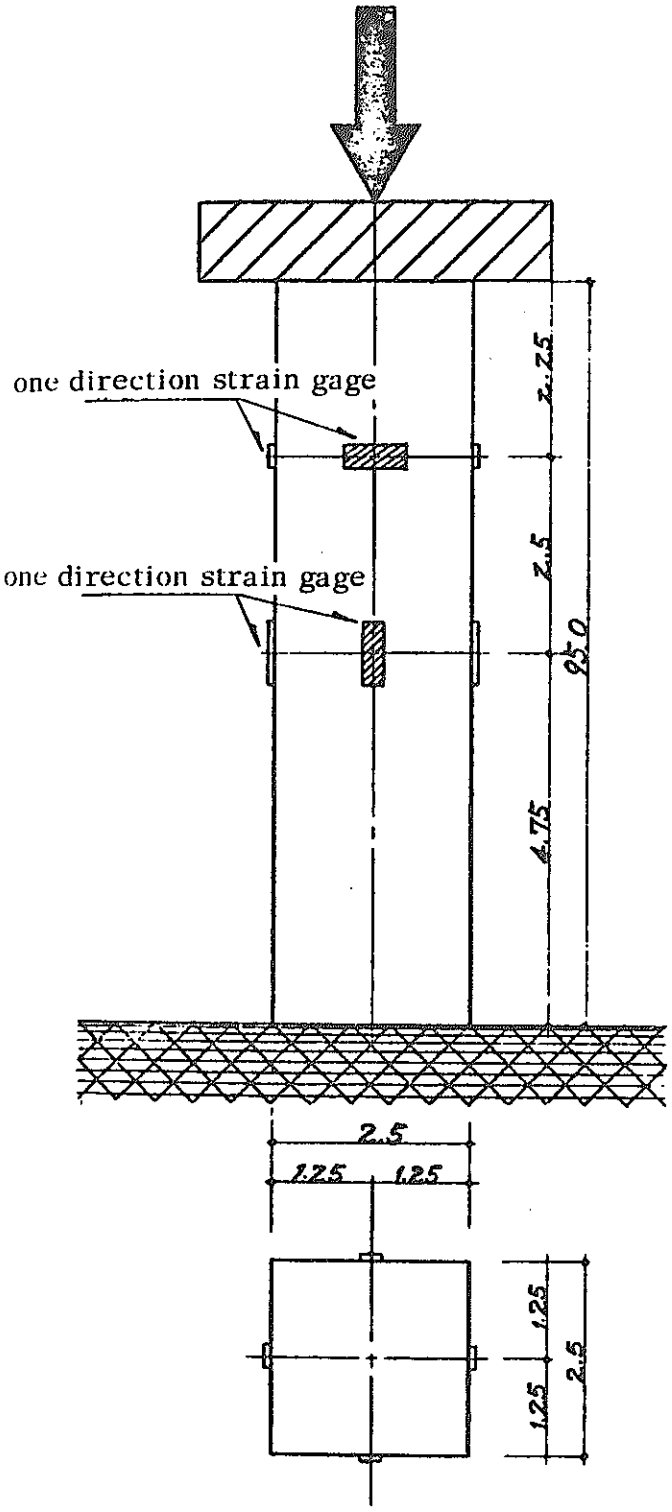

Fig. IV-I-II Dimensions of Specimen of Keys and Adhesion Location of Gauges (S: 1/1)

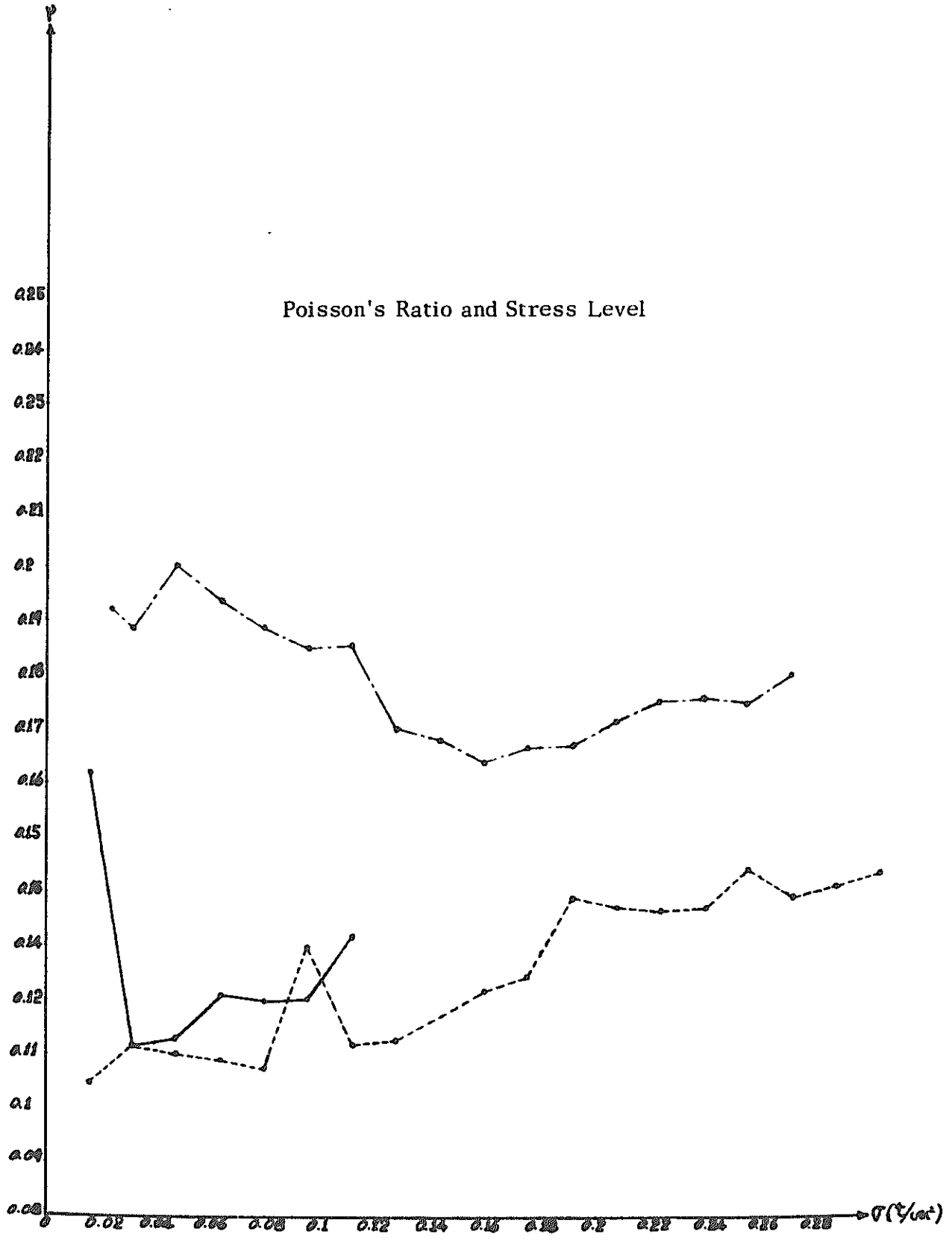
Poisson's Ratio and Stress Level
ν
0.25
0.24
0.23
0.22
0.21
0.2
0.19
0.18
0.17
0.16
0.15
0.13
0.14
0.12
0.11
0.1
0.09
0.08
0
0.02
0.04
0.06
0.08
0.1
0.12
0.14
0.16
0.18
0.2
0.22
0.24
0.26
0.28
σ(t/cm²)

Graph IV-I-2

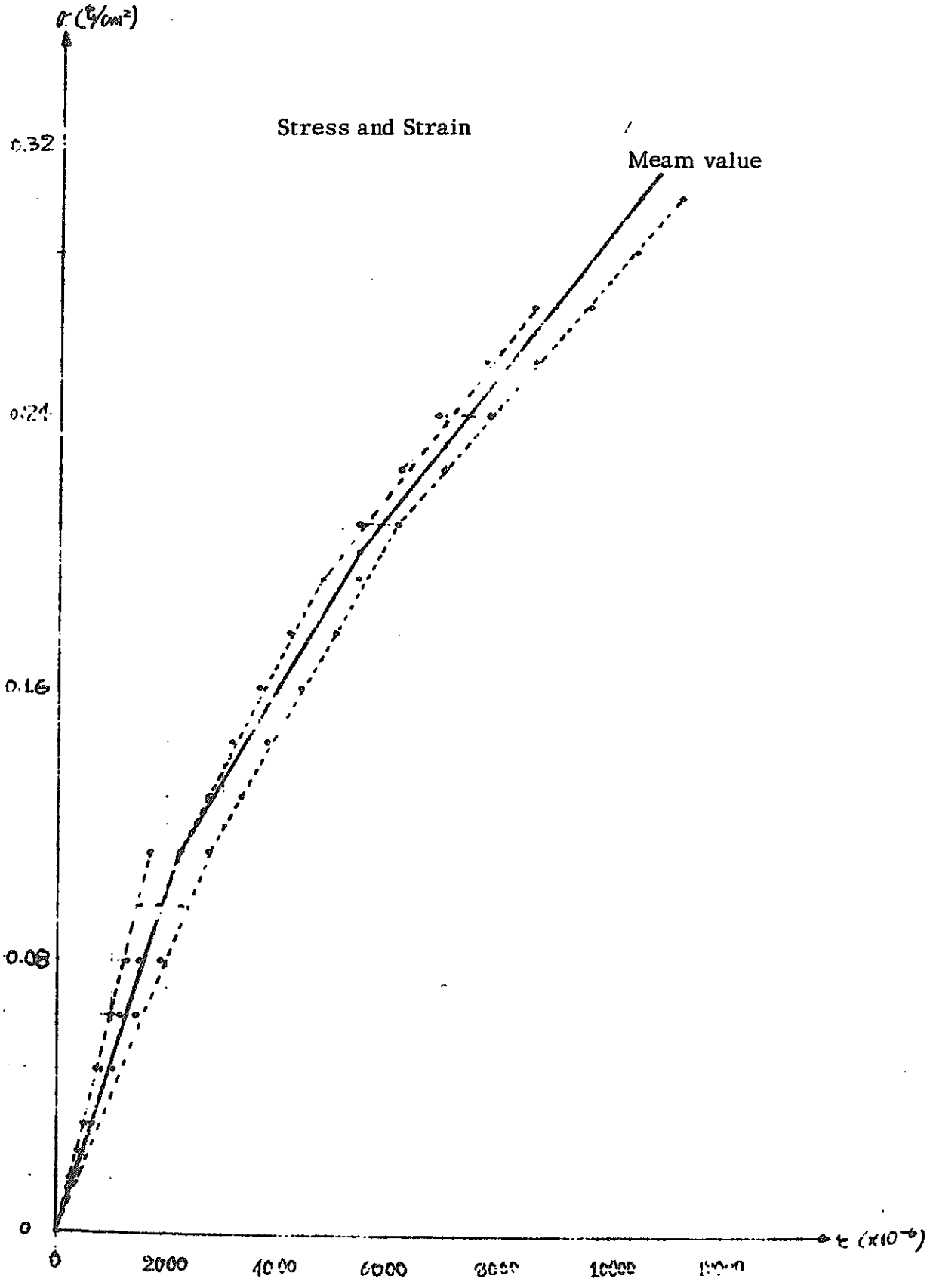
σ (kg/cm²)
Stress and Strain
Meam value
0.32
0.24
0.16
0.08
0
0
2000
4000
6000
ε (×10⁻⁶)

Graph IV-I-3

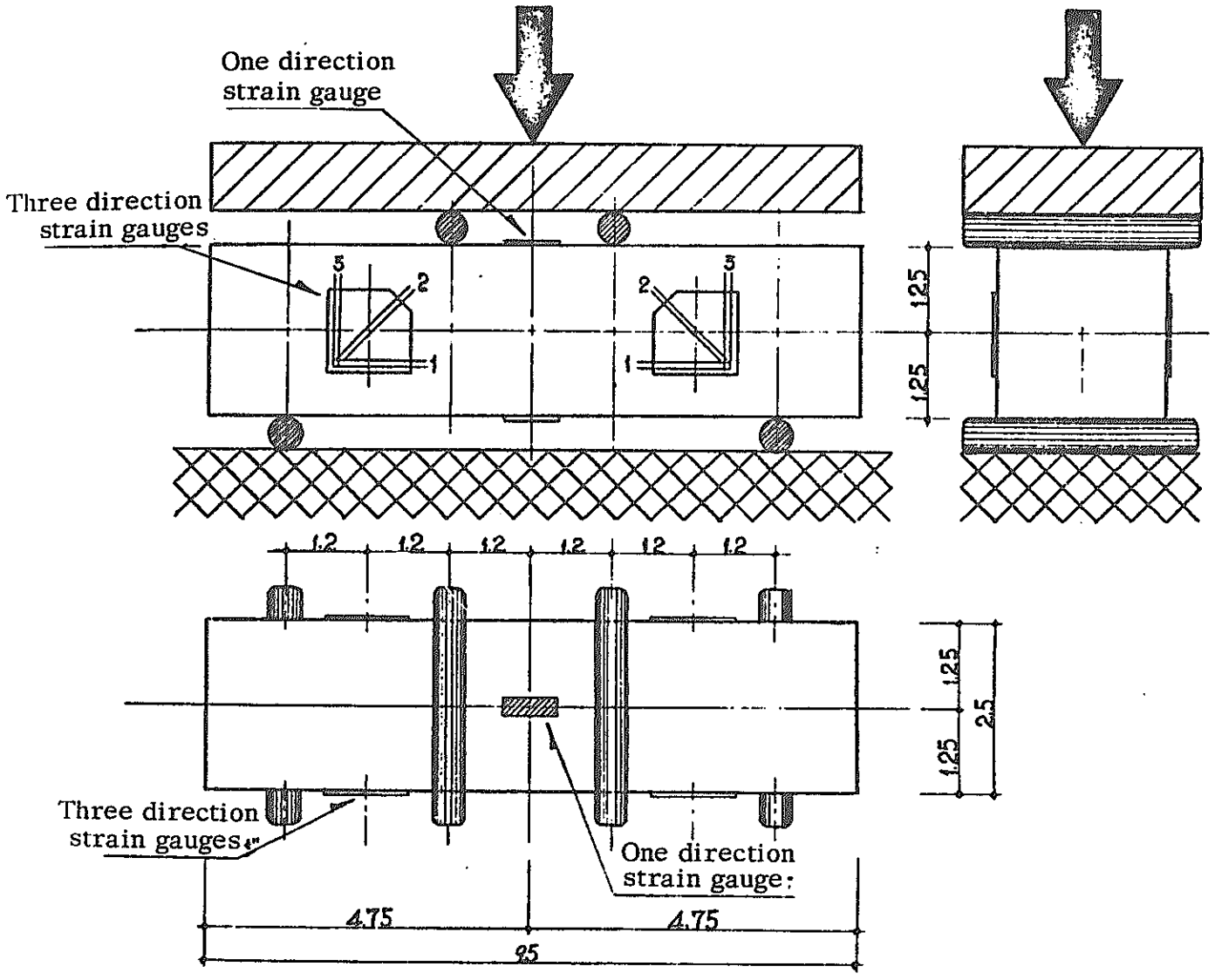
One direction
strain gauge
Three direction
strain gauges
3
2
1
2
3
1
125
125
1.2
1.2
1.2
1.2
1.2
1.2
125
25
125
Three direction
strain gauges
One direction
strain gauge
4.75
4.75
9.5

Fig. IV-I-III

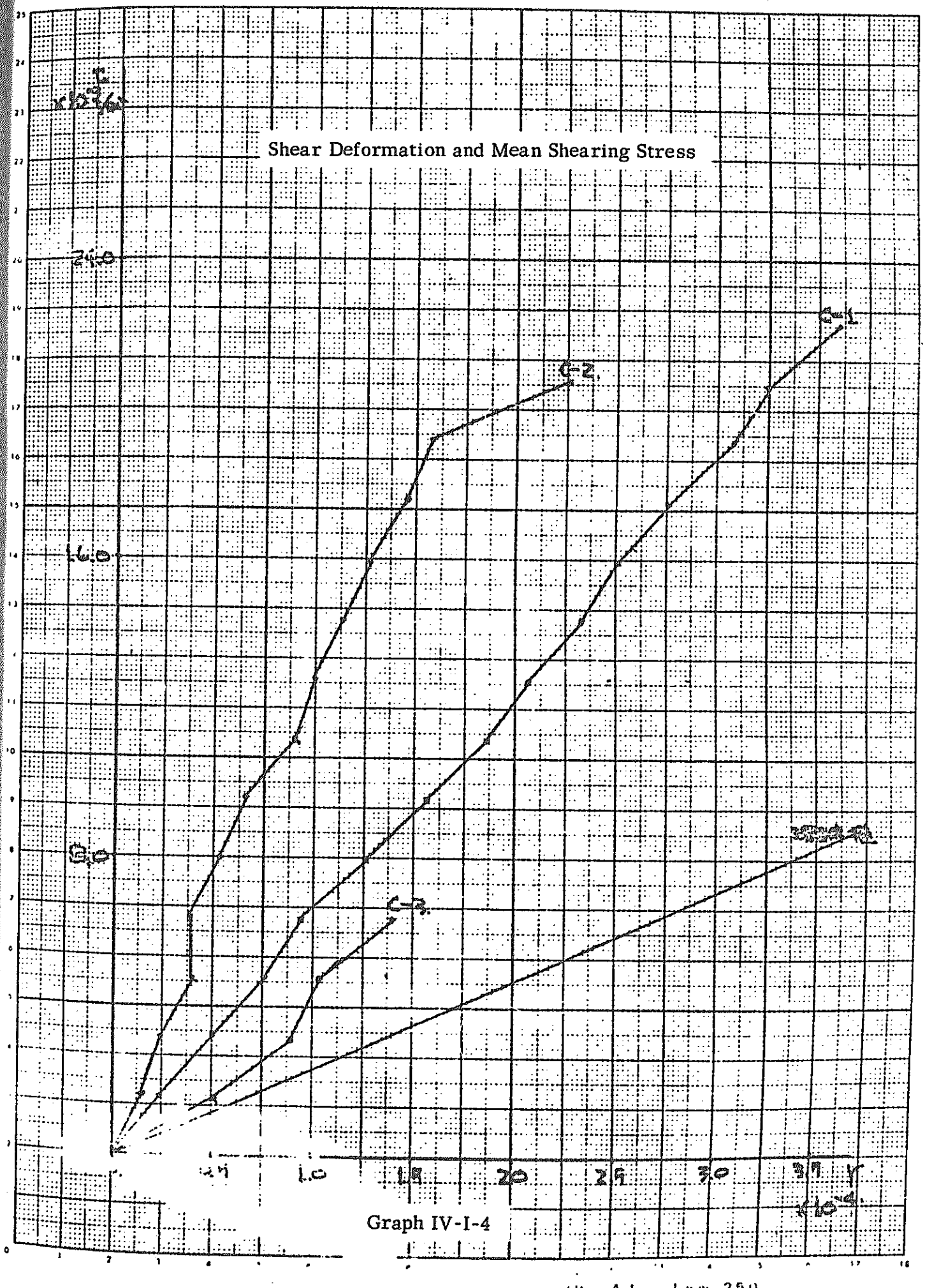
Shear Deformation and Mean Shearing Stress
kb2/cm2
24.0
16.0
8.0
C=1
C=2
C=3
1.0
2.0
3.0
γ
×10⁻⁴

Graph IV-I-4

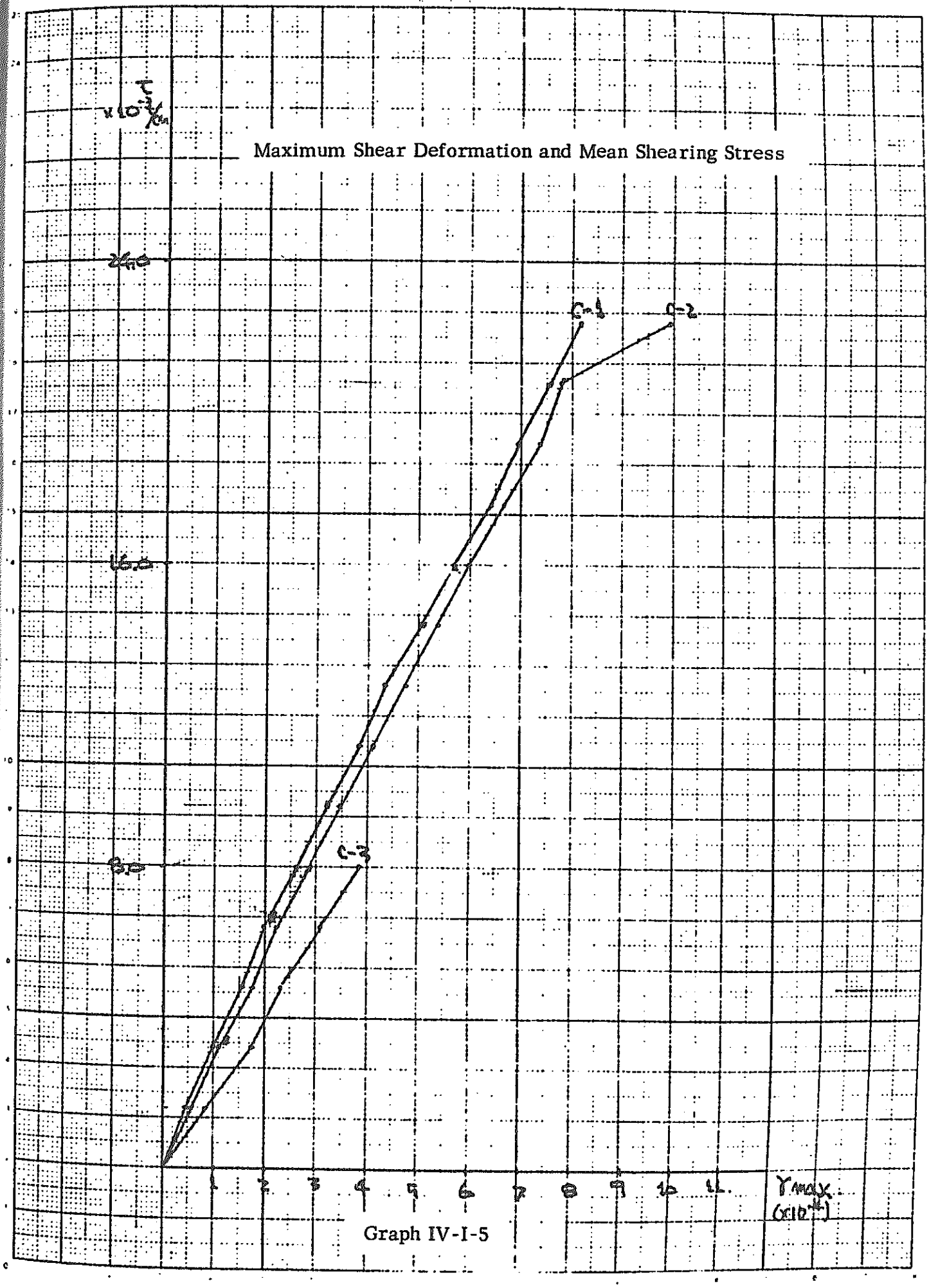
Maximum Shear Deformation and Mean Shearing Stress
C-1
C-2
C-3

Graph IV-I-5

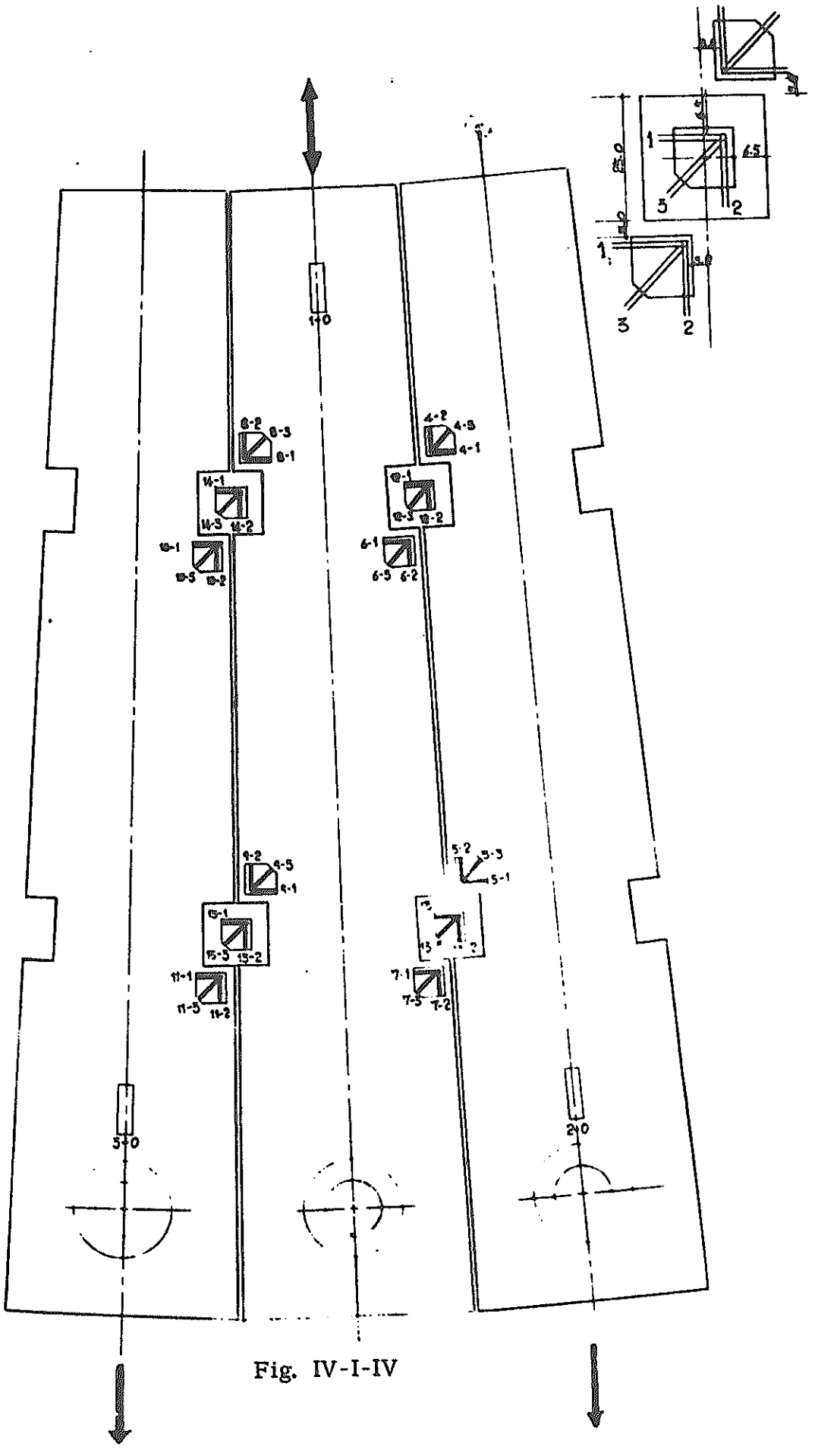

Fig. IV-I-IV

Principal Plan of Stress and Principal Stress

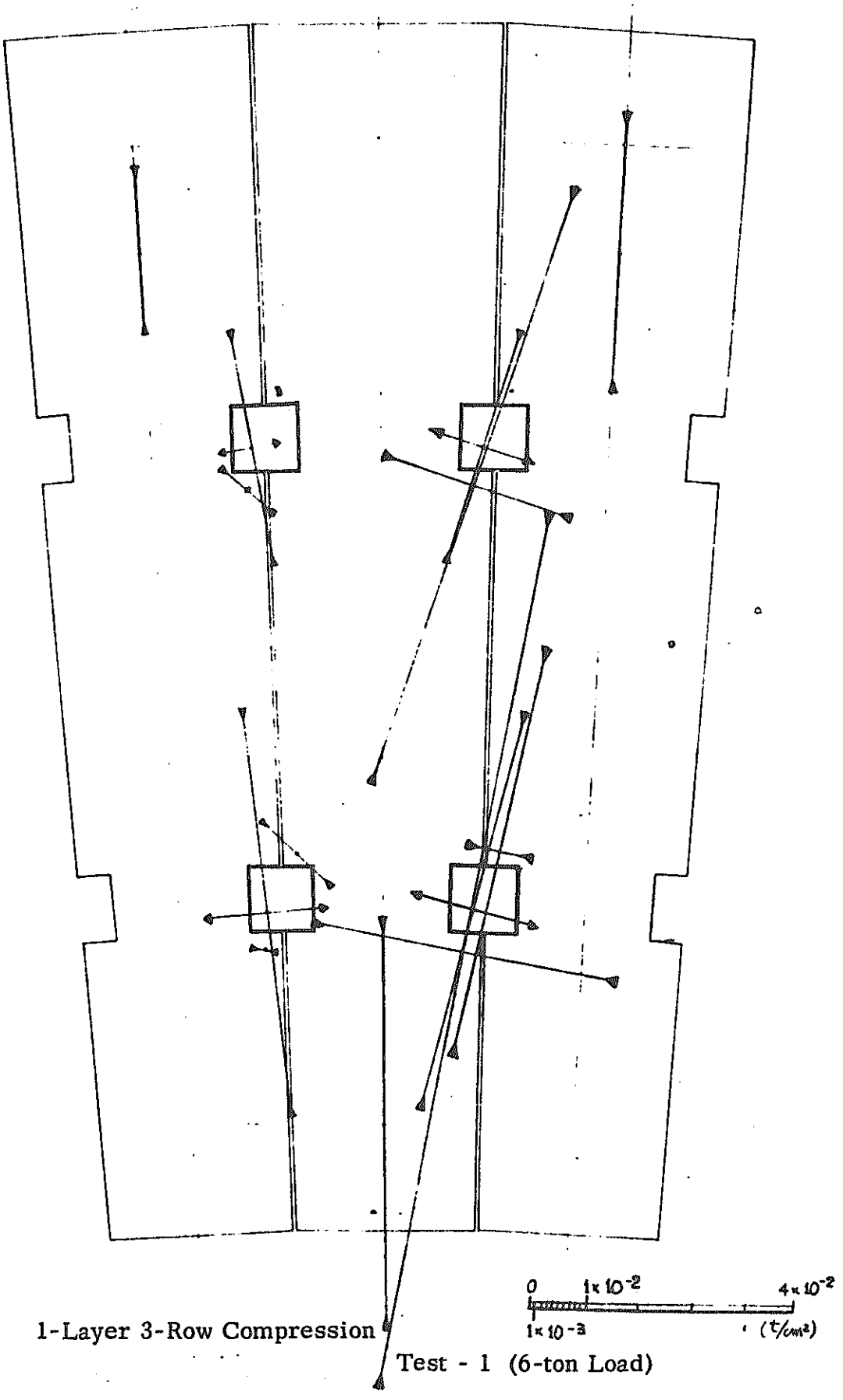

1-Layer 3-Row Compression Test - 1 (6-ton Load)

Fig. IV-I-3

Principal Plan of Stress and Principal Stress

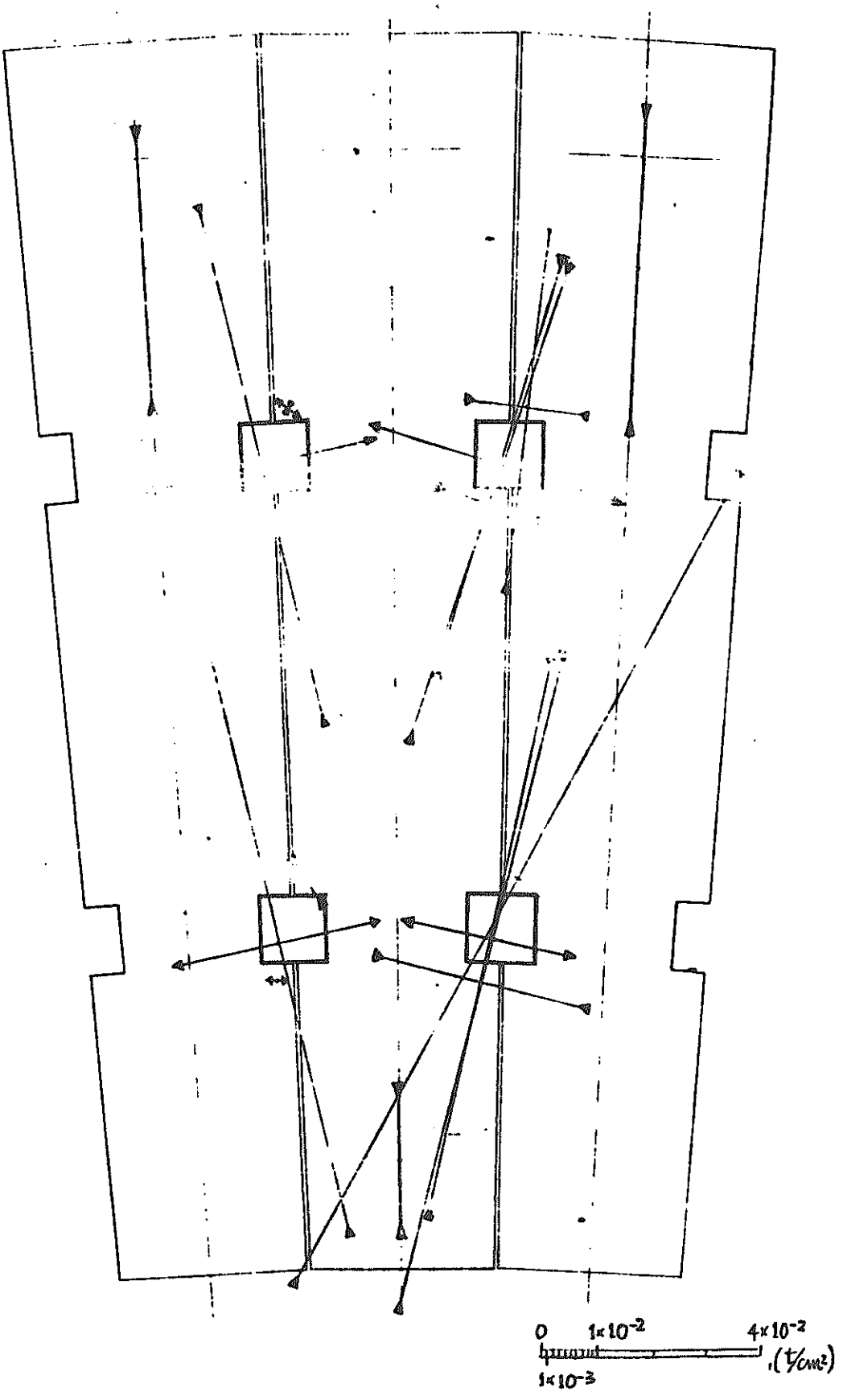

1-Layer 3-Row Compression Test - 2 (6-ton Load)

Fig. IV-I-6

Principal Plan of Stress and Principal Stress

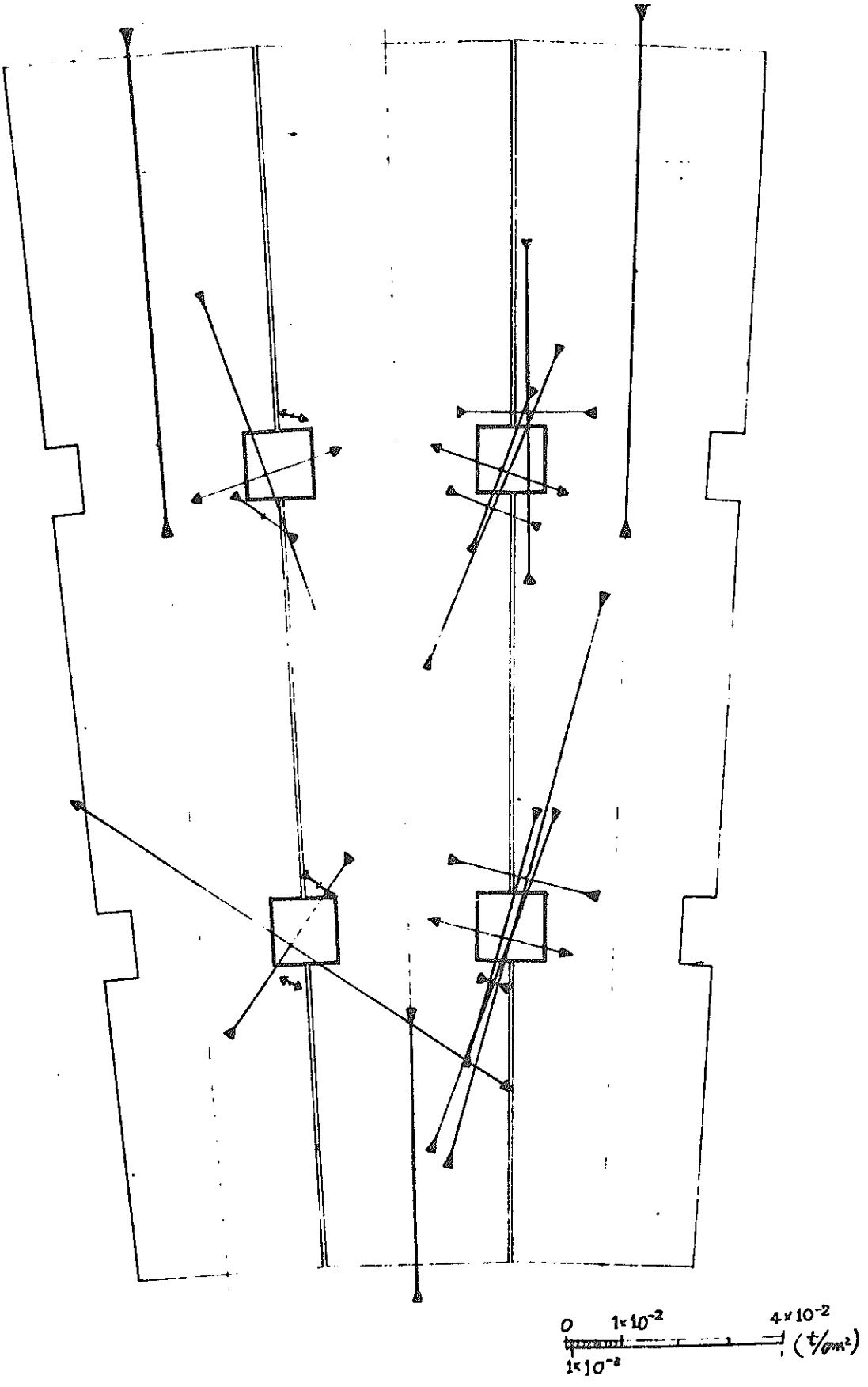

1-Layer 3-Row Compression Test - 3 (4-ton Load)

Fig. IV-I-8

Principal Plan of Stress and Principal Stress

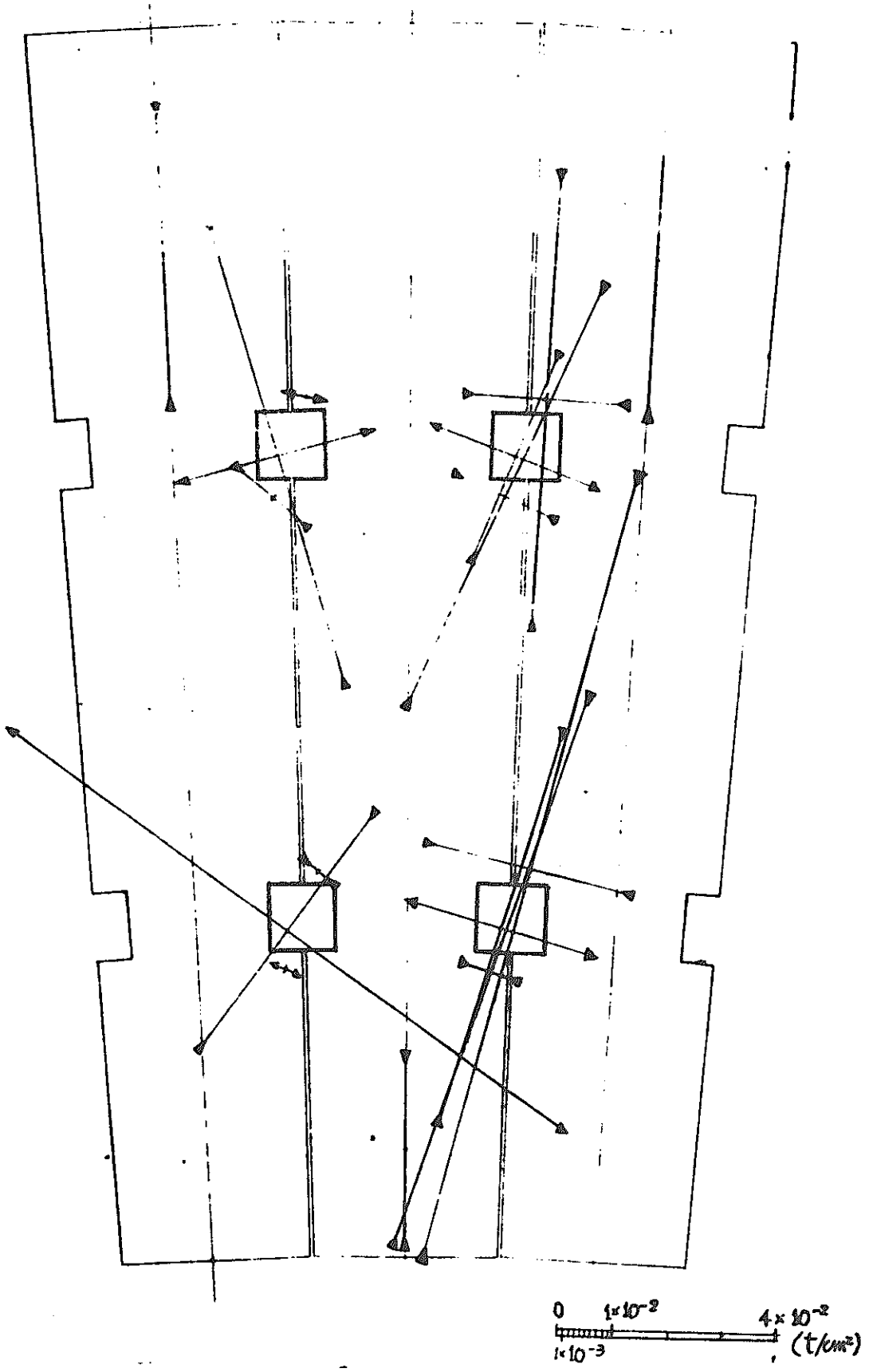

1-Layer 3-Row Compression Test - 3 (6-ton Load)

Fig. IV-I-9

Principal Plan of Stress and Principal Stress

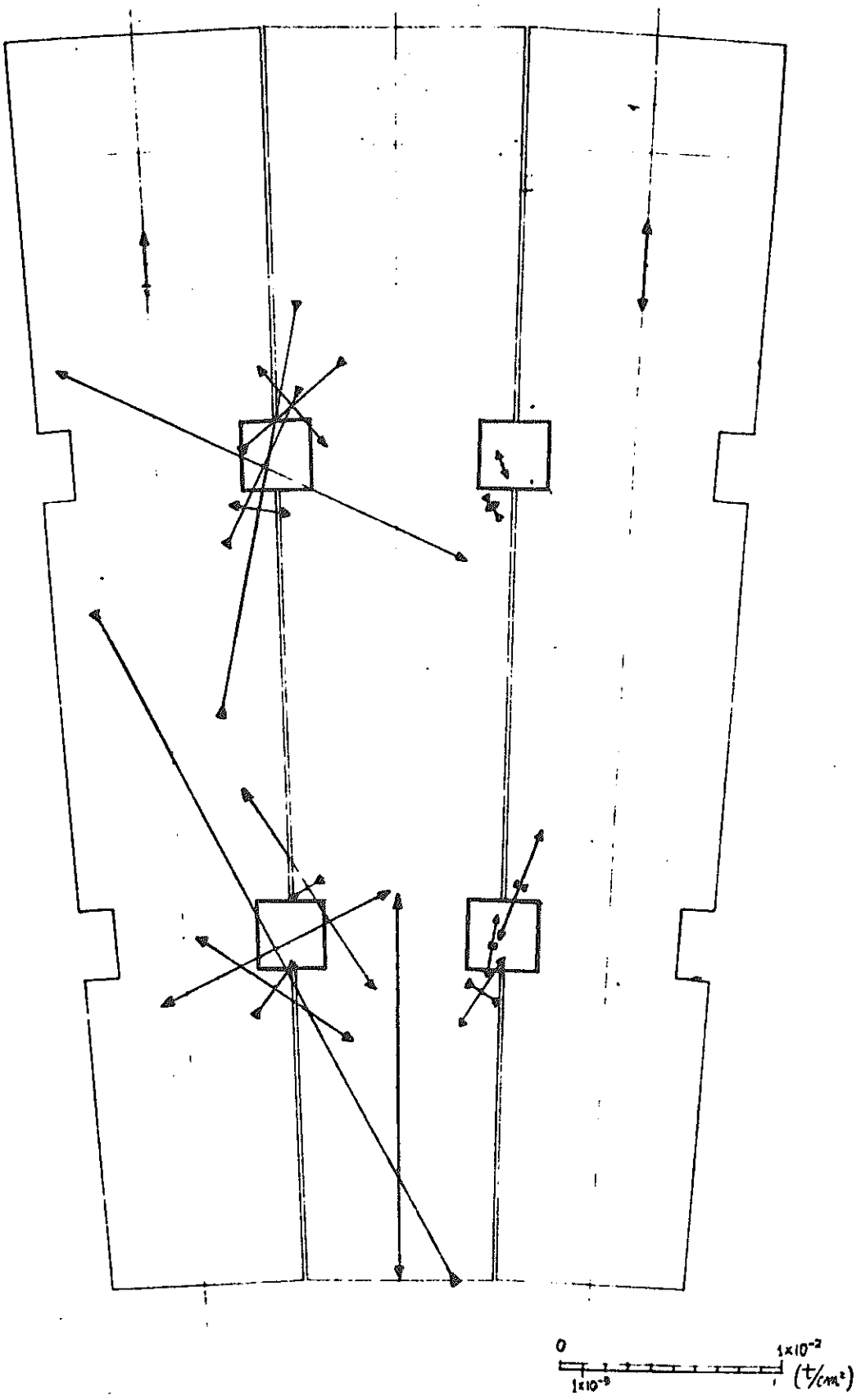

1-Layer 3-Row Tensile Test (1.5-ton Load)

Fig. IV-I-12

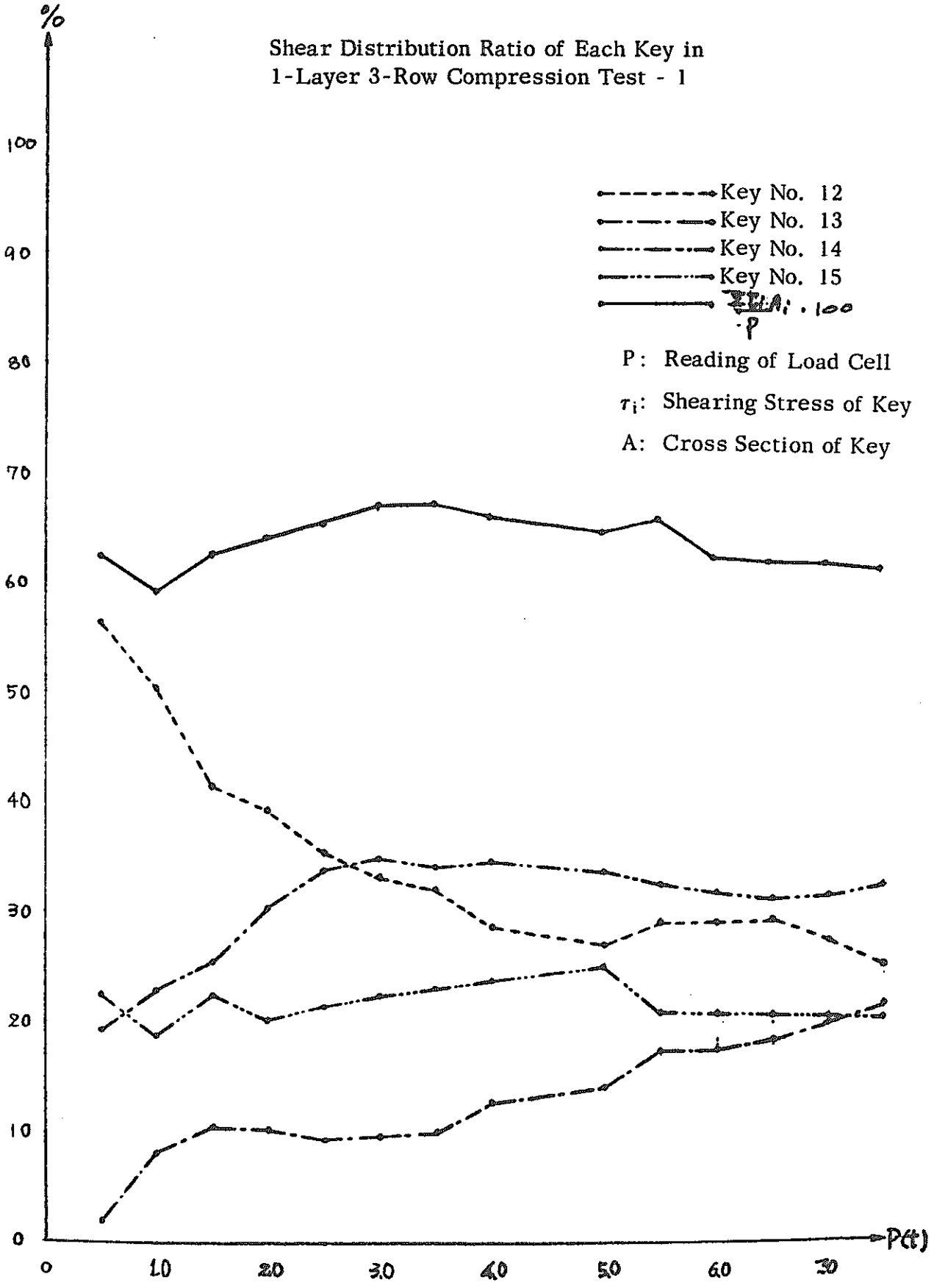
Shear Distribution Ratio of Each Key in
1-Layer 3-Row Compression Test - 1
%
100
90
80
70
60
50
40
30
20
10
0
0
10
20
30
40
50
60
30
P(t)
Key No. 12
Key No. 13
Key No. 14
Key No. 15
$\frac{\Sigma \tau_i A_i \cdot 100}{P}$
P: Reading of Load Cell
τ_i: Shearing Stress of Key
A: Cross Section of Key

Graph IV-I-6

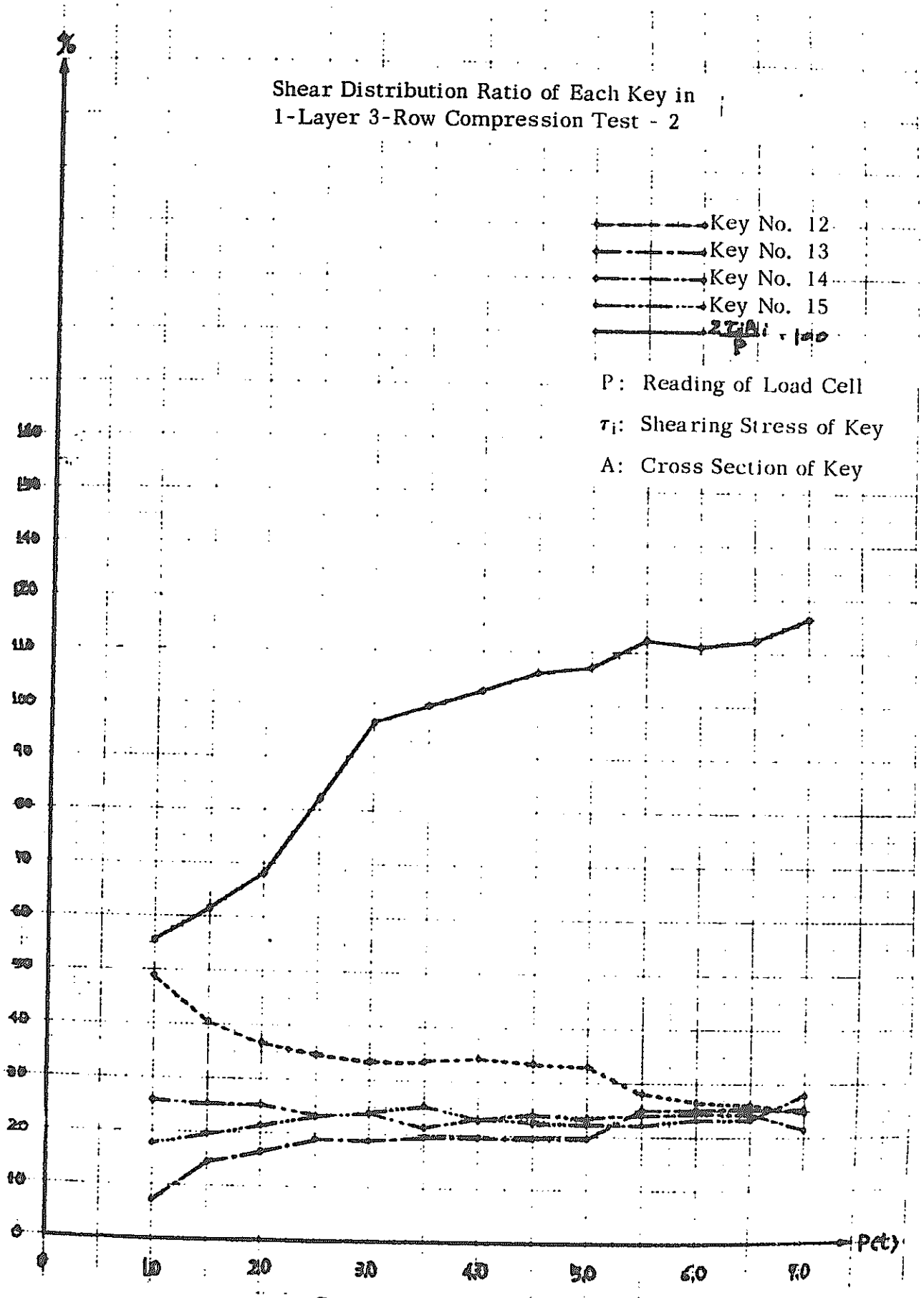
Shear Distribution Ratio of Each Key in
1-Layer 3-Row Compression Test - 2
Key No. 12
Key No. 13
Key No. 14
Key No. 15
P : Reading of Load Cell
τi: Shearing Stress of Key
A: Cross Section of Key
%
P(t)

Graph IV-I-7

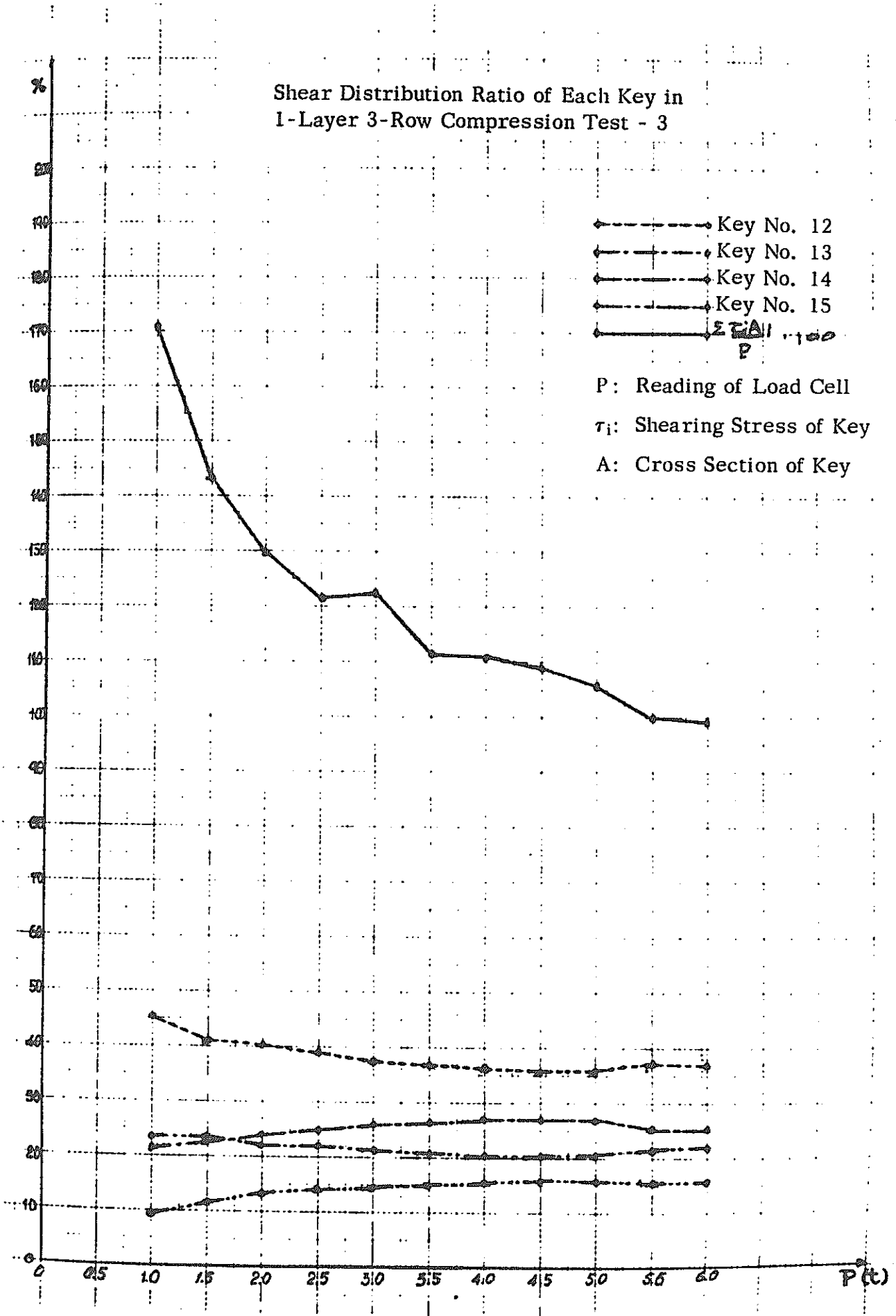
Shear Distribution Ratio of Each Key in
1-Layer 3-Row Compression Test - 3
%
Key No. 12
Key No. 13
Key No. 14
Key No. 15
P: Reading of Load Cell
τ_i: Shearing Stress of Key
A: Cross Section of Key
0
0.5
1.0
1.5
2.0
2.5
3.0
3.5
4.0
4.5
5.0
5.6
6.0
P (t)

Graph IV-I-8

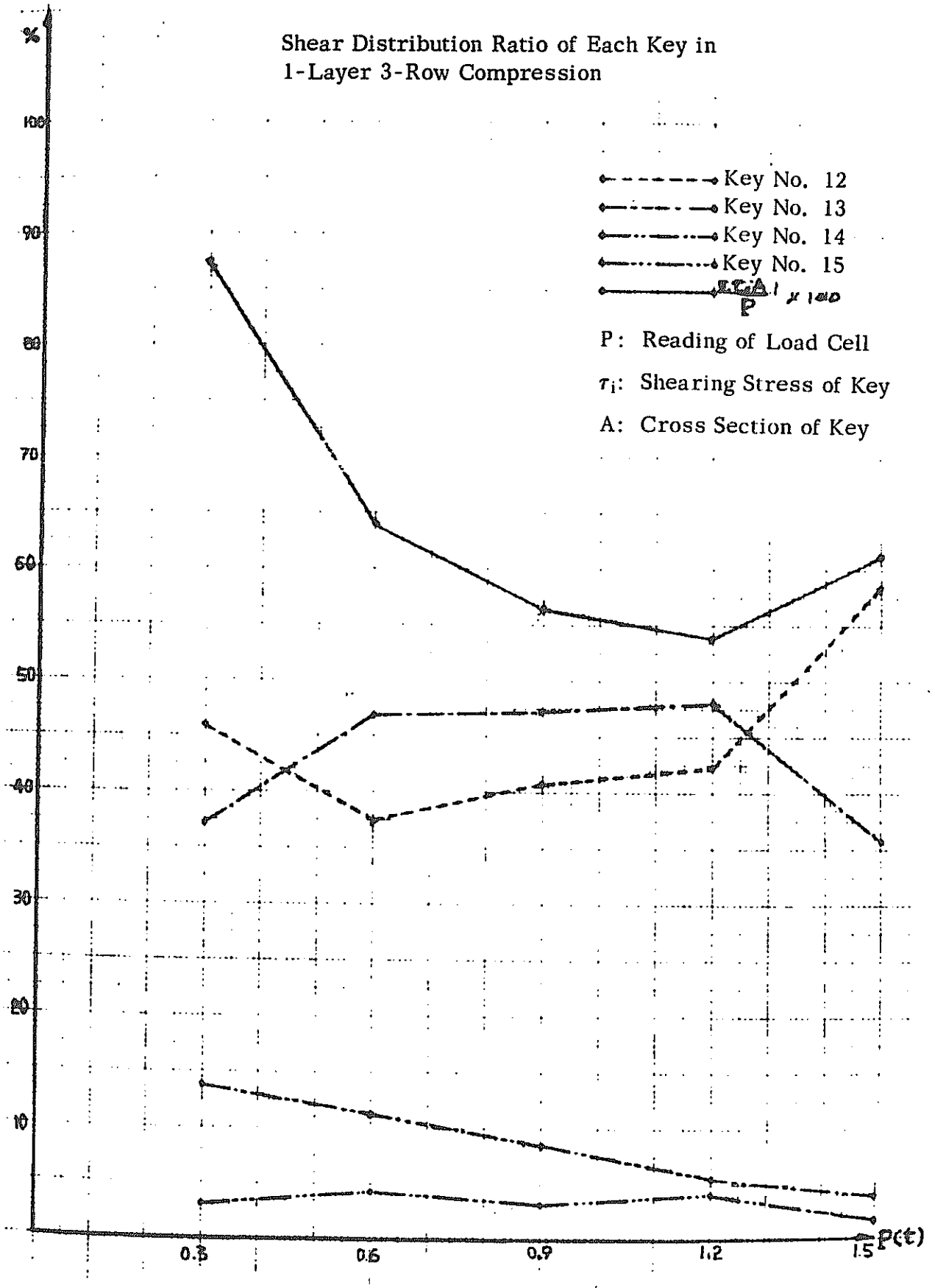
Shear Distribution Ratio of Each Key in
1-Layer 3-Row Compression
%
100
90
80
70
60
50
40
30
20
10
0.3
0.6
0.9
1.2
1.5
P(t)
Key No. 12
Key No. 13
Key No. 14
Key No. 15
P: Reading of Load Cell
τi: Shearing Stress of Key
A: Cross Section of Key

Graph IV-I-9

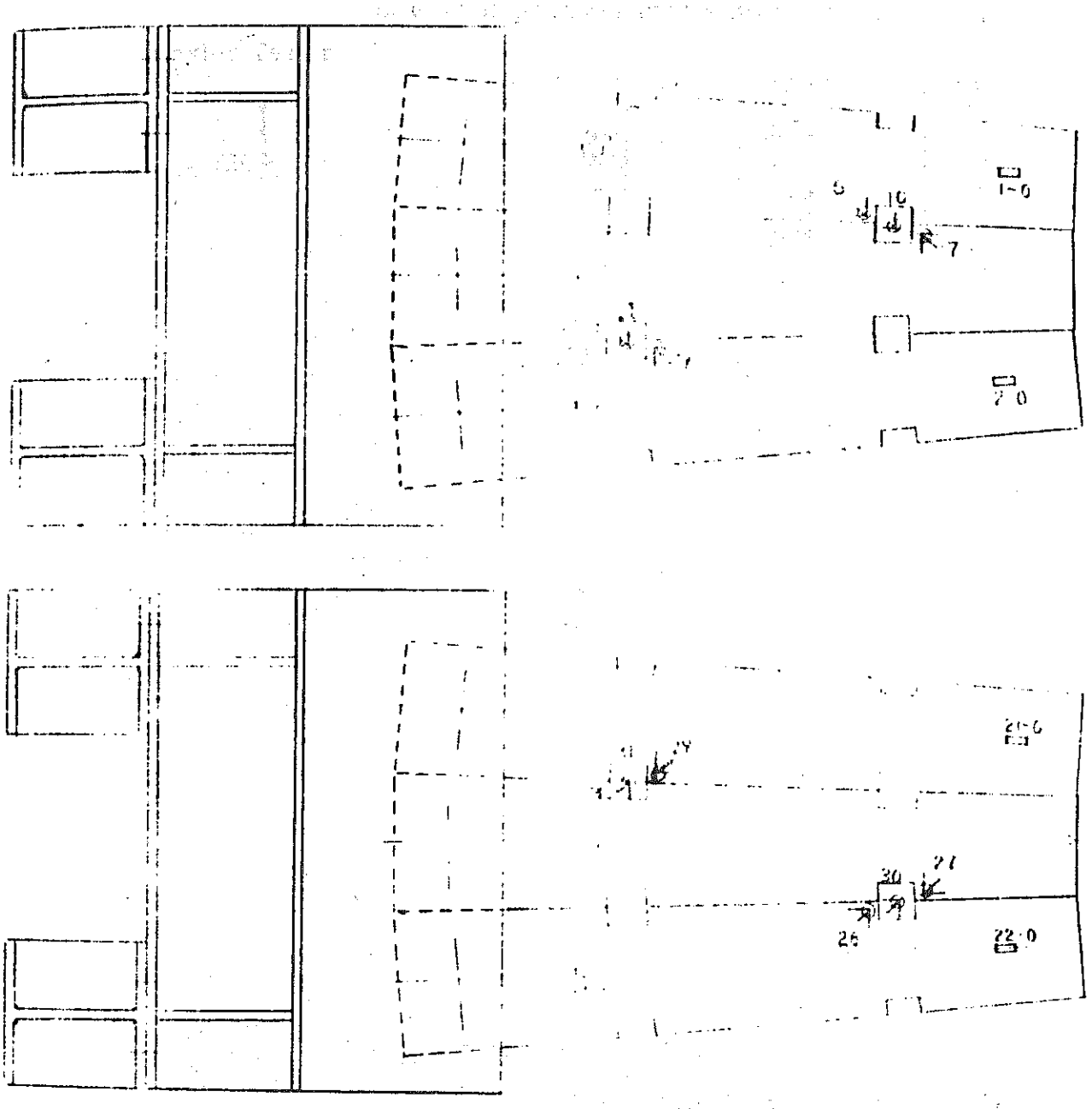

Gauge Positions in 3-Layer 3-Row Compression Bending Test

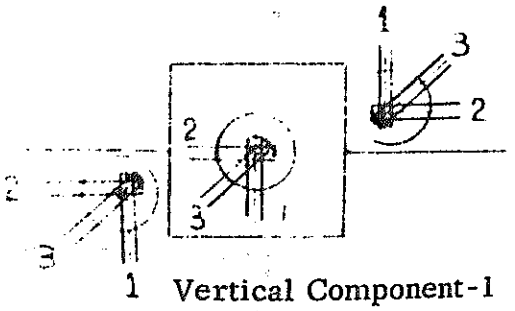

Vertical Component-1

Horizontal Component-2

45° Component-3

Fig. IV-I-V_1

Load in Steps in 3-Layer 3-Row Compression Test

Amsler Tester

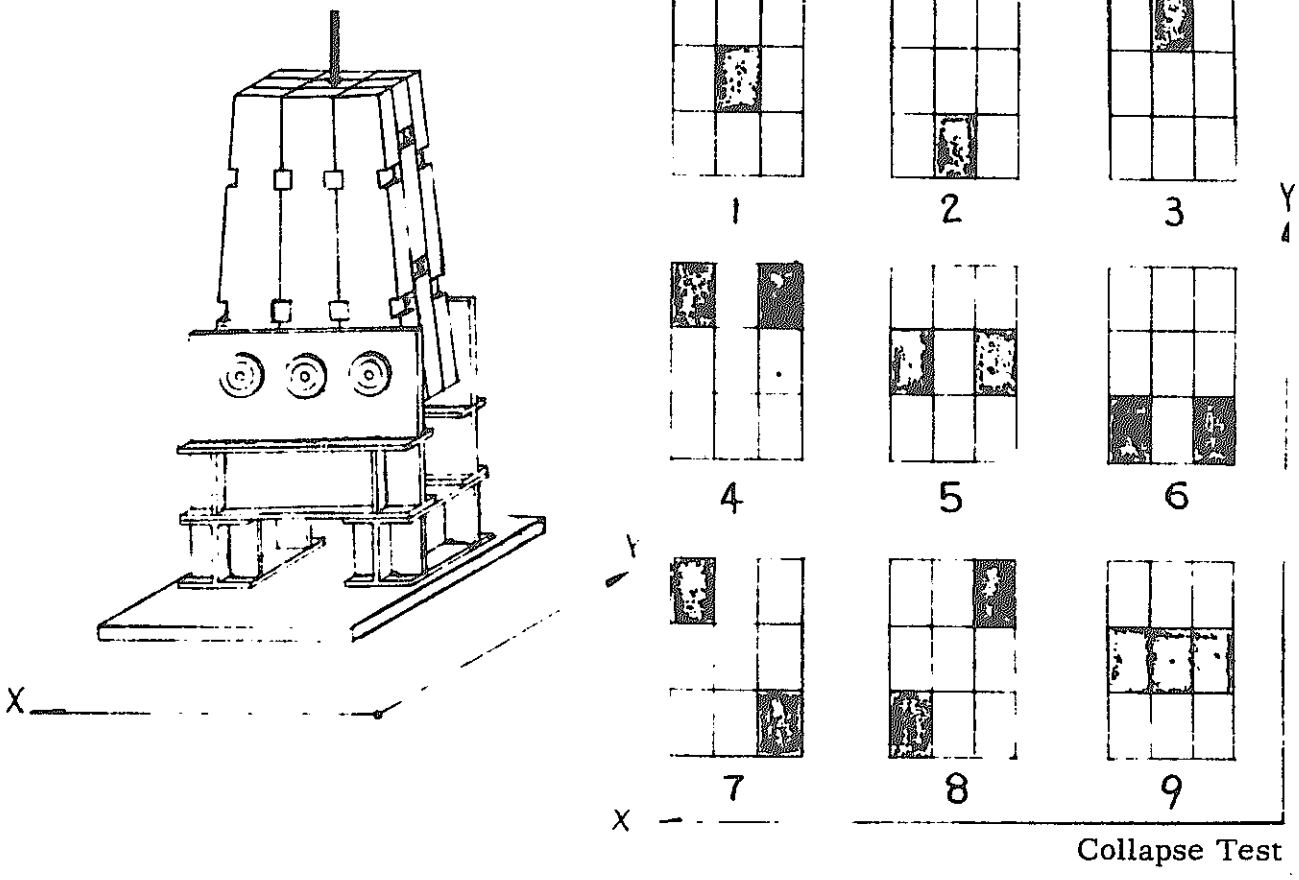

Load in Steps in 3-Layer 3-Row Bending Test

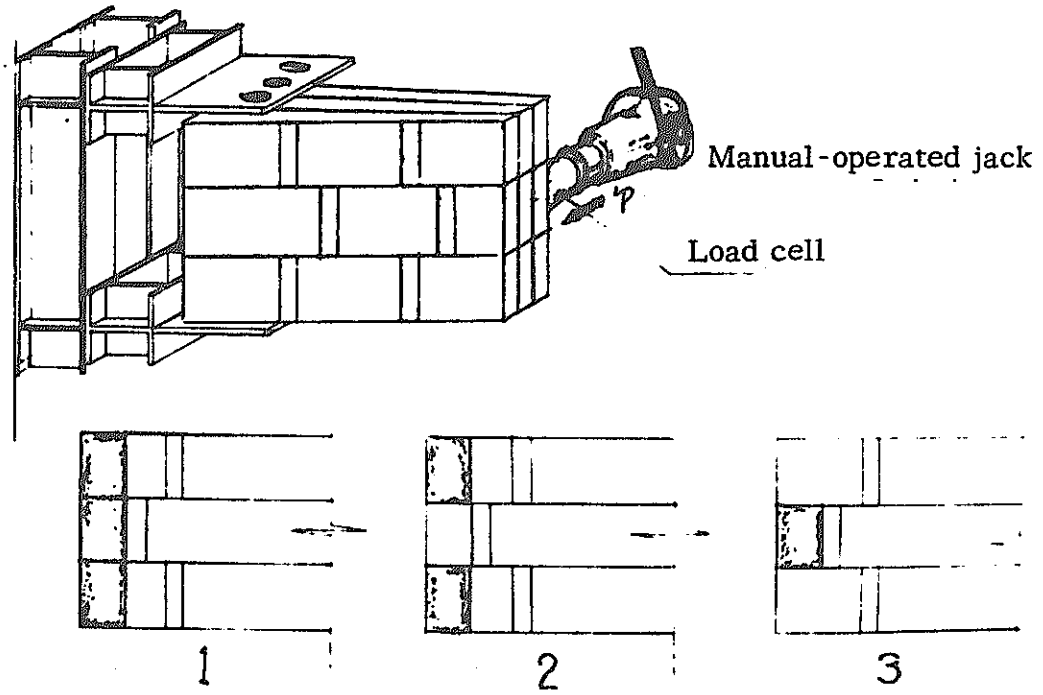

Fig. IV-I-V_2

Shear Distribution Ratio at Each Load Position of Block in
3-Layer 3-Row Compression Test

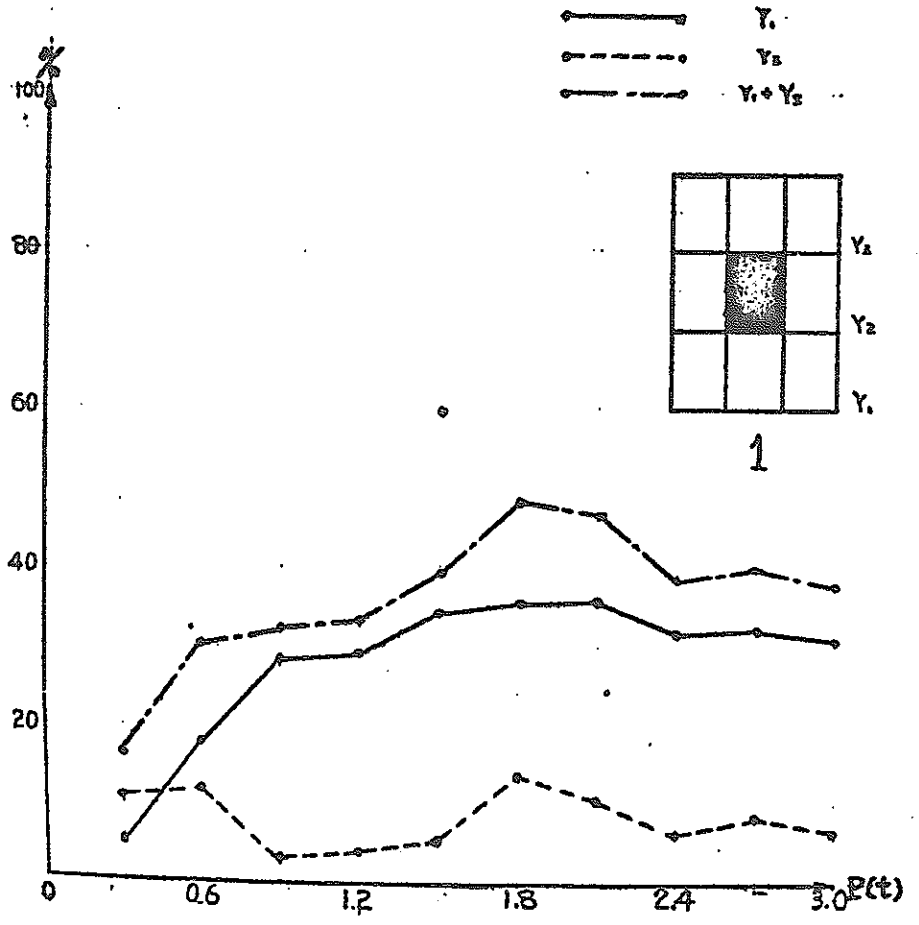

Graph IV-I-10

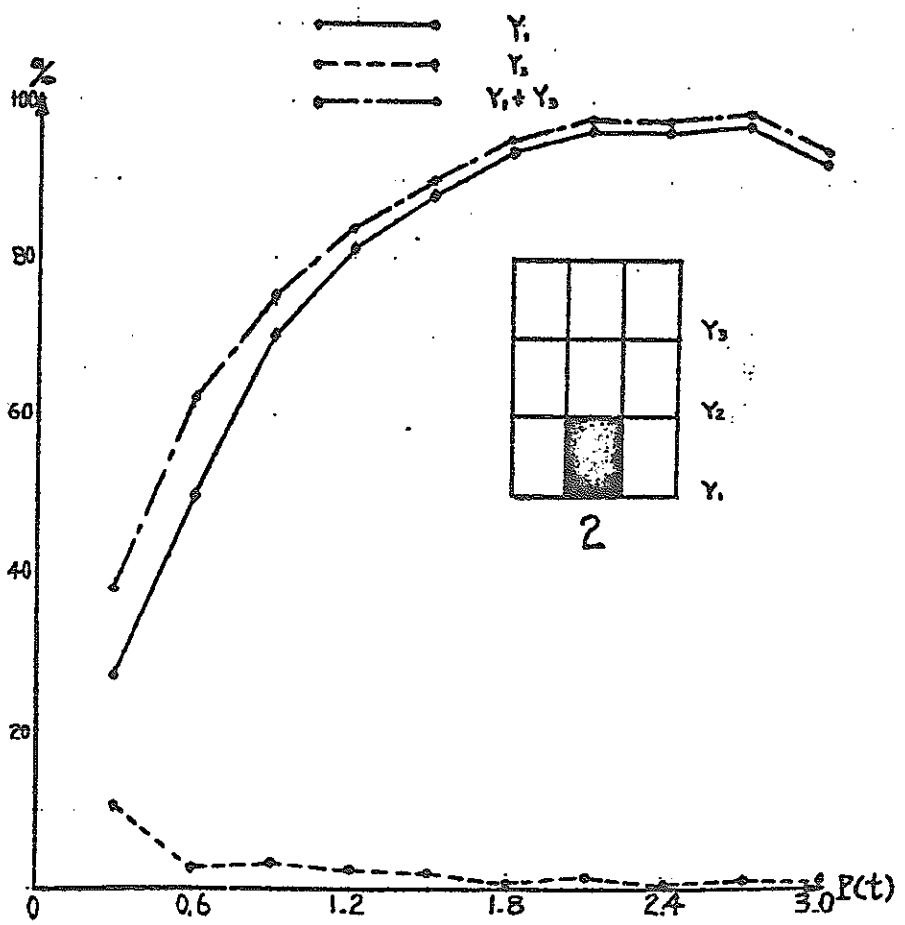

Graph IV-I-11

Shear Distribution Ratio at Each Load Position of Block in
3-Layer 3-Row Compression Test

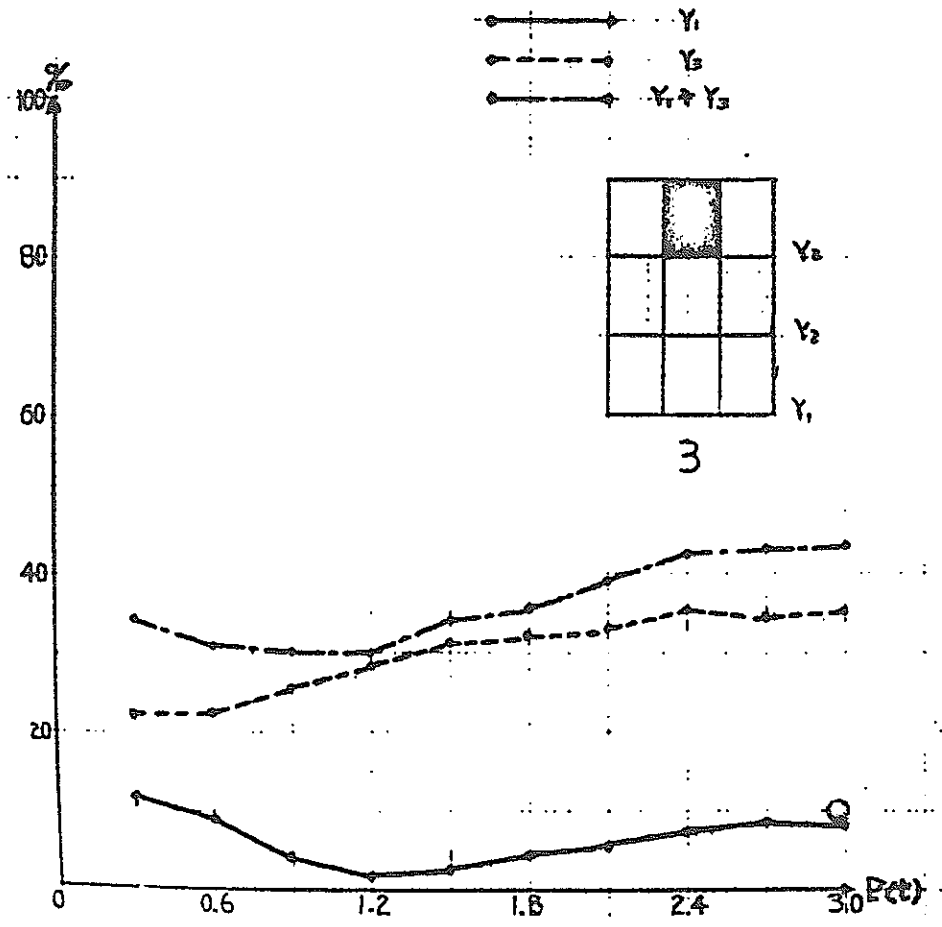

Graph IV-I-12

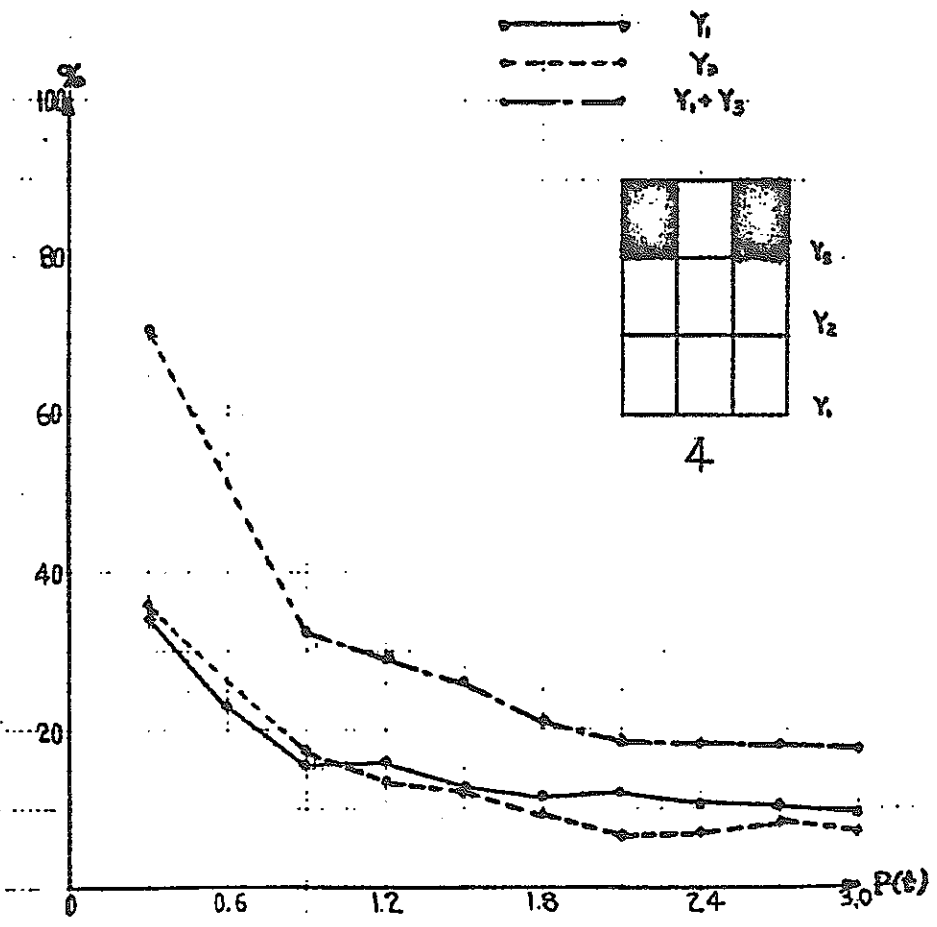

Graph IV-I-13

Shear Distribution Ratio at Each Load Position of Block in
3-Layer 3-Row Compression Test

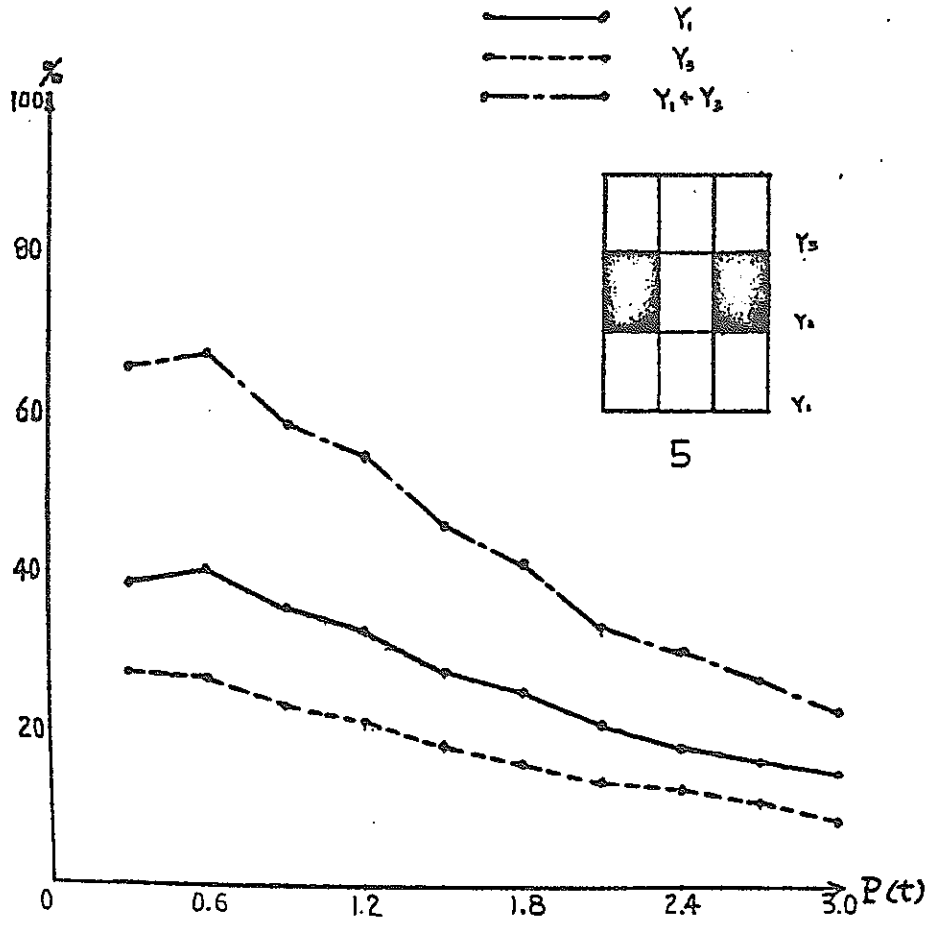

Graph IV-I-14

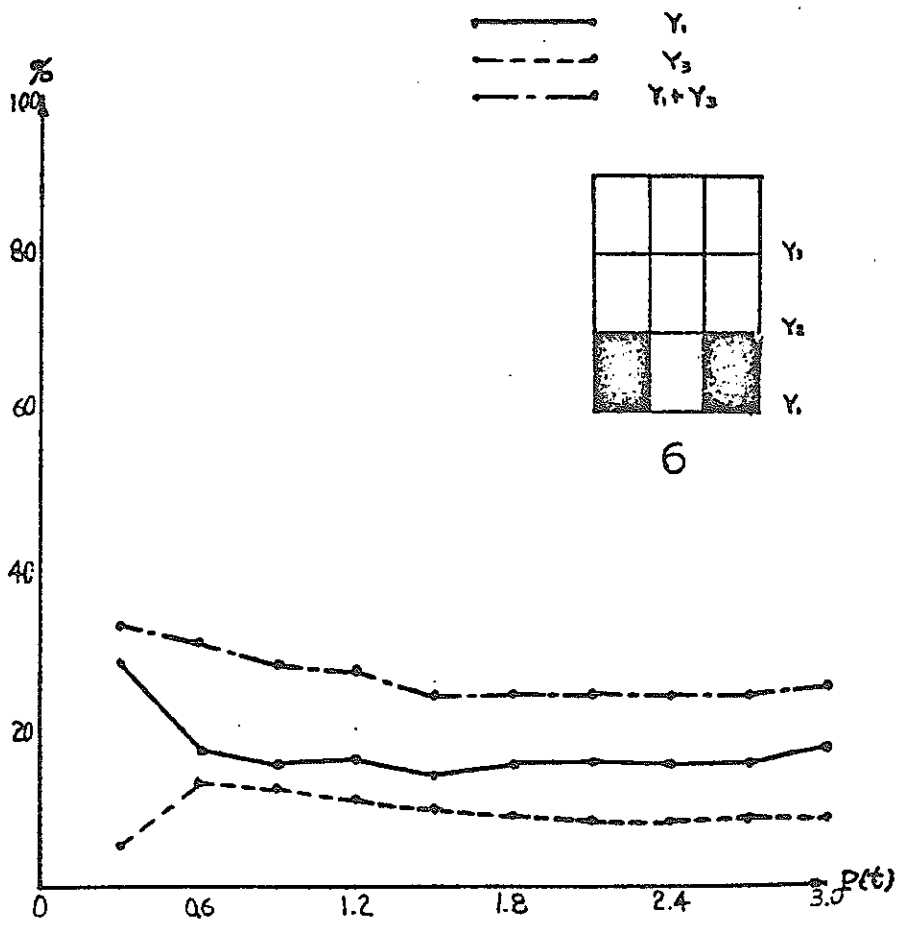

Graph IV-I-15

Shear Distribution Ratio at Each Load Position of Block in 3-Layer 3-Row Compression Test

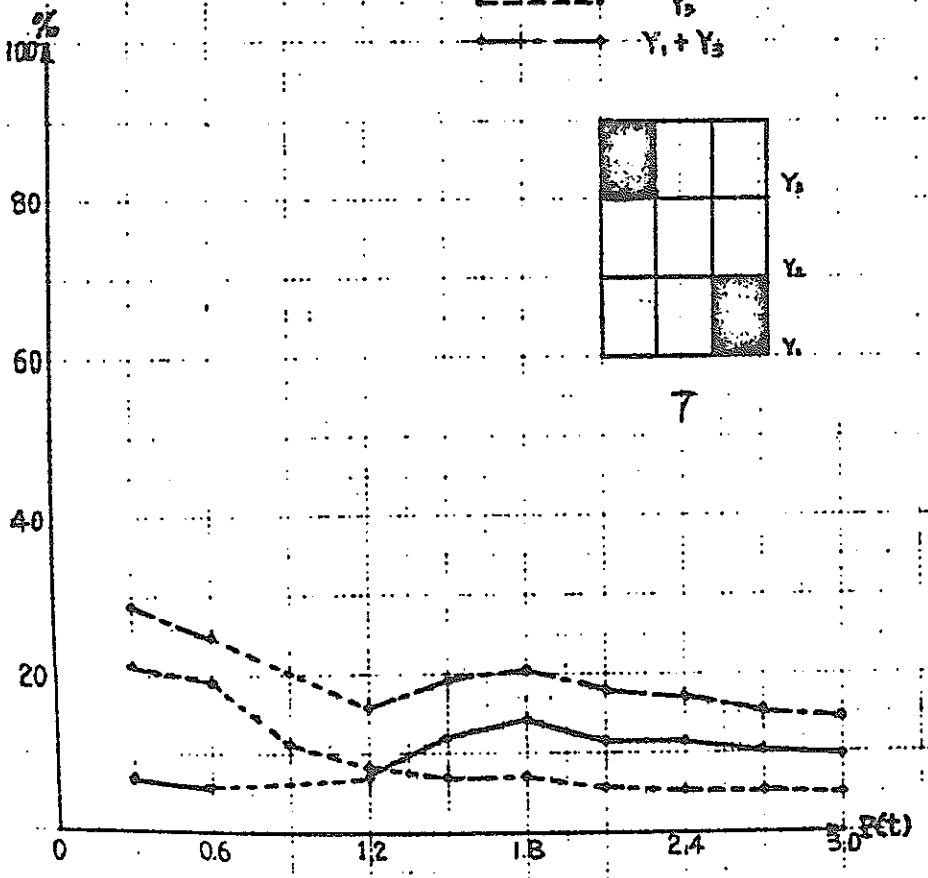

Graph IV-I-16

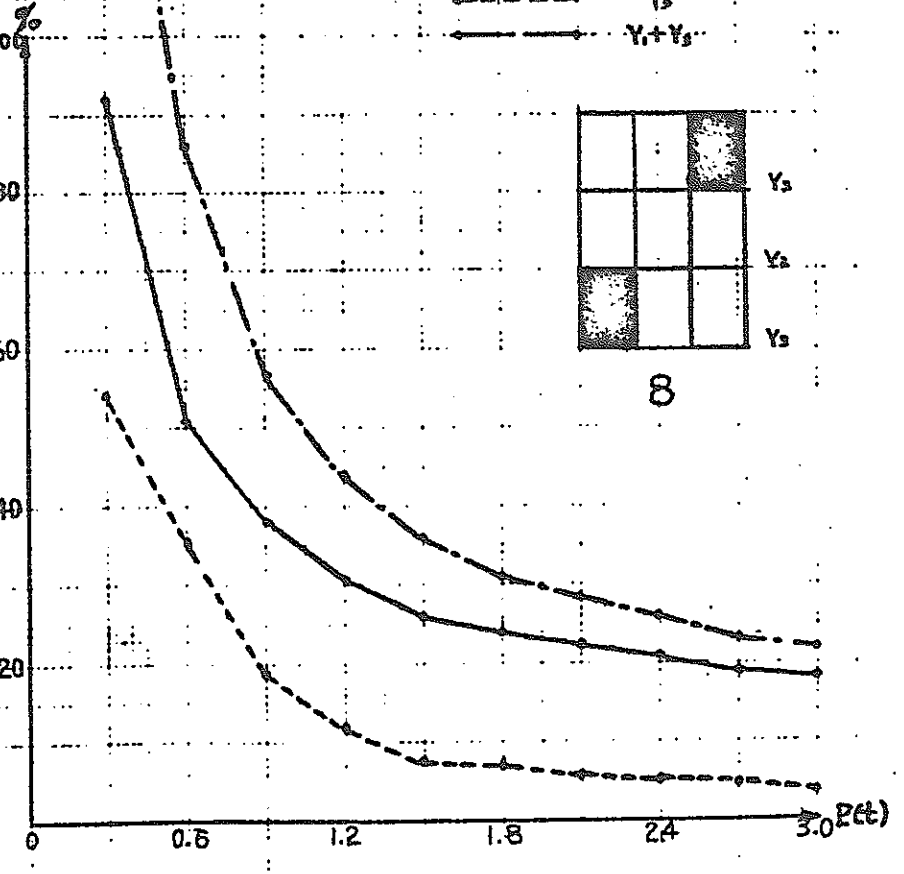

Graph IV-I-17

Shear Distribution Ratio at Each Load Position of Block in
3-Layer 3-Row Compression Test

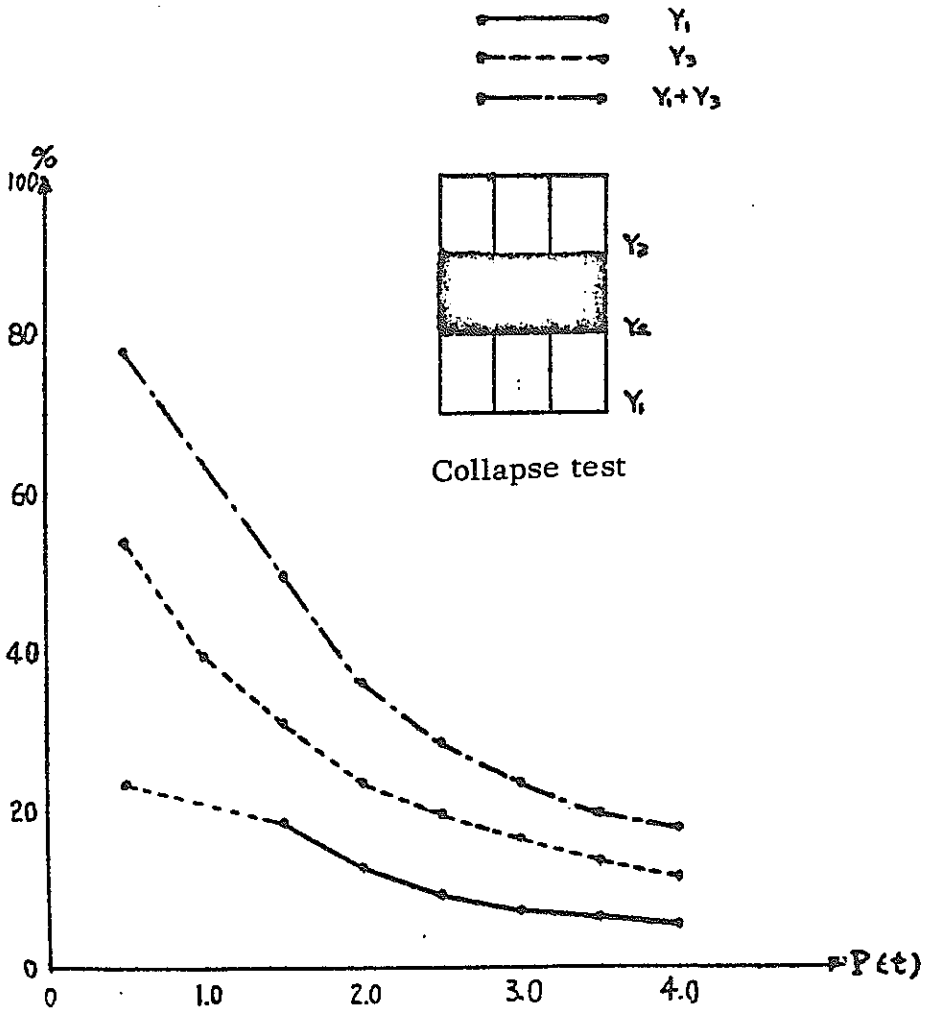

Graph IV-I-18

Collapse test

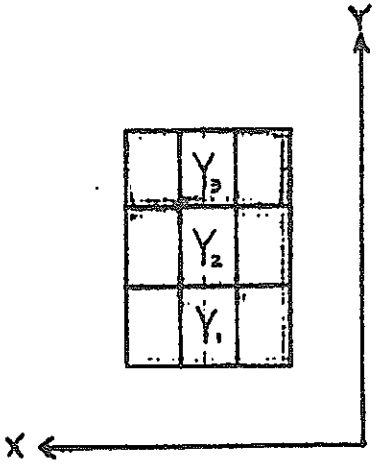

Pin's Moment at Each Load Position

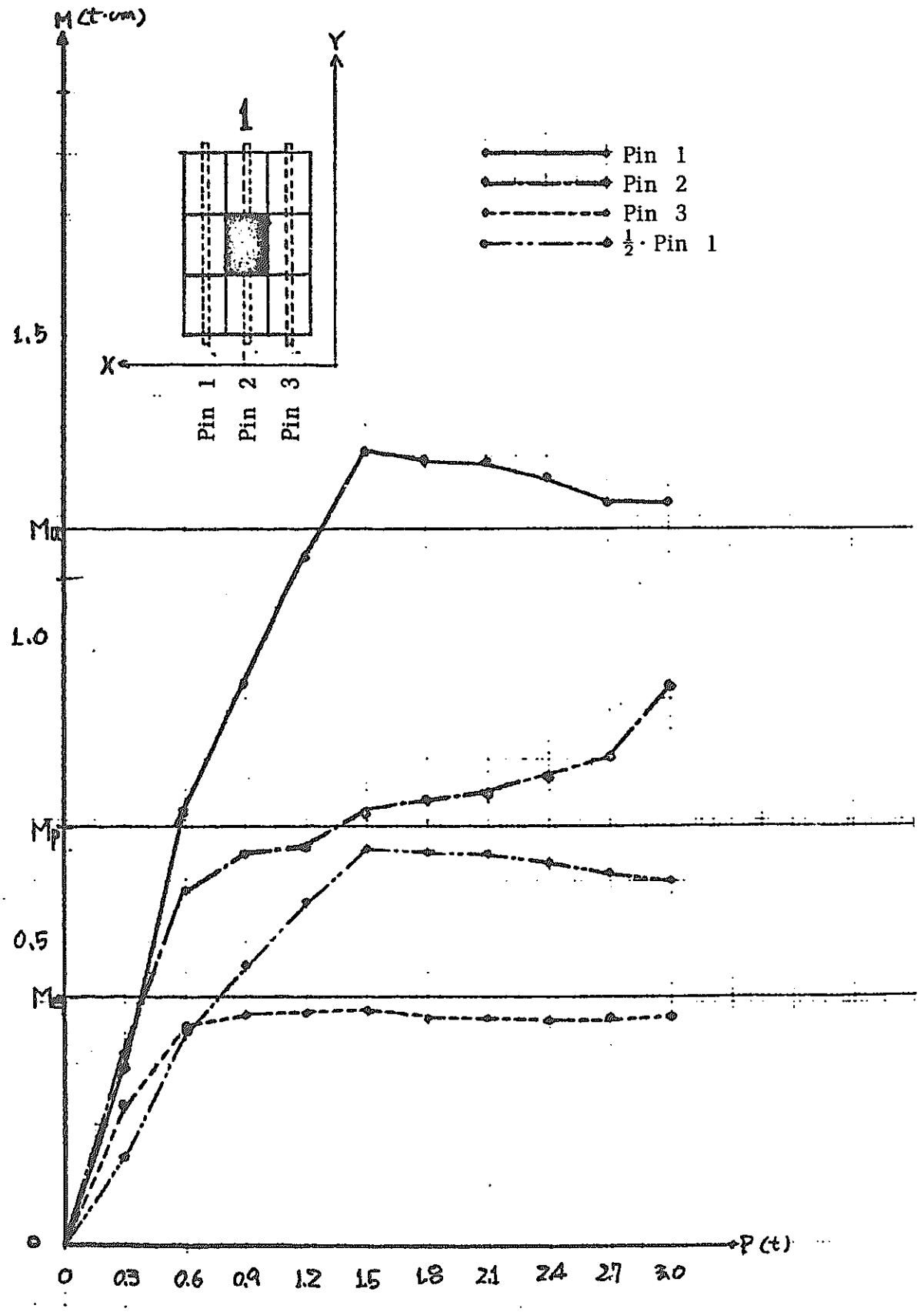

Graph IV-I-19

Pin's Moment at Each Load Position

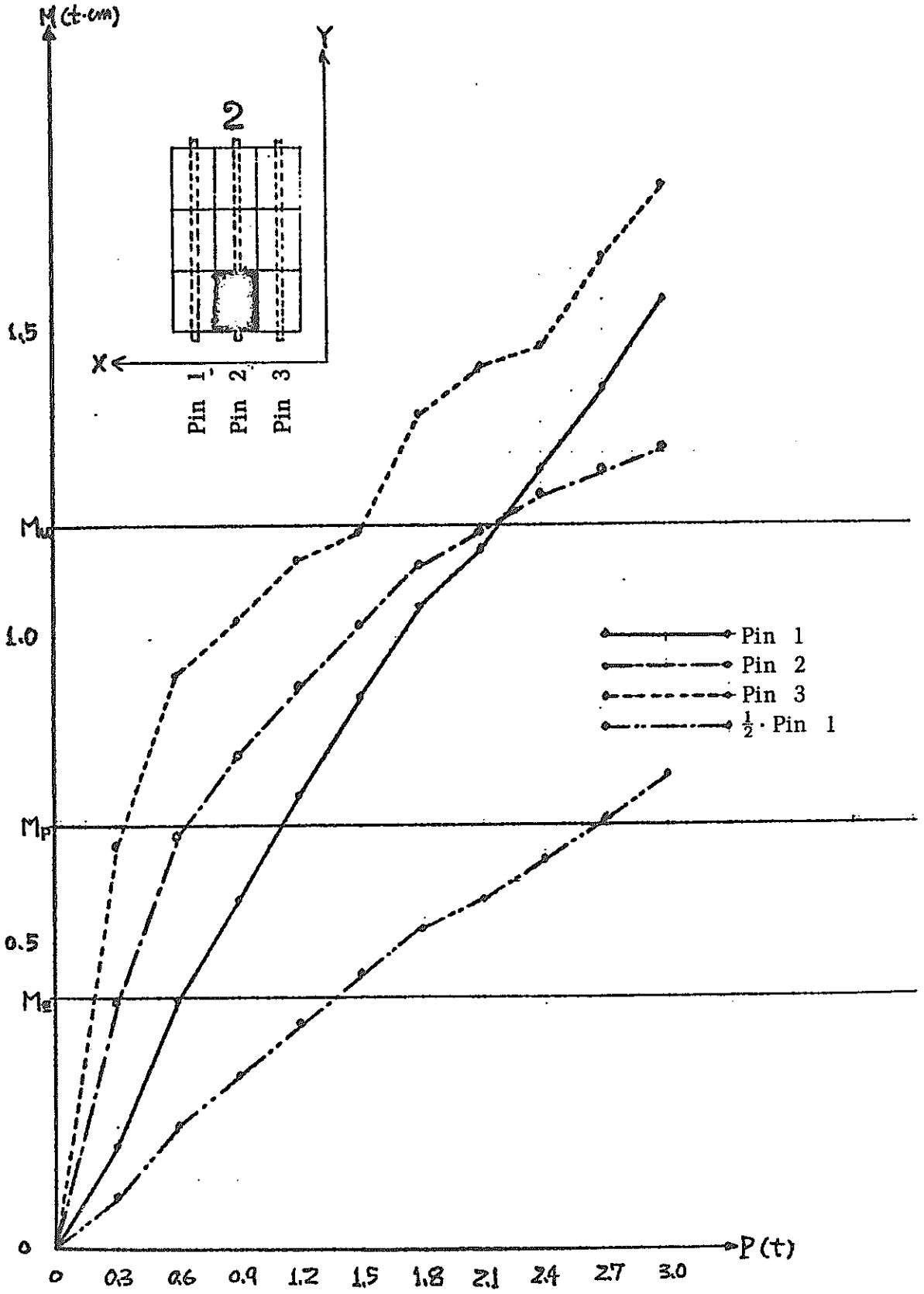

Graph IV-I-20

Pin's Moment at Each Load Position

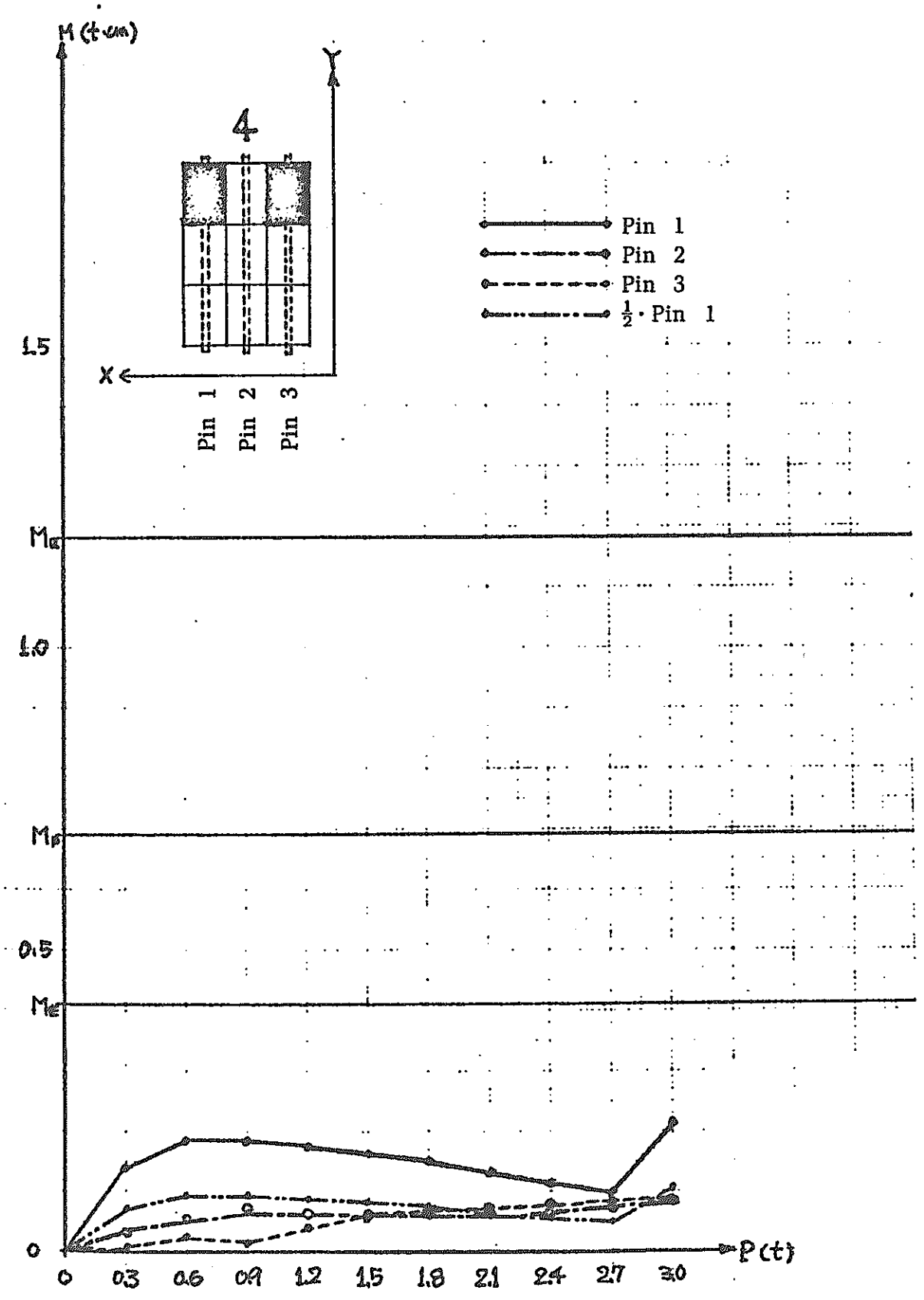

Graph IV-I-22

Pin's Moment at Each Load Position

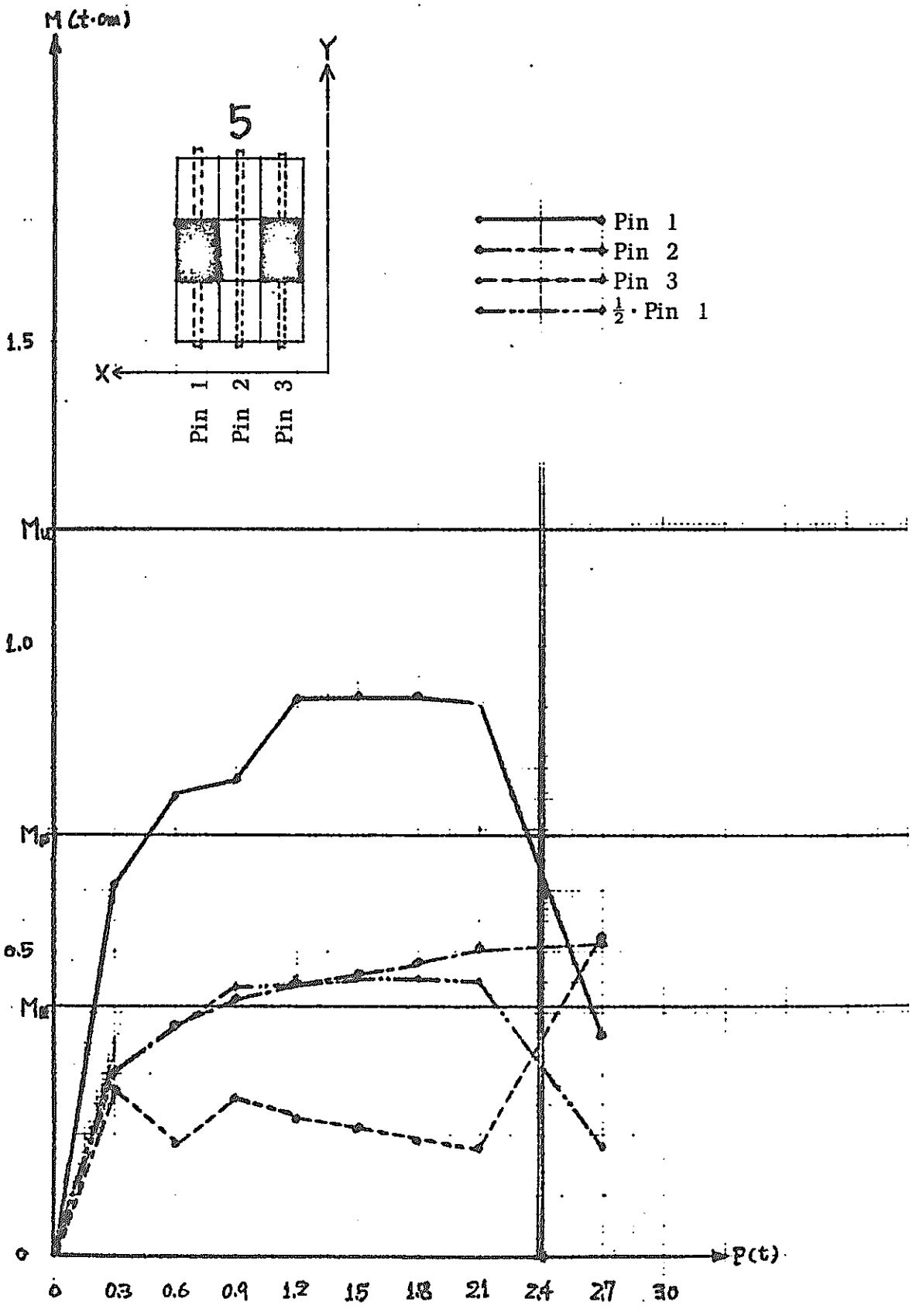

Graph IV-I-23

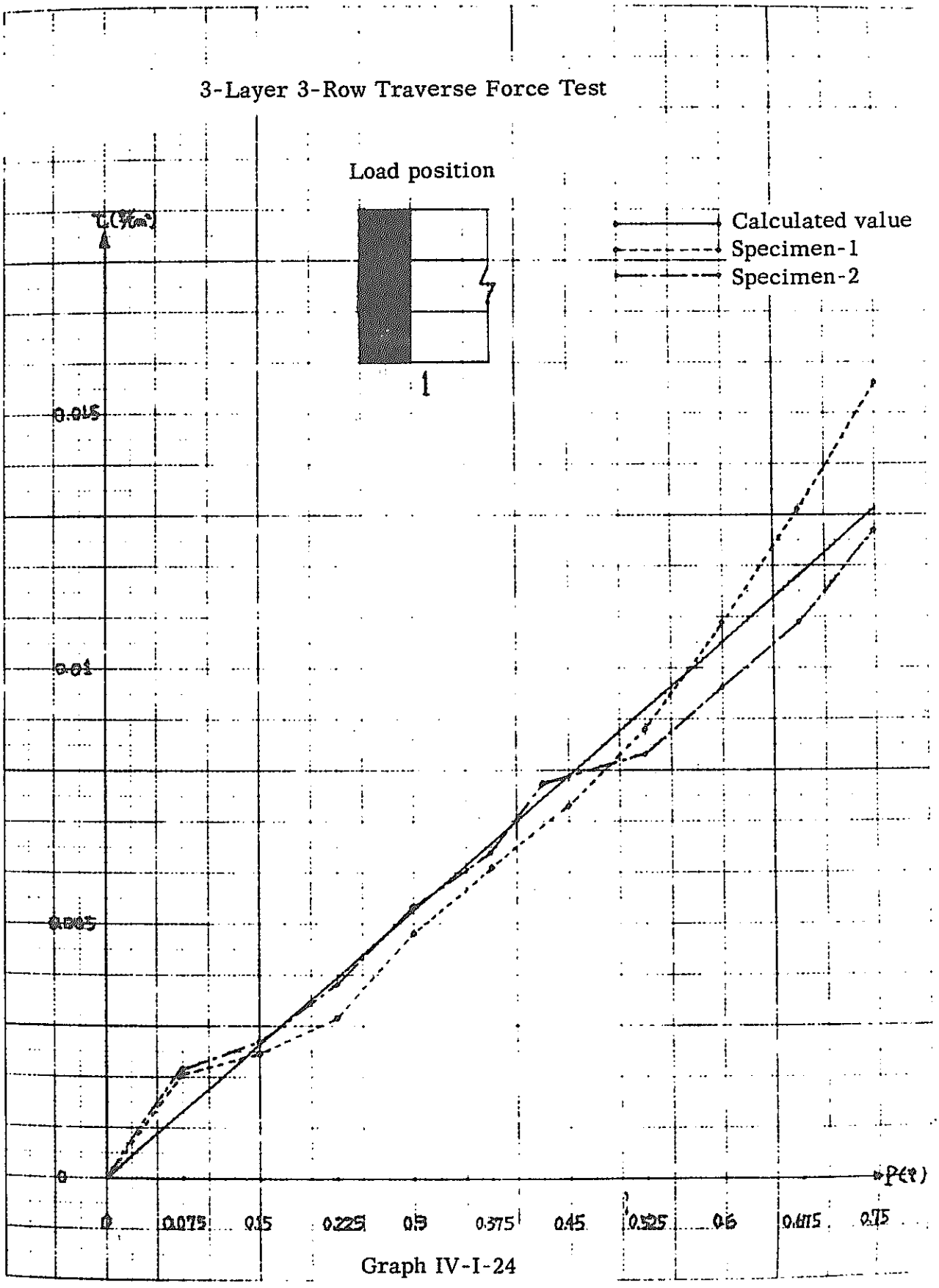
3-Layer 3-Row Traverse Force Test
Load position
Calculated value
Specimen-1
Specimen-2
0.015
0.01
0.005
0
0
0.075
0.15
0.225
0.3
0.375
0.45
0.525
0.6
0.675
0.75

Graph IV-I-24

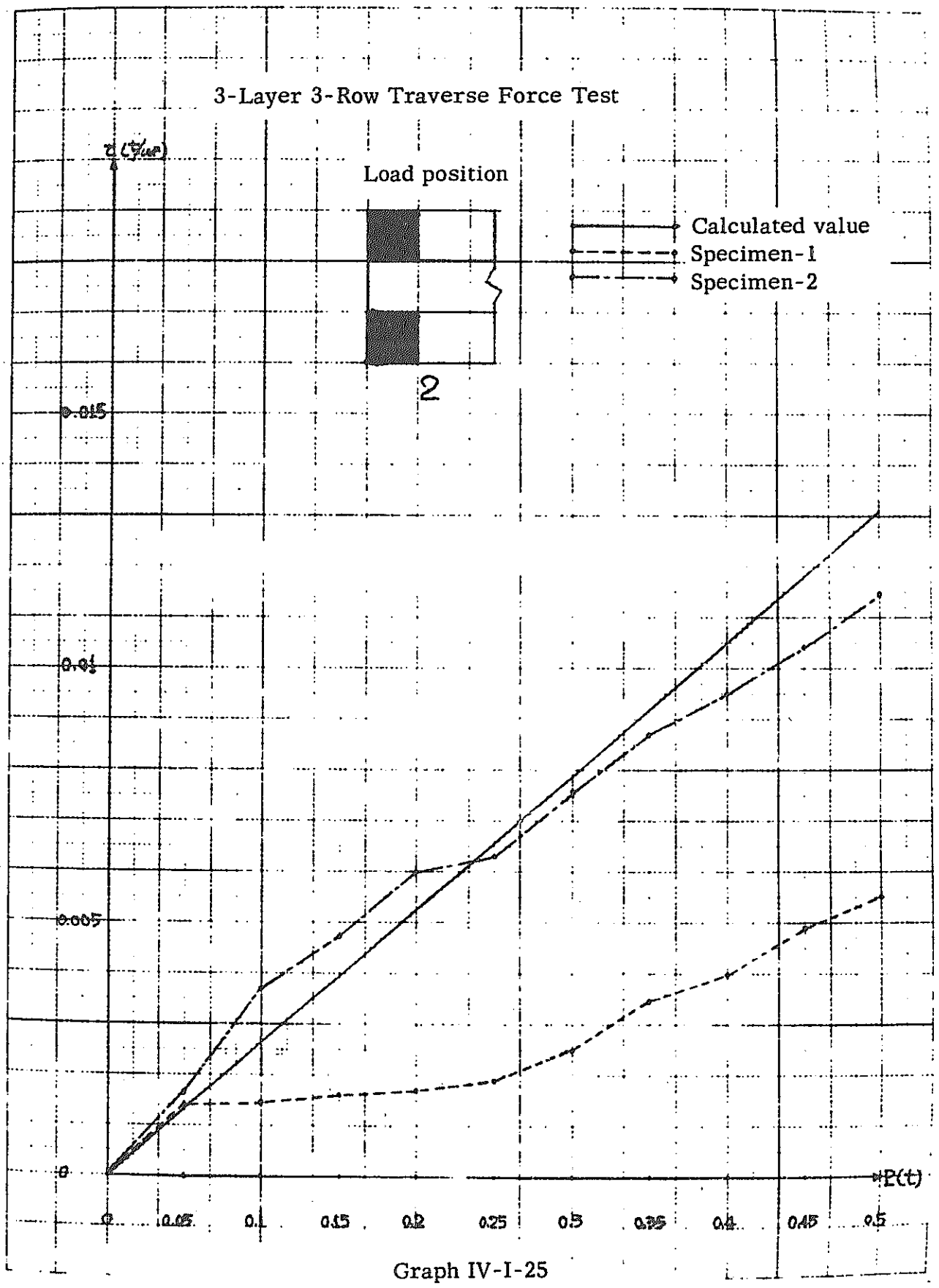
3-Layer 3-Row Traverse Force Test
Load position
Calculated value
Specimen-1
Specimen-2
2
0.015
0.01
0.005
0
P(t)
0
0.05
0.1
0.15
0.2
0.25
0.3
0.35
0.4
0.45
0.5

Graph IV-I-25

Chapter 5 Static Test by Tilting Test Model

5.1 Method of Test

The model is placed on a tilted table of which tilt angle is changed in the following degrees. At each changed angle, the model which tilted on its own dead weight is applied with a static force in a traverse direction by way of a component force in parallel with the inclined plane, and thus the strain and displacement of the model are measured:

$0^o \rightarrow 30^o \rightarrow 45^o \rightarrow 30^o \rightarrow 0^o$	$0^o \rightarrow 30^o \rightarrow 45^o \rightarrow 30^o \rightarrow 0^o$	Y-direction
$0^o \rightarrow 30^o \rightarrow 45^o \rightarrow 30^o \rightarrow 0^o$	$0^o \rightarrow 30^o \rightarrow 45^o \rightarrow 30^o \rightarrow 0^o$	X-direction

5.2 Measuring Method and Measuring Points

All the measuring instruments are arranged and provided in the control room on the 2nd floor. As the model is in a circular form, it is difficult, comparing with ordimary france structure, to specifically select for the measurment the points where the principal stress concentrates. So, the measuring gauges are adhered to the specimens in such directions as vertical, horizontal, and in 45^o and 22.5^o angles where are considered appropriate to measurean overall stress of the specimen as a whole.

5.3 Consideration on Static Tilting Test

The behavior of the blocks under static force is deduced as follows on the basis of the following hypothetic conditions:

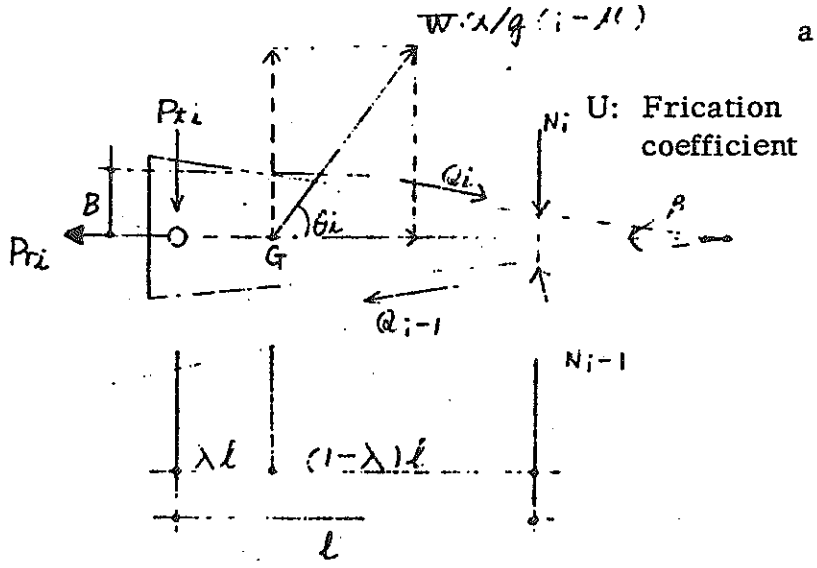

a) Hypothesis:

(1) The phase difference can be ignored in respect of all the blocks.

(2) Under the consideration that blocks can be rotated centering around the pin freely to a desired degree.

$$\Delta Q_i B - W\alpha/g\,(1-\mu)\,\sin\theta_i \lambda \ell + \Delta N_i \ell = 0 \quad (1)$$

$$\Delta N_i = N_i - N_{i-1}\cos\beta\,, \quad \Delta Q_i = Q_i - Q_{i-1}\cos\beta \quad (2)$$

$$P_{ti} + \Delta N_i - W\alpha/g\,(1-\mu)\sin\theta_i = 0 \quad (3)$$

$$P_{ri} = W\alpha/g\,(1-\mu)\cos\theta_i + \Delta Q_i + N_{i-1}\sin\beta \quad (4)$$

G : Center of gravity

α : Acceleration 1 g

W : Weight of one block, 6.5 kg

$\beta = \frac{90^o}{25} = 3.6^o = 0.0625$ rad = sin β cooβ = 1

ℓ = 40.6 cm λ = 0.44

B = 9.4 + 6.7/4.0 = 4.3 cm

μ = tan 7^o = 0.12278 = 0.12 (Friction factor)

When it is i = 1,

$N_{i-1} = 0$ $Q_i = 4.3 \times 9.5 \cos\theta_i$ (*1), kg

$Q_{i-1} = 0$

From Eq. (1), $\Delta N_i = N_i$ is obtained.

Pti is obtained by substituting $N_i = 4N_i$ for Eq. (3).

Pri is obtained by substituting $\Delta Q_i = Q_i$ for Eq. (4).

When a certain restraint condition is considered for the rotation of b) block centering around the pin:

$N_{i-1} = 0$

$\Delta Q_i = Q_i$

Calculating only with 3-4 blocks in front of the spring, and the boundary condition is (i = 1):

$\Delta Q_i B - W\alpha/g \cdot (1-\mu) \cdot \sin\theta_i \cdot \lambda\ell = 0$

$P_{ti} = W\alpha/g \cdot (1-\mu)\sin\theta$

$P_{ri} = W\alpha/g \cdot (1-\mu)\cos\theta_i + \Delta Q_i$

The results of an example of calculation made in respect of blocks No. 11 - 32 with load in Y-direction are shown is Table 5-3-1. While Table 5-3-2 shows the comparative figures between the above results and the results of the test made at 45^o tilt angle. In the conversion of measured strain factors obtained by the experiment into load factors, the figures in the following page have been adopted as the conversion coefficient:

Table 5-3-1 Y-Direction Load on Blocks No. 11 - 32 and X-Direction Load (Acceleration 1 g)

	i =	N_i kg	P_{ti} kg	P_{ri} kg	Q_i kg	ΔN_i kg	ΔQ_i kg
	1	0	0	5.72	40.85	0	0
	2	0.17	0.19	5.78	40.77	0.17	0.08
	3	0.45	0.44	5.93	40.52	0.28	0.25
	4	0.84	0.68	6.00	40.11	0.39	0.41
	5	1.39	0.82	6.03	39.58	0.55	0.53
	6	2.09	1.06	6.13	38.85	0.70	0.73
	7	2.90	1.25	6.16	37.99	0.81	0.86
	8	3.83	1.42	6.14	36.97	0.93	1.02
	9	4.91	1.66	6.20	35.78	1.08	1.19
Y	10	6.11	1.84	6.14	34.47	1.20	1.31
Direction	11	7.42	2.02	6.07	33.05	1.31	1.42
Load	12	8.85	2.20	6.06	31.45	1.43	1.60
	13	10.40	2.37	5.94	29.78	1.55	1.67
	14	12.06	2.55	5.79	27.98	1.66	1.80
	15	13.79	2.68	5.67	26.02	1.73	1.96
	16	15.61	2.79	5.42	24.02	1.82	2.00
	17	17.50	2.91	5.26	21.90	1.89	2.12
	18	19.47	3.03	5.06	16.69	1.97	2.21
	19	21.47	3.10	4.76	17.40	2.00	2.29
	20	23.55	3.21	4.57	15.03	2.08	2.37
	21	25.67	3.27	4.32	12.62	2.12	2.41
	22	27.82	3.34	3.98	10.17	2.15	2.45
	1	2.52	3.20	0	0	2.52	0
X	2	5.01	3.22	3.09	2.57	2.49	2.57
Direction	3	7.24	3.44	3.58	5.11	2.23	2.54
Load	4	9.44	3.42	4.06	7.64	2.20	2.53
	5	11.61	3.37	4.54	10.17	2.17	2.53
	6	13.74	3.31	4.95	12.62	2.13	2.45

	i =	N_i kg	P_{ti} kg	P_{ri} kg	Q_i kg	ΔN_i kg	ΔQ_i kg
X Direction Load	7	15.82	3.24	5.39	15.03	2.08	2.42
	8	17.85	3.15	5.81	17.40	2.03	2.37
	9	19.81	3.05	6.17	19.69	1.96	2.29
	10	21.69	2.92	6.53	21.90	1.88	2.21

Key: $Q(kg) = 0.574 \times 10^6 \cdot \gamma$

Q : Shearing force γ = shearing strain

Pin: $P_r = P_i\,(kg) = 0.01735 \times 10^6 \cdot \epsilon$

ϵ : 2-times bending strain caused to pins

Spring: $P\,(kg) = 1.0 \times 1.0^4 \cdot \epsilon$

ϵ : 2-times strain caused to the spring's circular curved end

	PINS			
		Test Value (kg)	Calculation Value (kg)	Calculation Value - ΔQ: kg
Y Direction	Pt7	2.01	1.25	
	Pr7	6.76	6.16	5.30
	Pt13	2.72	2.37	
	Pr13	2.42	5.14	3.47
	Pt19	1.25	3.10	
	Pr19	2.08	4.76	2.47
X Direction	Pt1	0.17	2.24	
	Pr1	0.17	0	0
	Pt8	3.95	2.25	
	Pt8	1.38	4.07	1.70

KEYS				
		Test Value (kg)A	Calculation Value (kg)B	Ratio B/A
Y Direction	Q7	9. 18	25. 9	2. 8 Average 2. 1-fold
X Direction	Q8	16. 6	12. 2	1. 4

SPRINGS (N_i)					
		Test Value (kg)	Calculation Value (kg)	$\sum_{\ell=1}^{\ell} \Delta N_{N-\ell}$	ℓ
Y Direction		1. 33	19. 47	1. 5	1
X Direction		2. 47	15. 18	2. 68	2

where, ℓ is expressed by $\sum_{\ell=1}^{\ell} \Delta N_{N-\ell}$

The maximum acceleration value (β) is assumable from this tilt test.

Under the force of 0. 707 g in Y-direction, there is seen a strain of 83. 5 (167/2)μ caused to 11 pins. This value, when cross section where the gauge adhered is considered, is 48. 2μ . Although 11 pins have the maximum degree of strain, this is eliminated because of the small strain on this point at the time of dynamic force application.

The yielding stress of pins is σ y = 2. 4 t/cm^2, and the ratio between this value and the ultimate load taking the ratio between the maximum yeilding force and maximum load at the time of the 3-layer 3-row as given in Table 4-2-2, it is 1. 34 times as higher.

$$\beta = \frac{2.4}{E \cdot 48 \cdot 2} \cdot 1.34 = 31.77$$ E: Young modulus = 2100 t/cm^2.

Similarly, β factors obtained from the actually measured values of the springs and keys are respectively:

(From S8) β (spring) = 19. 8 g (exceting S7)

(From K4b) β (Key) = 56. 9 g

As to the keys, if Qi = 40. 85 kg is the maximum value, it is: β = 63. 7 g.

$$\left(\beta = \frac{169 \text{ kg/cm}^2 \times 2 + 2.5 \times 9.5}{40.85 \text{ kg} \times 1.3 \text{ (stress concentration)} \times 2}\right)$$

This results may be considered as indicating a similar trend as in the case of the results of the static force experiment.

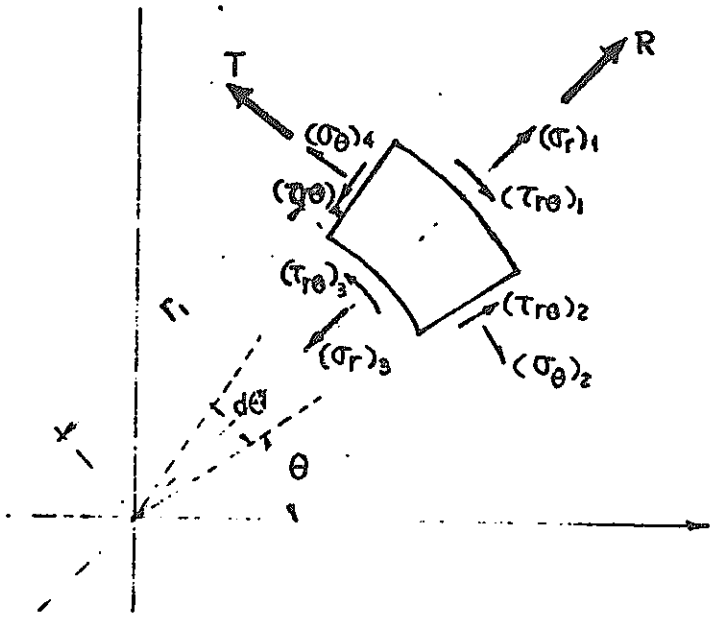

$$R \cdot \gamma d\theta d\gamma + (\sigma\gamma \cdot \gamma)_1 d\theta - (\sigma\gamma \ \gamma)_3 d\theta - (\sigma\theta)_2 d\gamma \frac{d\theta}{2} - (\sigma\theta)_4 d\gamma$$

$$\lim_{d \to 0} \quad \frac{\partial \sigma\gamma}{\partial \gamma} + \frac{1}{\gamma}\frac{\sigma \cdot \tau\gamma\theta}{\partial\theta} + \frac{\sigma\gamma\sigma\theta}{\gamma} + R = 0$$

$$\frac{1}{\gamma}\frac{\partial \sigma\theta}{\partial\theta} + \frac{\partial \tau\gamma\theta}{\partial\gamma} + \frac{2\tau\gamma\theta}{\gamma} + T = 0$$

Placing $\sigma\theta = 0$,

$$\frac{\partial \sigma\gamma}{\partial \gamma} + \frac{1}{\gamma}\frac{\partial \tau\gamma\theta}{\partial\gamma} + \frac{\sigma\gamma}{\gamma} + R = 0 \qquad (1)$$

$$\frac{\partial \tau\gamma\theta}{\partial\gamma} + \frac{2}{\gamma} \cdot \tau\gamma\theta + T = 0 \qquad (2)$$

$$R = -\alpha/g \cos\theta \cdot \rho$$
$$T = +\alpha/g \sin\theta \cdot \rho \qquad (\rho : \text{specific gravity}) \qquad (3)$$

By solving those (1) and (2) by application of Eq. (3), the following boundary conditions are introduced as substitutes:

$$\tau\gamma\theta \, 1\gamma = \gamma_1 = 0$$
$$\sigma\gamma 1\gamma = \gamma_1 = 0$$

$$\tau\gamma\theta = \frac{1}{3}\left[\left(\frac{\gamma_1}{\gamma}\right)^3 - 1\right] \gamma \cdot \sin\theta \cdot \alpha/g \cdot \rho$$

$$\sigma\gamma = \frac{1}{3}\left[\left(\frac{\gamma_1}{\gamma}\right)^3 - 3\left(\frac{\gamma_1}{\gamma}\right)^2 + 2\right] \gamma \cdot \cos\theta \cdot \alpha/g \cdot \rho$$

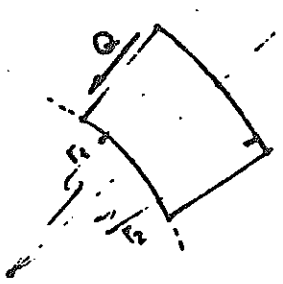

$$Q = \int_{\gamma_1}^{\gamma_2} \tau\gamma\theta \, d\gamma = \frac{1}{3} \alpha/g \cdot \rho \left\{ -\frac{\gamma_1^3}{\gamma_2} - \frac{1}{2}\gamma_2^2 + \frac{3}{2}\gamma_1^2 \right\} \quad \alpha/g \cdot \rho = 1.75 \times 10^{-3} \text{ kg/cm}^3$$

Where, $\gamma_1 = 113.5$ cm is applied, and

$Q = -0.43 \times 10 \cdot \sin\theta$

F. E. M. Model Showing Principal Stress Distribution

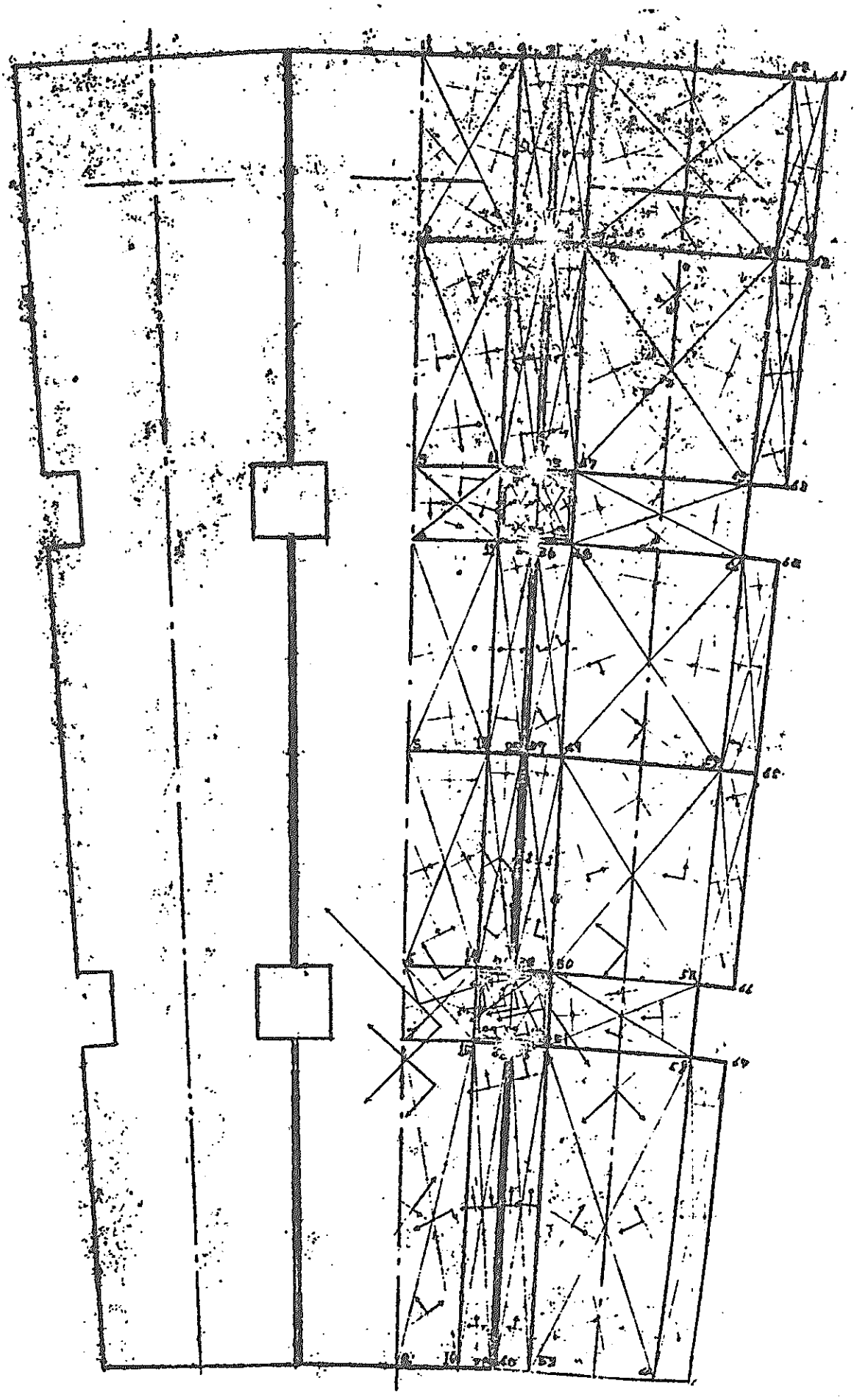

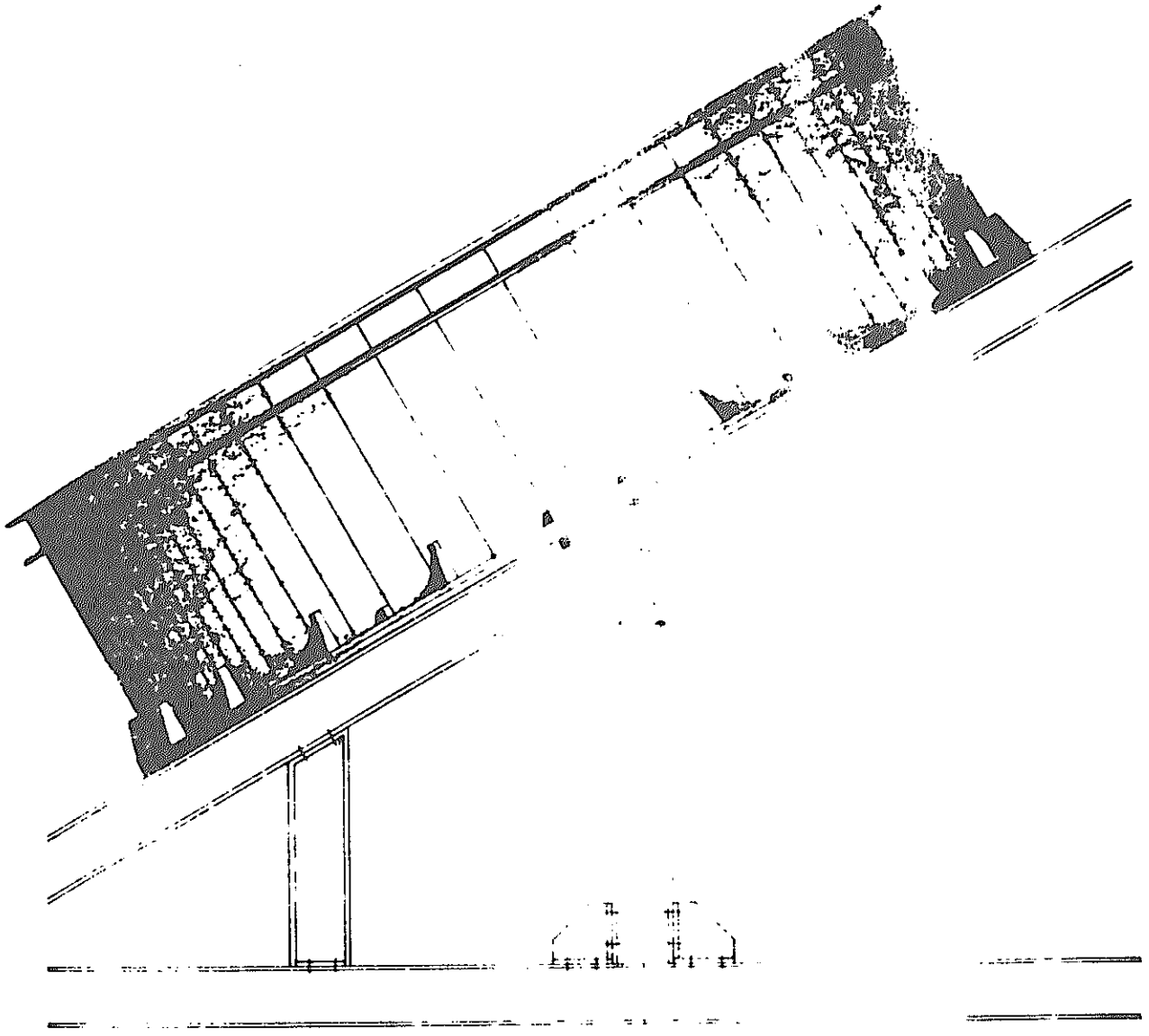

Static Force Test of Tilting Test Model (30^{o} Tilt Angle)

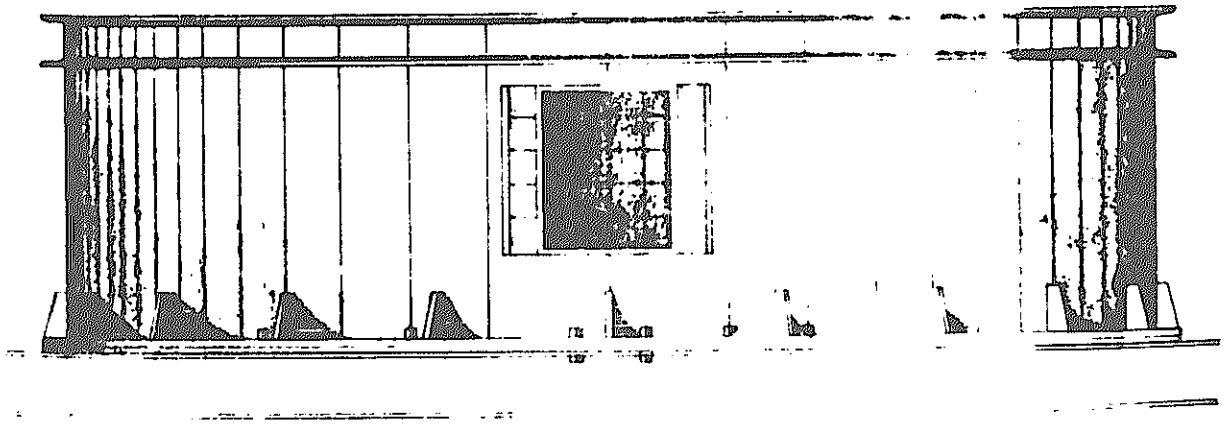

Schematic Drawing of Experimental Vibration Equipment

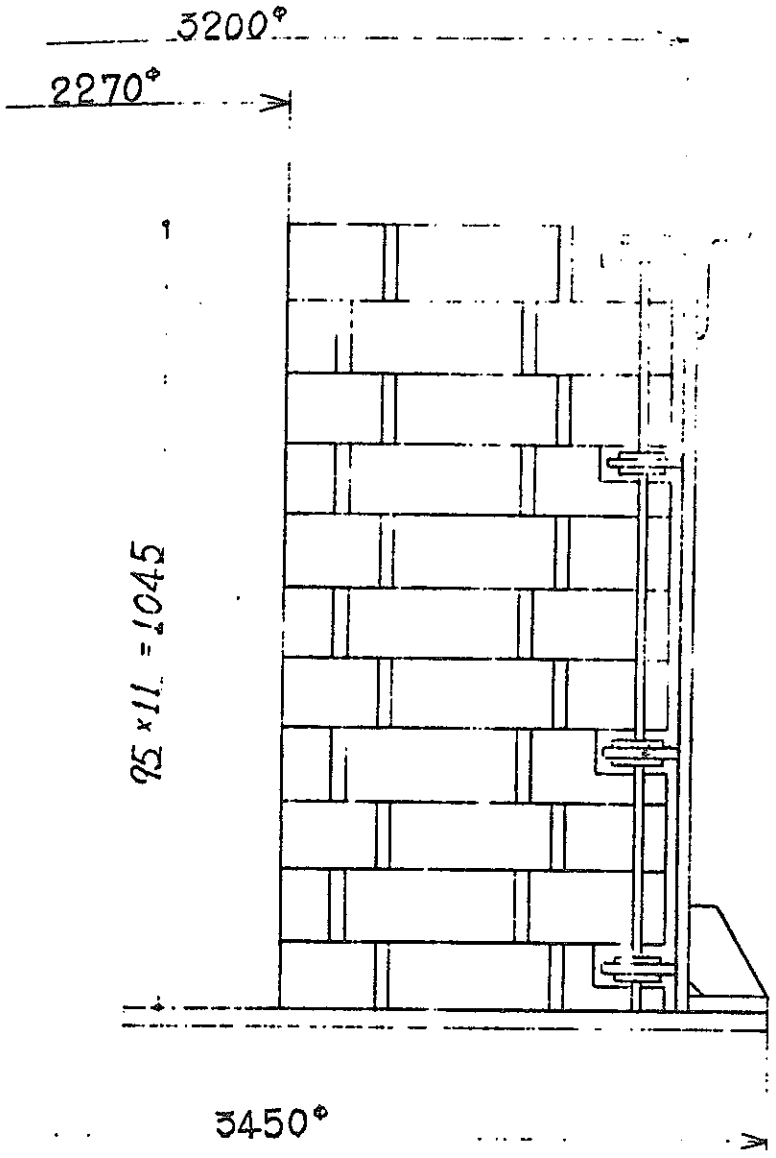

Cross Section (1/10)

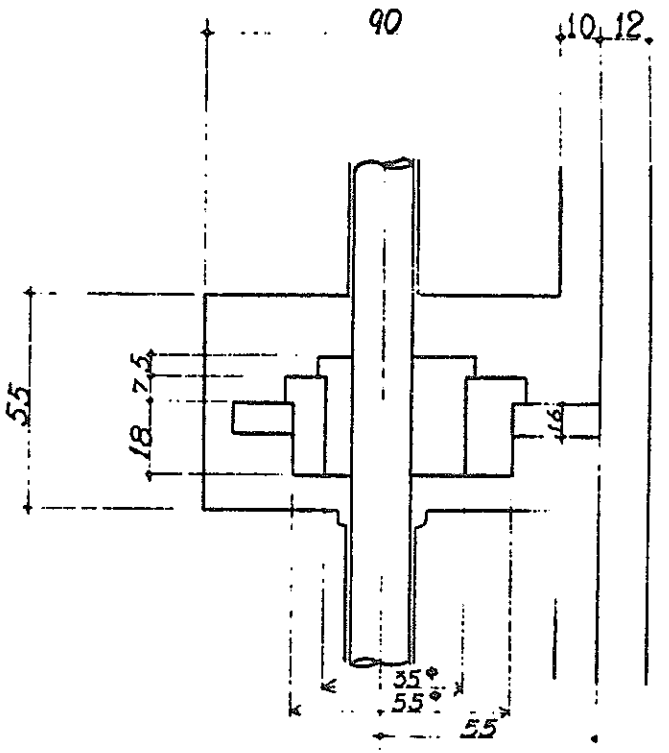

Details in D-Section (1/2)

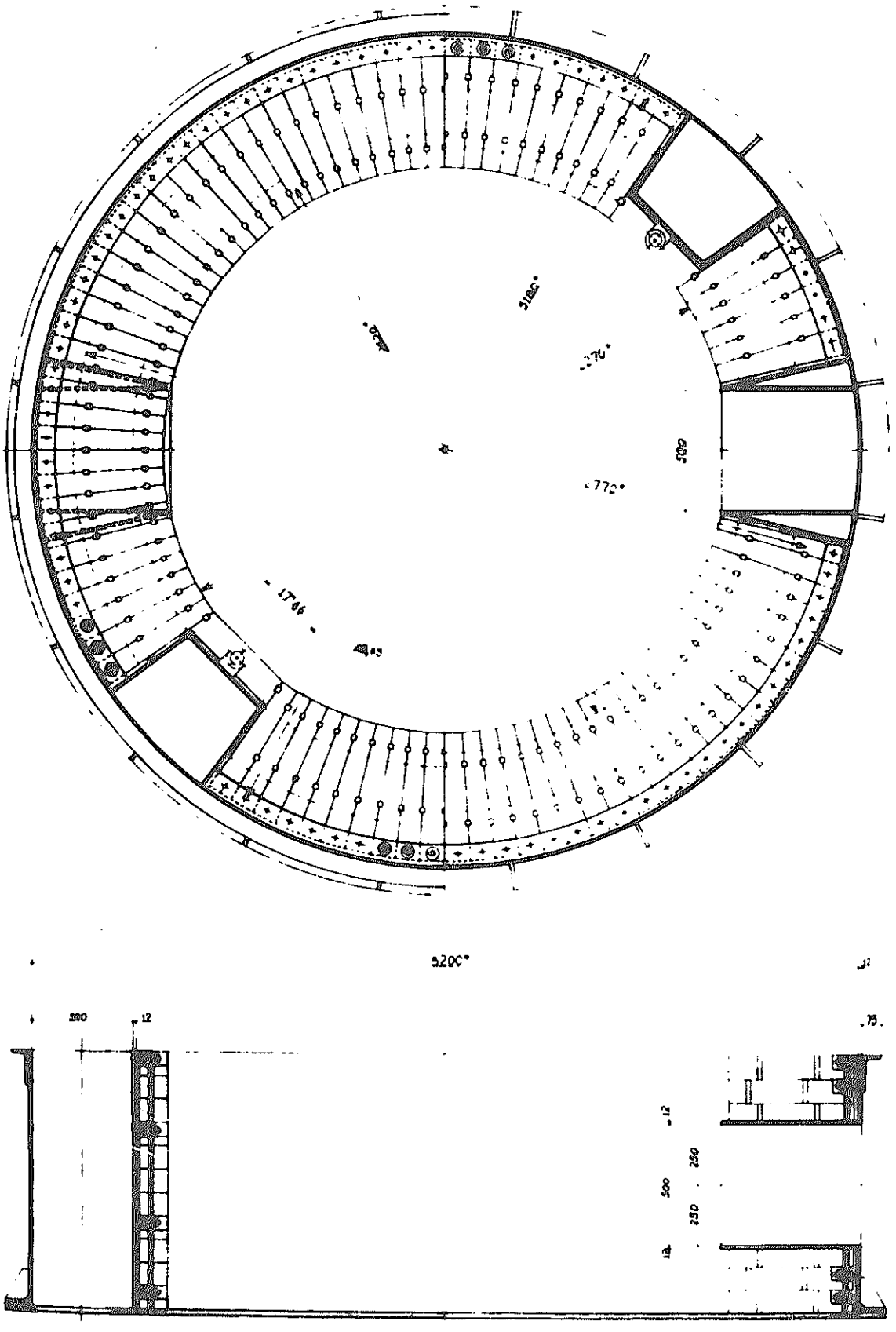

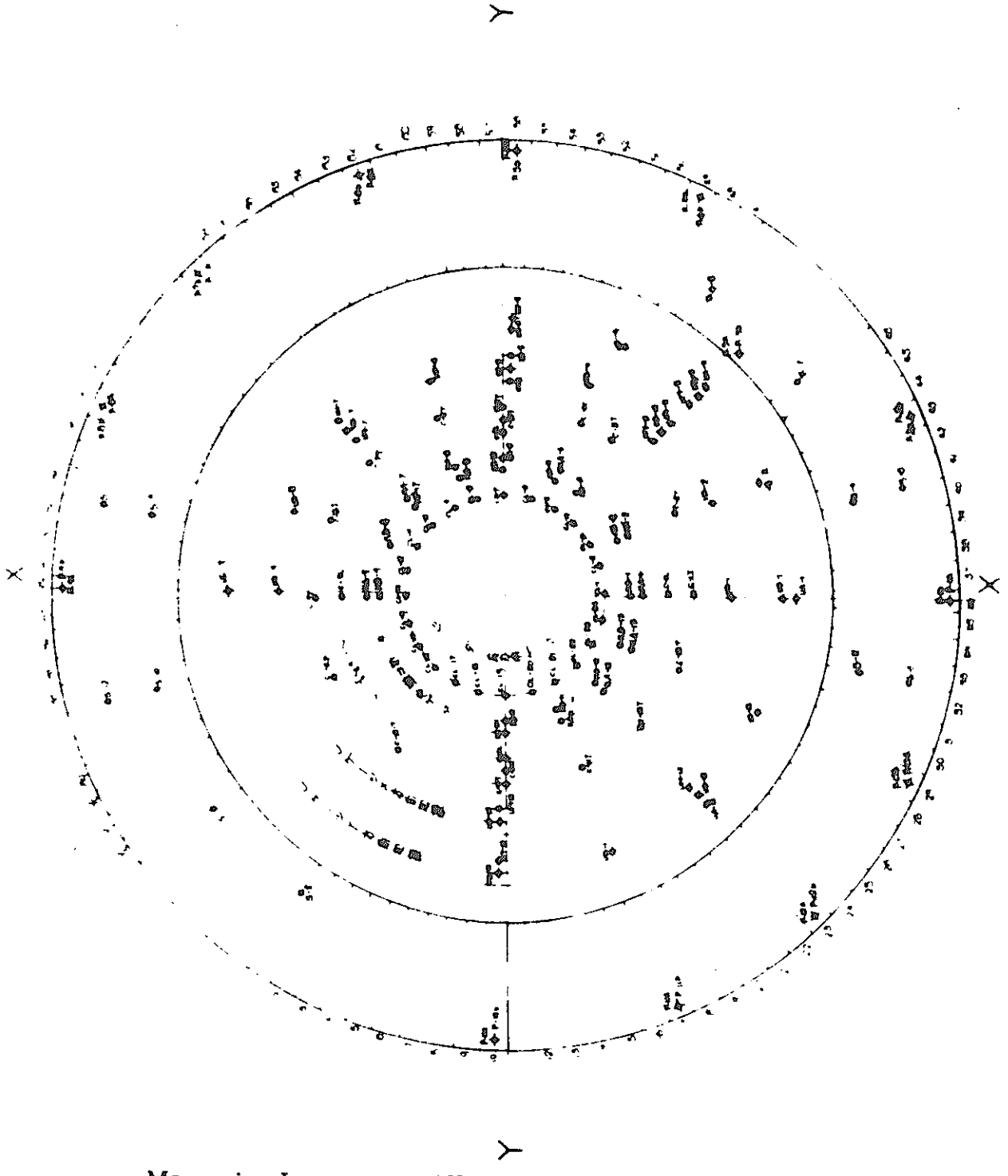

Measuring Instruments Allocated Positions in Vibration and Tilting Test Model

Test No. 12

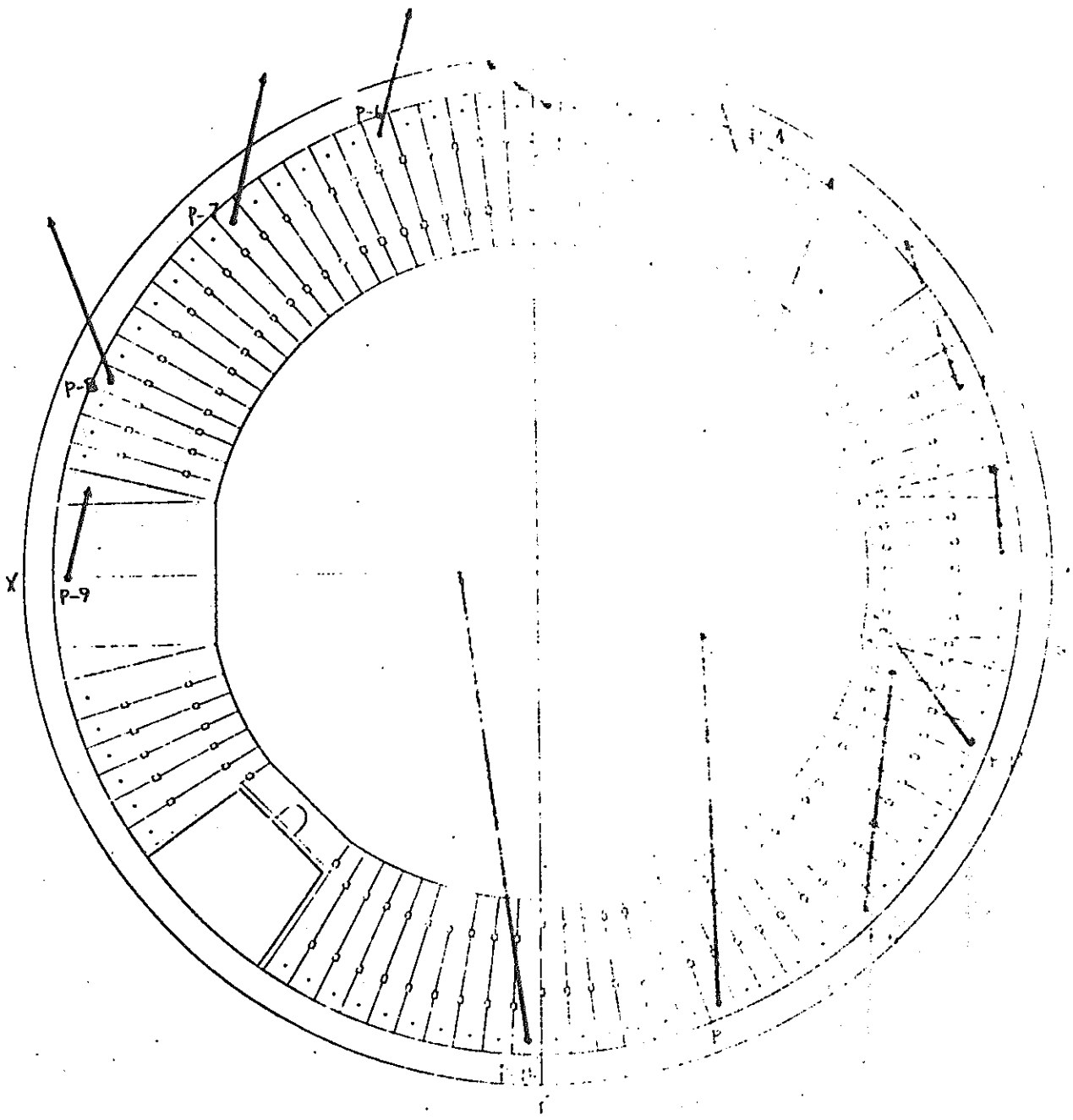

Pin Y-45°

Test No. 12

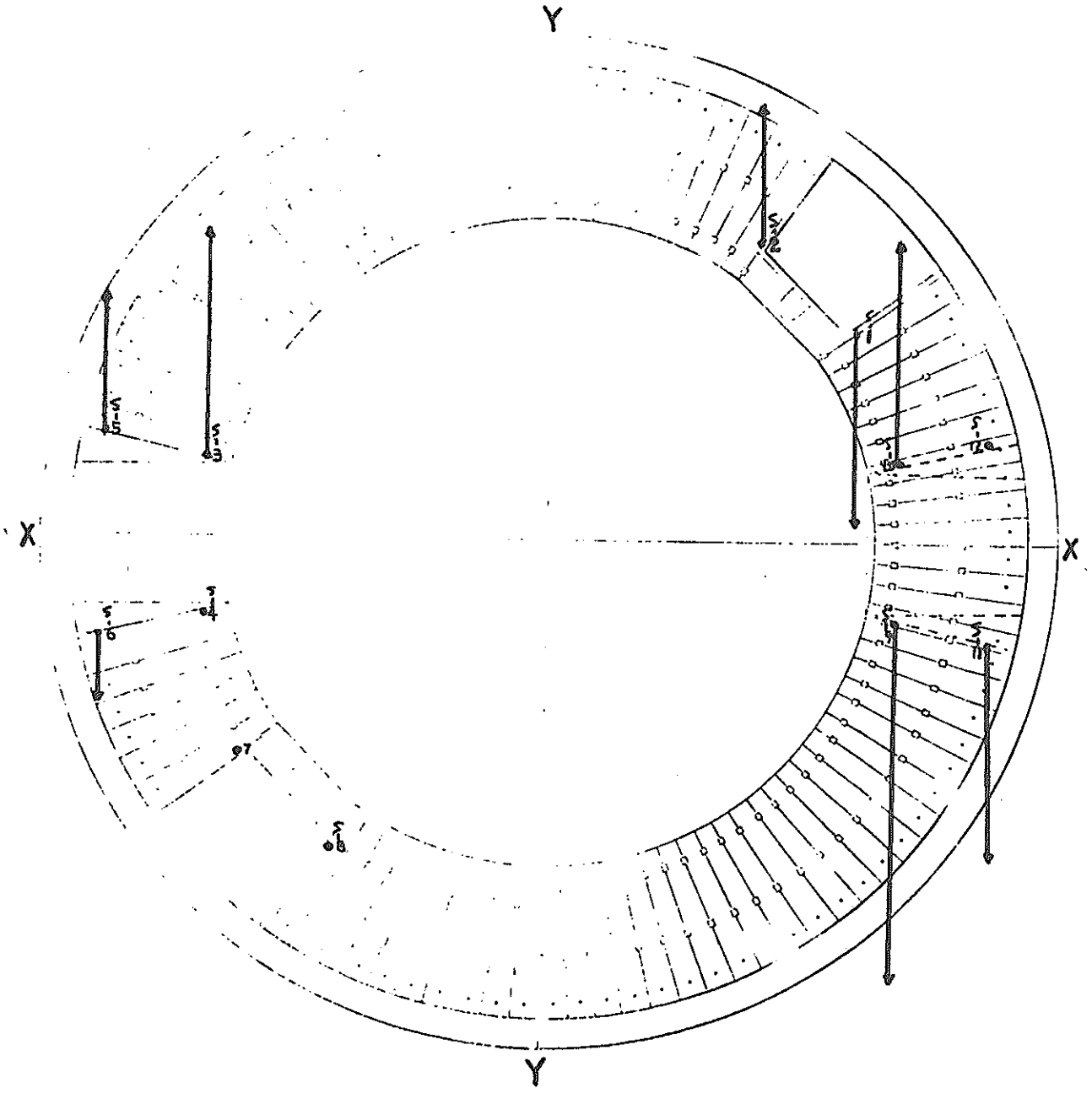

Spring Y-45°

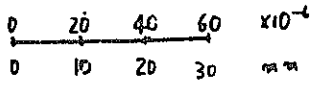

Test No. 12

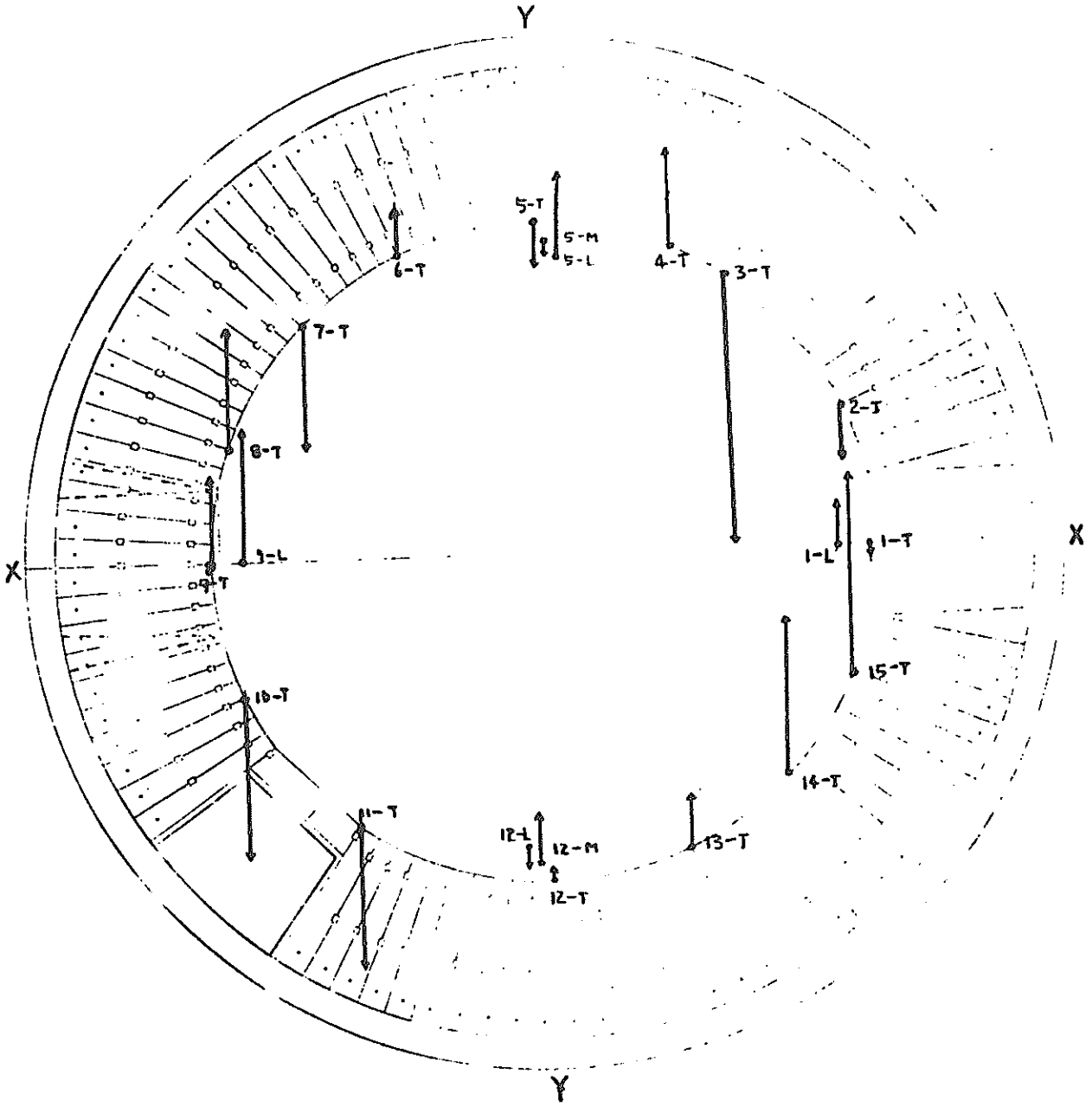

Clip Y-45°

Test No. 12

G = 23.75 ton/cm²

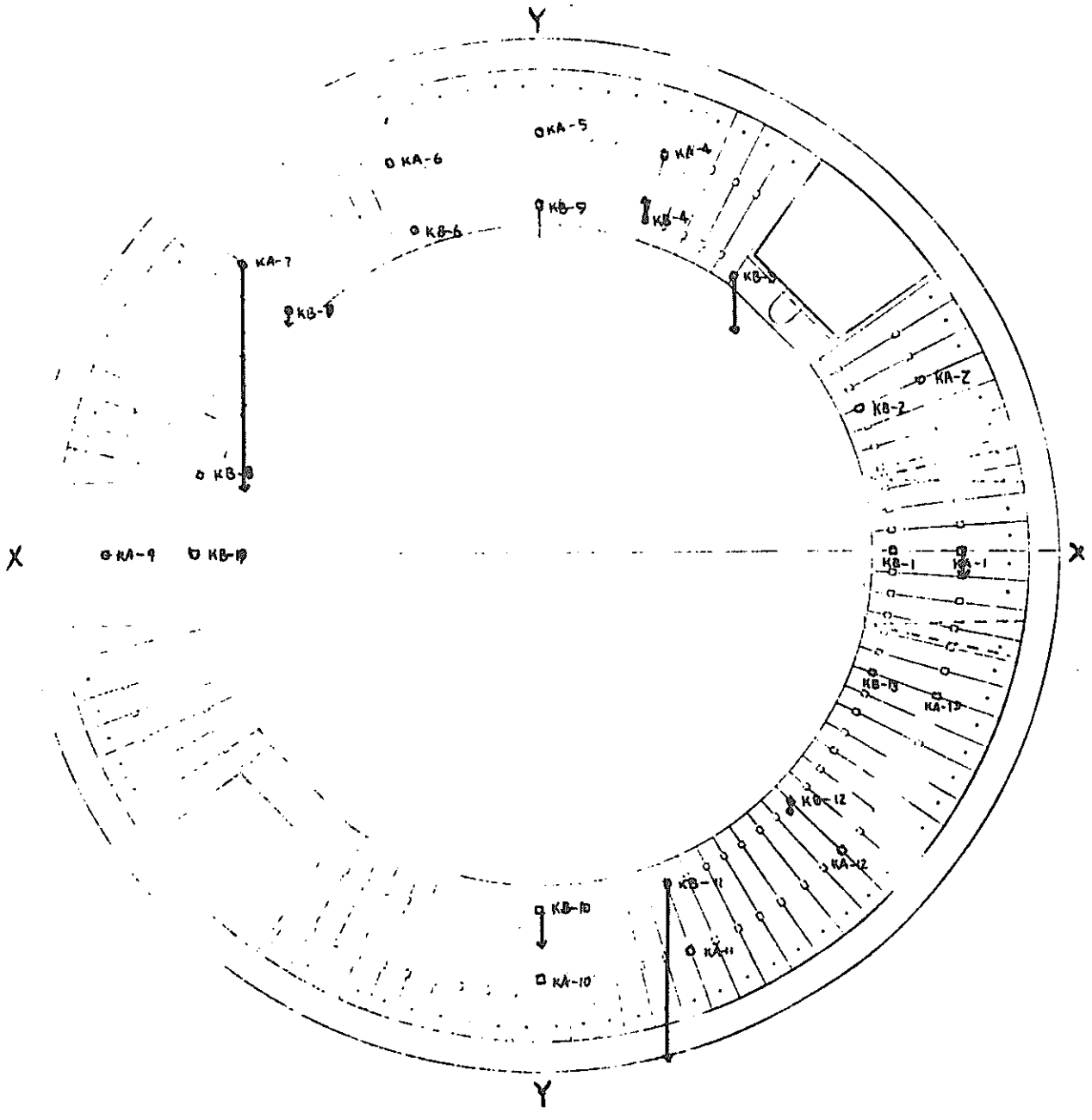

Key Y-45°

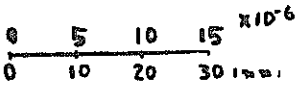

Test No. 12

$E_Z = 356.348 \text{ ton/cm}^2$

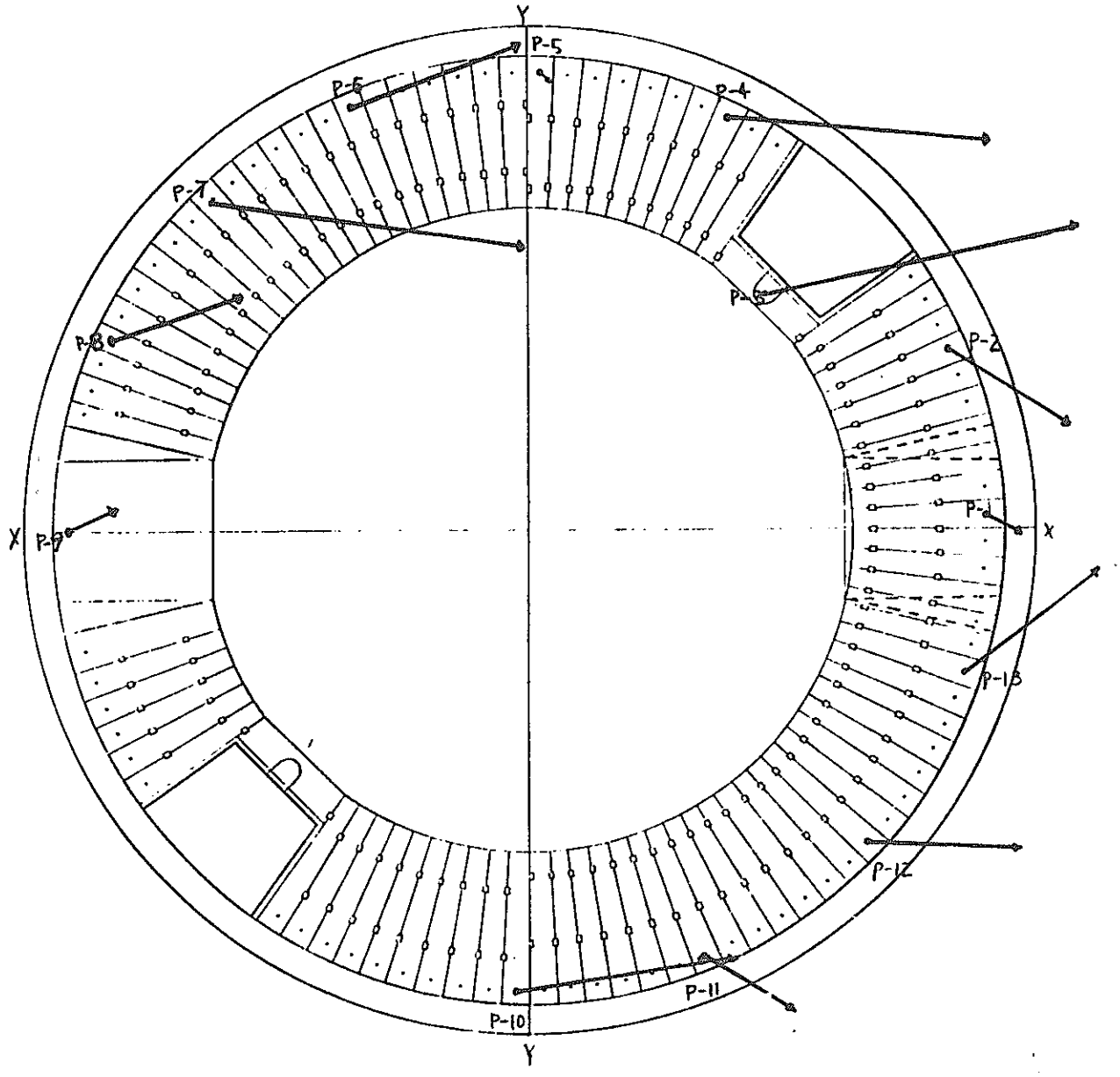

Pin X-45°

Test No. 12

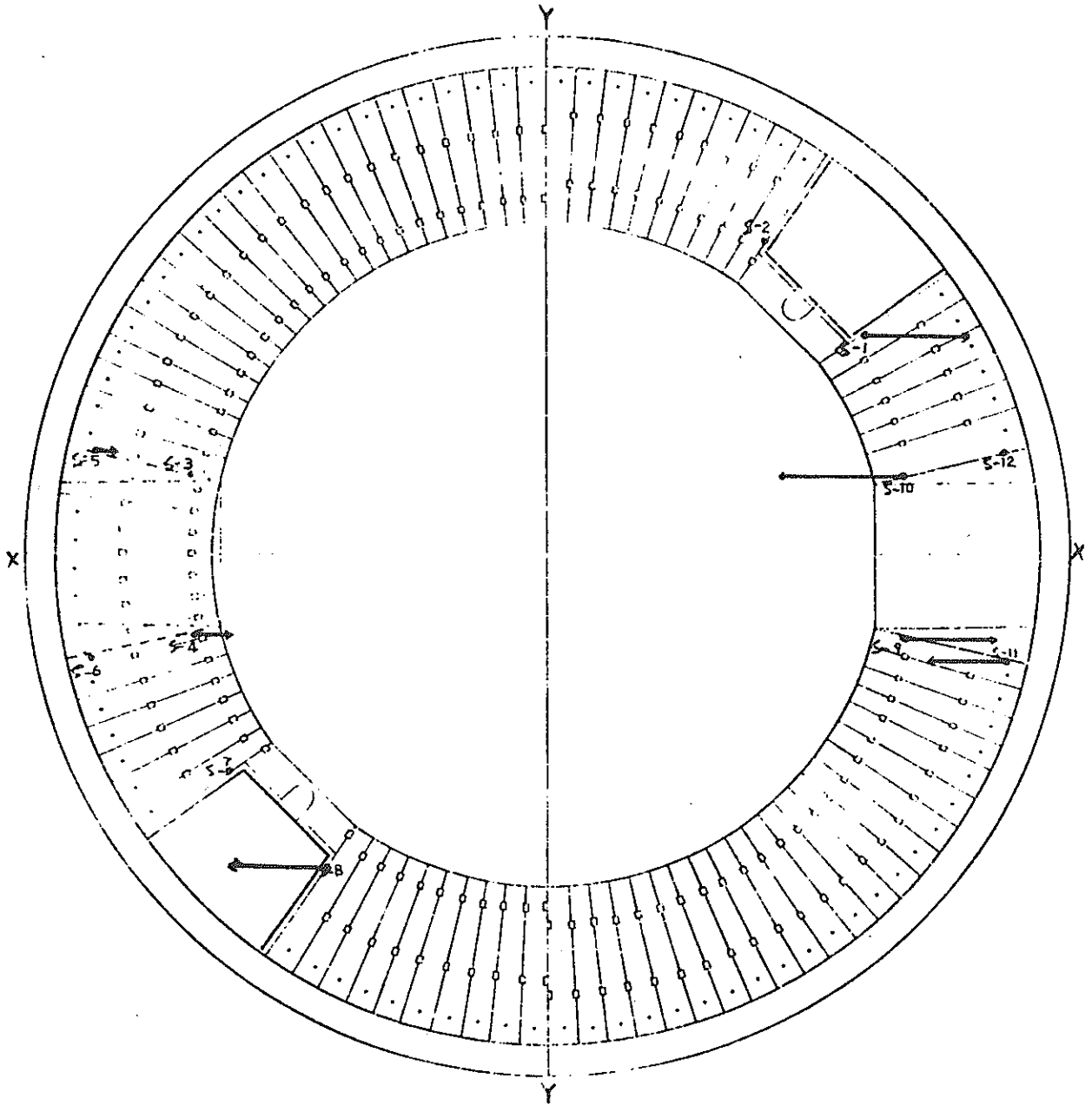

Spring X-45°

0 20 40 60 $\times 10^{-6}$

0 10 20 30

Test No. 12

G = 23.75 ton/cm²

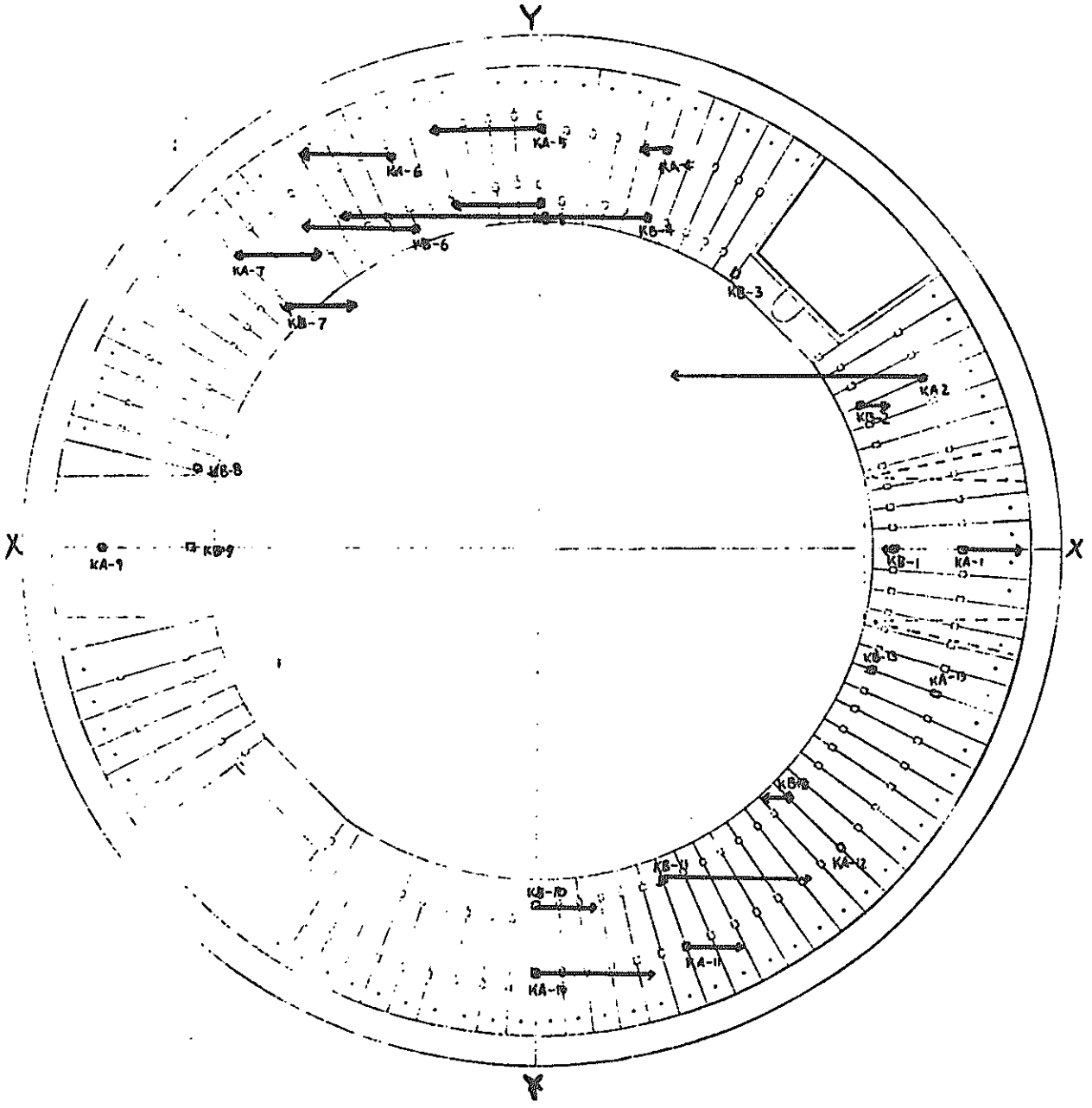

Key X-45°

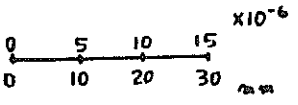

Test No. 12

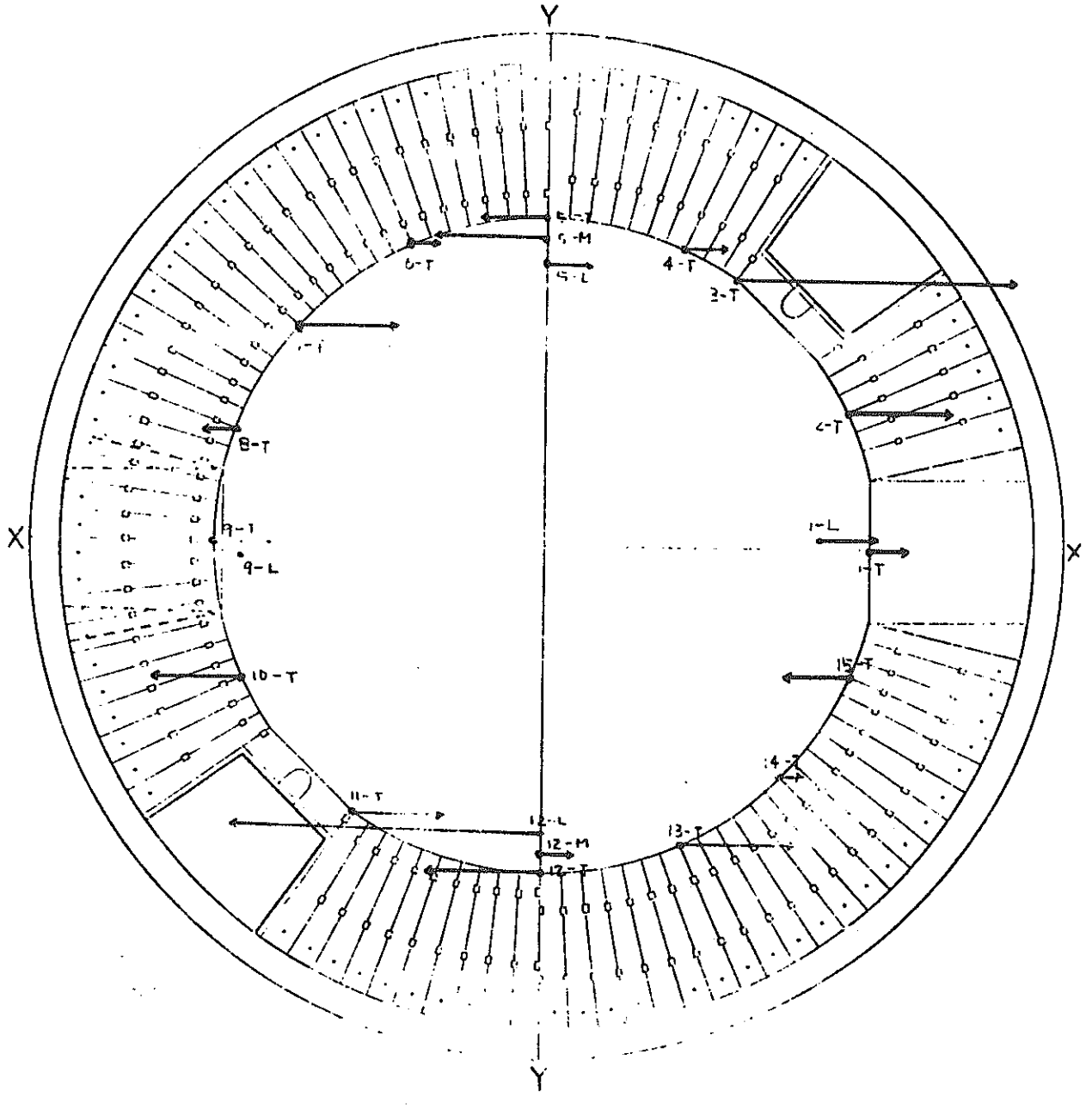

Clip X-45°

0 1.0 1.5 ..

Chapter 6 Vibration Test by Vibration Test Model

6. 1 Test Method and Vibration Table

The Specimen is placed horizontally on the vibration-shaking table. In this case, the specimen is fixed to the table by means of 68 bolts. In such places where bolt tightening is impossible, it is secured by means of welding which is performed with 6 mm of throat thickness and 20 mm of length for each one bolt replacement.

The so secured specimen is applied with various types of vibration such as free vibration, forced vibration, random vibration, etc. to measure the produced stress. For this vibration test, a large capacity electrically operated hydraulic pressure type vibration testing equipment which is installed in the National Disaster Defense Center (Frequency 0. 1 - 50 cps; maximum shaking and vibration force 360 t with sinusoidal and random waves; maximum amplitude ± 30 mm) is employed. The limited capacity of this equipment is shown in the following diagram:

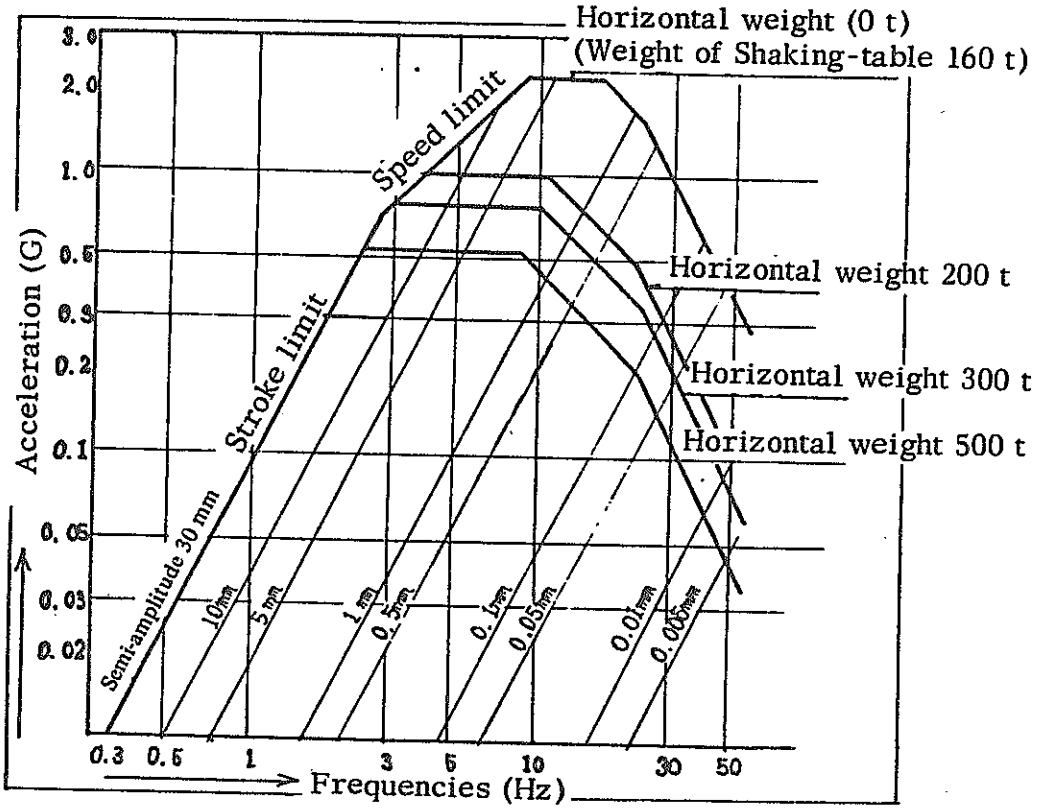

Diagram Showing Limited Capacity

6. 2. 1 Measuring Method and Measuring Points

The same as in the case of the static force test.

6. 2. 2 Results and Data of Vibration Tests

1) Strain and frequencies of Pins: 100, 200, 400 gal, Y-direction
P10b, P11a, 11b, 12a, 12b, 13a, 13b

2) Strain and frequencies of Springs: 100, 400 gal, Y-direction
S1, S7, S3, S5, S9, S11, S2, S8

3) Measured values of acceleration and frequencies: 100, 400 gal, Y-direction
A1, A4, A11, A14, A18, A2(400 gal) A3(400 gal) A12(400 gal)

4) Displacement and requencies of Slip-gauges: 400 gal, Y-direction

5) Strain and frequencies of Keys: 400 gal, Y-direction
K11 A. B K12 A. B K13 A. B

6) Strain distribution of Pins: 6 Hz 100 gal, 400 gal, Y-direction
X-direction (6. 25 Hz)

7) Strain distribution of Springs: 6 Hz 400 gal, Y-direction
X-direction (6. 25 Hz)

8) Gap distribution of Slip-gauges: 6 Hz 400 gal, Y-direction
X-direction (6. 25 Hz)

9) Strain distribution of Keys: 6 Hz, 400 gal, Y-direction

6. 3 Consideration on Vibration Test Results

6. 3. 1 General Characteristics of Vibration Test by Means of Sinusoidal Wave Input

Up until 200 gal of input sinusoidal waves, although the clear resonance point at 6 - 7 Hz and 17 - 18 Hz is considered as coming from the model proper, the resonance at 17 - 18 Hz may be because of, so to speak, the rocking phenomenon of the model since the perpendicular direction rigidity of the table on which the specimen is fixed may be lower than as expected. When the input sinusoidal waves are raised above 400 gal, the resonance phenomenon at around 6 - 7 Hz is not so conspicuous. From this fact, it may be considered the resonance phenomenon in this vicinity is produced by non-linear vibration phenomena. One way to explain this phenomenon is to regard it as a resonance produced by the vibration mechanism consisting of the springs and the blocks.

Here, when obtained the number of blocks which relate to the vibration mechanism to form the resonance point 7 Hz as in the case of the vibration system shown in the following diagram, it is 7.36 blocks:

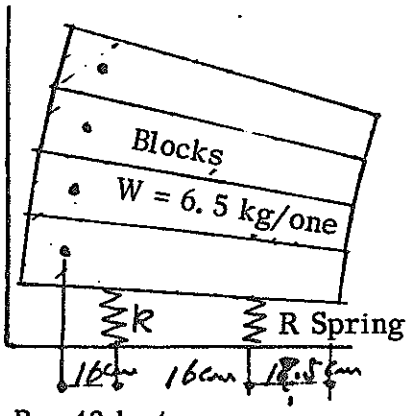

R = 42 kg/cm

Therefore, it is assumable that when input is increased, the amplitude becomes larger, and the number of blocks having relation with the vibration system decreases, and the resonance frequencies thereby change. With this method, however, the fact that the resonance phenomenon has occurred in the section 10 blocks away from the spring is difficult to be reasonably explained. Therefore, the following diagrammed non-linear vibration mechanism can be considered. The equilibrium equation of this mechanism is expressed in the following manner, when perpendicular direction vibration is ignored,

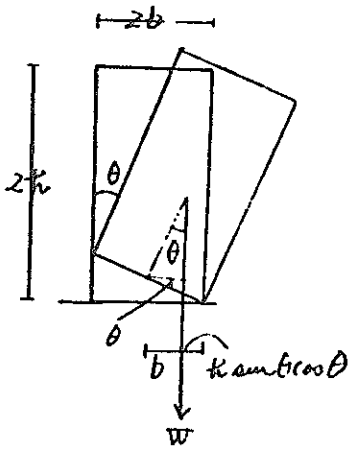

the force equilibrium is:

$$I\ddot{\theta} + W(b - h\sin\theta\cos\theta) = 0$$

and if θ is supposed to be sufficiently small;

$$I\ddot{\theta} + Wb = 0$$

If the initial condition at the top displacement and the initial speed are set as zero:

$$T = \sqrt{\frac{8}{3}} \cdot 2h \sqrt{\frac{\delta}{2gbh}} = 0.052 \cdot 2h\sqrt{\frac{\delta}{2hb}}$$

If it is T = 0.14 sec → 7 Hg, it will be (2h = 104.5 cm 2b = 8 cm) = 0.27 cm in the case of 11th step blocks.

The displacement in the oscillation numbers at 7 Hz corresponds to an acceleration of 530 gal, and if the center of rigidity exists at the 1/3 of the height, the input acceleration is 177 gal.

In the next, as another characteristics of this vibration test, here will be introduced the phenomenon producing a large acceleration in an extremely short limited time as the result of block collisions. The collision impact shock acceleration is tremendously larger than originally planned. In the oscillograph recording of the acceleration values shows highly irregular "sharp peaks" as shown here:

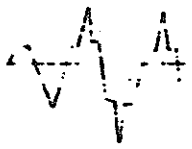

Vibration frequencies with this "sharp peaks" are so high that these exceed the measuring frequency range of the acceleration oscillometer (100 Hz - 10 Hz), and do not necessarily represent the actual acceleration values as recorded, and rather they may represent the velocity values. In accordance with *2, the test results with more conspicuous "sharp peaks" are classified into two categories of "sharp peak conspicuous" and "non-sharp peak mark".

In addition, the overing deformation at the most external periphery of the steel cylinder as originally expected is so minor that it has been almost impossible to detect it during the vibration test.

6. 3. 2 Behavior of Pins

The strain distribution of pins in 45° Y-direction of static tilting test and the strain distribution of pins at the time of 400 gal sinusoidal wave input in Y-direction are extremely similar. From this, the equivalent acceleration applied to graphite from the strain distribution of pins at 400 gal can be deduced from the tilting test.

	A Tilt 45° 700 gal (kg)	B 100 gal, 7. 5 Hz (kg)	Amp ratio B/A	C 400 gal, 2 Hz (kg)	Amp ratio C/A
11a	2. 01	1. 45	0. 73	8. 3	4. 1
12b	2. 42	1. 3	0. 47	8. 6	3. 6
13a	3. 10	1. 45	0. 47	12. 3	4. 0
13b	2. 08	1. 17	0. 57	(3. 45)	
Average			0. 56		3. 8
	100 gal 0. 56 x 700/100 = 3. 9			400 gal 3. 8 x 700/400 = 6. 8	

Note: Kg in this table represents the force applied to pin in the radial (a) and tangential (b) directions by a block and converted from the pin's strain.

From this table, the amplification factor converted into the equivalent acceleration at the time of 100 gal input is 3. 9 times as higher, and at 400 gal input, 6. 8 times as higher.

6. 3. 3 Behavior of Keys

As in the case of 6. 3. 2, the test data of 45° Y-direction and the test data at the time of 400 gal input are compared as shown in the following table:

Key No.	A Tilt test Kg	B 400 gal At input	Amp Ratio B/A
11a + 11b	9. 18	18. 4	2. 4
12a + 12b	14. 89	30. 0	2. 01
13a + 13b	8. 7	11. 2	(1. 25)

Magnification: 2 x 700/400 = 3. 5

From this table, the amplification factor converted into the equivalent acceleration at the time of 400 gal input is 3. 5 time as higher. This values is about 1/2 of the Magnification calculated from the measured value of pins.

6. 3. 4 Behavior of Springs

When comparison is made in the same way as in the case of Section 6. 3. 2, the amplification factor is 1. 75, which is about 1/2 of the magnitude computed from the measured values of keys.

6. 3. 5 Gap between Blocks

When the gap at the top, medium section and the bottom part of the blocks between No. 10 and No. 11 are examined during the 400 gal Y-direction vibration, the gap or the opening shows a perpendicular distribution as represented by the following diageam:

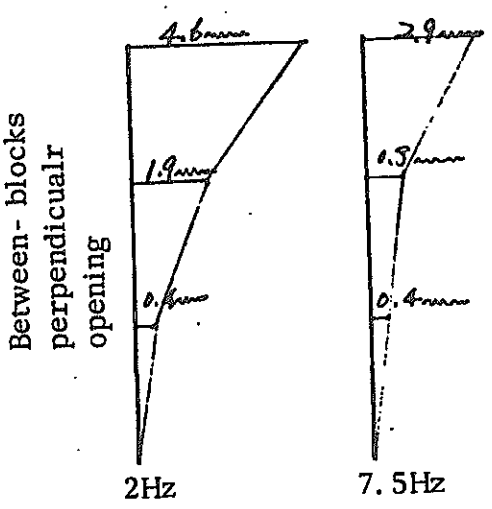

Generally, horizontal distribution of gap on radial direction of vibration is more remarkable on the top then on the bottom, and less on the perpendicular vibration direction. The values of gap, however, are indefinite and show only a general trend.

6.3.6 Acceleration Mode

The modes of the respective points of the model on the basis of acceleration input at the bottom section of the specimen under 100 gal and 400 gal inputs respectively are shown in the following diagram. (Refer to Page)

As self-explanatory from the graph, the acceleration amplification factor of the outer periphery of the cylinder in the perpendicular direction is between 0.85 - 2.60, while the internal perimeter graphite's acceleration amplification factor is between 0.85 - 2.26. In both cases, their respective amplitudes vary very widely. In the case of the "sharp peak conspicuous", the former's amplification factor is 1.0 - 5.20, and the latter is 1.0 - 9.23. These values, when compared, the latter has a considerably larger discrepancy. This trend more remarkably indicates itself in the case of 400 gal input than 100 gal input.

Meanwhile, viewing the acceleration distribution at the upper section of the horizontal plane, it is greater in the area above the internal graphite perimeter, particularly in the vicinity of 45^{o}, 22.5^{o} from the vibration direction. It is, however, difficult to find the generally applicable rules.

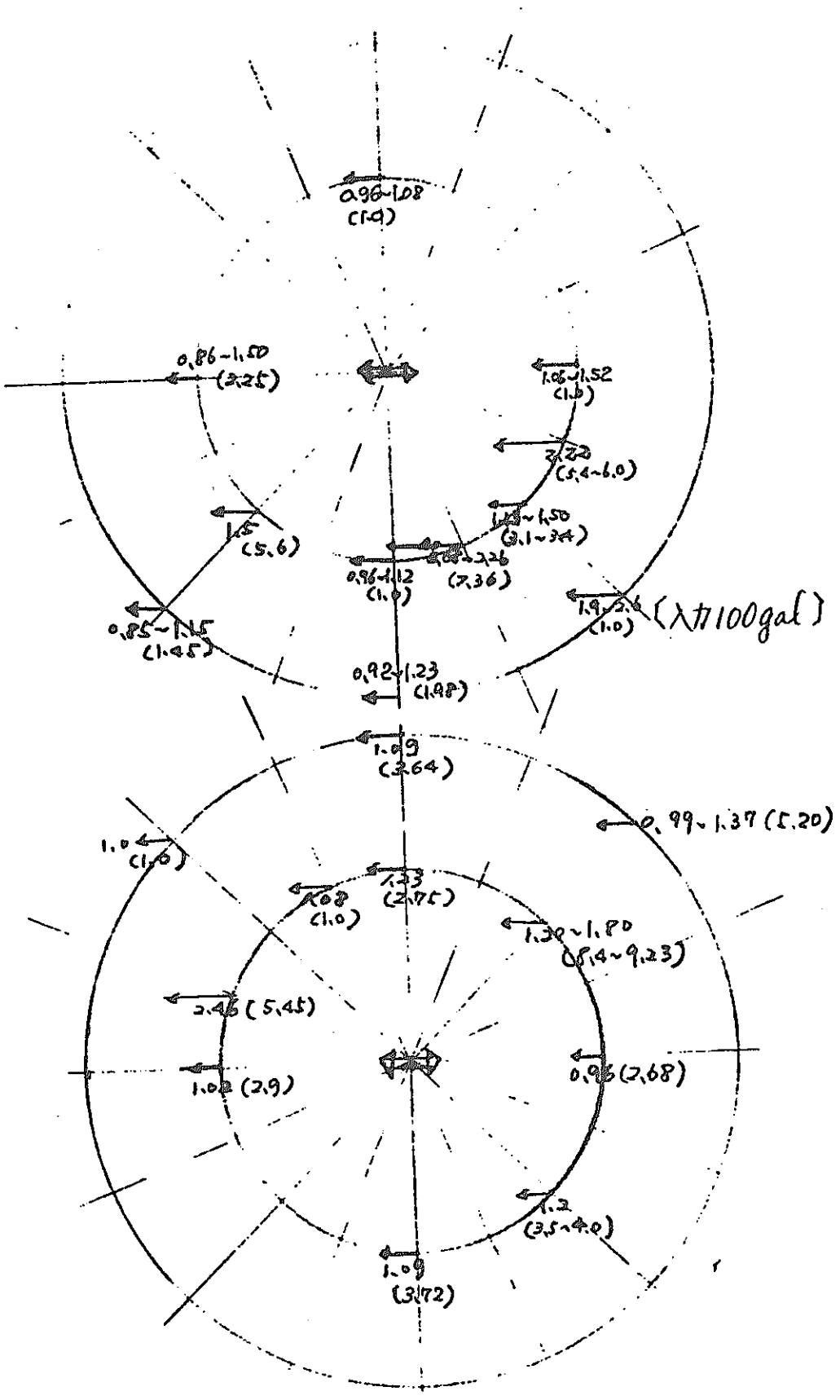

(Input 400 gal)

( ) shows the case of "sharp peak conspicuous"

6. 3. 7 Allowable Acceleration Values (β) Including Dynamic Amplification

Considering the maximum dynamic acceleration value (β) from Paragraphs 6. 3. 2, and 6. 3. 4, the static force value (β) of the tilting test is:

Pin: β = 31. 77 g Spring: β = 19. 8 g

Key: β = 113. 8 g

The amplification factor of dynamic force for pins, keys and springs at 400 gal are 6. 8, 3. 5, and 1. 75 respectively. When β values are divided by these values, there will be obtained the values of β including the dynamic amplification. These are

Pin : β = 4. 67 g

Key : β = 32. 5 g

Spring : β = 11. 3 g

On the other hand, judging from the responding amplification factors as indicated in Paragraph 6. 3. 6, the maximum responding amplification factor of the "sharp peak consipcuous" is 9. 23, and that of "non-sharp peak" is 2. 26 holds. The responding amplification factor, 6. 8, of pins is regarded as belonging to consederably a safety side with inclusion of certain elements of the "sharp peak conspicuous." Consequently, the pin's β value of 4. 67 g should be deemed virtually lower than the actual value and sufficiently a safe one.

6.4 Assumption of Response Analysis

The specific values have been sought by making a model of the vibration system of a nuclear reactor, reactor vessel and the reactor structure with the safety vessel and the graphite shielding structure installed.

Fig. 6.4.1 shows the model of the vibration system, and the perticipation functions of the respective mode numbers at the points where the graphite shielding structure is connected and obtained by the vibration system are shown in the following Table 6.4.1.

On the other part, a model of a safety vessel including graphite shielding structure is mode to obtain its own eigen values. Fig. 6.4.2 shows the model of this structure vibration system, and Fig. 6.4.3 represents the foundamental, second and third modes.

As is known from these results, the vibration period of resonance of the structure is short, and in the vicinity of this period, the participation functions at the points of the structure's contact in the nuclear power reactor building shows substantially lower values compared to the values of the foundamental and second modes.

E ℓ Center (NS)

1) If the damping coefficient in the response spectrum of E Centro (NS) and taft (EW) is 0.05 and $T < 0.5$ sec., then the acceleration response amplification factor is $\simeq 2.0$.

2) From the formulation proposed by Dr. Umemura for the approximate upper limiting value of the various response spectrum:

$Sd = 90\ T^2$ ($T < 0.5$ sec)

Sd = Response displacement

This is converted into a response acceleration. Then, it is, Sa constant 3600 gal 3.6 g. (If the input acceleration is 1.8 g, the acceleration response amplification factor is 2.0)

Table 6. 4. 1 Participation Functions at Each Order Number

Order No.	Cycle (sec)	Participation Functions	
		Upper Section	Bottom Section
1	0. 346	0. 659	0. 69965
2	0. 154	1. 049	3. 1162
3	0. 143	-0. 5614	-0. 41861
4	0. 140	0. 05476	1. 4389
5	0. 093	0. 11656	0. 023767
6	0. 089	-0. 00061967	-0. 00011075
7	0. 078	-0. 43432	-0. 14854
8	0. 066	0. 0982	0. 04693
9	0. 058	0. 00824	0. 0075477
10	0. 045	-0. 000562	0. 000000295
11	0. 03936	0. 0089767	0. 00052016
12	0. 03060	0. 00086507	0. 012661
13	0. 02973	-0. 00020847	-0. 032101
14	0. 027311	-0. 0071432	0. 033554
15	0. 02512	-0. 00022897	0. 00036848
16	0. 024785	0. 0099906	-0. 014005
17	0. 021587	-0. 00120	0. 00071269
18	0. 020569	-0. 00000087485	0. 00000053348
19	0. 016675	-0. 00055357	0. 000020979
20	0. 01548	-0. 00000014448	-0. 000000021188
21	0. 01311	-0. 000011622	-0. 0000042851
22	0. 0122	-0. 00000019929	-0. 0000018236
23	0. 01095	-0. 000000002896	-0. 0000000010002

The natural periods of the respective mode number of vibration system model as shown in Fig. 6. 4. 1 are not more than 0. 5 seconds. Assuming that the response amplification factor is the constant value of 2. 0, response values at the points where the graphite shielding streucture directly contacts within the reactor building have the value of 2. 8739, which is derived by multiplying the root mean square value of the structure base by the response amplification factor. This value is likewise nearly the same as

the values on the upper section of the structure. This fact means that at the time of an earthquake, the structure has no particular amplification of vibration, thus maintaining almost the similar behavior as that of its base.

6.5 General Comments

i) The size of the model used for this vibration test is a 1/2 scale model of the actual size structure. Therefore, in the case of a bending deformation wrought upon this 1/2 scale model, it means that it has a 2 times valuel of vibration frequency in the case of the real size structure, and thereby the vibration acceleration factors to be applied to examine the vibration characteristics must be twice as much of the actual size values.

Also in respect to the deformation phenomenon produced by the specimen in the axial direction, it will have the same vibration characteristics as in the case of the actual size counterpart without regard to its reduced model scale. The vibration acceleration factor to examine its strength is likewise the same as that of the actual size structure. These facts may be well understood by the both behaviors at the time of the application of a horizontal vibration and vertical vibration force to the square column canty lever model.

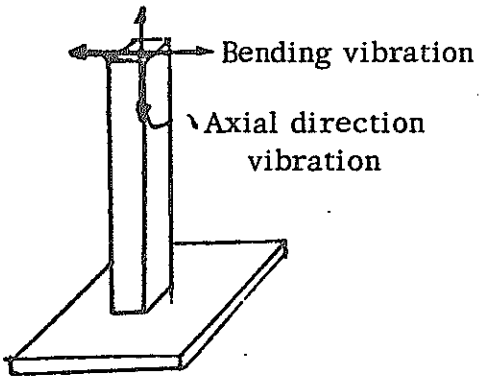

In this experiment, bending deformation has more controlling emphasis, and therefore, the bending deformation simulation laws should be observed. But since an axial direction deformation is also included in the experiment, it is taken into consideration of that effect.

The actual seismological recording experiments were undertaken as follows:

1. El Centro Earthquakes (May 18, 1940, NS maximum 330 gal)
2. El Centro Earthquakes (May 18, 1940, NS maximum 330 gal)
   PRV bottom section response acceleration wave.
3. Tokachi Off-Shore Earthquakes, Hachinoe Port, EW (May 16, 1968, maximum 185 gal)
4. Hidaka Sankei (Mountain Range) Earthquakes, Hiroo records EW (Jan. 21, 1970, maximum 437 gal)

Transformed into 1/2 actual hour, and the maximum acceleration value is made twice as much of the above, namely:

1. El Centro Earthquakes (May 18, 1940, NS maximum 660 gal)
2. El Centro Earthquakes (May 18, 1940, NS maximum 660 gal)
3. Tokachi Off-Shore Earthquakes, Hachinoe Port EW (May 16, 1968, maximum 370 gal)
4. Hidaka Sankei (Mountain Range) Earthquakes, Hiroo records EW (Jan. 21, 1970, maximum 874 gal)

The vibration force of these records were applied to either direction of X and Y, but neither collapse and damage on the vibration model were observed.

ii) The Maximum Allowable Dynamic Acceleration Factor β

When values β, which have been obtained as the results of the static strength test, tilting test, and be the vibration test, are summarized as shown in Table 6. 5. 1. But these values have no meaning of respective equivalences, rather, they should be interpreted as indicating certain computation approach for obtaining β factors for the vibration test.

iii) In case that the entire structure including building is considered as one model of vibration system, the separated portion of the vibration system is considered as equivalent system for the graphite shielding structure. Where by it becomes necessary to show a volume to represent the mutual relationship of the entire and separated system. This is, therefore, described as the response consideration in Chapter 6. 4, of which ground acceleration, if assumed.

Table 6. 5. 1

	Pin (g)	Key (g)	Spring (g)
One block obtained by the static strength test	52. 4	57. 3	
Blocks as an entire assembly obtained by the tilting test	31. 8	56. 9	19. 8
Blocks as an entire assembly obtained by the vibration test considering response amplification factor	4. 67 (2. 34)	32. 5 (16. 25)	11. 3 (5. 65)

Note: Figures in parenthesis represent 1/2 reduced values in consideration of the model rules.

as 1, is concluded to become 2.87. The β values as considered on the basis of the simulation laws and is indicated in Paragraph ii) hereabove;

β = 2.34 is used for the allowable maximum ground acceleration, which produces 2.34/2.87 = 0.815 g. As the final conclusion. 1) When the obtained actual earthquake records are considered as the vibration input, this graphite shielding structure is sufficiently safe. 2) The block supporting pins are hypothetically determined to break or damage by the high degree of vibration sharp peak caused by block collision. As an evaluation of its safety factor, it may be assumed, when sufficient safety is considered, the allowable maximum ground acceleration is 799 gal or 0.815 g in the case when an input of the ground movement having the similar type of spectrum as obtained from the actual earthquakes is introduced.

*2 If the vibration of equation for one mass system is expressed by;

$$m\ddot{y} + c\dot{y} + ky = p(t)$$

At the time of accelerameter p (t) = 0, but

$$\ddot{y} = \ddot{y} + x$$

$$m\ddot{y} + cy + ky = -mx$$

$$\omega^2 = \frac{k}{h} \qquad To = 2\pi\sqrt{\frac{m}{k}}$$

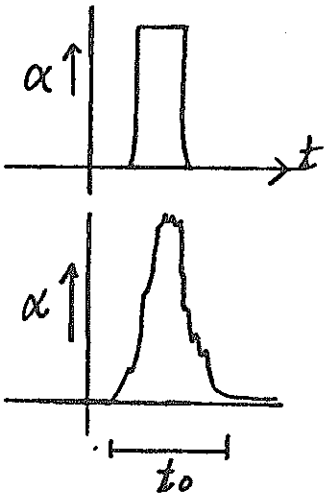

When an extremely short time acceration is applied, namely when, to << To

assuming $\ddot{y} \rightarrow$ const α, as the displacement y is an order of t^2o, it is nearly 0.

Then, the general impulse equation is:

$$m\Delta\dot{y} = \int_o^t [\ p(t) - k \cdot y(t)\ ]\ dt$$

($y(t)$: nearly 0)

$$\therefore m\Delta\dot{y} = \int_o^t [\ p(t)\ ]\ dt = \int_o^t -m\alpha\, dt = -m\int_o^t dt$$

$$\Delta\dot{y} = -\int_o^t \alpha\ dt$$

When the initial displacement 0 and the initial speed $\dot{y}(0)$ is given to the one system of particles, it is;

$$y(t) = e^{-h\omega t} \cdot \frac{\dot{y}(0)}{\omega D} \cdot \sin \omega Dt = e^{-h\omega t} \frac{-\int_o^t \alpha \, dt}{\omega_0} \cdot \sin \omega Dt$$

But $h = \frac{c}{2m\omega}$

$$\omega D = \omega\sqrt{1 - h^2}$$

peak valve $\sin \omega Dt = 1 \quad (t = \frac{\pi}{2\omega})$

$$y(t)\,max = e^{-h\cdot\omega\cdot\frac{\pi}{2\omega}} \cdot \frac{-\int \alpha \, dt}{\omega D}$$

Supposing h = 0.7

$$y(t)\,max = e^{-0.7\cdot 3.14/2} \frac{-\int_o^t \alpha \, dt}{\sqrt{1-0.7^2\cdot\omega}}$$

$$\simeq \frac{1}{2.718} \frac{\int_o^t \alpha \, dt}{0.7\,\omega} \simeq \frac{1}{1.9\cdot\omega} \int_o^t \alpha \, dt$$

On the other part when it is To < to (normal time)

$$y(t) = \frac{-m}{k} \alpha_0 \cdot \frac{1}{\sqrt{(1-\beta^2)^2 + 4h^2\beta^2}} \rightarrow 1$$

$$y(t) = \frac{-1}{\omega^2}\alpha_0$$

If the amplification ratio of electro-magnet is k.

$$y(t)\cdot k = l_0 \quad (mm)$$

$$\frac{-1}{\omega^2} = x_0 \cdot k = l_0 \quad (mm) \quad k = \frac{-l_0}{\alpha_0} \cdot \omega^2$$

On the other part, when it is To >> to

$$y(t)\cdot k = 1 \quad (mm)$$

$$\frac{-1}{1.9\omega} \int_o^t \alpha \, dt \cdot k = 1 \quad (mm)$$

$$\frac{-1}{1.9\omega} \int_o^t \alpha \, dt \cdot \frac{-l_0}{\alpha_0} \cdot \omega^2 = 1 \quad (mm)$$

$$\int_o^t \alpha \, dt = y = \frac{1\cdot\alpha_0}{l_0} \cdot \frac{1.9}{\omega} = \frac{1}{l_0} \frac{\alpha_0}{\omega} 1.9$$

Reference data

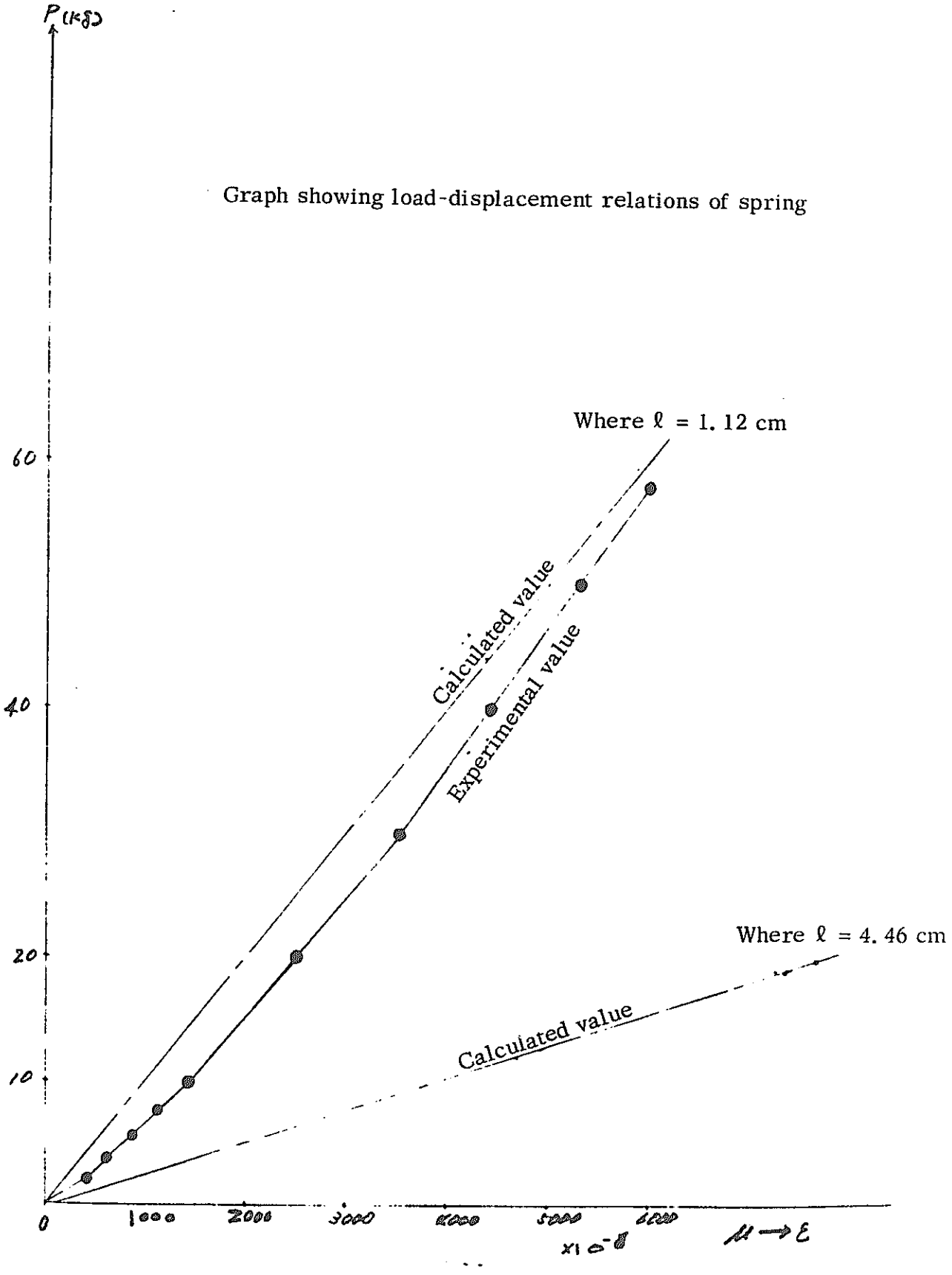

Graph showing load-displacement relations of spring

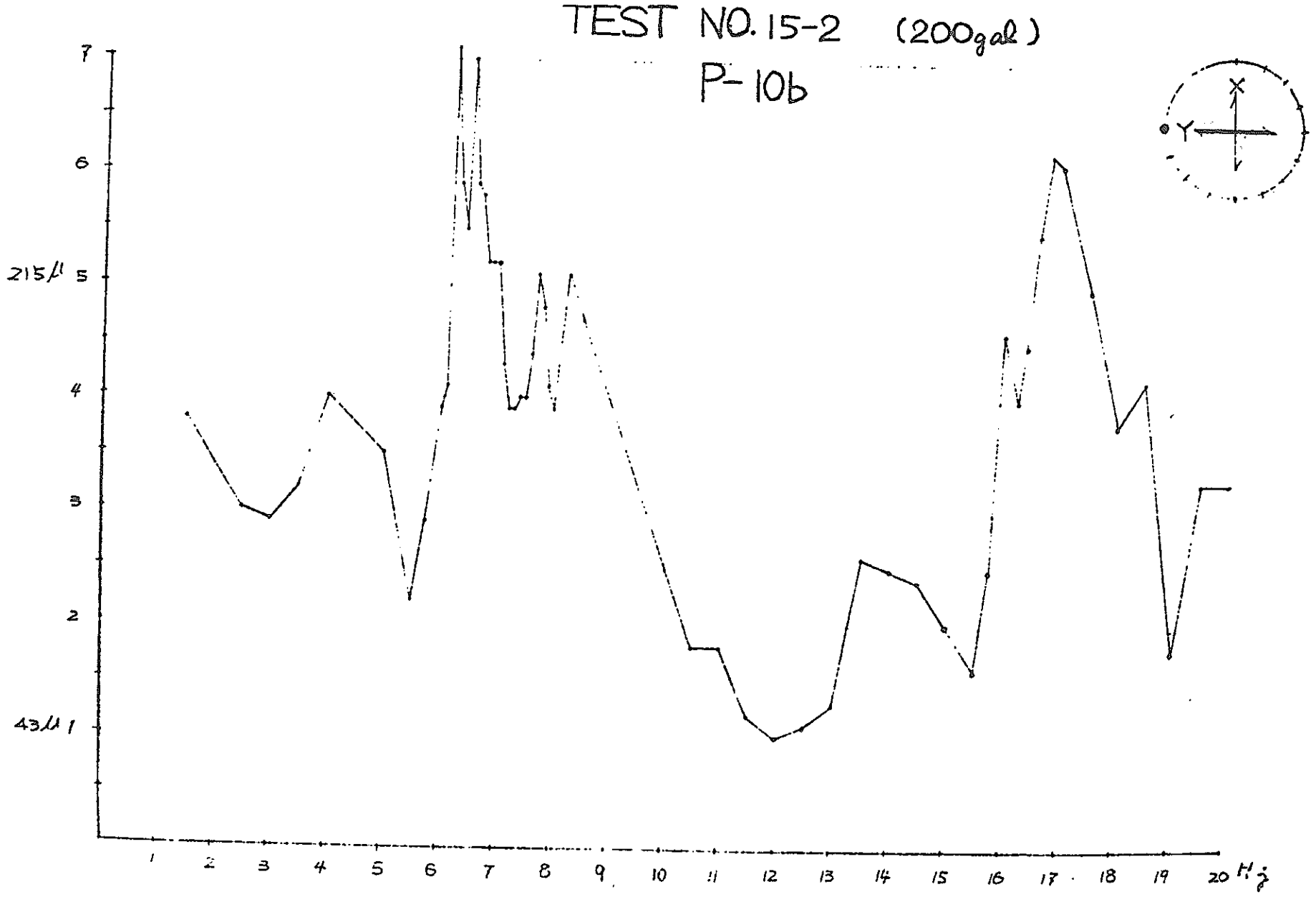
TEST NO. 15-2 (200gal)
P-10b
X
Y
7
6
215μ 5
4
3
2
43μ 1
1 2 3 4 5 6 7 8 9 10 11 12 13 14 15 16 17 18 19 20 Hz

TEST NO.15-3 (400gal)

P-10b

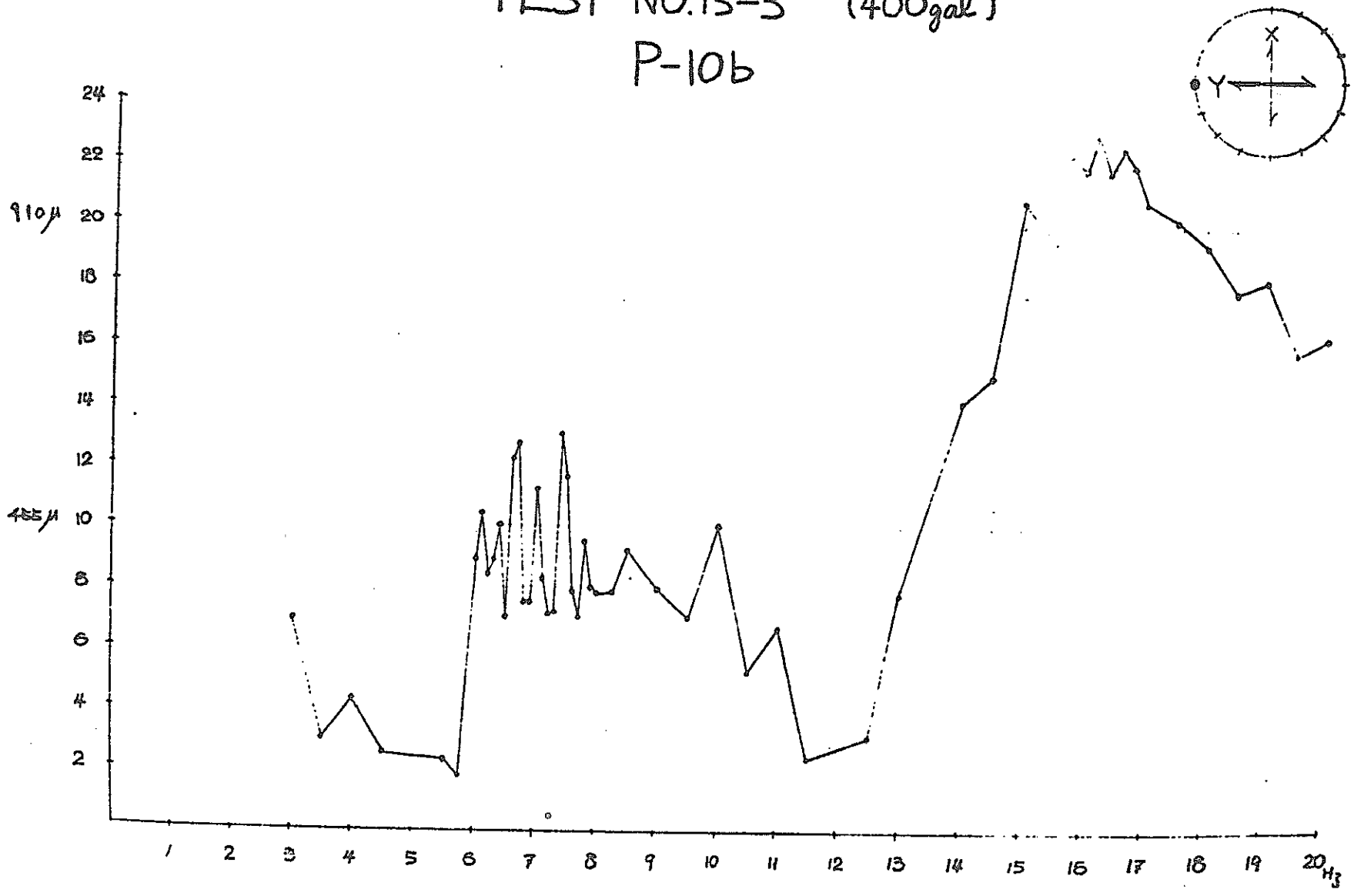

TEST No 16-T (100gal)

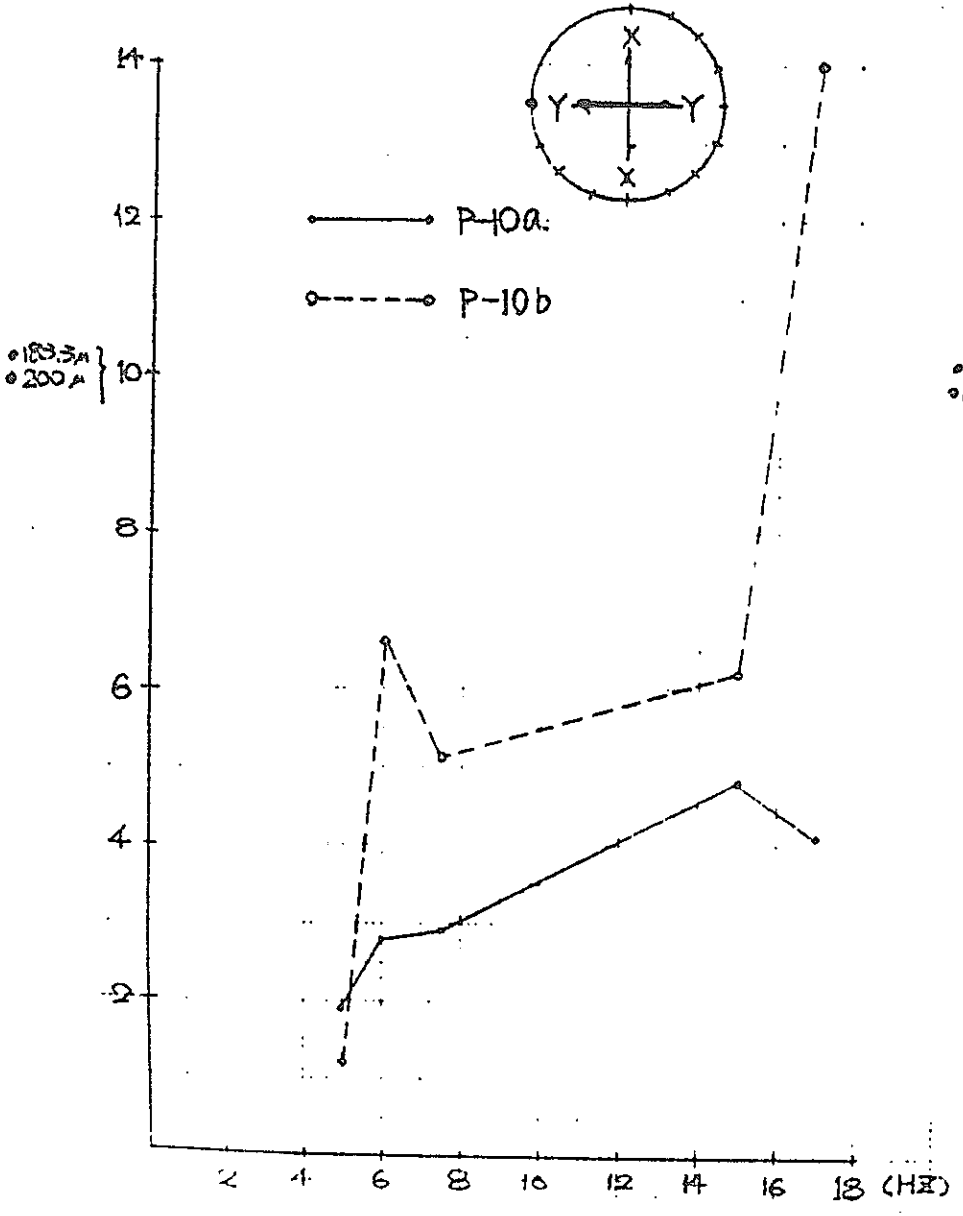

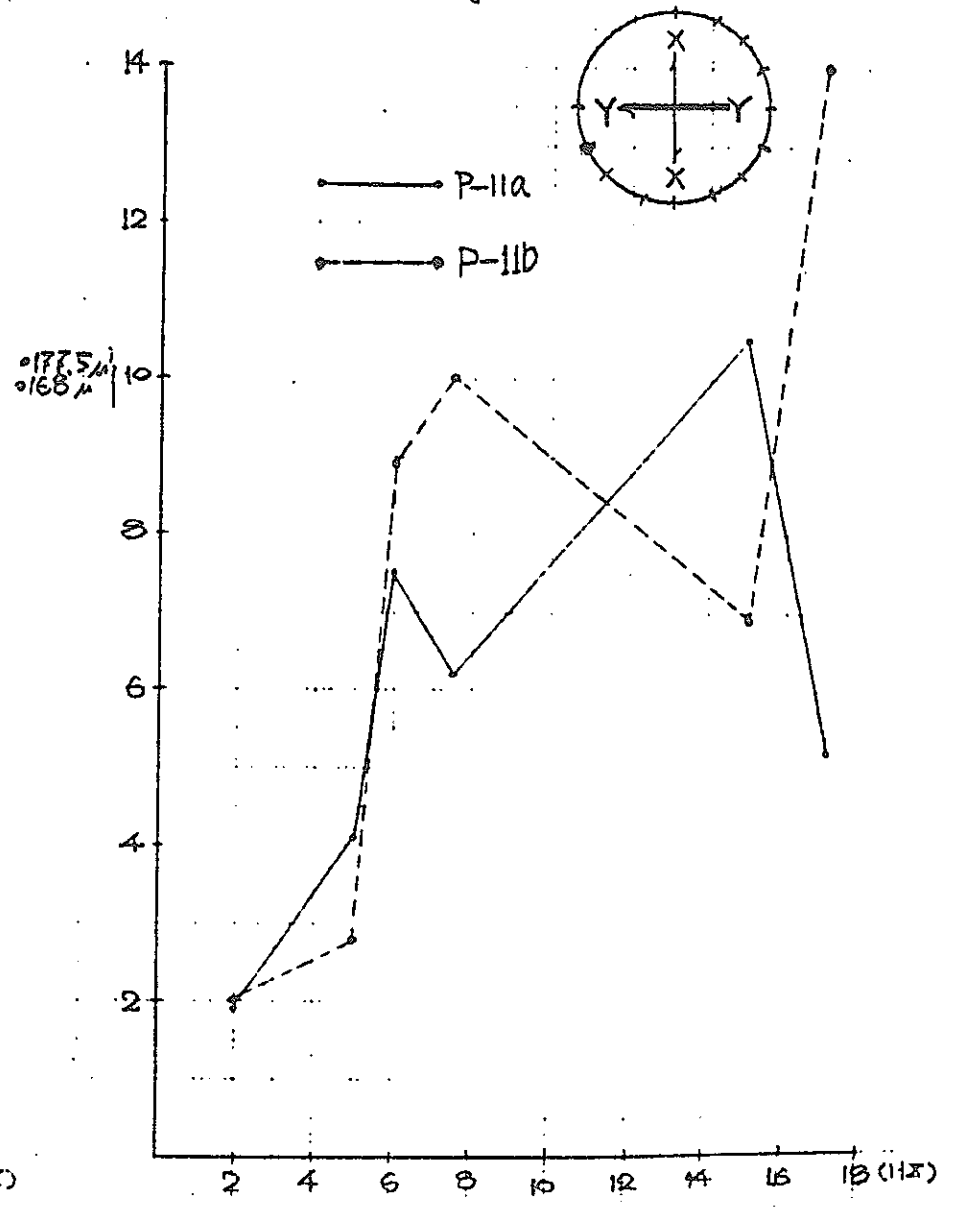

TEST NO 16-7 (100gal)
P-13a
P-13b
P-12b
X
Y
Y
X
12
8
6
4
2
2
4
6
8
12
14
16
18
Hz

TEST NO.16-8 (400gal)

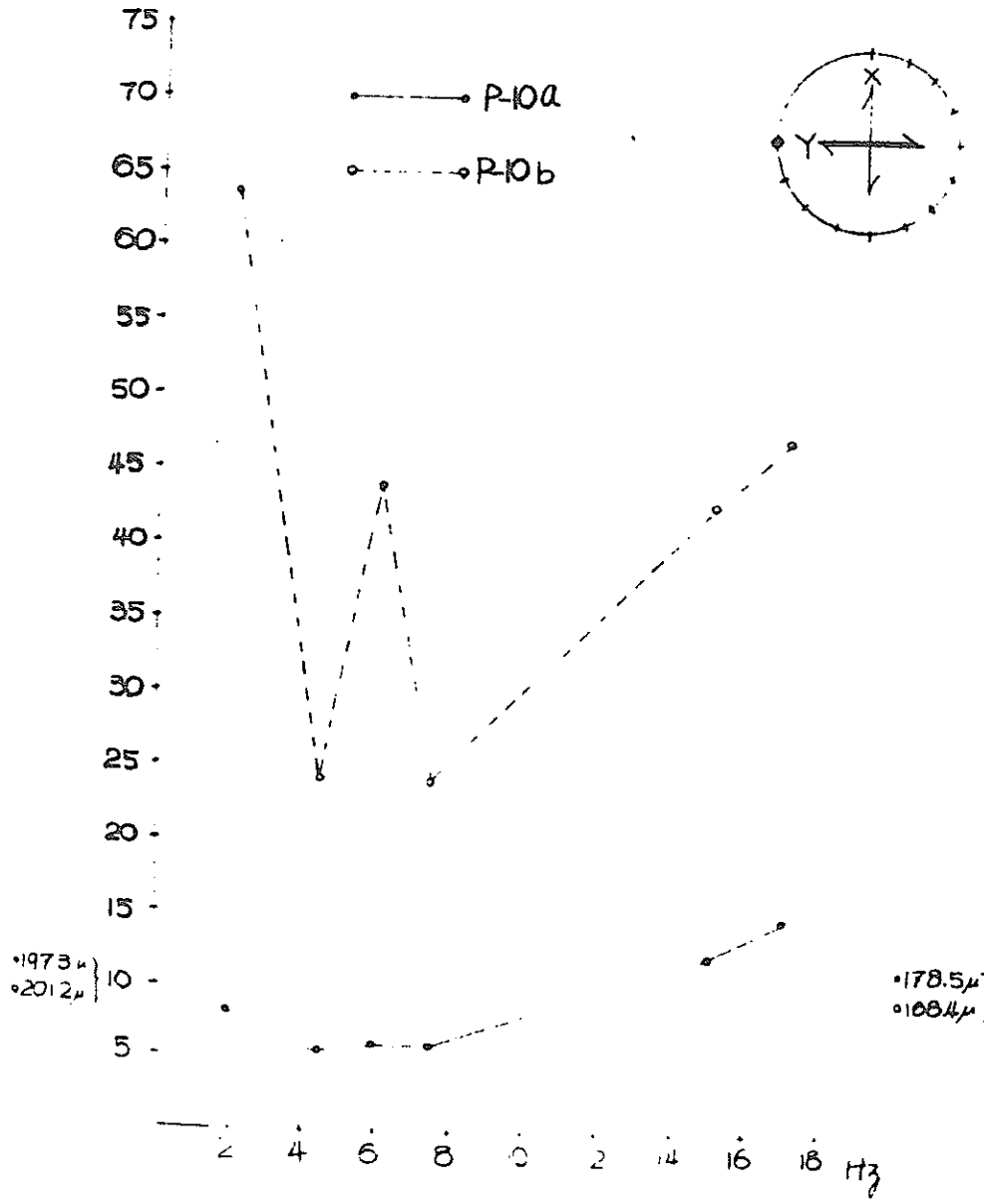

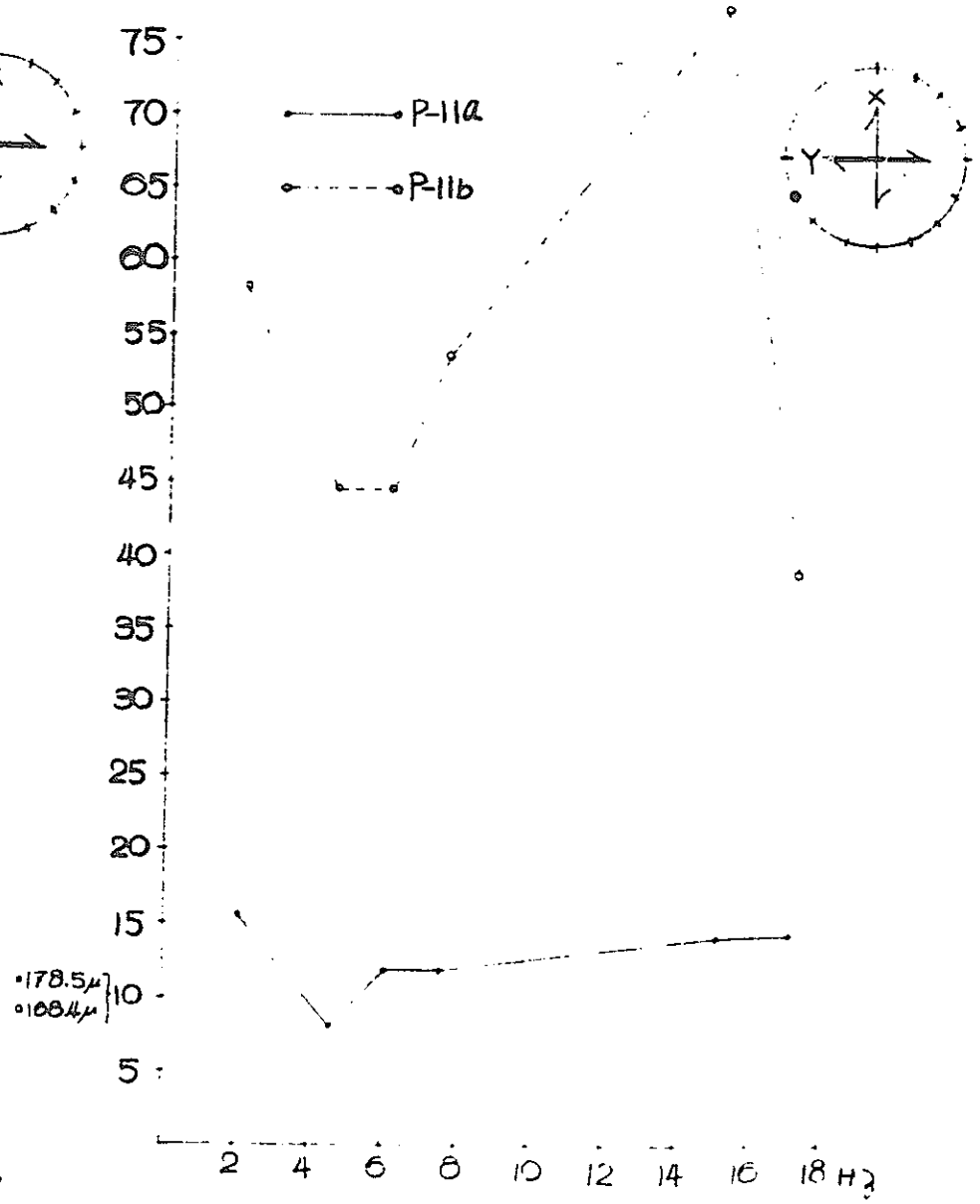

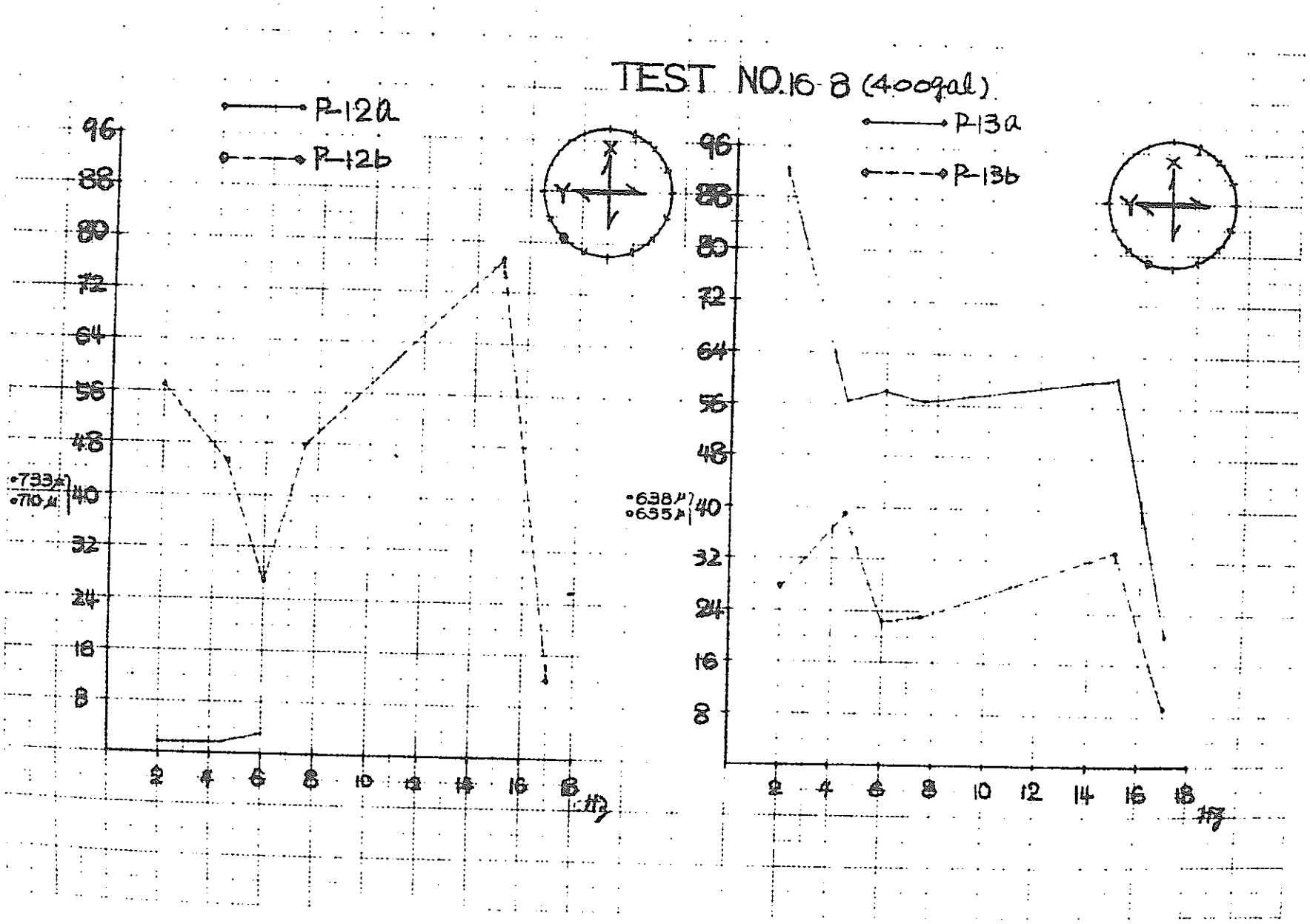
TEST NO.16-8 (400gal)
P-12a
P-12b
P-13a
P-13b
96
88
80
72
64
56
48
40
32
24
16
8
.733A)
.710A)
.638A)
.635A)
2
4
6
8
10
12
14
16
18
Hz

TEST No 16-7 (100gal)

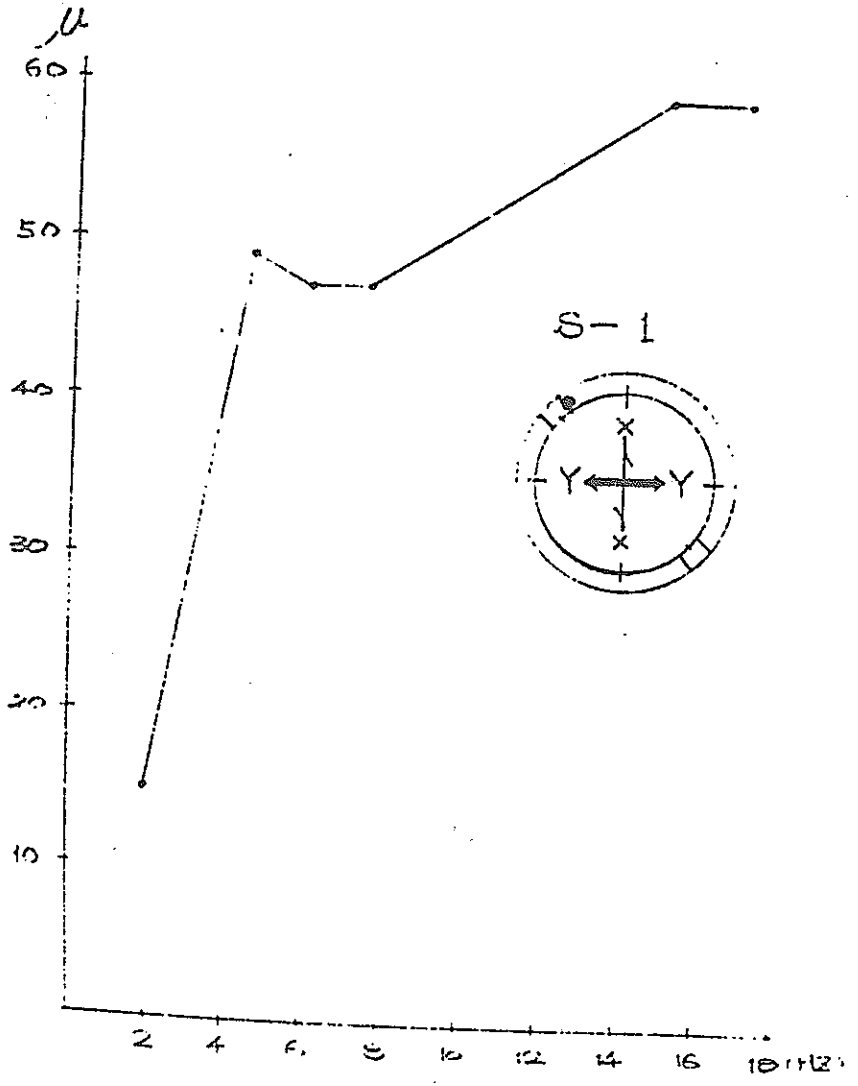

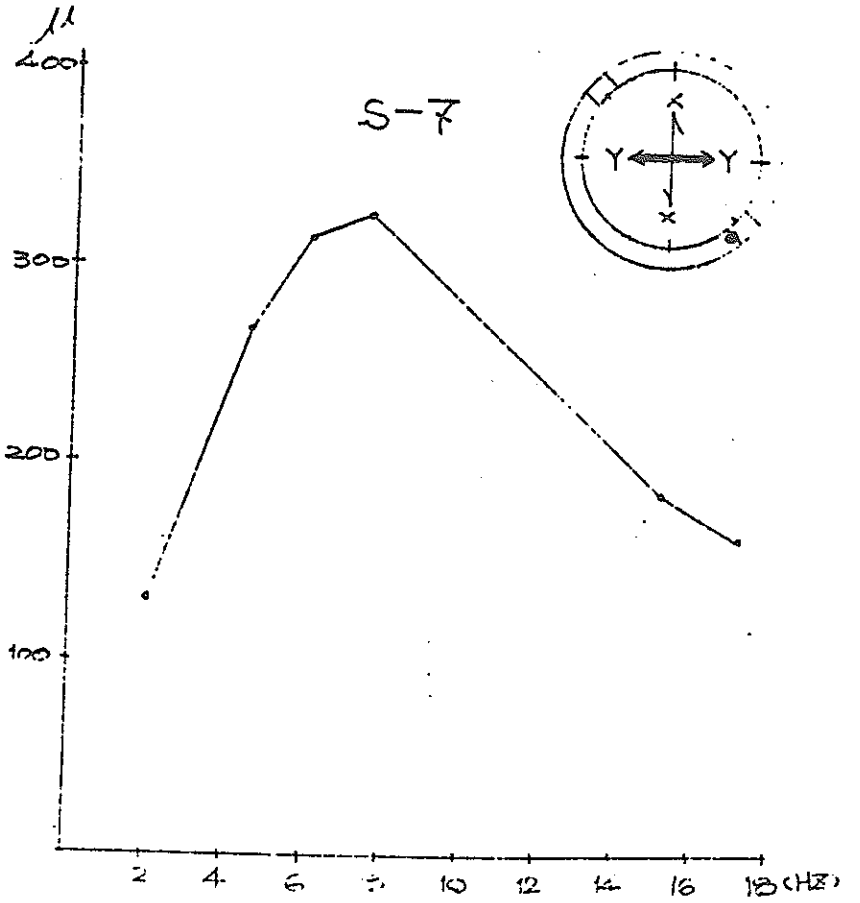

TEST No. 16-7 (100 gal)

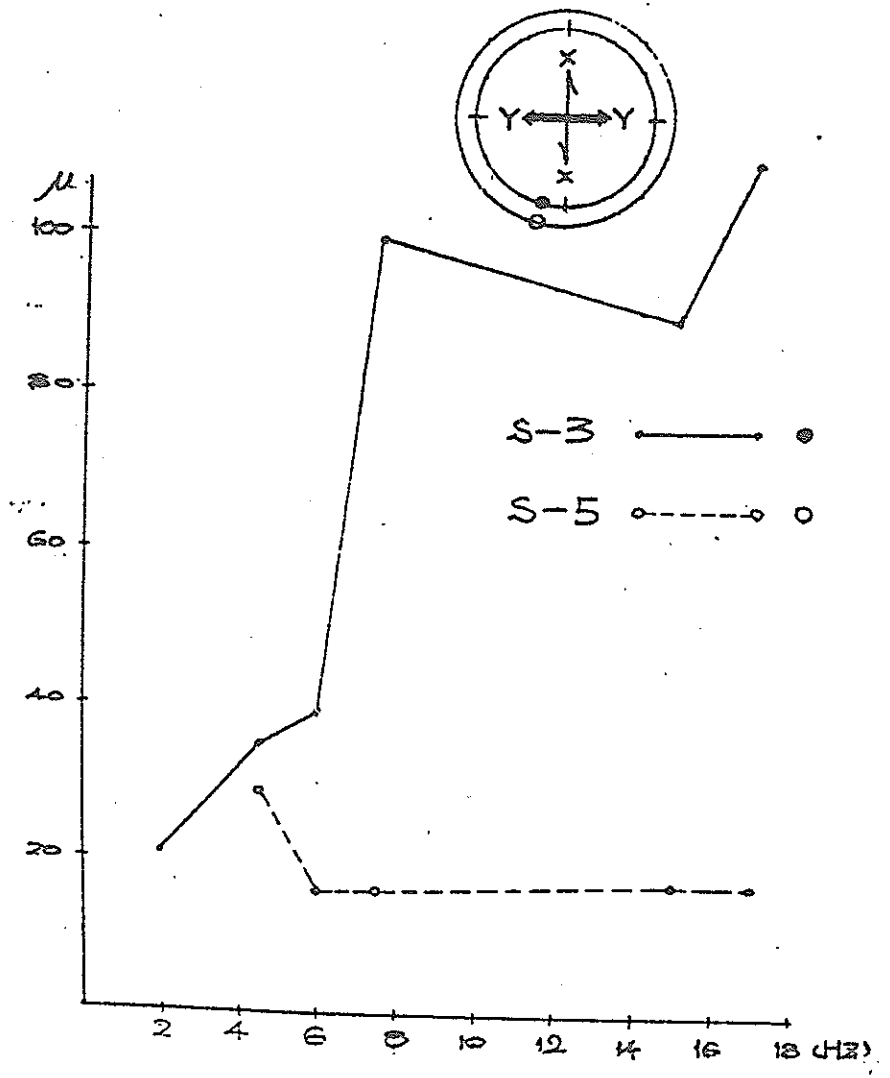

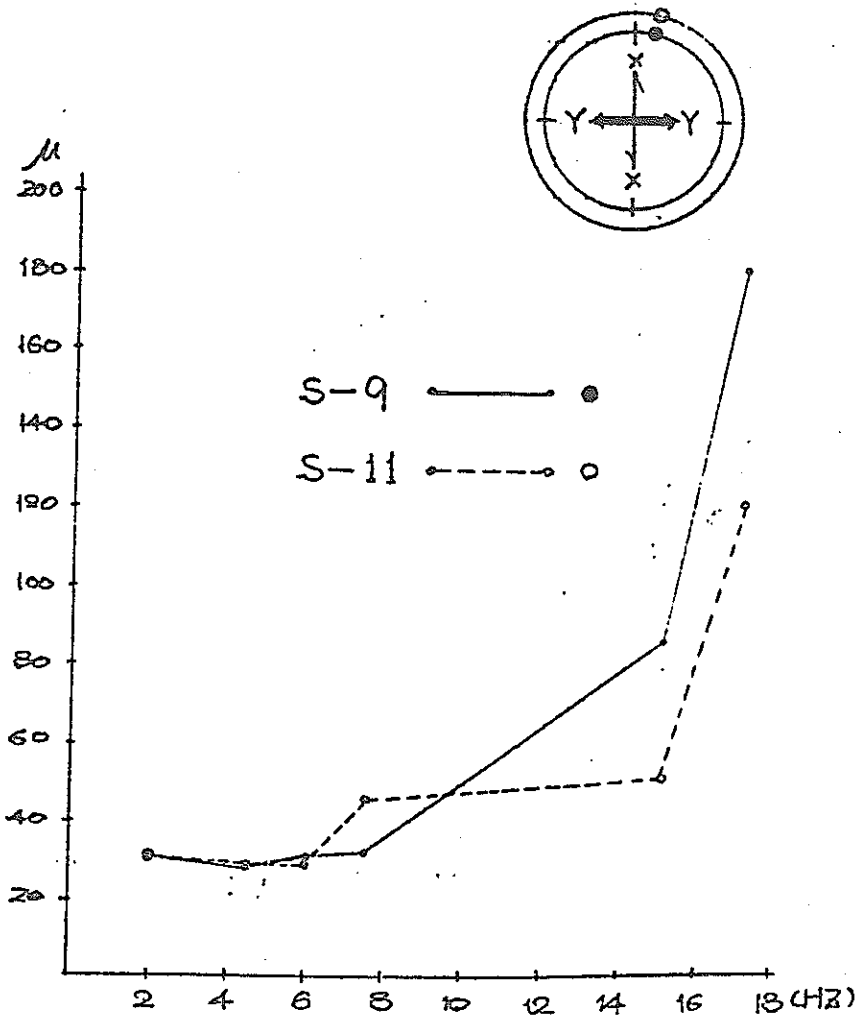

TEST No 16-8 (400gal)

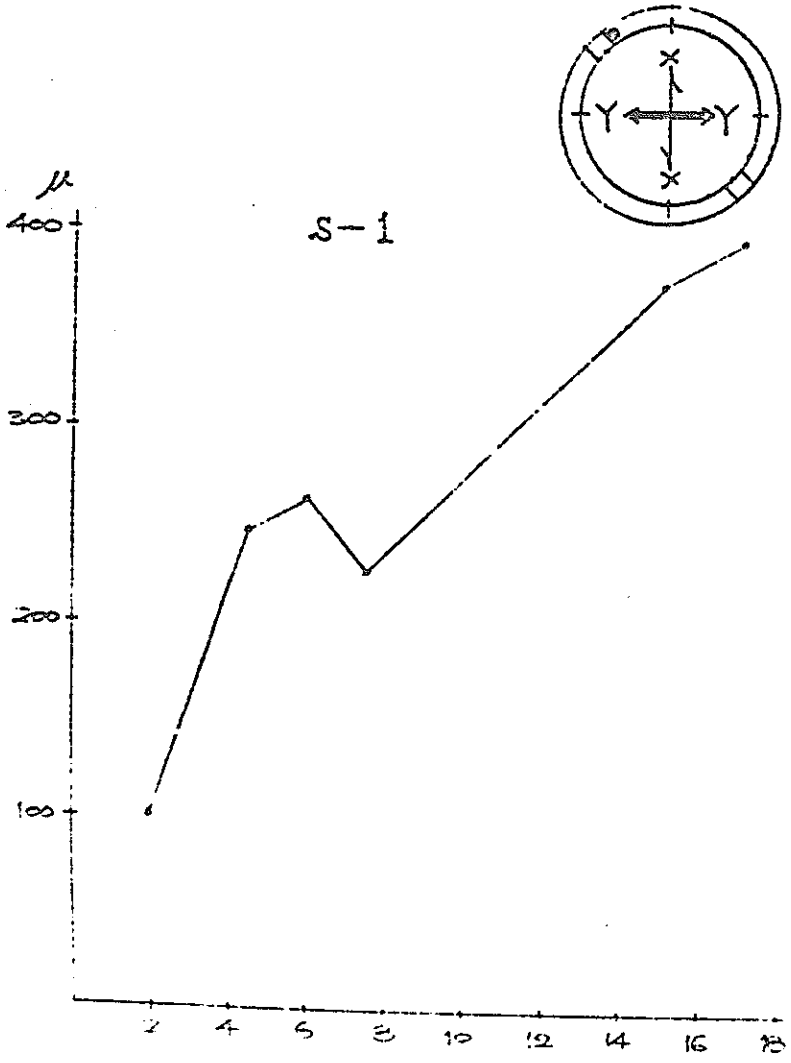

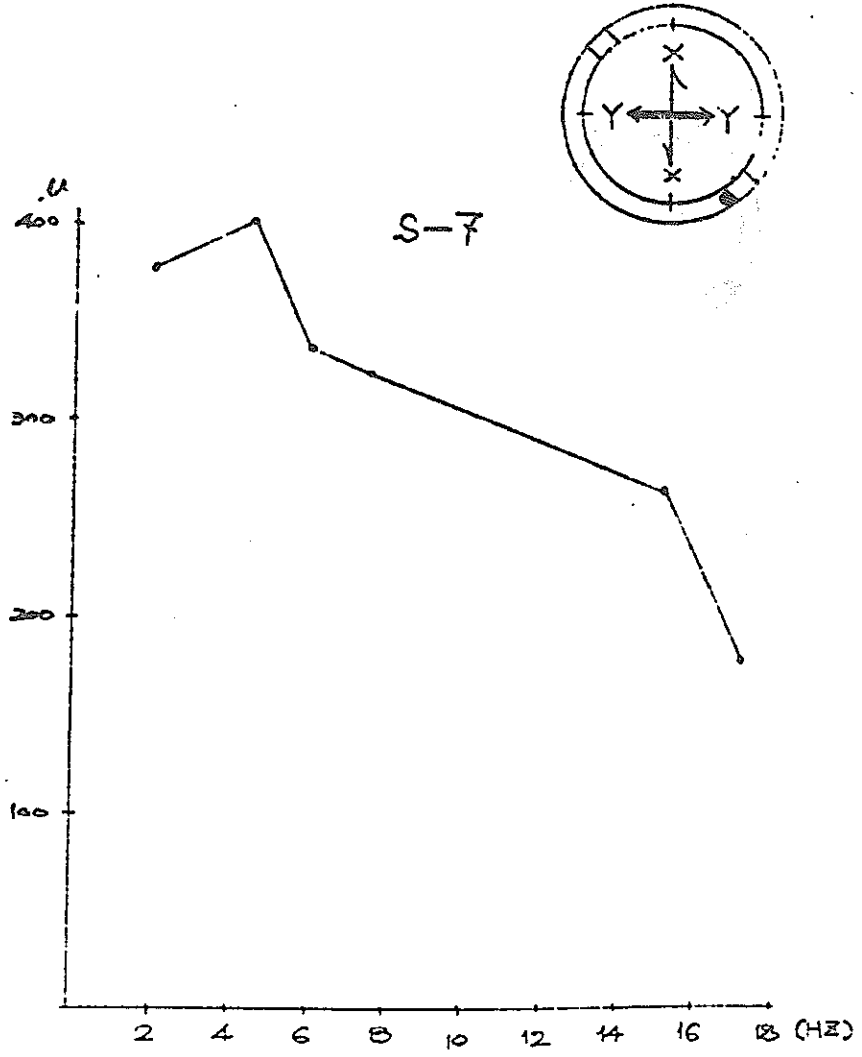

TEST No 16-8 (400gal)

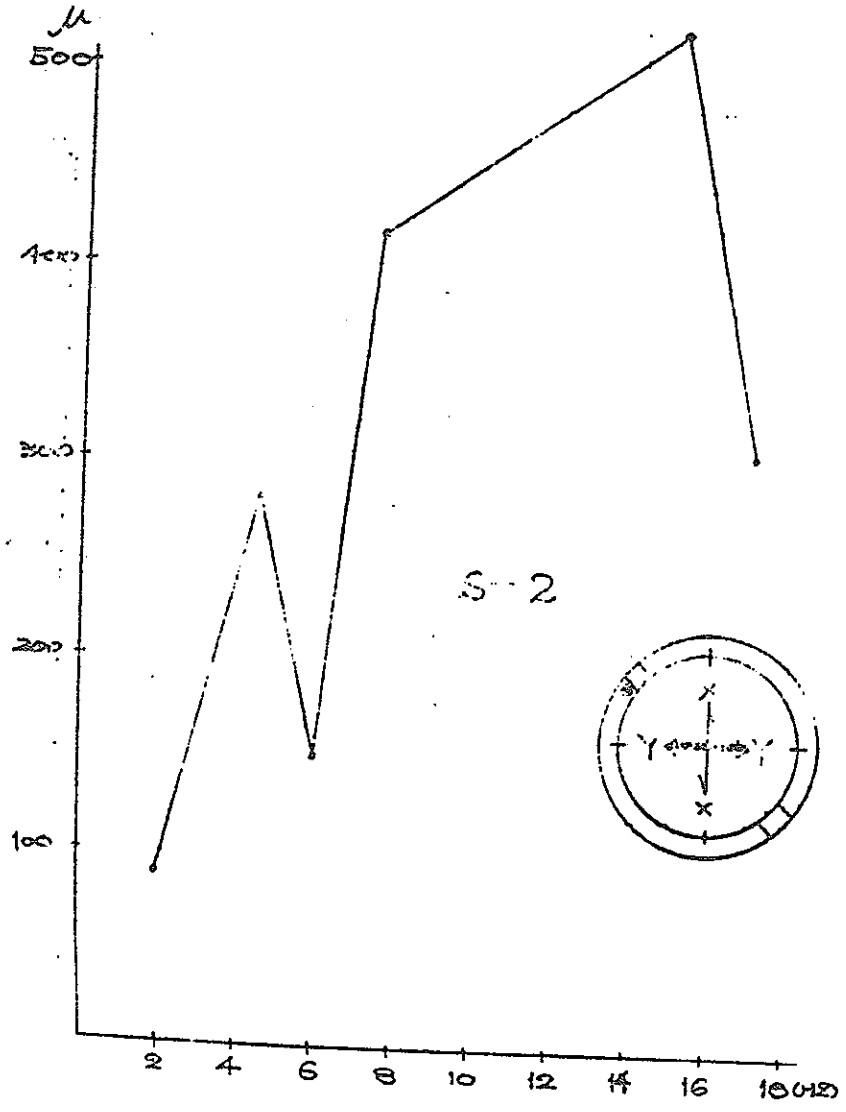

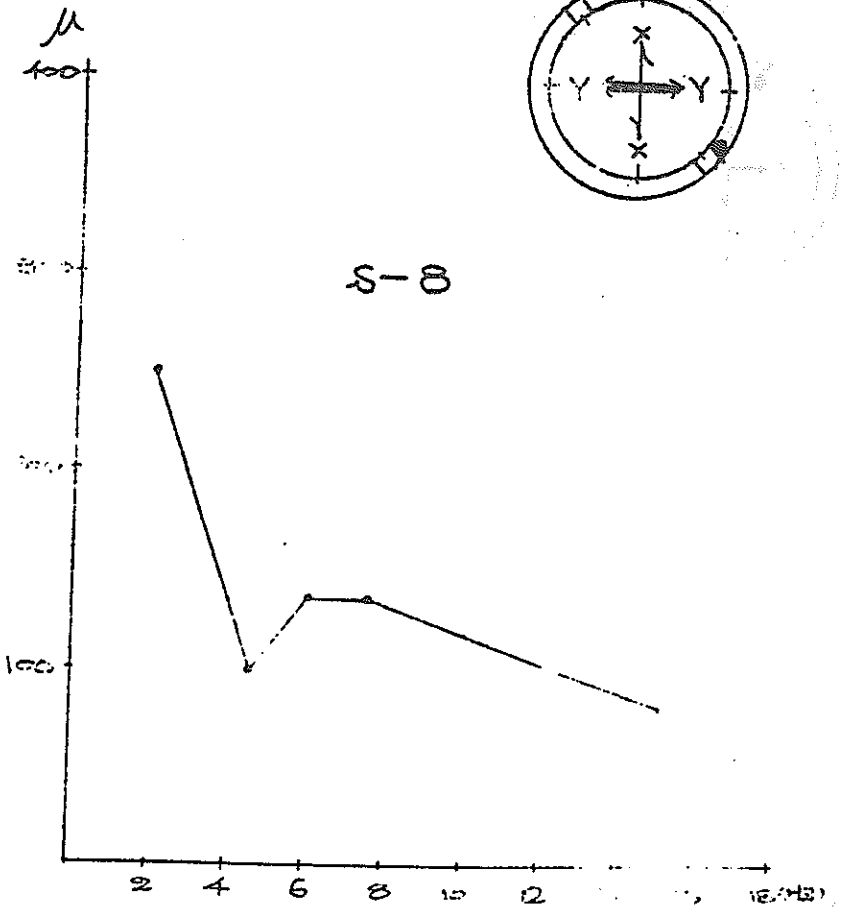

TEST No 16-8 (400gal)

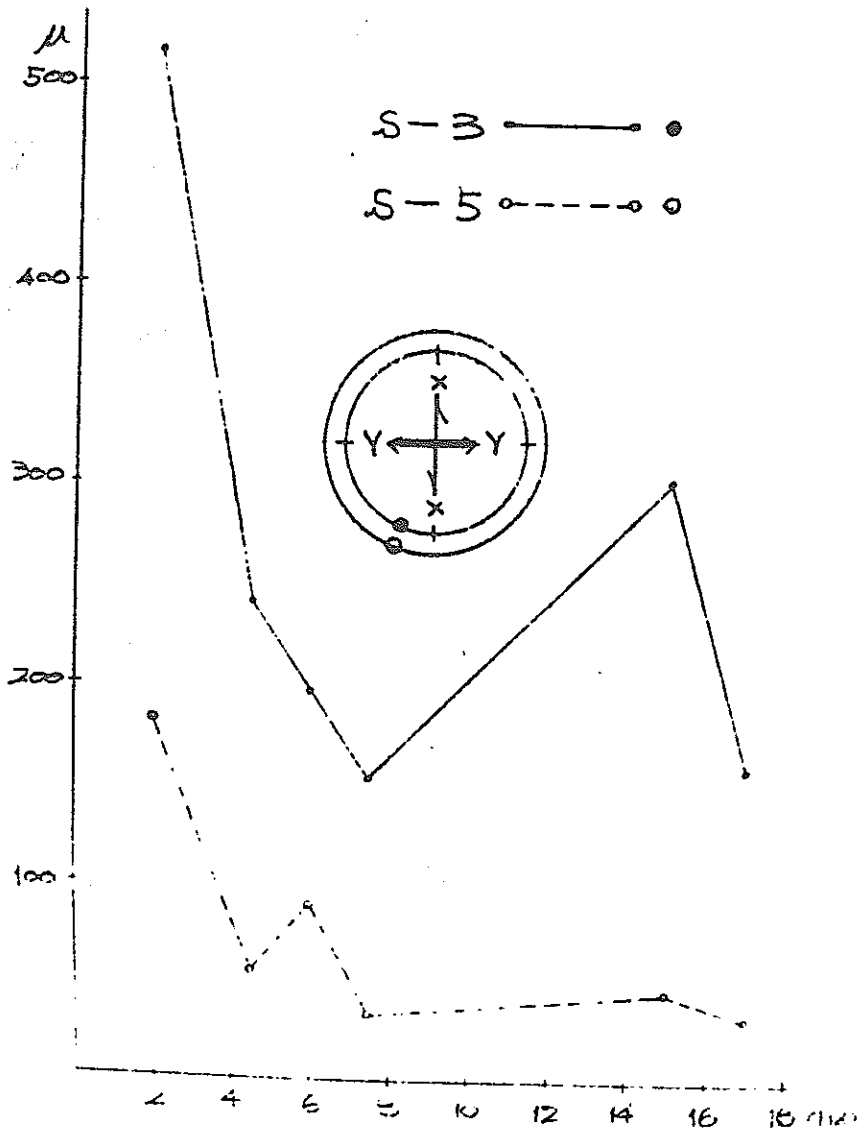

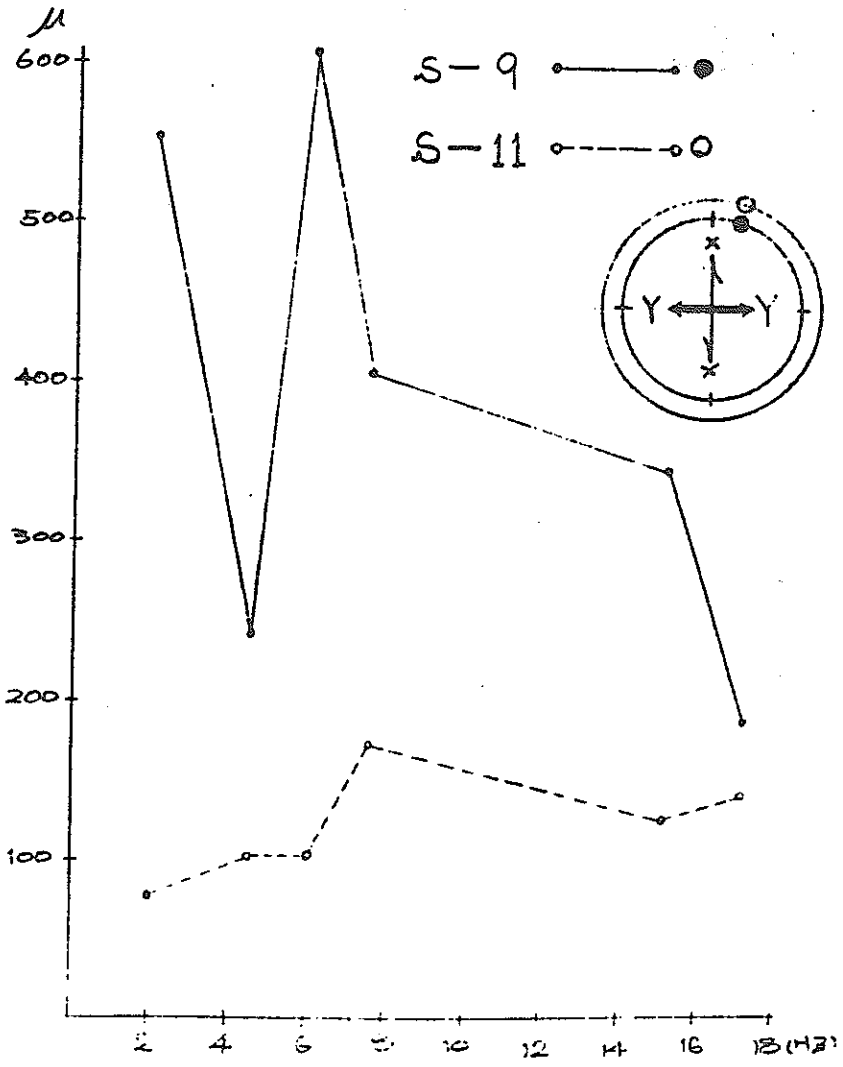

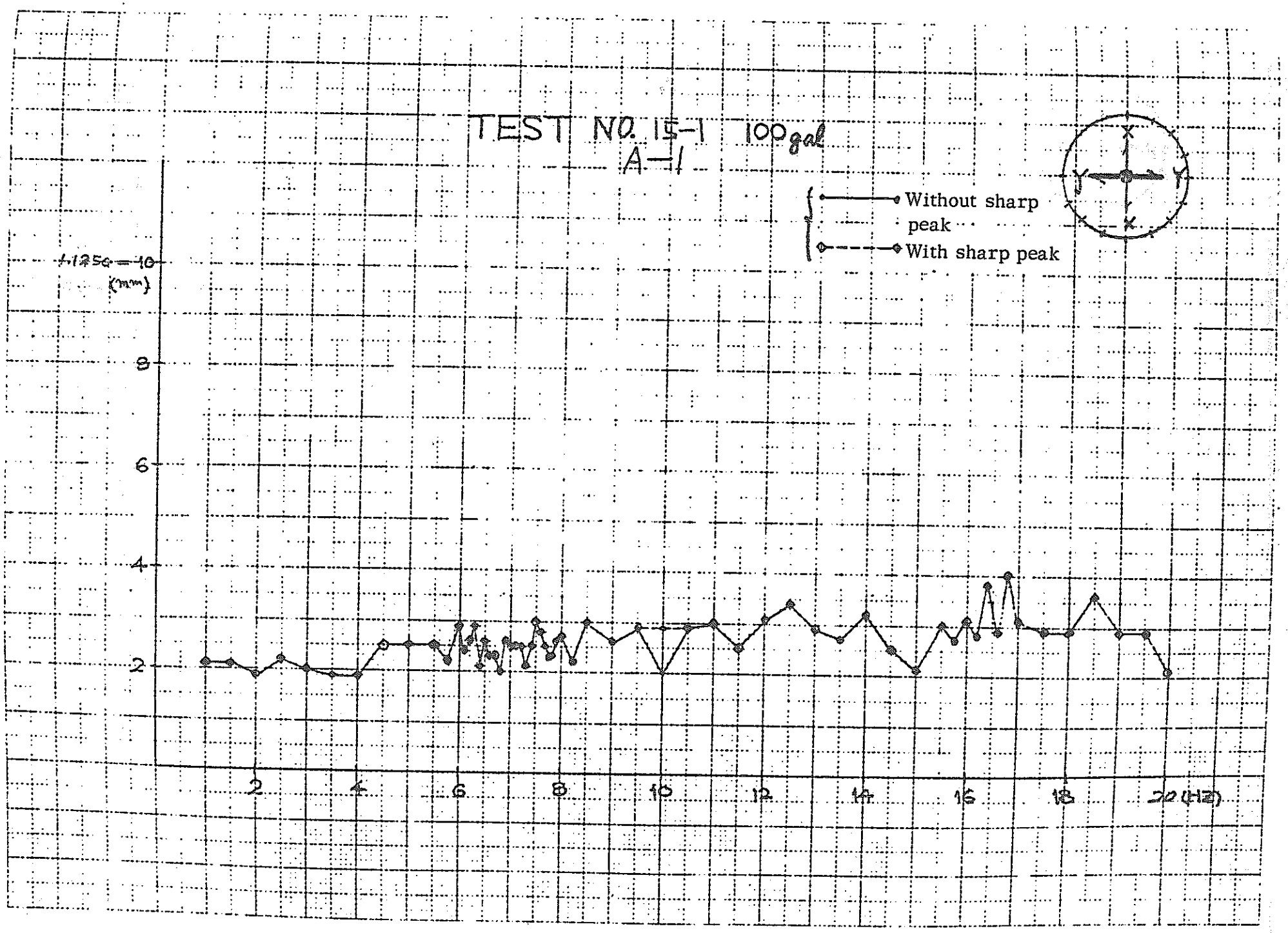
TEST NO. 15-1 100gal
A-1
Without sharp peak
With sharp peak
1/125=10 (mm)
8
6
4
2
2
4
6
8
10
12
14
16
18
20 (HZ)

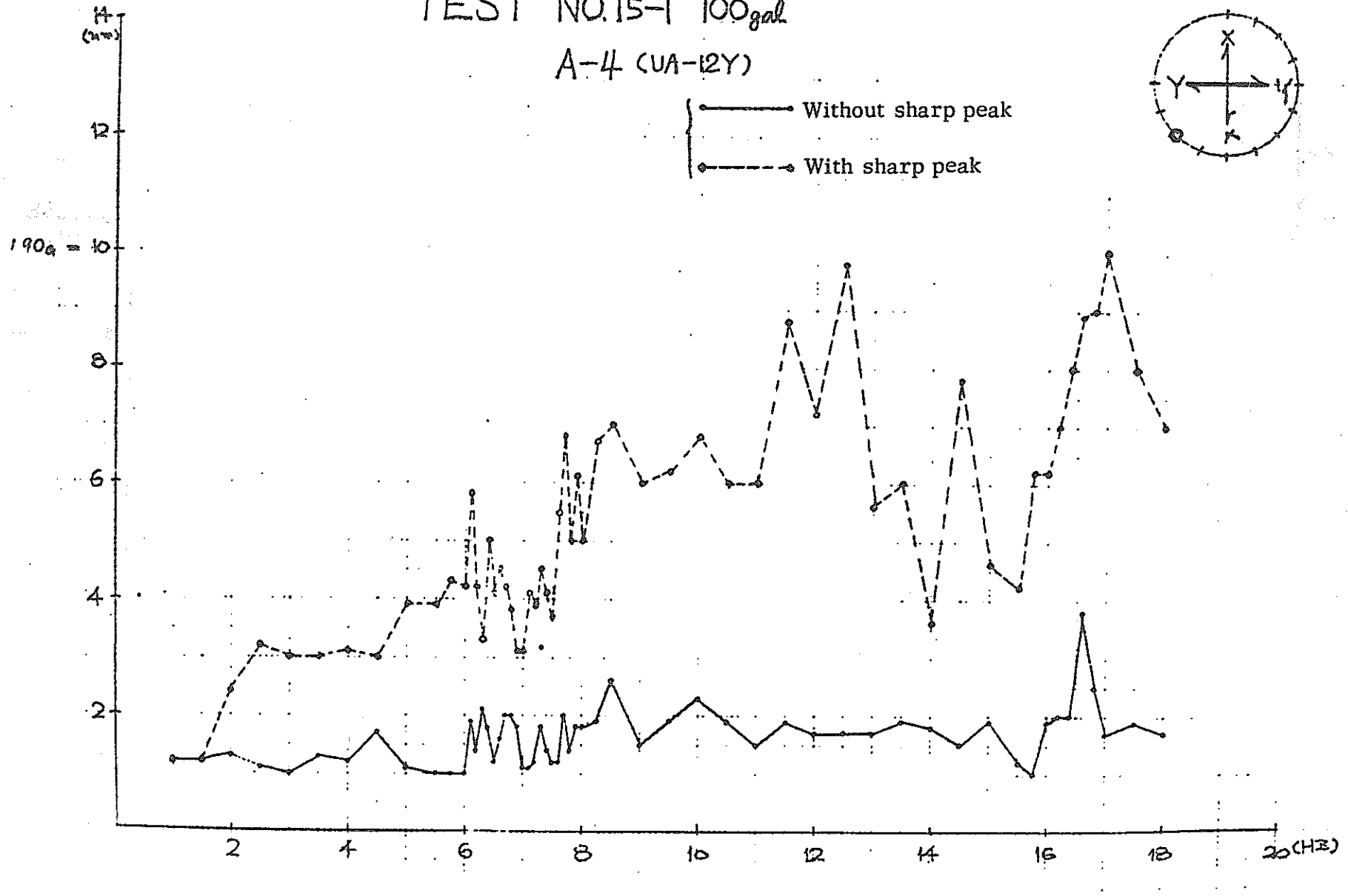
TEST NO.15-1 100gal
A-4 (UA-12Y)
Without sharp peak
With sharp peak
X
Y
190gal = 10
14
12
8
6
4
2
2
4
6
8
10
12
14
16
18
20(HZ)

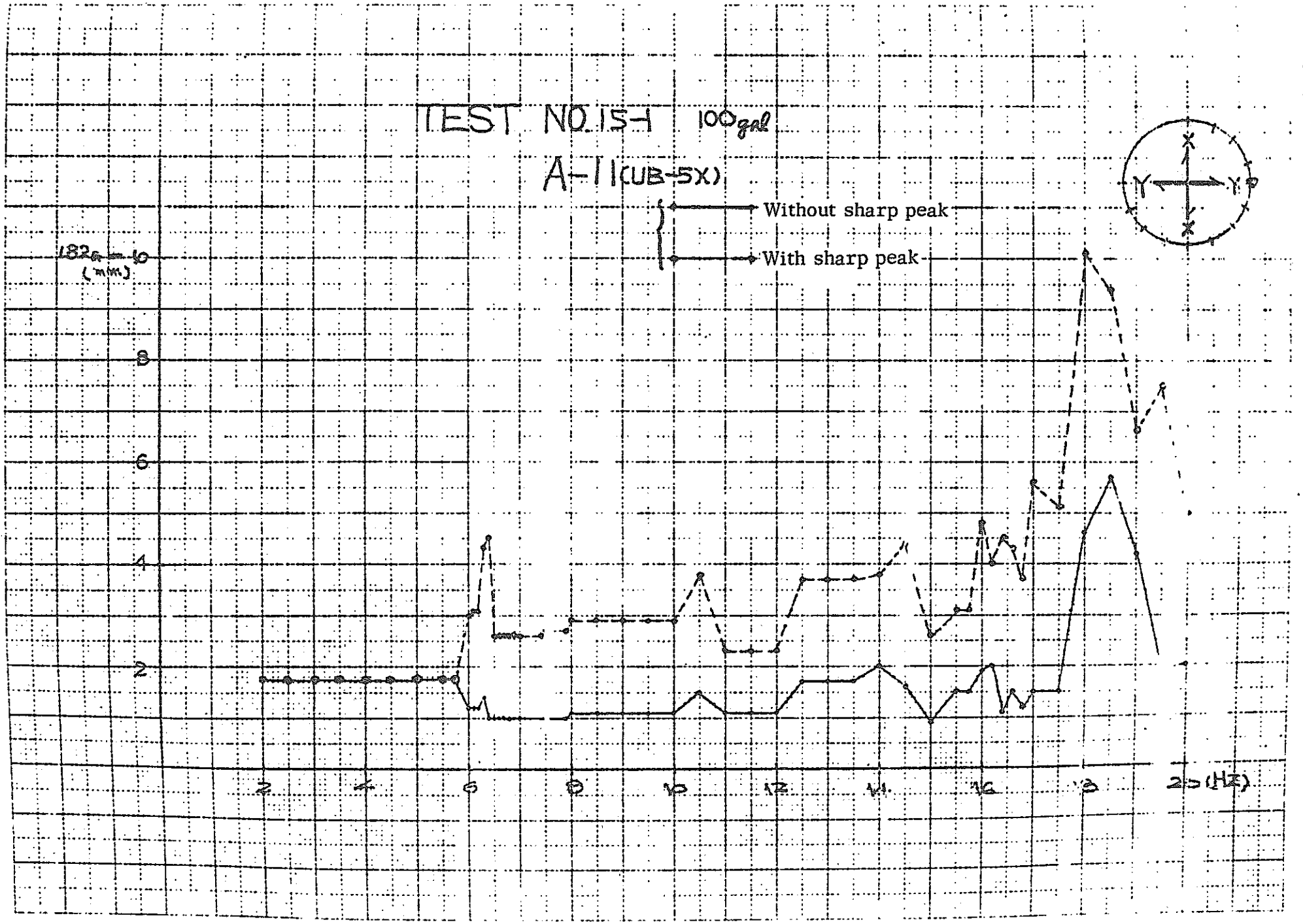
TEST NO.154 100gal
A-11(UB-5X)
Without sharp peak
With sharp peak
182 (mm)
2
4
6
8
10
12
14
16
18
20 (Hz)

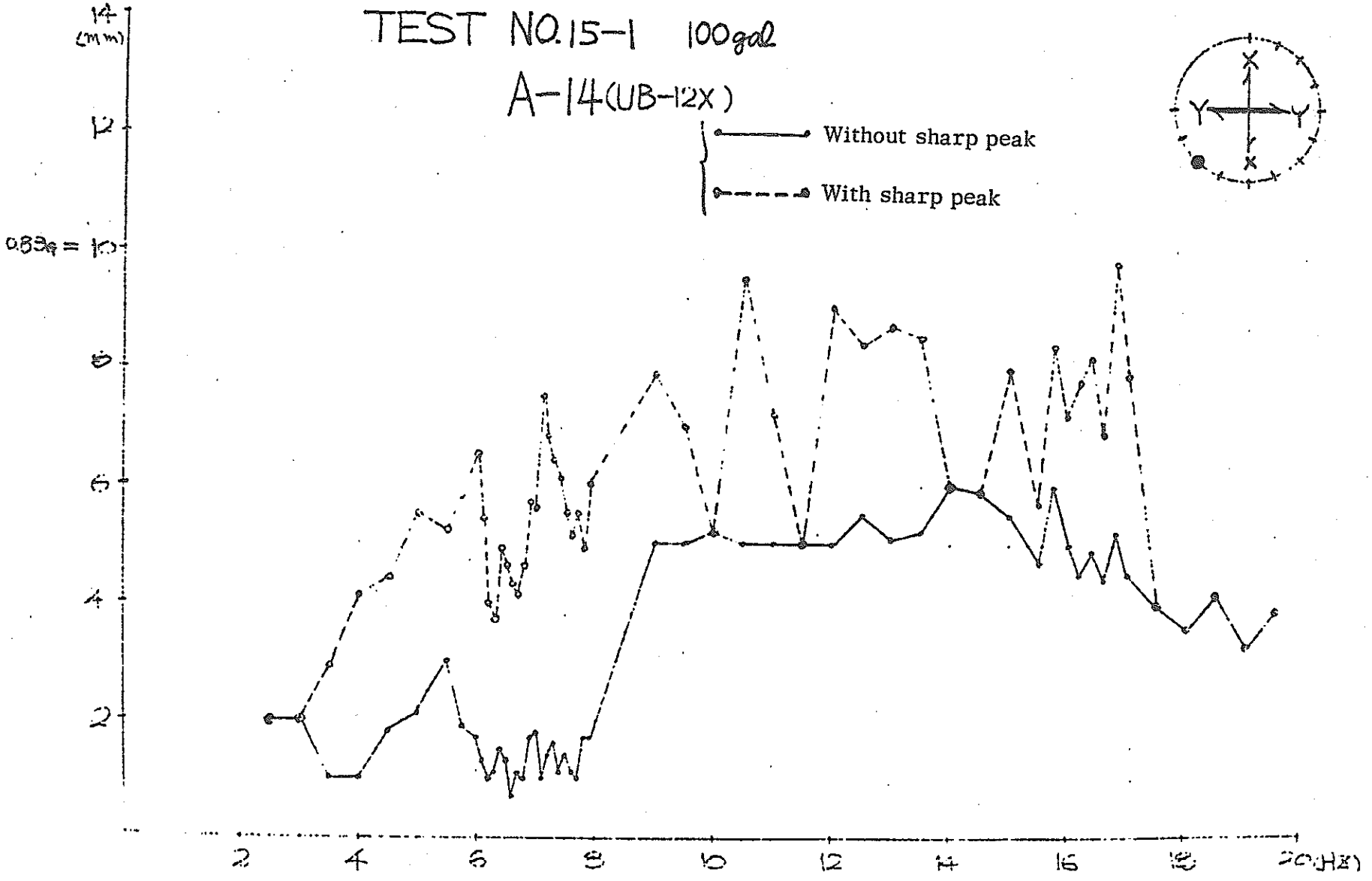
TEST NO.15-1 100gal
A-14(UB-12X)
Without sharp peak
With sharp peak
X
Y
Y
X
14
(mm)
12
10
8
6
4
2
0.83g = 10
2
4
6
8
10
12
14
16
18
20(HZ)

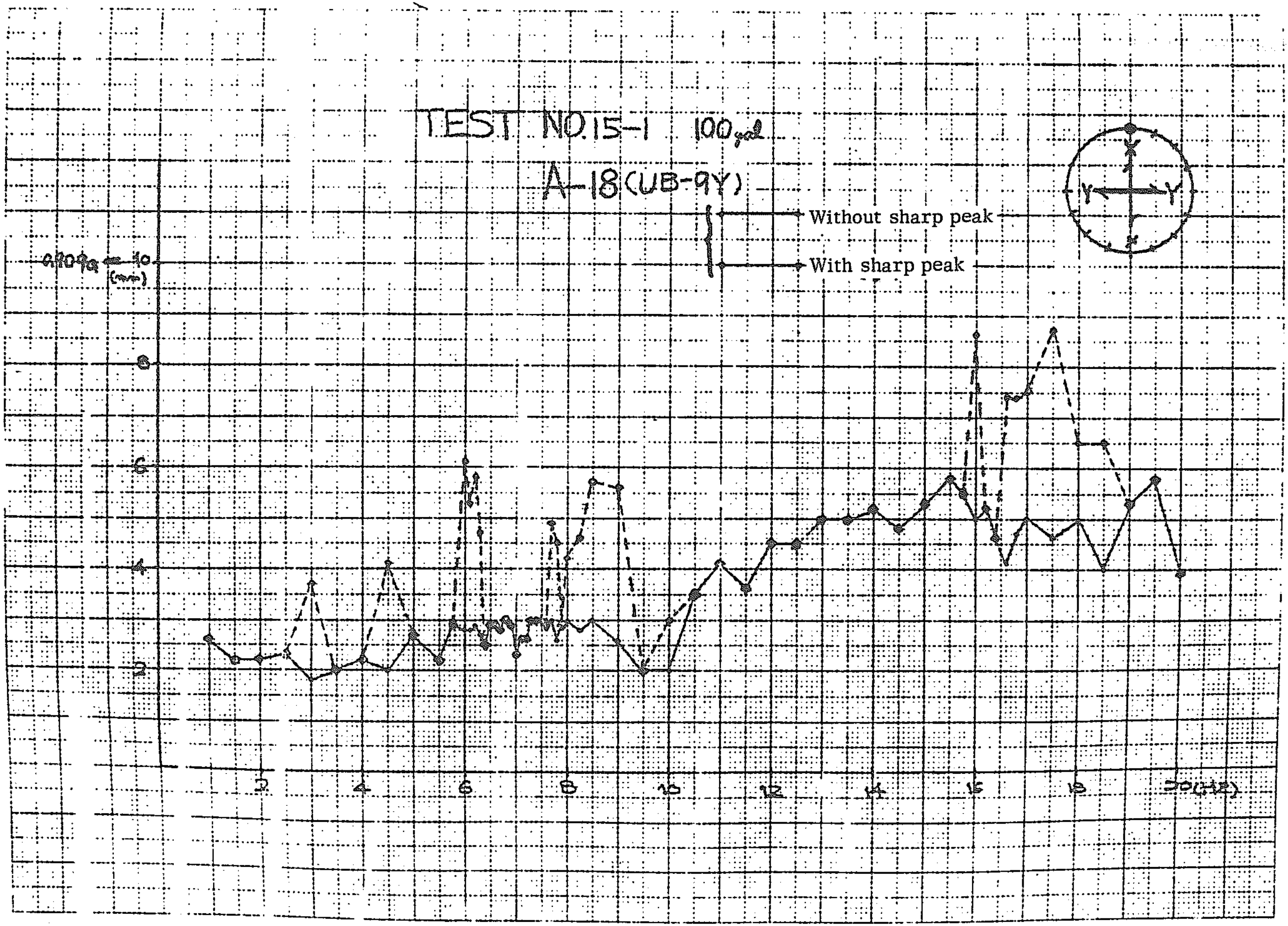
TEST NO.15-1 100gal
A-18(UB-9Y)
Without sharp peak
With sharp peak
Y
X
2
4
6
8
10
12
14
16
18
20(Hz)

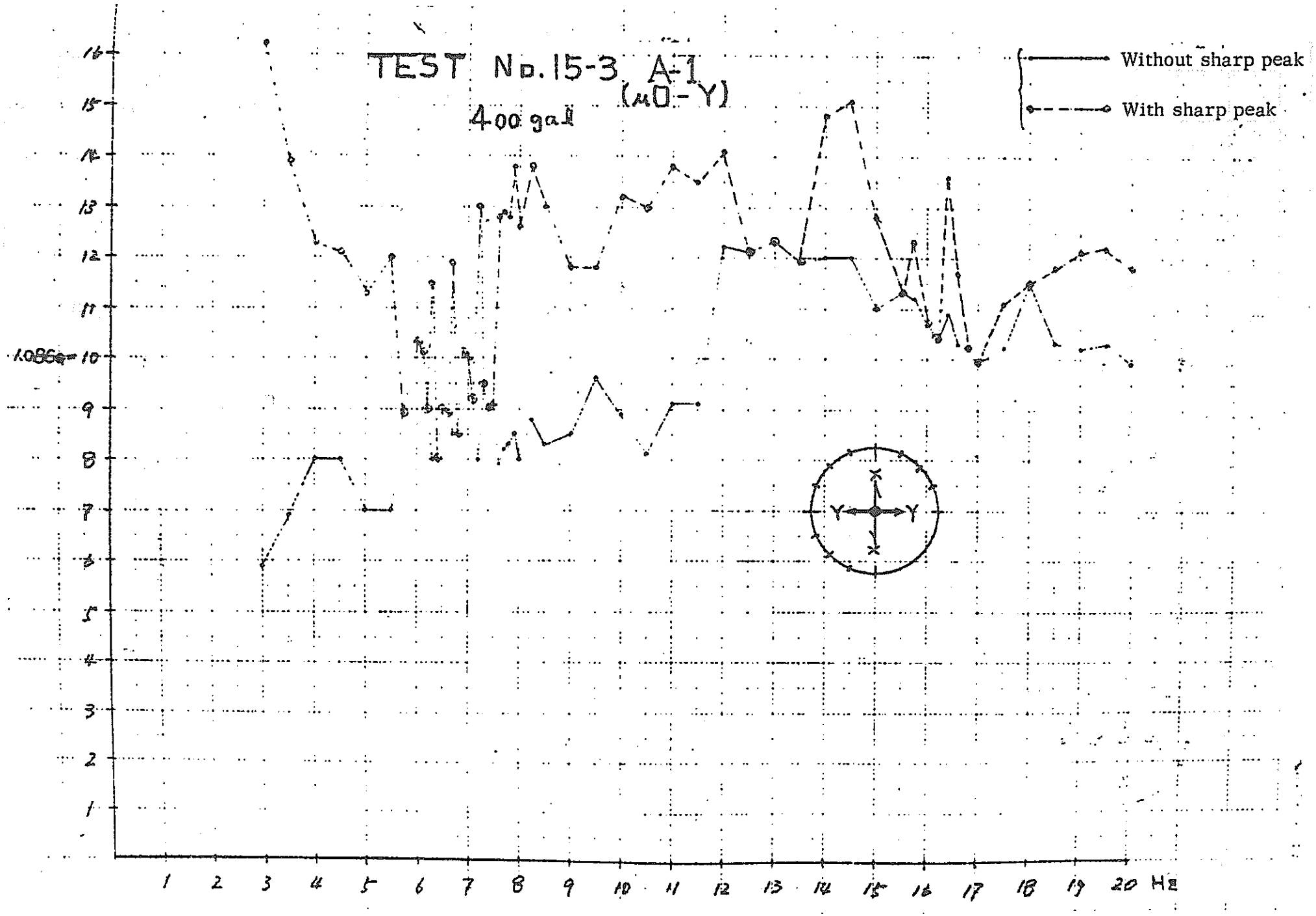
TEST No. 15-3 A-1
(μ0-Y)
400 gal
Without sharp peak
With sharp peak
X
Y
Y
X
1086
16
15
14
13
12
11
10
9
8
7
6
5
4
3
2
1
1 2 3 4 5 6 7 8 9 10 11 12 13 14 15 16 17 18 19 20 Hz

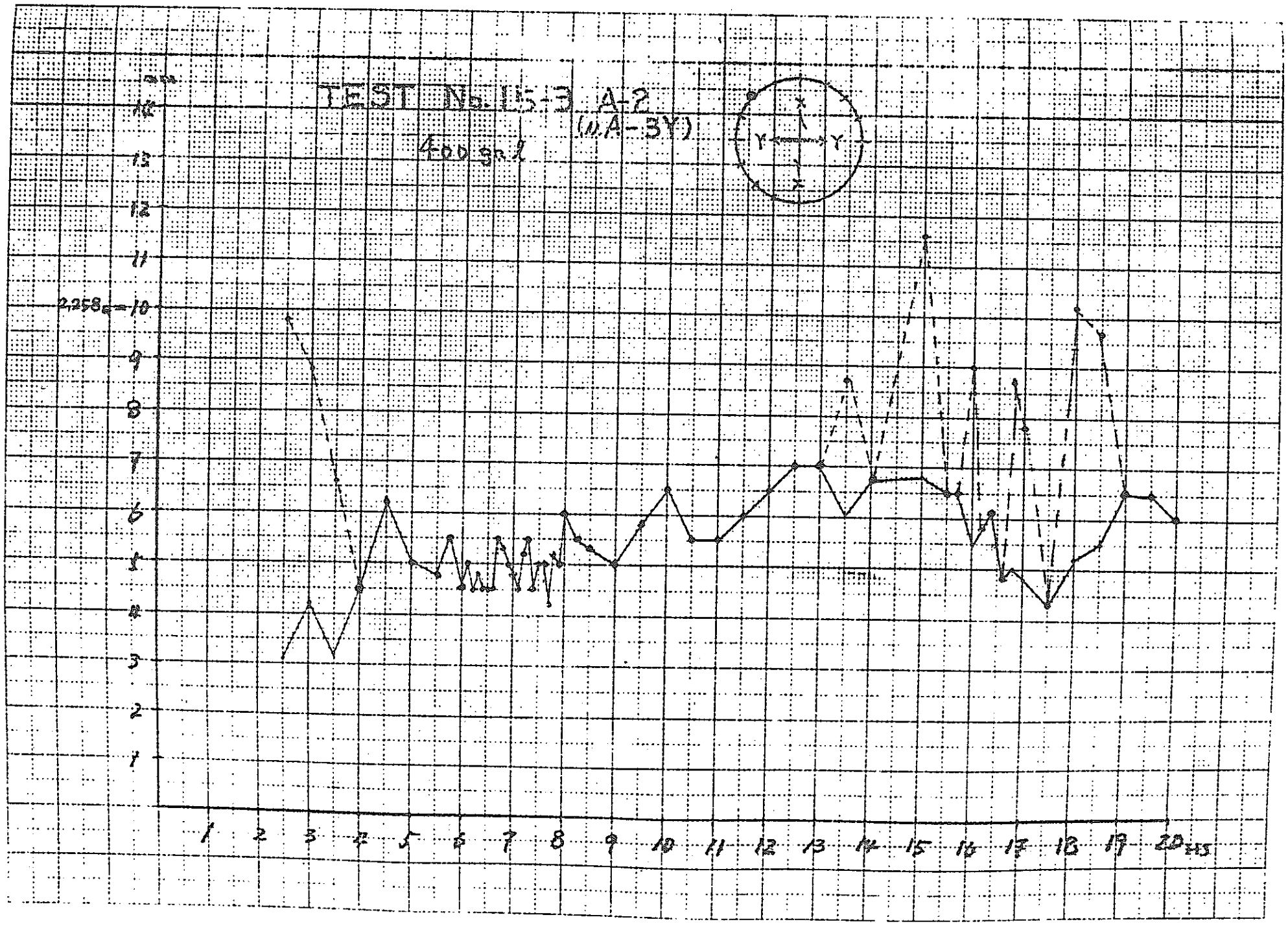
TEST No. L5-3 A-2
(1) A-3Y)
Y
Y
Z
X
2,258
1 2 3 4 5 6 7 8 9 10 11 12 13 14 15 16 17 18 19 20 HS

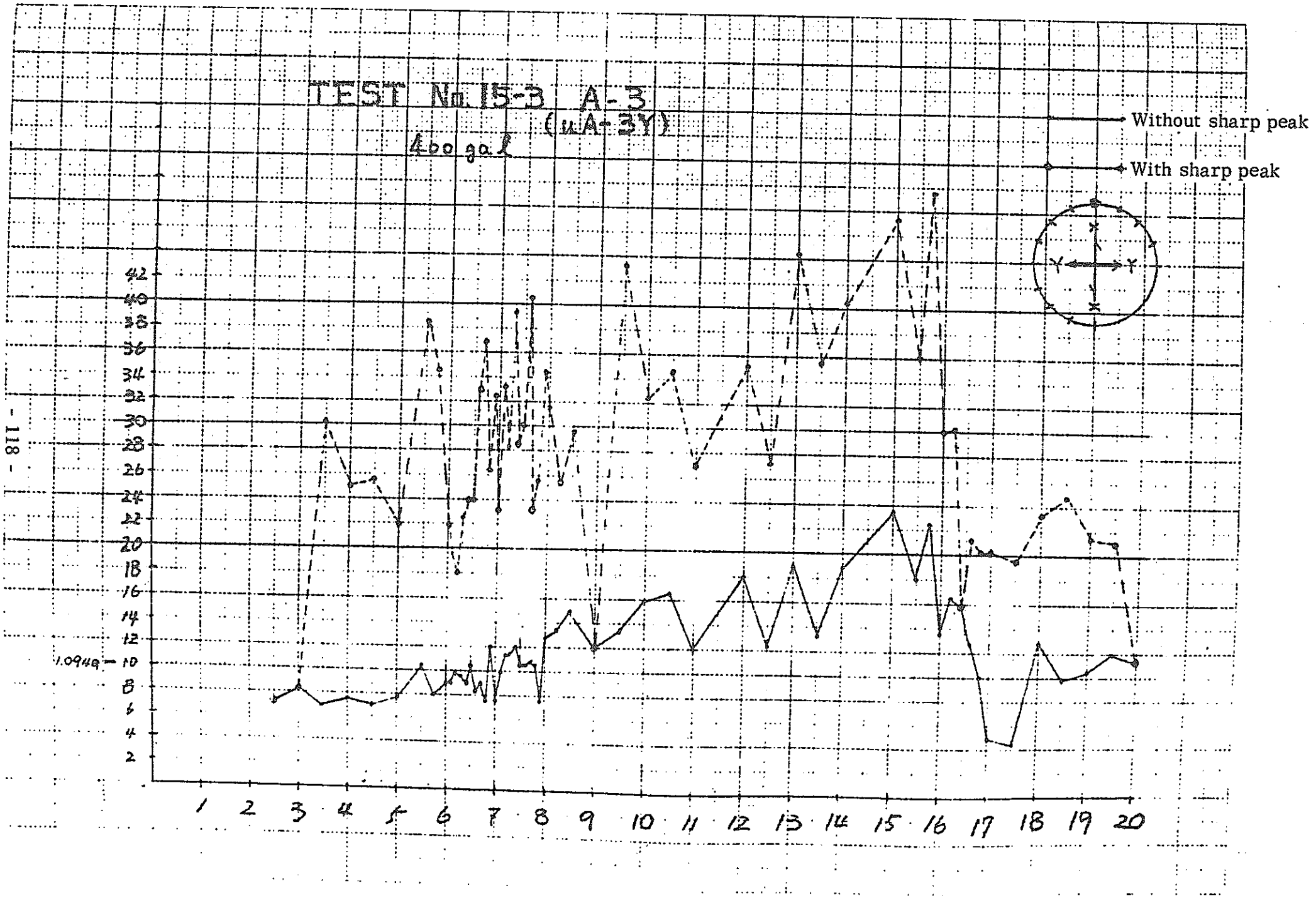
TEST No. 15-3 A-3
(uA-3Y)
400 gal
Without sharp peak
With sharp peak
42
40
38
36
34
32
30
28
26
24
22
20
18
16
14
12
1.094g — 10
8
6
4
2
1 2 3 4 5 6 7 8 9 10 11 12 13 14 15 16 17 18 19 20

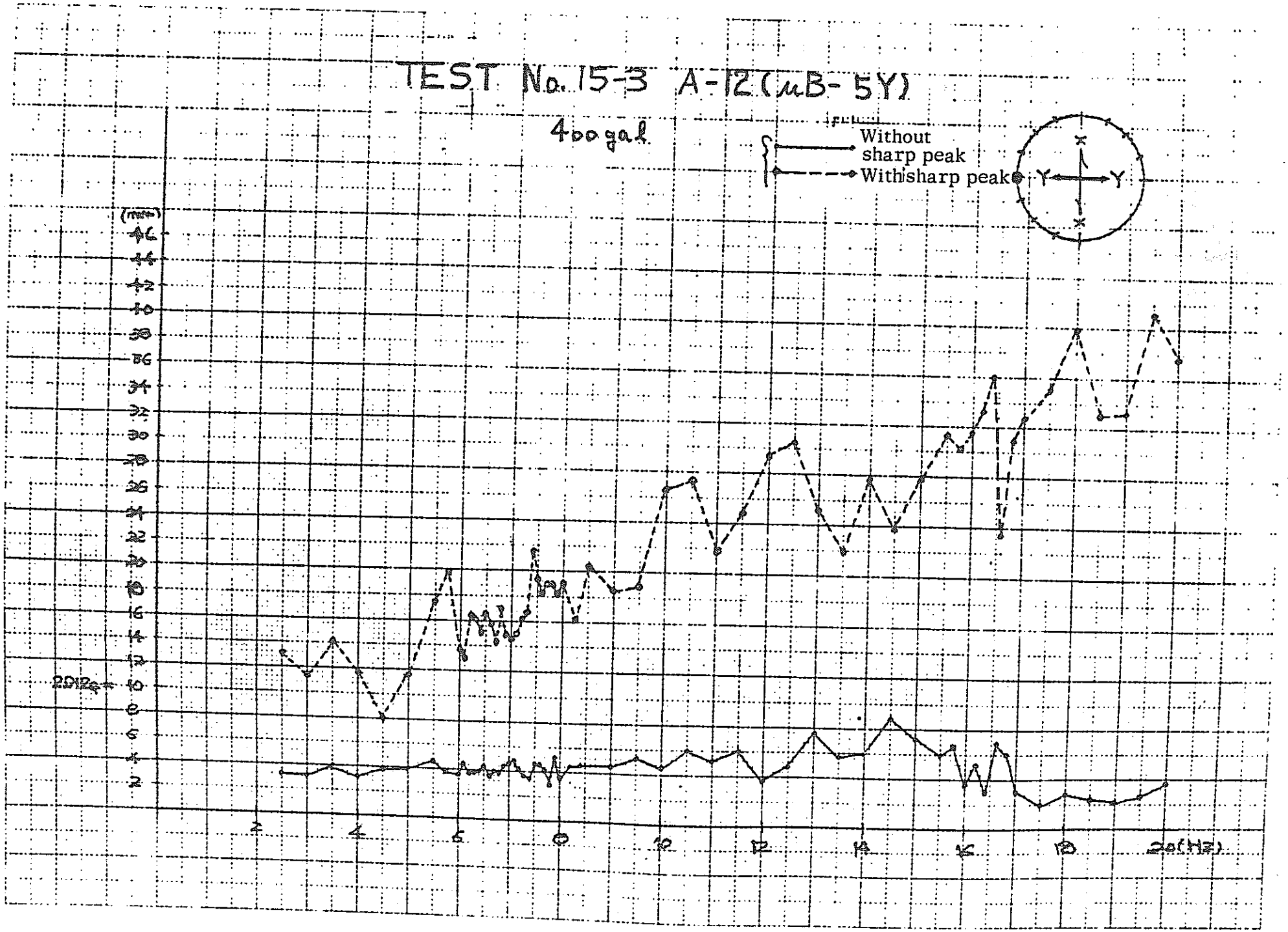
TEST No. 15-3 A-12 (uB-5Y)
400 gal
Without sharp peak
With sharp peak
X
Y
Y
X
(mm)
2SI12
2
4
6
8
10
12
14
16
18
20(Hz)

TEST No 16-2 (400 gal)

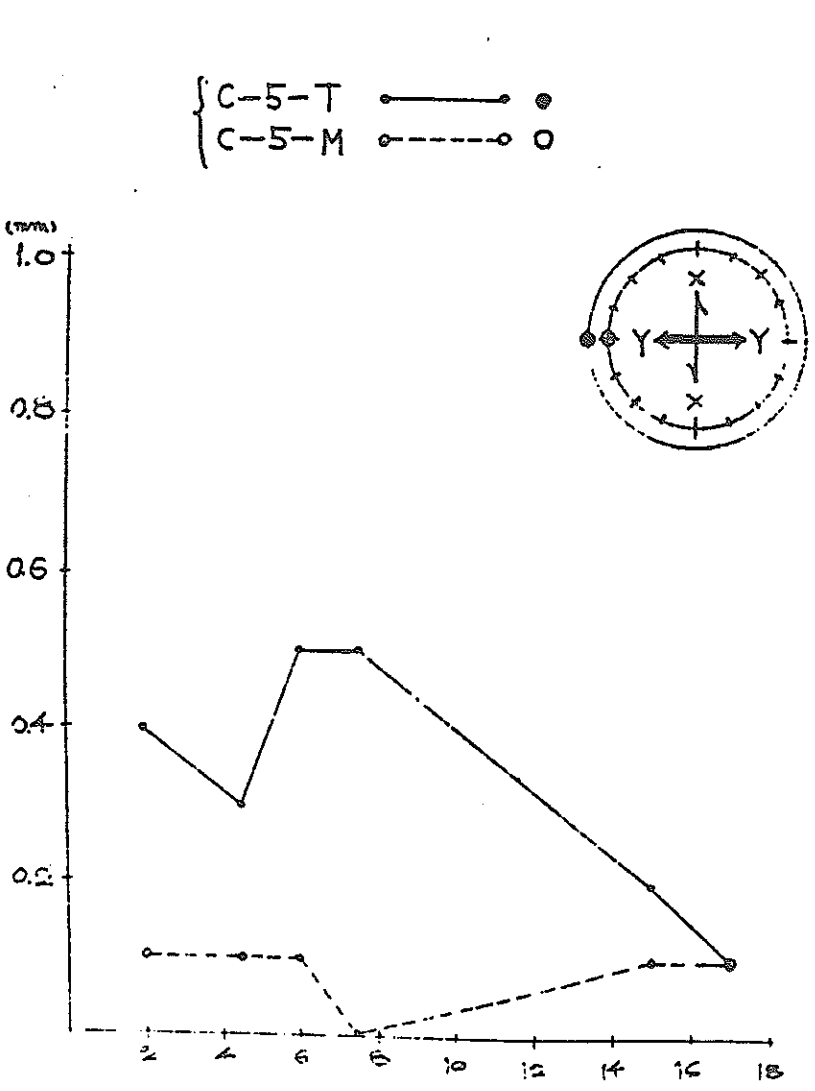

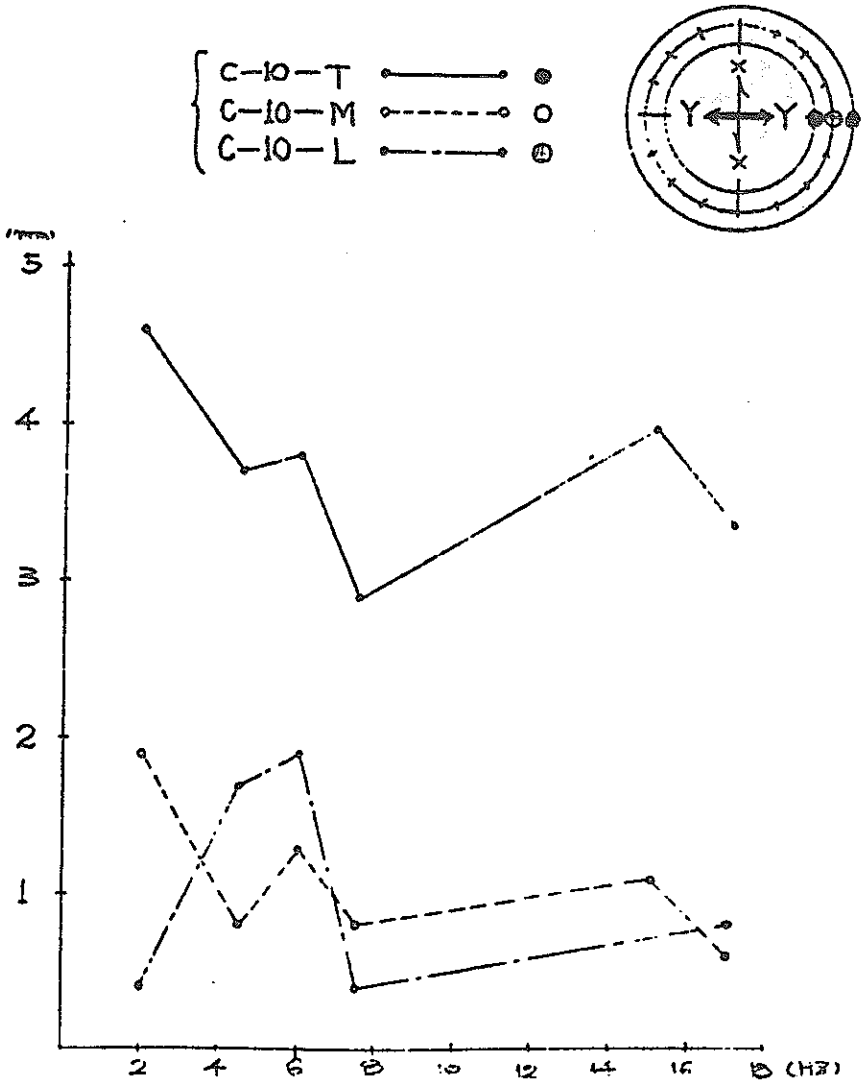

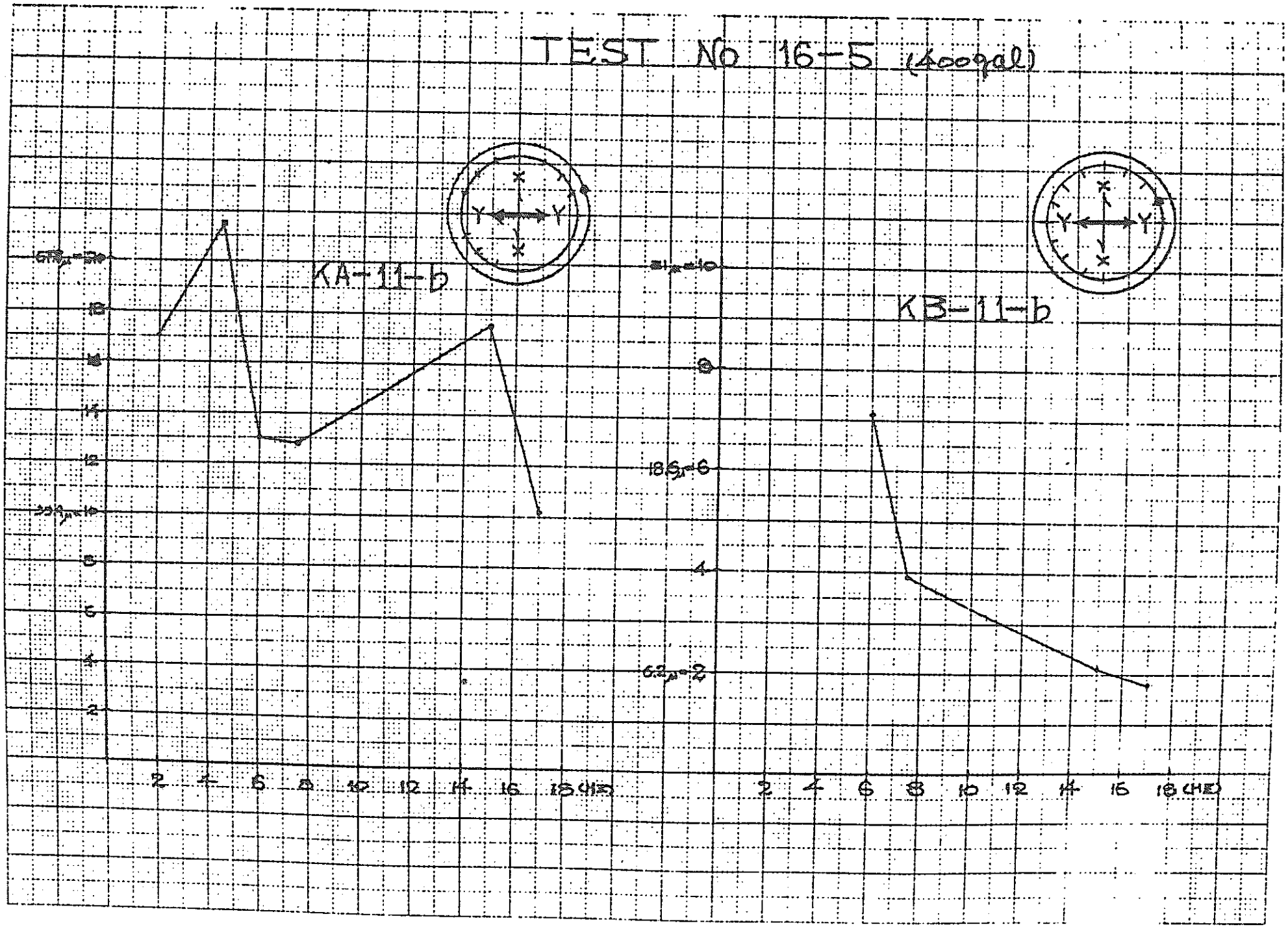
TEST No 16-5 (400gal)
KA-11-b
KB-11-b
Y
Y
X
X
18
16
14
12
10
8
6
4
2
2 4 6 8 10 12 14 16 18 (HZ)

TEST No 16-5 (400gal)

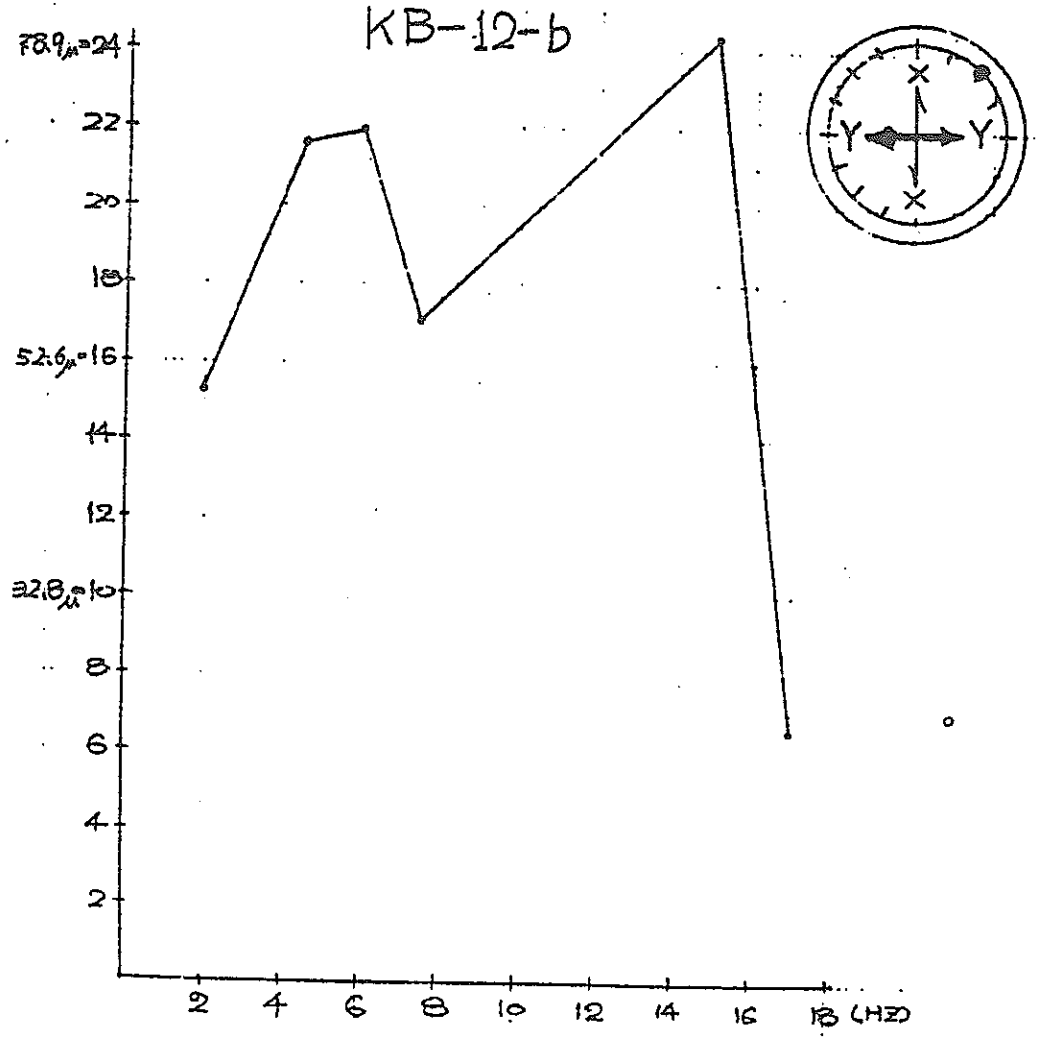

TEST No 16-5 (Accel)
KA-13-D
KB-13-D
X
Y
X
Y
f(Hz)
f(Hz)

TEST No. 16-7

F_X = 356.348 ton/cm²

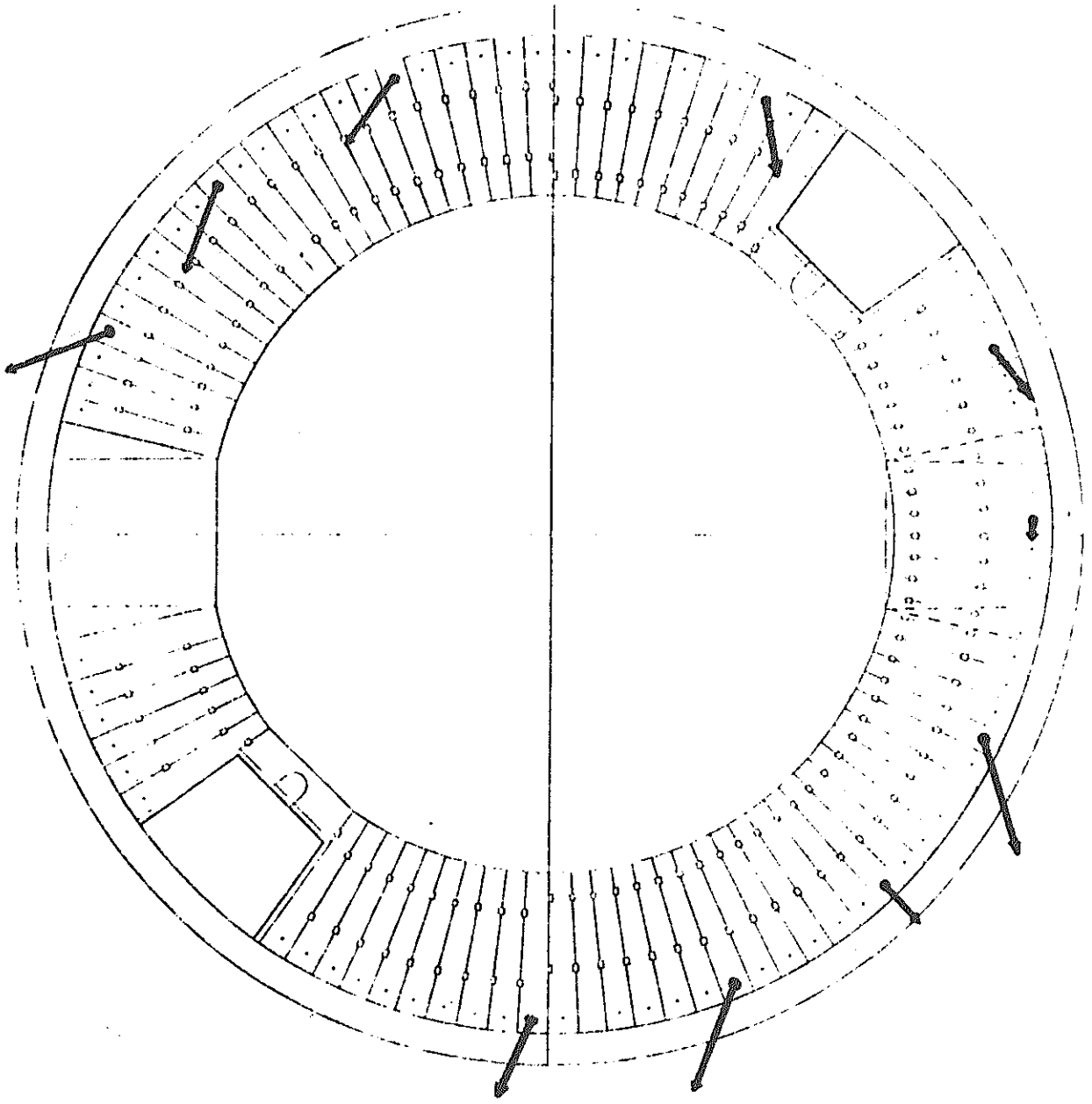

Y-Direction Vibration 100 gal

Pin 1~13 5Hz

10mm 50μ

TEST No. 16-8

EI = 356.348 t·m·cm

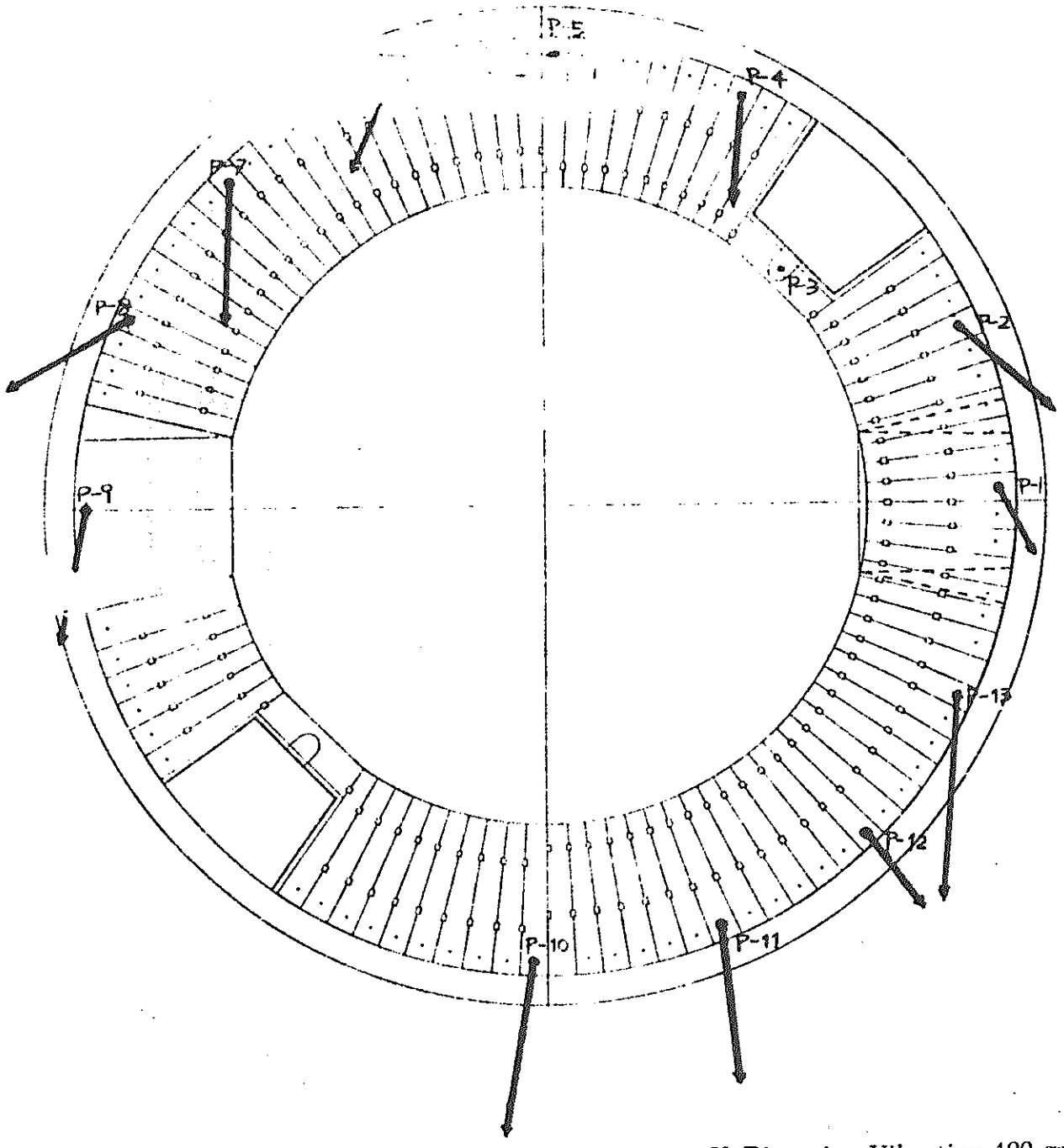

Y-Direction Vibration 400 gal

Pier 1~13 6H

10 75

TEST No. 16-8

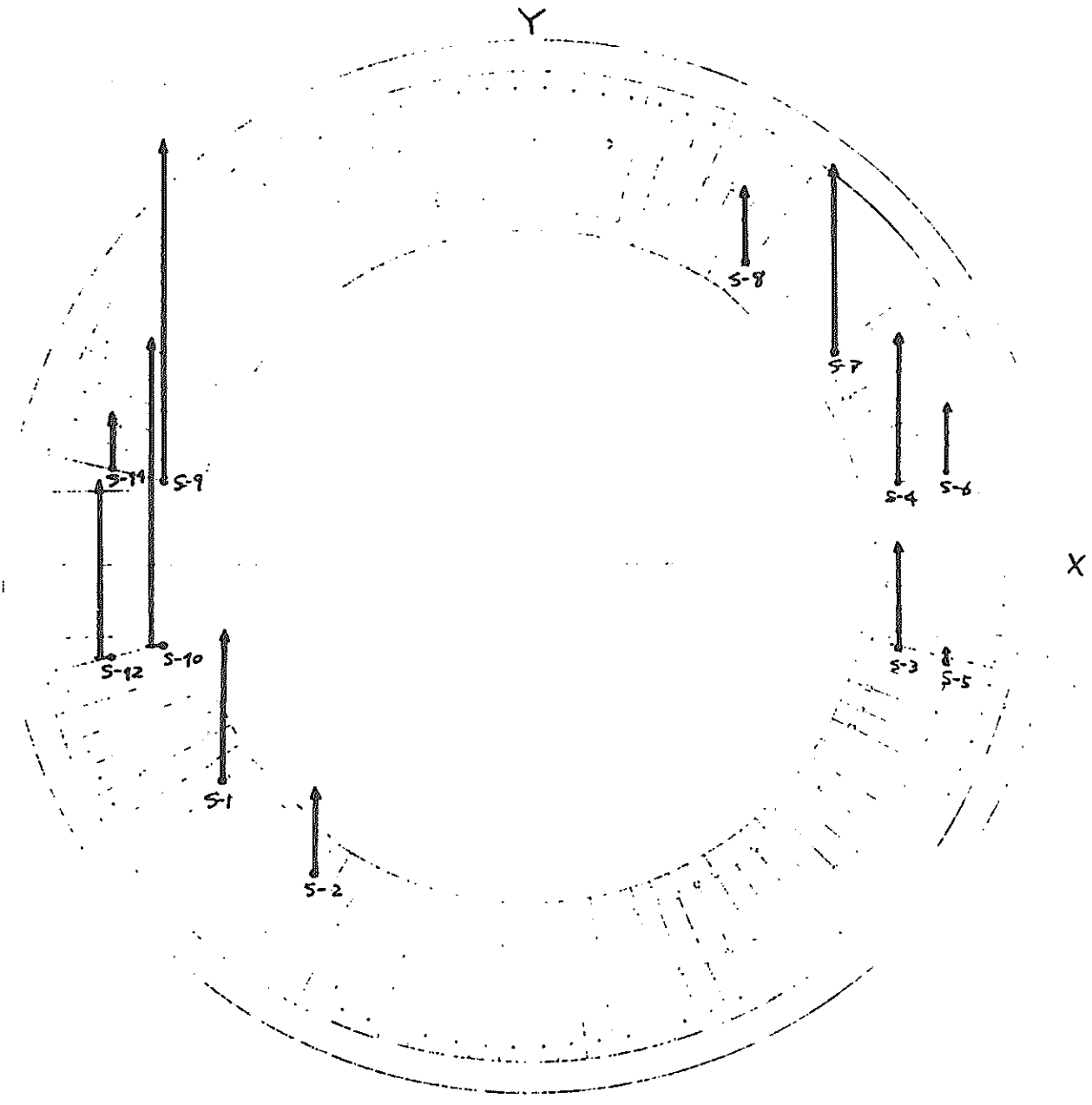

Y-Direction Vibration 400 gal

Spring 6Hz

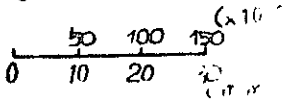

TEST No. 16-2

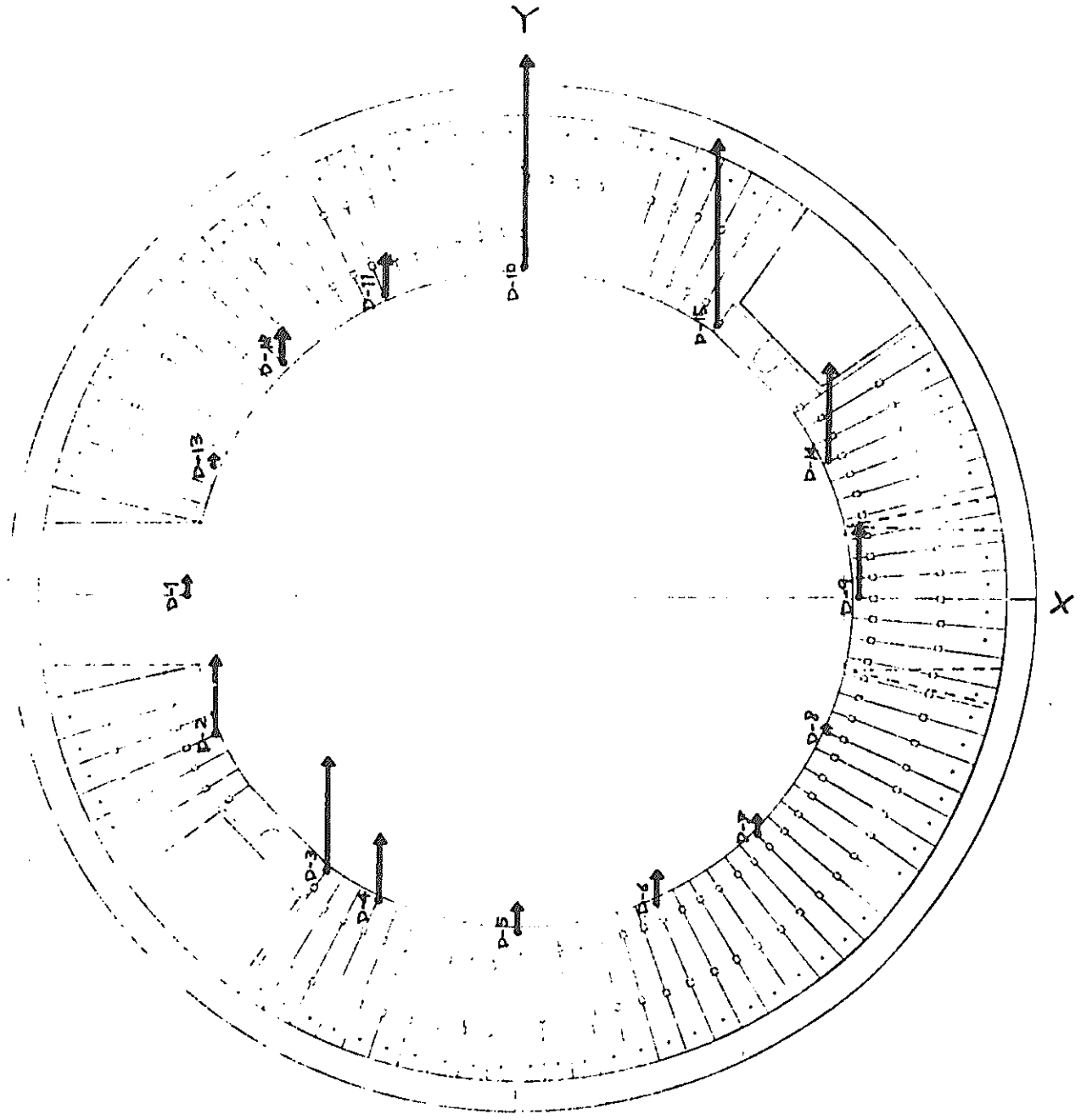

Y-Direction Vibration 400 gal

D1 ~ D15 6Hz

S, D= 1 2 3 (mm)

0 10 20 30 (mm)

TEST No. 16-5

$\theta = 23.75$ ton/cm²

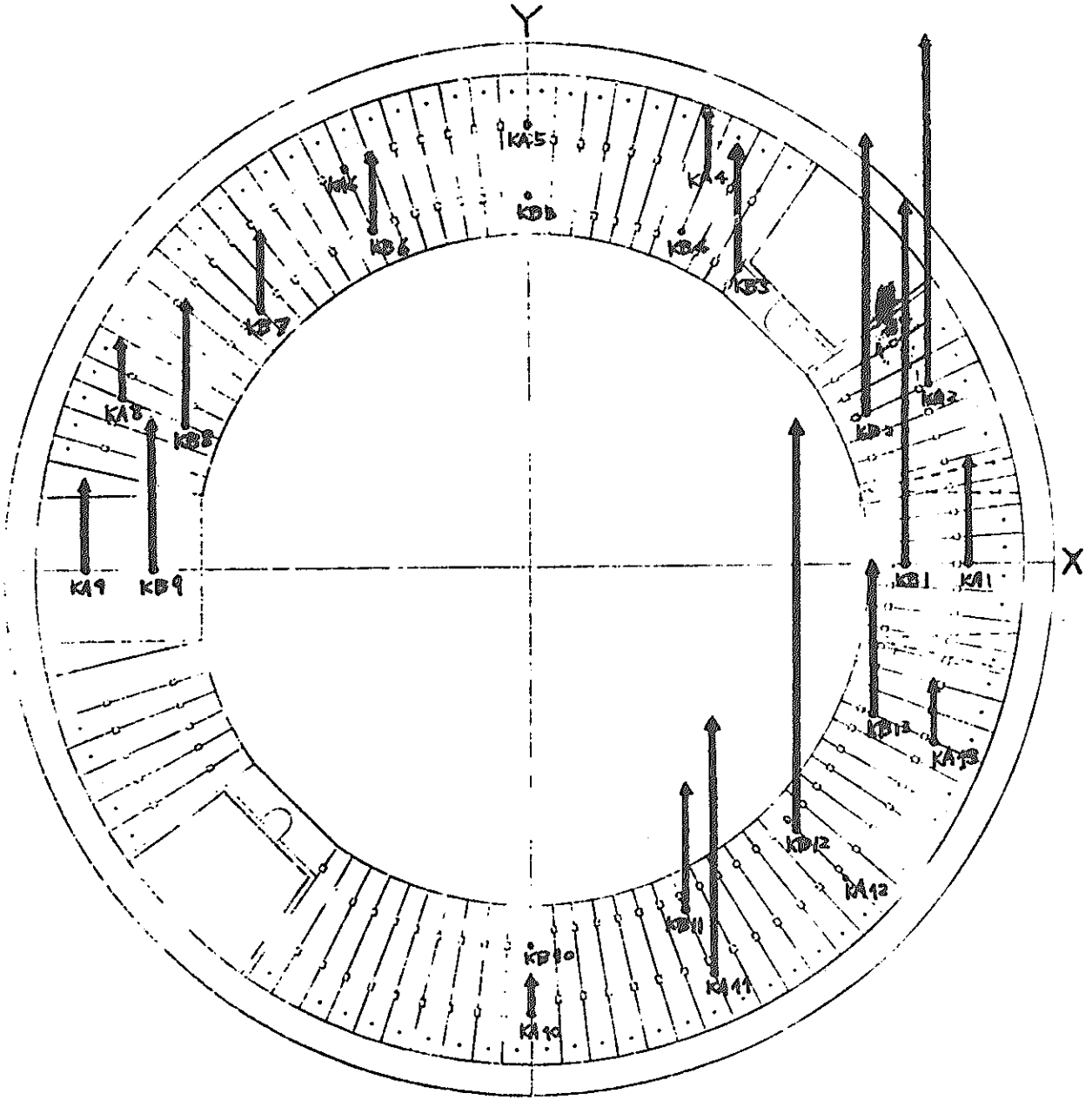

Y-Direction Vibration 400 gal

Key 6Hz

(×10⁻⁶)

5 10 15

0 10 20 30

(mm)

TEST NO 21-2

400 gal EZ = 356.348 kg/cm²

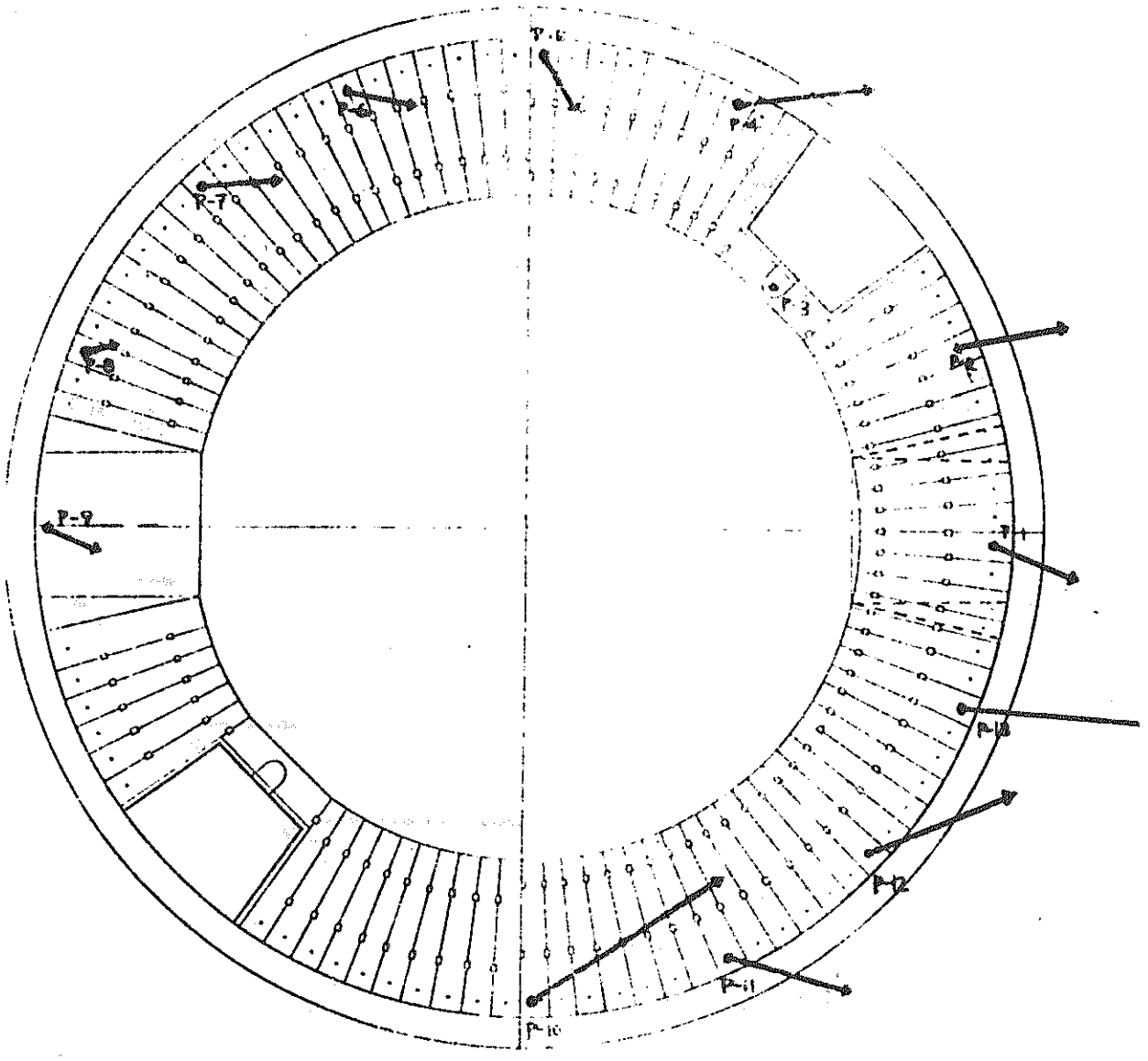

X-Direction Vibration

Pin 1 ~ 13 6.25H

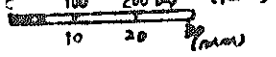

TEST No. 21-2

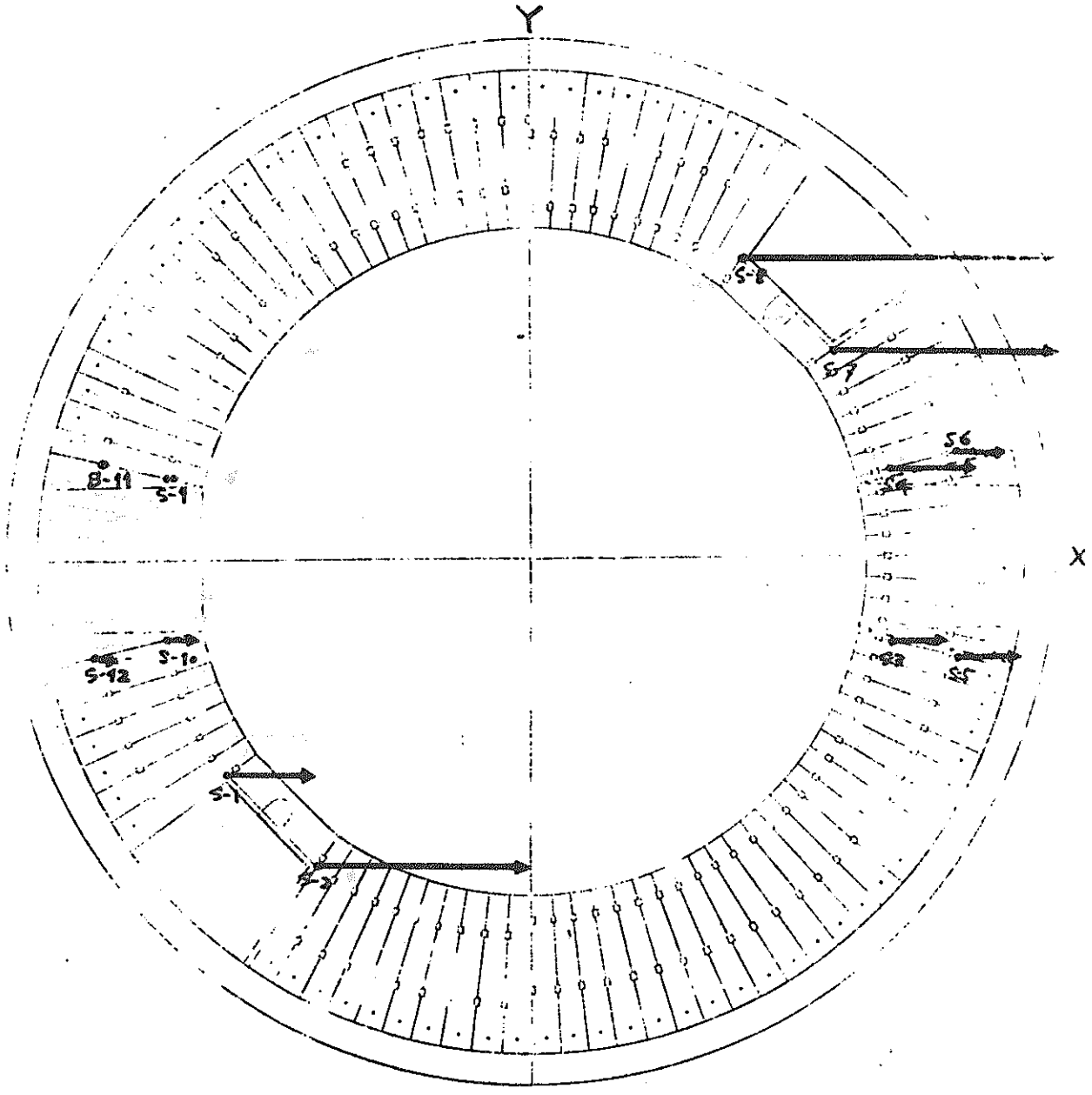

X-Direction 400 gal

Spring 6.25Hz

TEST No. 19-2

400 gal

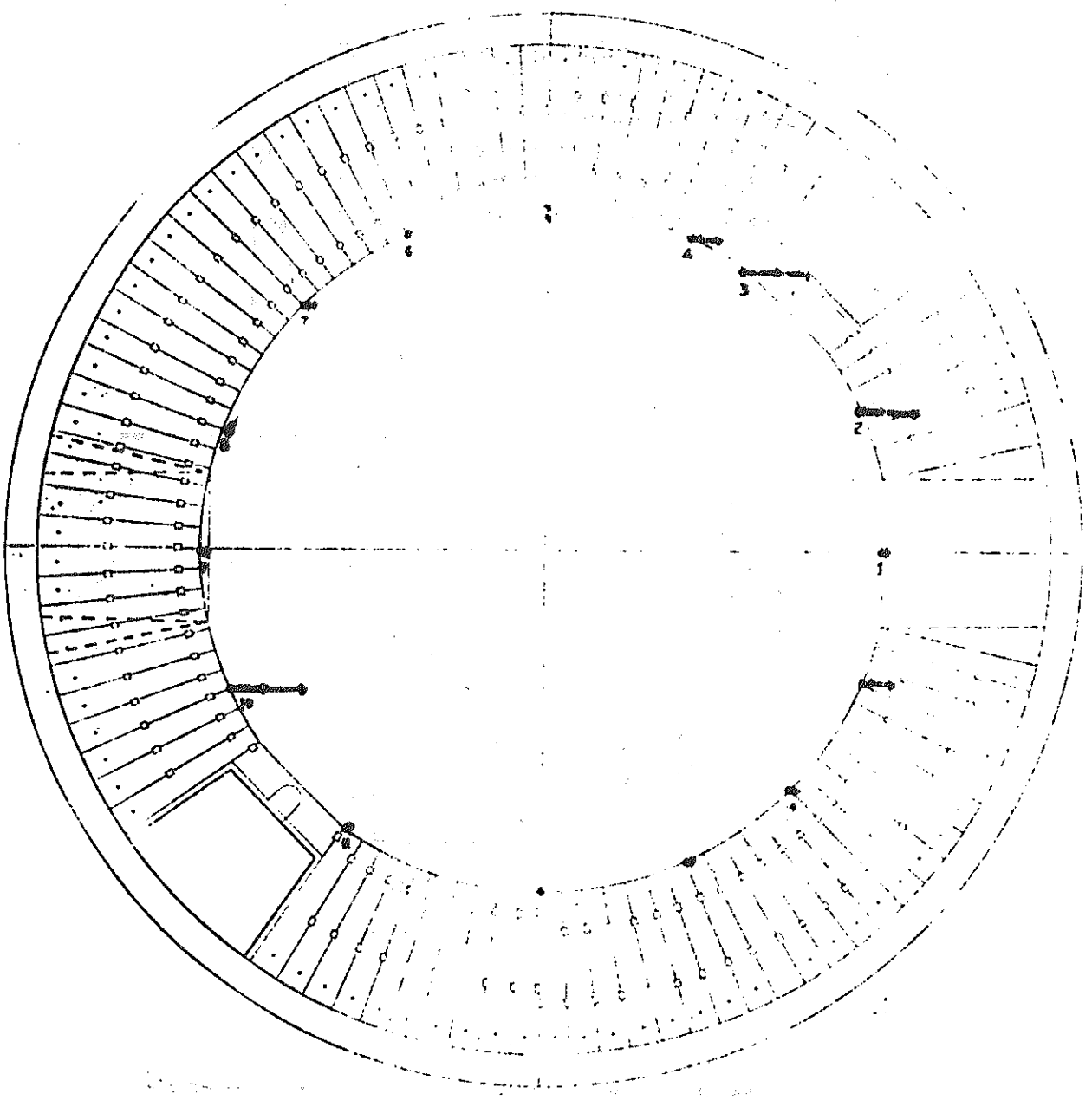

X-Direction Vibration (6.25Hz)

0 5 10 15 (mm)

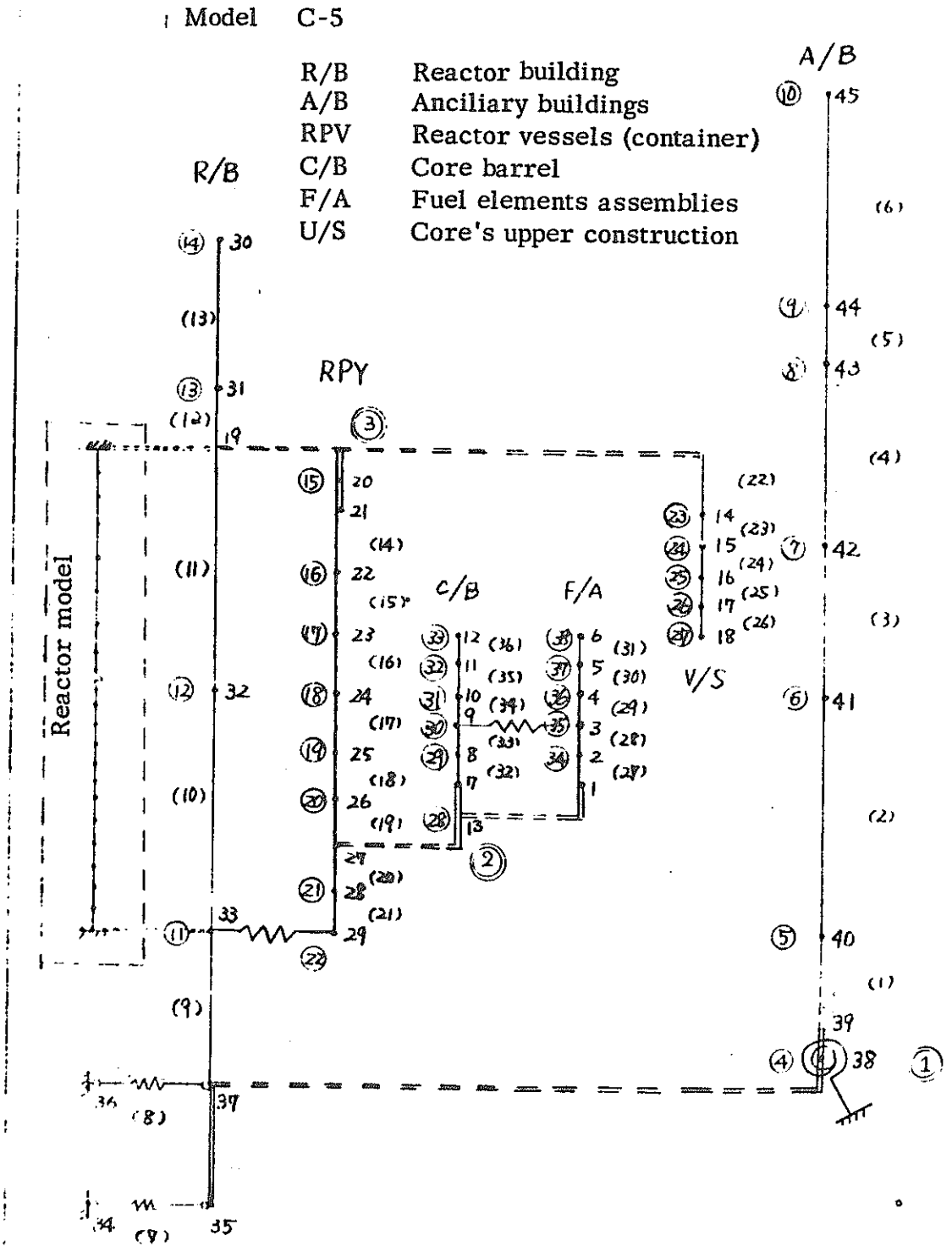

Fig. 6-4-1 General System Model

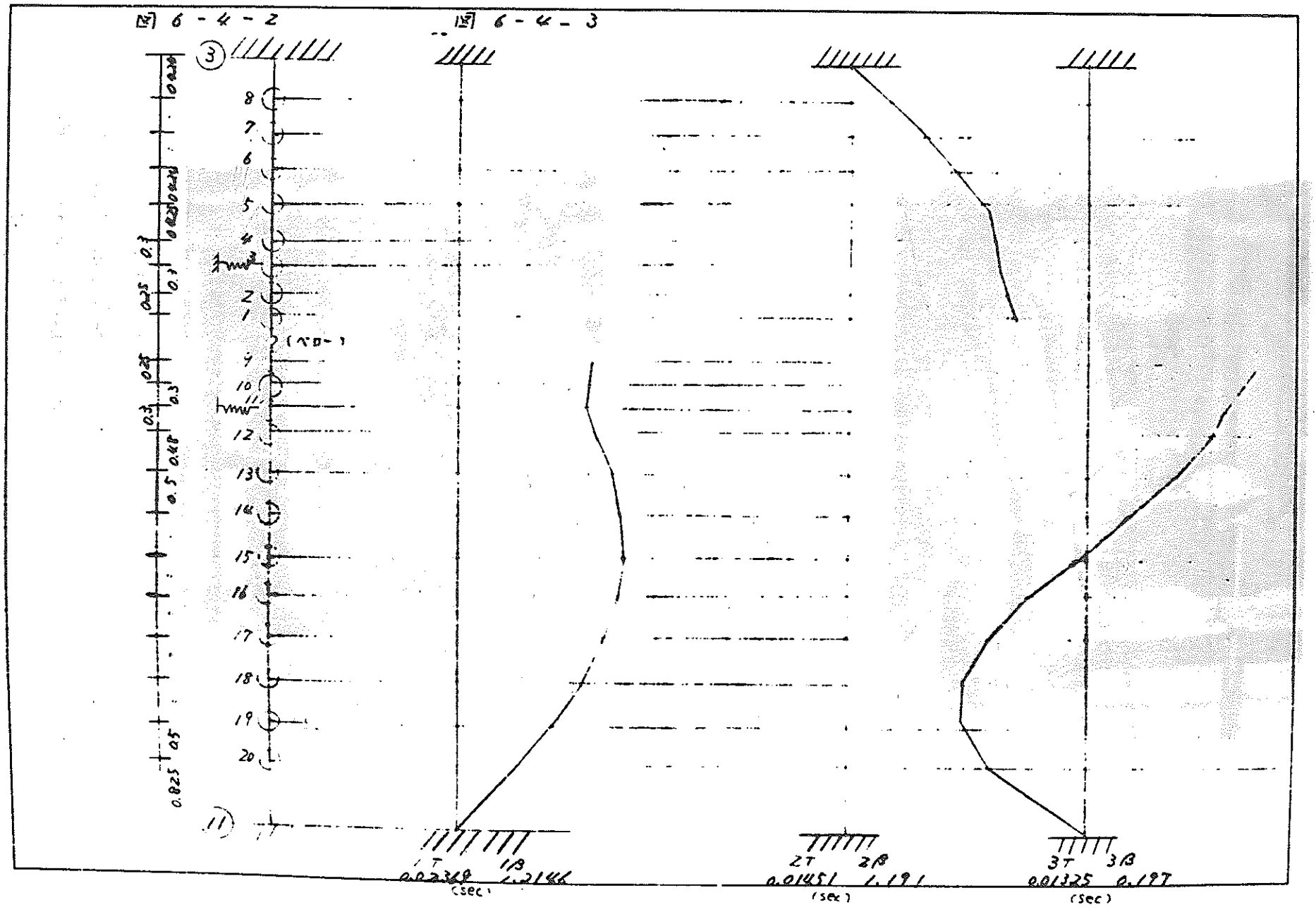
6 - 4 - 2
6 - 4 - 3
1T 1B
0.02348 1.2146
(sec)
2T 2B
0.01451 1.191
(sec)
3T 3B
0.01325 0.197
(sec)

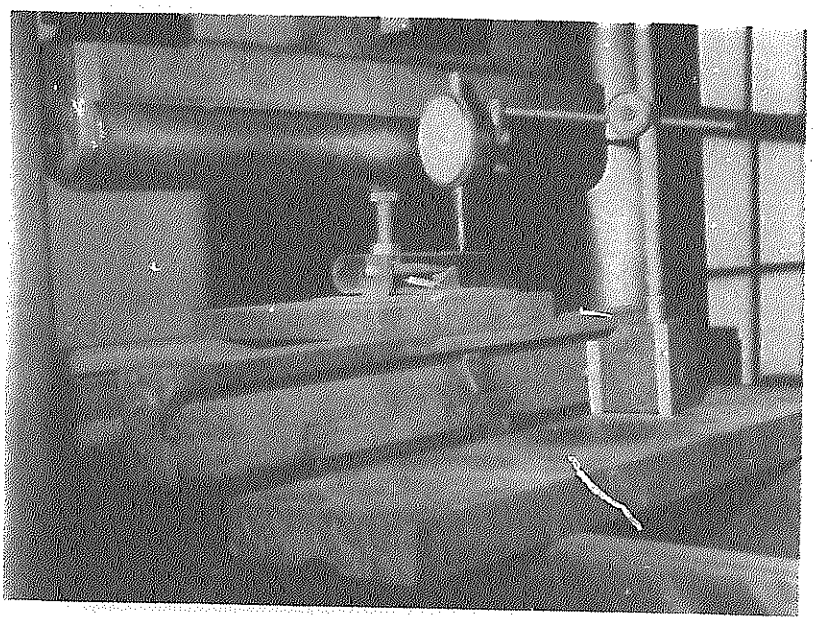

PH - 1. Plate Spring Rigidity Test

1,000 kg Amsler Tester is used to press the plate spring until it contacts the shaft bearing in order to obtain relation among pressure, strain and deformation.

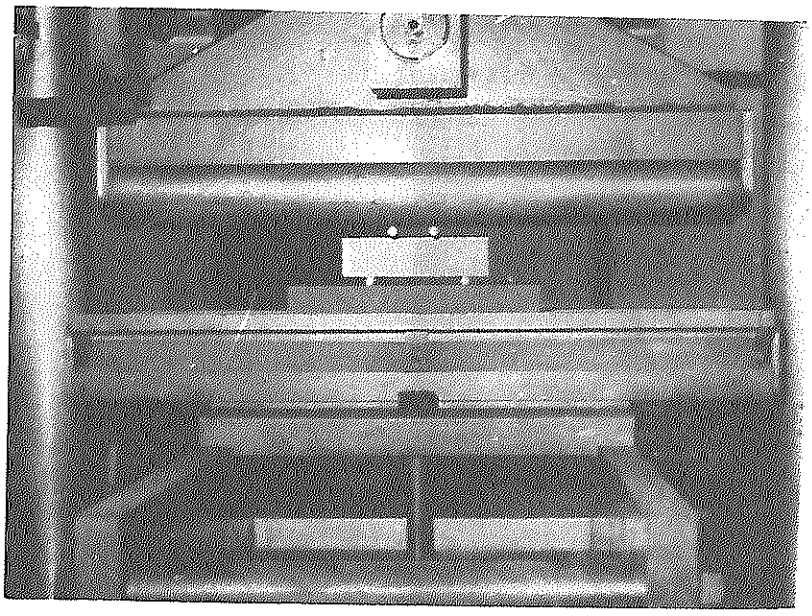

PH - 2. Key's Bending Test

1,000 kg Amsler Tester is used to apply compression load.

The compression load is applied 20 kg in each step.

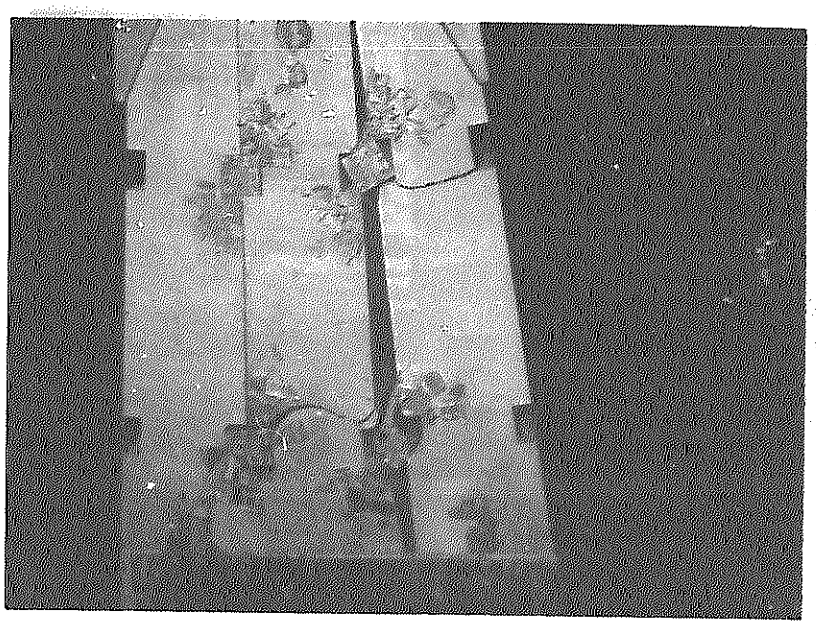

PH - 3. 1-Layer 3-Row Compression Test

The crevice for the key on the upper section of the block assembly is yielding under pressure while the keys are working as wedges to widen the opening.

PH - 4. 1-Layer 3-Row Tensile Test

The block is broken down under tensile force and eccentric bending.

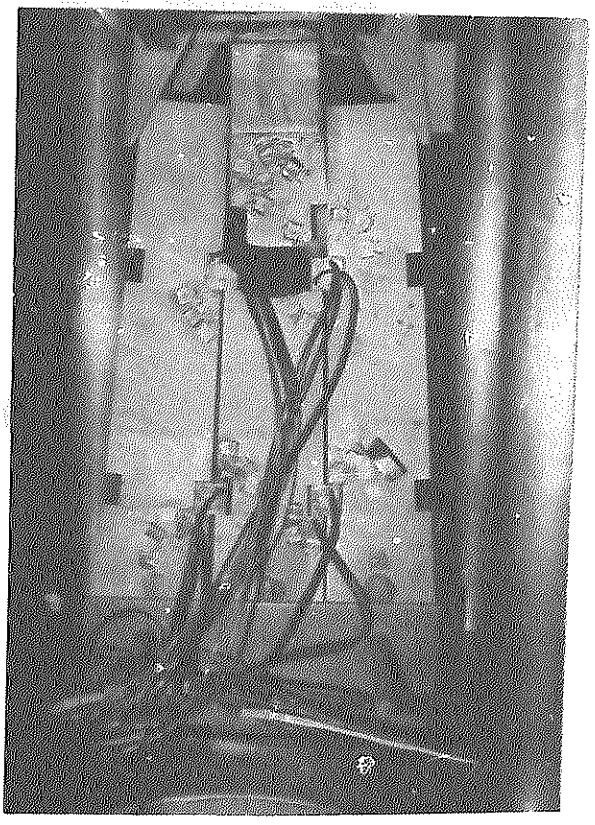

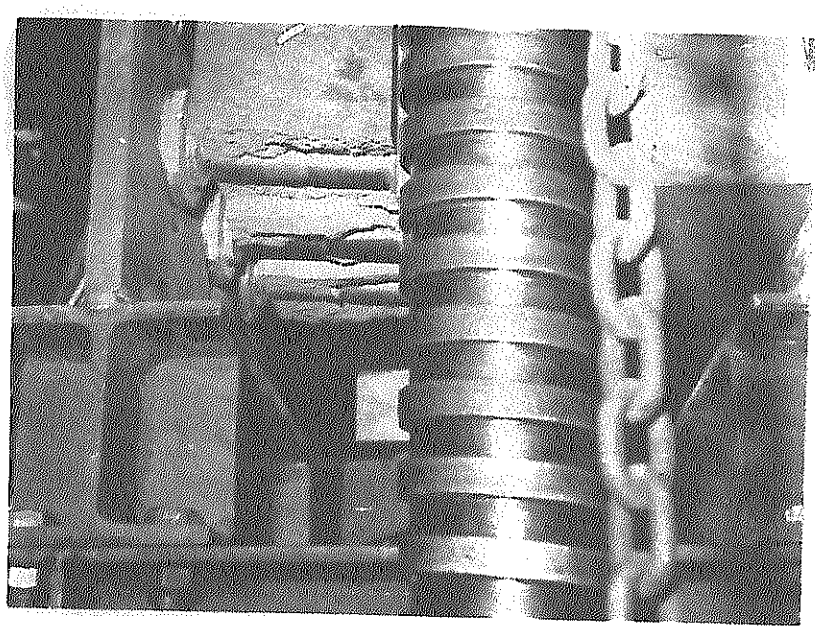

PH - 5. 3-Layer 3-Row Compression Test

The lower pin suffered a great deformation under bending stress and has broken down under the tensile stress applied on the graphite.

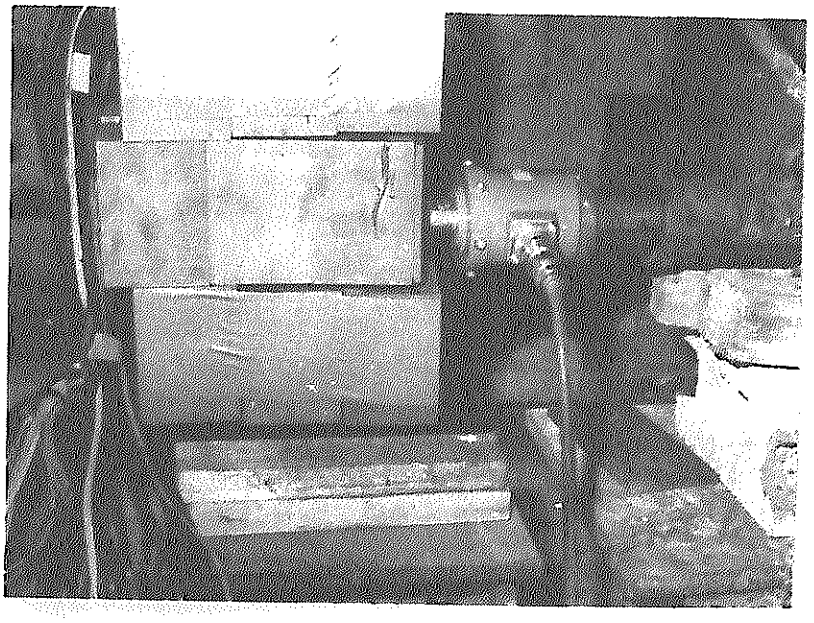

PH - 6. 3-Layer 3-Row Traverse Force Test

Test at the load position 3.

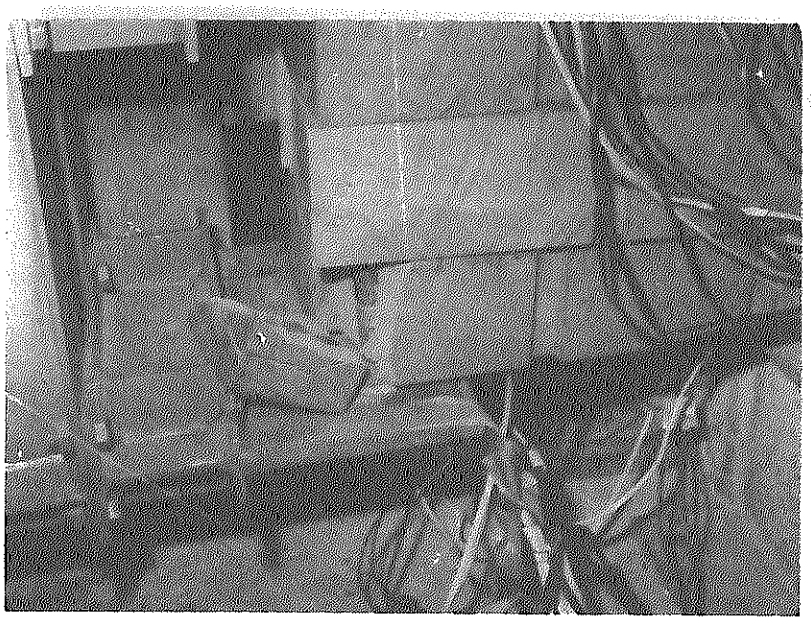

PH - 7. 3-Layer 3-Row Traverse Force Test

A pin suffered a great deformation under bending stress and damaged a corner section of the graphite.

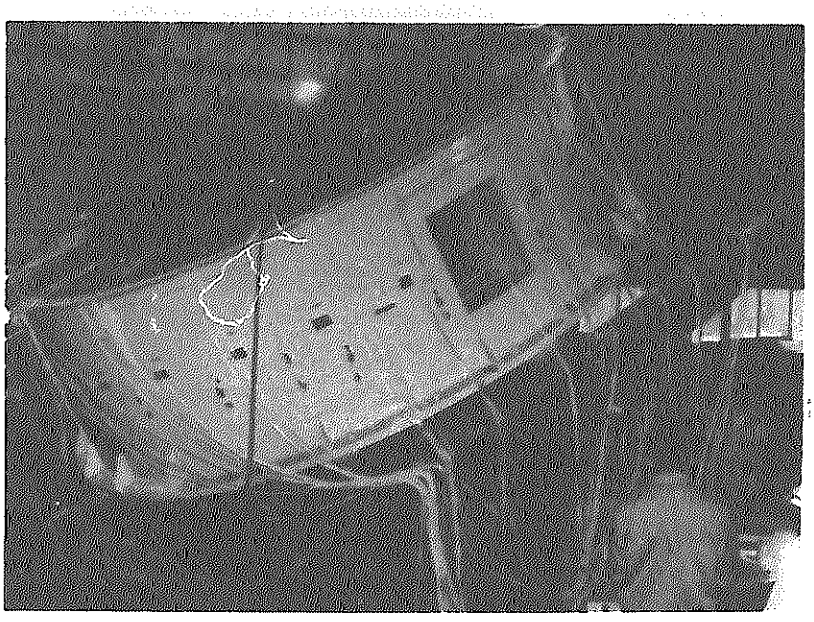

PH - 8. Tilting Test

Y-direction 45^{o} tilt

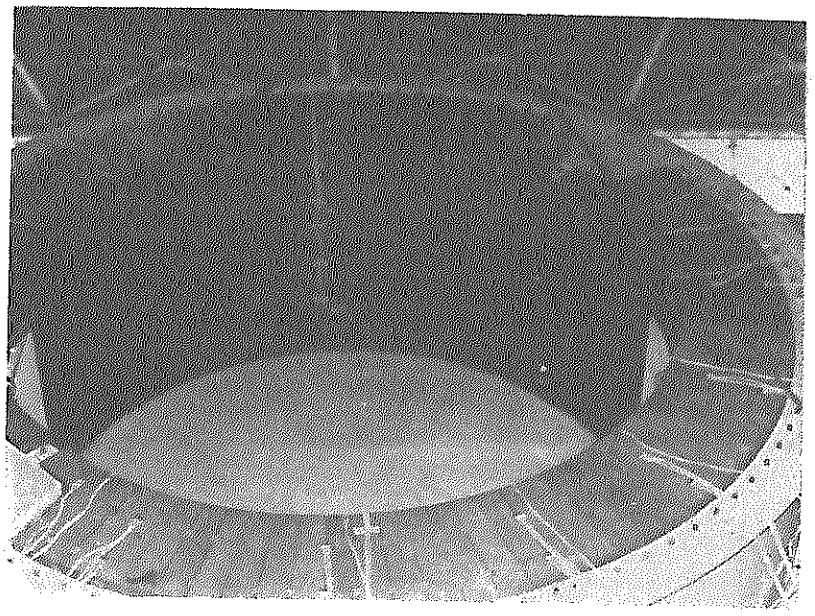

PH - 9. Tilting Test

Y-direction 45^{o} tilt

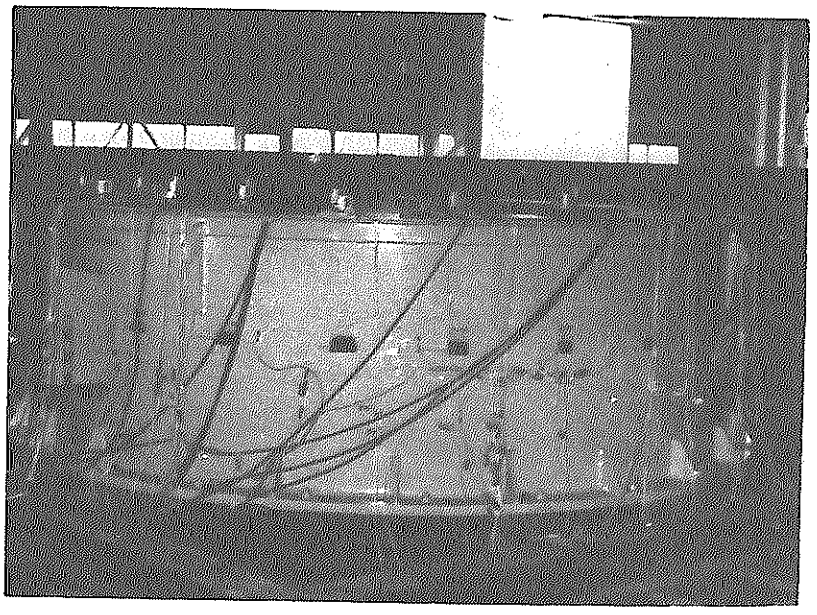

PH - 10. Vibration Test

PH - 11. Wider Opening between Blocks

Maximum opening, 24. 5 mm (Test opening)